POLITECHNIKA POZNAŃSKA

WYDZIAŁ INŻYNIERII MATERIAŁOWEJ I FIZYKI TECHNICZNEJ

Instytut Badań Materiałowych i Inżynierii Kwantowej

Zakład Inżynierii i Metrologii Kwantowej

mgr inż. Maciej Chomski

ROZPRAWA DOKTORSKA

Właściwości magnetyczne holmu w stanach wzbudzonych

Promotor: **dr hab. Bogusław Furmann, prof. PP**

Dyscyplina: Inżynieria materiałowa

Poznań, 2023

ABSTRACT

In this work, consisted of 6 thematically coherent papers, the research results of investigating hyperfine structure of holmium atom, are presented. This element has been gaining interest as the candidate for the quantum material in quantum engineering experiments and quantum information processing in recent years. The research was focused on identification of new electronic energy levels of the holmium atom, as well as the quantitative analysis of their characteristic parameters - magnetic dipole and electric quadrupole hyperfine structure constants, and Landé g_J factors. All the presented investigations, the method of laser spectroscopy with optical detection by laser induced fluorescence in a hollow cathode discharge lamp, was used.

As part of this doctoral thesis, based on the analysis of the hyperfine structure of unclassified spectral lines, 62 hitherto unknown electronic levels of the holmium atom have been identified. For all new energy levels the hyperfine structure constants and J quantum numbers were determined. In addition, as part of the research, the values of the hyperfine structure constants were measured for 27 known energy levels, for which these are the first experimental results. In total, experimental values of hyperfine structure constants for 89 electron levels of the holmium atom were published for the first time. The analysis of the hyperfine structure splitting in external magnetic field, caused by the Zeeman effect, allowed to determine Landé g_J factors for 51 energy levels of holmium atom, for the first time.

The presented results significantly extend the current state of knowledge about the hyperfine structure of the holmium atom, which may facilitate the implementation of the investigated element as a quantum material through the development of efficient optical trapping and cooling techniques for quantum engineering experiments. As part of this work, a spectrally narrow optical transition has been proposed, which can be used for second-stage laser cooling of holmium in a magneto-optical trap.

STRESZCZENIE

Niniejsza praca, na którą składa się cykl 6 spójnych tematycznie publikacji naukowych, zawiera wyniki badań struktury nadsubtelnej atomu holmu. Pierwiastek ten w ostatnich latach zyskuje na znaczeniu w kontekście wykorzystania jako materiał kwantowy w eksperymentach z zakresu inżynierii kwantowej oraz przetwarzania informacji kwantowej. Badania zostały skoncentrowane na identyfikacji nowych poziomów elektronowych atomu holmu, a także analizie ilościowej parametrów charakteryzujących te poziomy energetyczne, takich jak stałe struktury nadsubtelnej – magnetyczna dipolowa i elektryczna kwadrupolowa, a także czynniki g_J Landégo. We wszystkich przedstawionych pracach badawczych wykorzystano metodę spektroskopii laserowej z detekcją optyczną za pomocą metody laserowo indukowanej fluorescencji, w lampie wyładowczej z katodą wnękową.

W ramach niniejszej pracy doktorskiej, na podstawie analizy struktury nadsubtelnej niesklasyfikowanych linii spektralnych, zidentyfikowane zostały 62 nieznane dotąd poziomy elektronowe atomu holmu. Dla wszystkich nowych poziomów energetycznych wyznaczono doświadczalnie wartości stałych struktury nadsubtelnej oraz przypisano wartości liczb kwantowych J. Ponadto, w ramach prowadzonych badań zmierzono wartości stałych struktury nadsubtelnej dla 27 znanych poziomów energetycznych, dla których są to pierwsze wyniki eksperymentalne. Łącznie, po raz pierwszy opublikowano wartości doświadczalne stałych struktury nadsubtelnej dla 89 poziomów elektronowych atomu holmu. Na podstawie analizy rozszczepienia struktury nadsubtelnej w zewnętrznym polu magnetycznym, wynikającym ze zjawiska Zeemana, wyznaczono po raz pierwszy wartości czynników g_J Landégo dla 51 poziomów elektronowych atomu holmu.

Przedstawione wyniki znacząco rozszerzają aktualny stan wiedzy na temat struktury nadsubtelnej atomu holmu, co może ułatwić implementację badanego pierwiastka w roli materiału kwantowego poprzez rozwój technik wydajnego pułapkowania i chłodzenia atomów dla celów eksperymentów z dziedziny inżynierii kwantowej. W ramach niniejszej pracy zaproponowane zostało wąskie spektralnie optyczne przejście chłodzące, które może zostać wykorzystane do chłodzenia laserowego drugiego stopnia w pułapce magnetooptycznej.

Spis treści

1. Wstęp

Holm jest pierwiastkiem należącym do grupy lantanowców, posiadającym jeden stabilny izotop - $^{165}_{67}Ho$. Ze względu na swoją masę klasyfikowany jest pośród cięższych metali ziem rzadkich (ang. *heavy rare earths elements* - HREE). Czysty holm charakteryzuje się srebrzystym kolorem, stosunkowo dużą miękkością względem innych metali oraz, podobnie jak pozostałe metale ziem rzadkich, intensywnie reaguje z powietrzem atmosferycznym tworząc tlenek Ho_2O_3. Z tego powodu praktycznie nie występuje naturalnie w swojej czystej formie. Holm został odkryty przez szwajcarskich chemików Jacques'a Louisa Soreta i Marca Delafontaine'a, którzy sklasyfikowali go na podstawie badań spektroskopowych tlenku erbu w 1878 roku, a także niezależnie w tym samym roku przez szwedzkiego chemika Pera Theodora Cleve'a, który skutecznie wyizolował ten pierwiastek z rudy tlenku erbu [1].

Charakterystyczną cechą pierwiastków z grupy lantanowców jest otwarta powłoka $4f$ oraz bogata struktura energetyczna, skutkująca bardzo dużą ilością linii widmowych, których duża część leży w zakresie widzialnym promieniowania elektromagnetycznego. Z tego powodu metale ziem rzadkich znajdują liczne zastosowania, między innymi przy produkcji źródeł światła oraz w domieszkowaniu matryc ekranów telewizyjnych. Lasery na ciele stałym domieszkowane holmem (Ho:YAG) są szeroko stosowane w zabiegach medycznych, okulistycznych oraz dentystycznych. Matryce typu Ho:YIG wykorzystywane są w produkcji izolatorów optycznych oraz urządzeń mikrofalowych. Domieszkowanie holmem jest wykorzystywane również w celu barwienia szkieł i cyrkonii na kolor żółty lub różowy. Szkła zawierające tlenek holmu znajdują zastosowanie w kalibracji spektrofotometrów, ze względu na silną absorpcję w całym zakresie widzialnym, stanowiąc bardzo dobre filtry. Ponadto, materiał ten może pełnić rolę moderatora w reaktorach jądrowych [2] [3] [4].

Holm, w warunkach normalnych, jest materiałem paramagnetycznym posiadającym przejście do fazy ferromagnetycznej poniżej 20 K. Ze względu na wyjątkowe właściwości magnetyczne – największy moment magnetyczny wśród znanych pierwiastków, wynoszący $10,6\mu_B$ – holm stał się jednym z podstawowych materiałów wykorzystywanych przy produkcji silnych magnesów trwałych. Domieszki holmu w magnesach pozwalają na koncentrację strumienia magnetycznego lub wzmocnienie pola magnetycznego bezpośrednio na biegunach. Nadzwyczajny moment magnetyczny atomu holmu sprawia, że stał się on najważniejszym kandydatem do implementacji pamięci magnetycznych opartych o kodowanie bitów informacji w stanie magnetycznym pojedynczych atomów.

Naniesienie pojedynczych atomów holmu na podłoże utworzone z cienkiej warstwy tlenku magnezu (MgO) powoduje powstanie dużej anizotropii magnetycznej, w wyniku wystawienia atomu na działanie asymetrycznego potencjału elektrostatycznego.

Zachowanie momentu magnetycznego w takiej sytuacji silnie zależy od kierunku działania zewnętrznego pola magnetycznego. Pozwala to na bezpośredni zapis i odczyt bitów informacji zakodowanych w spinie indywidualnego atomu Ho, za pomocą analizy sygnału spinowego rezonansu elektronowego (ang. *electron spin resonance* - ESR) z wykorzystaniem spinowo spolaryzowanego skaningowego mikroskopu tunelowego [5].

Atomy holmu na podłożu MgO wykazują wysoką stabilność i stosunkowo długi czas relaksacji magnetycznej w niskich temperaturach, konieczny do skutecznej implementacji magnetycznego przechowywania danych. Koncepcja ta stanowi limit klasycznej realizacji nośnika pamięci magnetycznej, w kontekście możliwej gęstości zapisu informacji. Magnesy jednoatomowe są również interesujące z punktu widzenia przetwarzania informacji kwantowej. Układ Ho/MgO/Ag(100) wyróżnia się na tle innych badanych układów magnesów atomowych i molekularnych zarówno stabilnością w obecności zewnętrznego pola magnetycznego jak i termiczną. Materiał ten stanowił pierwszą realizację trwałego magnesu atomowego [6] [7].

Holm jest pierwiastkiem posiadającym względnie dużą wartość spinowego momentu pędu jądra atomowego $I = 7/2$, co w połączeniu z wysokimi wartościami momentów jądrowych, magnetycznego dipolowego oraz elektrycznego kwadrupolowego, skutkuje dużym rozszczepieniem struktury nadsubtelnej poziomów energetycznych. Właściwość ta sprawia, że holm jest materiałem pożądanym w eksperymentach z dziedziny inżynierii i metrologii kwantowej oraz przetwarzania informacji kwantowej. Jednym z interesujących zastosowań badanego pierwiastka jest implementacja procesora kwantowego opartego o dużą liczbę kubitów [8]. Układ poziomów energetycznych w atomie holmu oraz rozszczepienie Zeemana poziomu podstawowego są korzystne do przygotowania stanu kwantowego i przeprowadzenia odczytu informacji. Kluczowym aspektem do realizacji eksperymentów z dziedziny inżynierii kwantowej jest odpowiednie spreparowanie materiału kwantowego. Wydajną metodą zapewniającą znaczne obniżenie temperatury materiału kwantowego, z jednoczesnym zlokalizowaniem go w ograniczonej przestrzeni, jest chłodzenie laserowe w pułapkach magnetooptycznych (ang. *magneto-optical trap* – MOT). Ze względu na duże zainteresowanie pierwiastkami ziem rzadkich, jako dobrymi kandydatami na materiały kwantowe, w ostatnich latach zrealizowano MOT dla różnych lantanowców, w tym również dla holmu [9]. Duża liczba przejść promienistych, konkurencyjnych dla przejścia chłodzącego, daje okazję do przejścia atomów do stanów metastabilnych, nie biorących udziału w chłodzeniu laserowym. Przez wiele lat fakt ten utrudniał skuteczną realizację pułapki magnetooptycznej dla atomu holmu, przez potencjalną konieczność wykorzystania wielu laserów repompujących, przenoszących atomy z powrotem do stanów biorących udział w przejściu chłodzącym. Kluczem do przezwyciężenia problemu, napotkanego dla niektórych pierwiastków ziem rzadkich, był rozwój wiedzy na temat struktury nadsubtelnej, konieczny do zaprojektowania zamkniętego cyklu chłodzącego, wykorzystującego zaledwie jedno przejście repompujące. Obecnie,

8

dla atomu holmu zaproponowane zostało 6 przejść optycznych realizujących chłodzenie drugiego stopnia w zamkniętym cyklu [9] [10]. Wydajne pułapkowanie i chłodzenie laserowe atomów holmu jest konieczne do spreparowania tego materiału kwantowego w formie kondensatu Bosego-Einsteina (ang. *Bose-Einstein condensate* - BEC), będącego niezwykle atrakcyjnym stanem materii do zastosowań w inżynierii kwantowej [11].

Pomimo dziesiątek tysięcy poziomów energetycznych, przewidywanych dla pierwiastków ziem rzadkich przez teorię kwantową atomów złożonych, do tej pory stan wiedzy na temat wartości liczbowych podstawowych parametrów opisujących elektronowe poziomy energetyczne (stałe struktury nadsubtelnej czy też czynniki g_J Landégo) jest niekompletny. Poziom podstawowy atomu holmu został po raz pierwszy opisany za pomocą parametrów takich jak stałe struktury nadsubtelnej oraz czynnik g_J Landégo przez Haberstroha, Morana oraz Penselina w 1972 roku [12]. Wyznaczone wartości liczbowe zostały następnie skorygowane w 1974 r. przez Dankworta i Fercha, którzy w obliczeniach uwzględnili teorię zaburzeń drugiego rzędu [13]. Struktura nadsubtelna nisko leżących poziomów energetycznych była następnie badana przez Livingstona i Pinningtona [14], Burghardta *et al.* [15], Childsa *et al.* [16]. Poza przytoczonymi powyżej, również prace Wyarta *et al.* [17] [18] oraz Krőger *et al.* [19] dostarczyły wielu danych na temat struktury nadsubtelnej w atomie holmu.

Rozwój technik laserowych pozwolił na zwiększenie precyzji badań struktury nadsubtelnej w szerokim zakresie spektralnym Grupa badawcza, do której przynależę, działająca w Zakładzie Inżynierii i Metrologii Kwantowej na Politechnice Poznańskiej, przez lata dostarczyła licznych wartości stałych struktury nadsubtelnej różnych pierwiastków ziem rzadkich, w tym holmu [20] [21] [22] [23]. W przytoczonych badaniach jako źródło atomów wykorzystana została lampa wyładowcza z katodą wnękową, natomiast detekcja sygnału optycznego realizowana była metodą laserowo indukowanej fluorescencji (LIF). Bardziej szczegółowy opis metodyki badawczej zawarty został w kolejnym rozdziale. Badania prowadzone w ramach przytoczonych prac były kontynuowane oraz rozwijane w ramach części dorobku naukowego składającego się na niniejszą pracę doktorską. Potencjalne zastosowania holmu w roli materiału kwantowego dla eksperymentów w dziedzinie inżynierii kwantowej stanowią motywację do prowadzenia dalszych badań, w ramach niniejszej pracy doktorskiej, nad strukturą nadsubtelną tego pierwiastka.

Przygotowywanie materiału kwantowego w pułapce magneto-optycznej opiera się o chłodzenie laserowe atomów w gradientowym polu magnetycznym, którego wartość w centrum pułapki jest zerowa. Do realizacji tej techniki konieczne jest przewidzenie rozsunięcia poziomów energetycznych, które nastąpi w zmiennym polu magnetycznym w wyniku zjawiska Zeemana. Przeprowadzenie odpowiednich obliczeń wymaga znajomości m.in. wartości czynników g_J Landégo dla poziomów energetycznych, na których oparte jest przejście chłodzące. Po wstępnym schłodzeniu atomów w MOT

konieczne jest zastosowanie chłodzenia laserowego drugiego stopnia, aby obniżyć temperaturę materiału poniżej 100 μK. W ramach badań struktury nadsubtelnej atomu holmu, szczegółowo opisanych w publikacji nr 3 przedłożonej jako część niniejszej pracy doktorskiej, zmierzone zostały podstawowe parametry takiego przejścia. Zasoby danych eksperymentalnych o wartościach czynników g_J poziomów struktury nadsubtelnej w atomie holmu, pomimo ich dużego znaczenia, są wciąż dość ubogie [24]. Główne prace traktujące na temat czynników g_J związane były z obliczeniami ich wartości za pomocą metod pół-empirycznych [21] [25] [26]. Wyniki badań przedstawione w niniejszej pracy doktorskiej stanowią znaczny wkład w stan wiedzy na temat doświadczalnych wartości tych parametrów.

Badania prowadzone w ramach niniejszej pracy skierowane są na doświadczalne wyznaczenie wielkości fizycznych charakteryzujących poziomy elektronowe atomu holmu: wartości ich energii, stałe struktury nadsubtelnej oraz czynniki Landégo g_J. Poszerzenie zakresu wiedzy na temat tych parametrów struktury nadsubtelnej umożliwia lepszy opis oddziaływań między jądrem a chmurą elektronową oraz w istotny sposób poszerza możliwości zastosowania atomów holmu w roli materiału kwantowego. Prace badawcze, prowadzone w celu pomiaru dotąd nieznanych wartości czynników Landégo g_J, pozwalają określić wpływ zewnętrznego pola magnetycznego na strukturę nadsubtelną w wyniku zjawiska Zeemana. Znajomość wartości tych parametrów jest kluczowa w procesie przypisywania poziomów energetycznych do danych konfiguracji, a także pomaga w identyfikacji lantanowców występujących w atmosferze gwiazd [27] [28].

Dostarczanie nowych i wiarygodnych danych eksperymentalnych wspomaga też dalszy rozwój wiedzy na temat struktury energetycznej atomów ziem rzadkich. Symulacje niezwykle bogatej struktury poziomów energetycznych lantanowców metodami *ab initio* są bardzo utrudnione, z powodu kolapsu funkcji falowej elektronów na powłoce $4f$, który powoduje mieszanie konfiguracji. Wykorzystanie pół-empirycznych metod obliczeniowych daje w tej sytuacji lepsze wyniki, jednak wymagają one uzupełniania danych doświadczalnych, co stanowi kolejną motywację badań prowadzonych w ramach niniejszej pracy doktorskiej.

2. Metody pomiarowe

Badania prowadzone w trakcie realizacji niniejszej pracy skoncentrowane były na rejestracji struktury nadsubtelnej linii widmowych atomu holmu za pomocą metod spektroskopii laserowej, z detekcją laserowo indukowanej fluorescencji (LIF). Źródłem atomów holmu w przeprowadzonych eksperymentach była lampa wyładowcza z katodą wnękową, natomiast źródłem światła wzbudzającego przejścia w zakresie optycznym były stabilizowane przestrajalne lasery barwnikowe o pracy ciągłej.

Wyładowanie elektryczne w gazie buforowym, spowodowane przyłożeniem pola elektrycznego o potencjale rzędu kilkuset woltów, prowadzi do odparowania atomów badanego materiału ze ścianki otaczającej otwór w katodzie wnękowej. Tak przygotowane opary są następnie wzbudzane optycznie. Światło lasera, o częstotliwości przestrajanej w sposób ciągły, przenosi badane atomy do wyższego stanu energetycznego, z którego następuje spontaniczna depopulacja wraz z emisją fluorescencji. Wzbudzony atom może zrelaksować do różnych stanów o niższej energii, dozwolonych przez reguły wyboru. Skutkuje to powstaniem kanałów fluorescencji, które można rozdzielić za pomocą urządzeń dyspersyjnych, np. monochromatora.
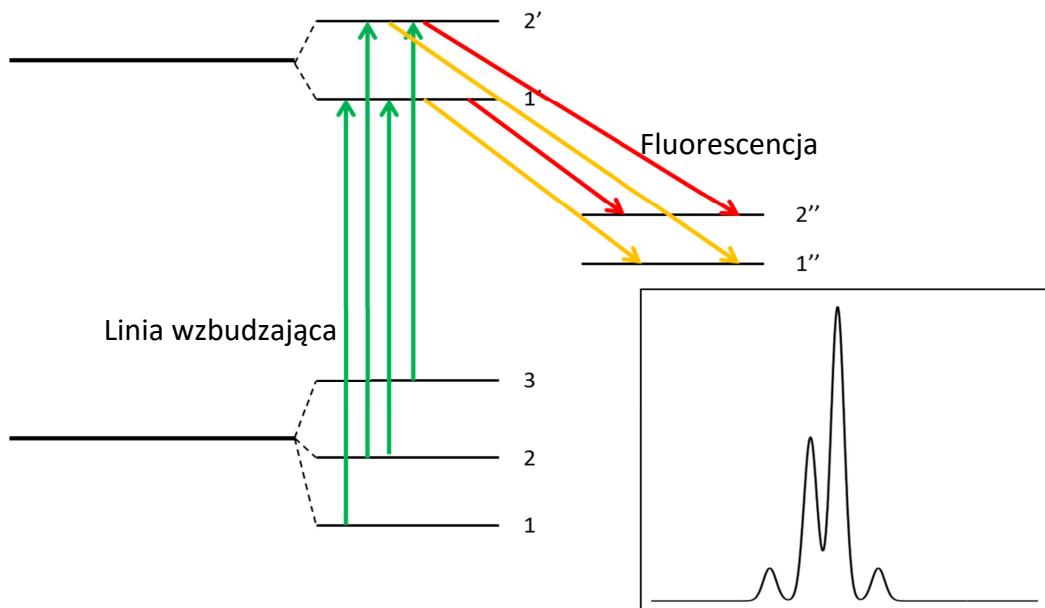
Rys. 1 Schemat poglądowy powstawania sygnału rejestrowanego metodą laserowo indukowanej fluorescencji.

Gęstość atomów holmu, w postaci odparowanej chmury wewnątrz katody wnękowej, jest zbyt mała aby analiza sygnału absorpcyjnego pozwoliła na rozpoznanie konkretnych składowych struktury nadsubtelnej. Rejestracja sygnału LIF, wraz z analizą zmiany jego natężenia, pozwala na odtworzenie linii wzbudzającej oraz określenie położenia i względnego natężenia wywoływanych przejść między podpoziomami struktury nadsubtelnej górnego i dolnego poziomu elektronowego badanej linii widmowej.

2.1. Układ eksperymentalny do badań struktury nadsubtelnej atomu holmu

Układ pomiarowy wykorzystywany podczas realizacji badań ukierunkowanych na analizę ilościową struktury nadsubtelnej atomu holmu składa się z trzech głównych części: źródła laserowego światła wzbudzającego, wraz z elementami kontrolującymi częstotliwość promieniowania oraz pracę jednomodową, źródła atomów holmu oraz układu detekcji. Schemat układu eksperymentalnego służącego do analizy struktury nadsubtelnej atomu holmu został przedstawiony na Rys. 2.
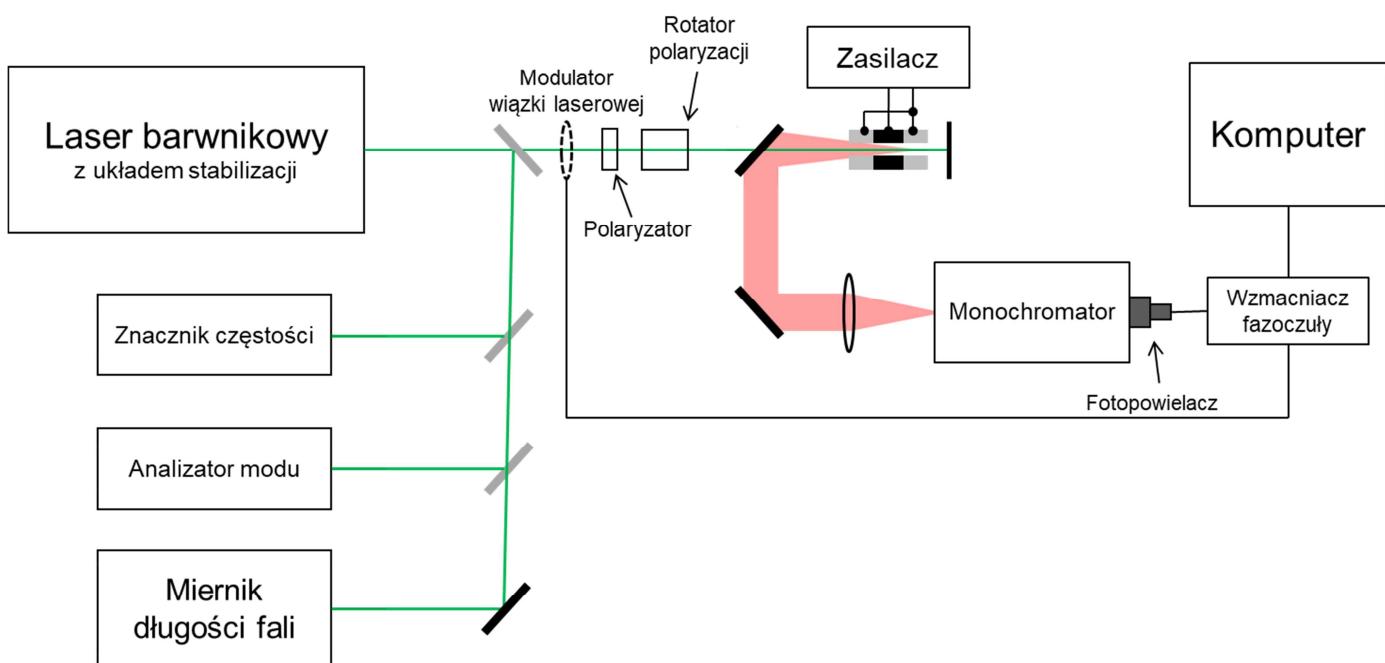
Rys. 2 Schemat blokowy układu eksperymentalnego wykorzystywanego do badania struktury nadsubtelnej atomu holmu.

Źródłem światła wzbudzającego atomy holmu są trzy stabilizowane jednomodowe przestrajalne lasery barwnikowe o pracy ciągłej pracujące przemiennie na czterech rodzajach barwnika, w zależności od badanego zakresu spektralnego. Podczas realizacji niniejszej pracy doktorskiej przeprowadzono pomiary wielu linii widmowych z zakresu od około 480 do około 670 nm. Dwa lasery wykorzystywane w prowadzonych badaniach to zmodyfikowane modele Coherent CR699–21. Pierwszy z nich generuje światło laserowe w zakresie 480-525 nm, przy pompowaniu optycznym barwnika Coumarin 498 światłem o długości fali 445 nm, generowanym przez niebieski laser diodowy. Przytoczony układ laserowy może również pracować na mieszance dwóch barwników: Coumarin 498 oraz Pyrromethene 556, pompowanej tym samym laserem diodowym. Takie rozwiązanie umożliwia generację światła laserowego z wykorzystaniem transferu energii pomiędzy dwoma barwnikami i pozwala na pokrycie zakresu około 540-

565 nm, który nie jest osiągalnym przy zastosowaniu dostępnych barwników laserowych [29].

Drugi ze zmodyfikowanych laserów Coherent CR699–21 zapewnia pracę w zakresie około 565-620 nm poprzez optyczne pompowanie barwnika Rhodamine 6G za pomocą zielonego lasera na ciele stałym Nd^{3+}:YVO_4 z podwajaniem częstości, emitującym wiązkę pompującą o długości fali 532 nm. Zakres czerwony wykorzystywany podczas badań spektroskopowych (około 625-670 nm) uzyskano poprzez zastosowanie zmodyfikowanego liniowego lasera firmy Coherent (model CR599-21) pracującego na barwniku DCM, pompowanym tym samym laserem zielonym co barwnik Rhodamine 6G.

Długość fali światła emitowanego przez laser i wzbudzającego badany materiał jest mierzona za pomocą miernika długości fali WA-1500 firmy Burleigh. W badaniach z zakresu spektroskopii laserowej istotne jest nie tylko kontrolowanie częstotliwości fali wzbudzającej przejścia w atomie, ale również utrzymywanie pracy jednomodowej źródła światła. W prowadzonych eksperymentach do monitorowania pracy jednomodowej lasera wykorzystano analizator modów oraz znacznik częstotliwości w postaci stabilizowanego interferometru Fabry-Perota o parametrze $FSR = 1500\ MHz$.
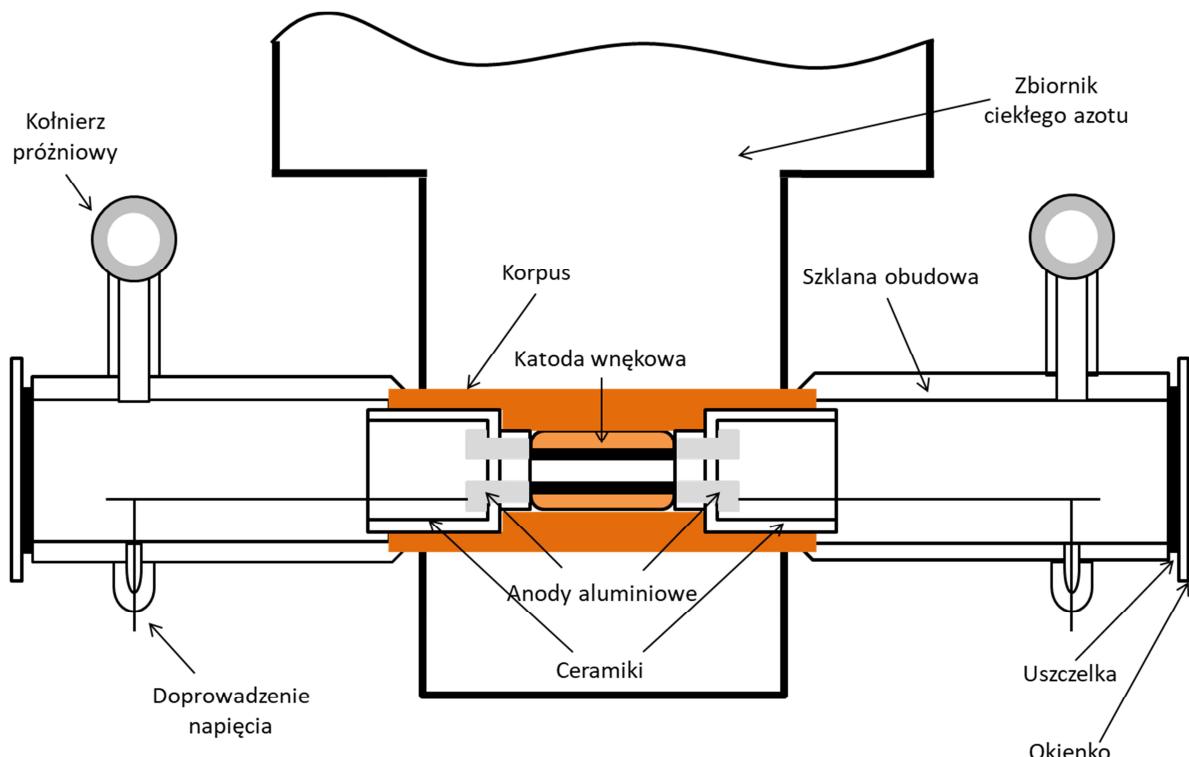
Rys. 3 Schemat lampy wyładowczej z katodą wnękową, wykorzystywaną w badaniach spektroskopowych w ramach niniejszej pracy doktorskiej.

Źródłem atomów jest lampa wyładowcza z katodą wnękową. Stabilizowany zasilacz (INCO Warszawa, typ IZS – 5/71) wytwarza wysokie napięcie, które za pośrednictwem doprowadzeń elektrycznych przekazywane jest na anody aluminiowe. Ze względu na brak kontaktu elektrycznego pomiędzy anodami, a katodą wnękową powstaje

wyładowanie, jonizując gaz buforowy, wypełniający lampę wyładowczą (w przypadku prezentowanych badań wykorzystano w tej roli argon). Powstała w ten sposób plazma argonowa pozwala na odparowanie atomów holmu z powierzchni katody, jednocześnie wzbudzając część z nich do wyższych stanów energetycznych, co znacznie poszerza zakres dostępnych stanów wzbudzonych holmu w ramach optycznego pompowania światłem laserowym w zakresie widzialnym. Stabilizacja wyładowania osiągana jest poprzez zastosowanie układu rezystorów pomiędzy zasilaczem, a lampą wyładowczą. W zależności od wymogów eksperymentu wybierana jest jedna z 4 wartości oporu balastowego: 0,77 kΩ, 1,55 kΩ, 2,35 kΩ lub 3,5 kΩ.

Natężenie prądu wyładowania w katodzie wnękowej kontrolowane jest za pomocą napięcia ustawianego na zasilaczu. Podczas początkowej fazy eksperymentu wymagane jest stosowanie wyższych napięć (powyżej 400 V), które w trakcie stabilizacji pracy lampy wyładowczej zostaje sukcesywnie redukowane do typowych wartości 220-270 V. Ze względu na ciągły przepływ prądu elektrycznego przez katodę wnękową i wynikające z niego ciepło uwalniane do układu pomiarowego lampa wyładowcza podlega stałemu chłodzeniu ciekłym azotem. Natężenie prądu wyładowania może być również modyfikowane za pośrednictwem ciśnienia gazu buforowego, które w początkowej fazie eksperymentu zmniejsza się, w wyniku ochładzania lampy ciekłym azotem, aż do ustalenia się równowagi termodynamicznej. Ciśnienie argonu wewnątrz układu pomiarowego jest stale kontrolowane i może być zwiększane poprzez zawór dozujący gaz buforowy z rezerwuaru, lub redukowane za pomocą zaworu odcinającego rotacyjną pompę próżniową. Natężenie prądu wyładowania jest podstawowym parametrem odpowiadającym za ilość atomów holmu odparowanych z katody wnękowej. W zależności od natężenia badanej linii spektralnej natężenie prądu wyładowania może być modyfikowane - standardowo utrzymywane jest w przedziale 30 – 50 mA, dla znacznej większości wykonanych pomiarów. Ciśnienie gazu buforowego dostosowywane jest do stanu wypełnienia katody wnękowej badanym materiałem. Podczas prowadzonych badań utrzymywano je w granicach 0,3 – 0,6 mbar, z typową wartością 0,45 mbar.

Aluminiowe anody w lampie z katodą wnękową umieszczone są w izolujących ceramikach wykonanych z Macoru i podobnie jak katoda są wydrążone, tak aby przepuszczać wiązkę laserową wzbudzającą optycznie atomy holmu. Przy pomiarze struktury nadsubtelnej linii spektralnych o niewielkim natężeniu fluorescencji stosowane jest zwierciadło zawracające wiązkę laserową z powrotem w kierunku chmury badanych atomów. Zabieg ten pozwala na dodatkowe wzbudzenie optyczne, przekładające się na lepszy stosunek sygnału do szumu, jednak wymaga umiejętnego poprowadzenia zawracającej wiązki laserowej tak aby nie docierała do rezonatora lasera wzbudzającego oraz nie podnosiła tła pomiarowego podczas rejestracji widma.

Układ detekcji stanowi monochromator SPM-2, firmy Carl Zeiss Jena, który rozdziela poszczególne kanały fluorescencji emitowanej przez relaksujące atomy holmu i kieruje światło na fotopowielacz Hamamatsu R-375. Ze względu na wysoką precyzję pomiarową, wymaganą przy analizie ilościowej rejestrowanej struktury nadsubtelnej, konieczne jest zwiększenie stosunku sygnału do szumu. W tym celu wykorzystywana jest technika detekcji fazoczułej, realizowana przez wzmacniacz fazoczuły (Princeton Applied Research Model 5101). Modulacja wiązki laserowej ze stałą częstotliwością, jaką zapewnia wirująca perforowana tarcza (*chopper*) pozwala na wzmocnienie składowych rejestrowanego sygnału o stałej fazie względem sygnału modulacji, ograniczając szum, którego faza jest chaotyczna.

Fotoprąd, o natężeniu proporcjonalnym do natężenia indukowanej laserowo fluorescencji, jest rejestrowany podczas przestrajania lasera barwnikowego, wzbudzającego badane atomy. Równolegle, rejestrowany jest fotoprąd indukowany w fotodiodzie znajdującej się za stabilizowanym interferometrem Fabry-Perot, który stanowi znacznik częstotliwości (tzw. „marker") w postaci wąskich, równo rozsuniętych pików, odpowiadających selektywnej transmisji wybranych częstotliwości. Odległość pomiędzy kolejnymi znacznikami markera jest stała i odpowiada FSR interferometru. Zarówno proces przestrajania częstotliwości lasera barwnikowego, jak i proces rejestracji widma fluorescencji sterowany jest za pomocą układu pomiarowego zaprojektowanego i wykonanego przez mgr inż. Patryka Gałczyka, w ramach pracy magisterskiej realizowanej w Zakładzie Inżynierii i Metrologii Kwantowej na Politechnice Poznańskiej. Układ sterujący rejestracją struktury nadsubtelnej badanych linii widmowych składa się z przetwornika analogowo-cyfrowego (MCP3204), przetwornika cyfrowo-analogowego (DAC8531) oraz mikrokontrolera (ATMEGA32). Przytoczony układ elektroniczny obsługiwany jest komputerowo za pomocą dedykowanego programu, dającego możliwość manipulacji trzema parametrami przestrajania lasera wzbudzającego: akumulacji (ilość pomiarów przypadających na jeden stopień przestrajania), czasu przestoju (czas pomiędzy podaniem napięcia wejściowego, a wykonaniem pomiaru) oraz rozdzielczości skoku (ilość skoków częstotliwości na podane napięcie wejściowe). Przez odpowiedni dobór wymienionych parametrów można poprawić jakość rejestrowanego widma, wydłużając czas skanowania częstotliwości lasera. Poza zoptymalizowaniem ilości zebranych próbek i rozdzielczości kroku skanowania konieczne jest dostosowanie stałej czasowej wzmacniacza fazoczułego do czasu rejestracji. Zbyt krótki czas całkowania wzmacnianego sygnału pogarsza stosunek sygnału do szumu, jednak wybór zbyt długiej stałej czasowej może wpłynąć na kształt rejestrowanych pików.

Wykorzystywany program pomiarowy zapisuje w dwóch oddzielnych kanałach sygnał laserowo indukowanej fluorescencji oraz sygnał markera, co pozwala na kontrolę liniowego przestrajania długości fali światła laserowego. Każda nieliniowa zmiana częstotliwości światła wzbudzającego jest niepożądana i może wpłynąć na późniejszą

analizę ilościową parametrów struktury nadsubtelnej. Niekontrolowany przeskok częstotliwości lasera ujawnia się w widmie markera, poprzez zmianę odległości między sąsiednimi maksimami, zapobiegając włączeniu do dalszej analizy zniekształconych pomiarów.

Przedstawiony układ doświadczalny wykorzystano w takiej samej formie we wszystkich badaniach spektroskopowych struktury nadsubtelnej, których wyniki zostały włączone do niniejszej pracy doktorskiej. Pewne modyfikacje, które zostaną omówione w dalszej części tego rozdziału, zostają wprowadzone w badaniach ukierunkowanych na pomiar czynników g_J Landégo.

2.2.   Pomiary stałych struktury nadsubtelnej atomu holmu

Zarejestrowany sygnał przedstawia układ pików reprezentujących przejścia pomiędzy poszczególnymi poziomami struktury nadsubtelnej atomu. Struktura nadsubtelna atomu powstaje w wyniku oddziaływania momentu magnetycznego jądra atomu z momentem magnetycznym chmury atomowej. Poziom energetyczny atomu opisany momentem pędu J rozszczepia się na podpoziomy o całkowitym momencie pędu opisanym liczbą kwantową F:

$$F = J + I, J + I - 1, \ldots, |J - I|, \tag{1}$$

gdzie I jest momentem pędu jadra atomowego. Ilość podpoziomów struktury nadsubtelnej dla danego poziomu energetycznego wynosi $2I + 1$, jeśli $J \geq I$, lub $2J + 1$ w odmiennym przypadku. Holm charakteryzuje się wartością momentu pędu jądra atomowego $I = 7/2$, zazwyczaj mniejszą niż moment pędu chmury elektronowej, dlatego dla większości poziomów energetycznych spodziewane jest obserwowanie rozszczepienia na osiem podpoziomów struktury nadsubtelnej. Ich przesunięcie zależy od stałych struktury nadsubtelnej magnetycznej dipolowej A oraz elektrycznej kwadrupolowej B i opisane jest wzorem:

$$E_{hfs} = h \left(\frac{K}{2} A + \frac{3K(K+1) - I(I+1)\,J(J+1)}{8I(2I-1)\,J(2J-1)} B \right) = h \left(\alpha A + \beta B \right), \tag{2}$$

gdzie h jest stałą Plancka, natomiast $K = F(F+1) - J(J+1) - I(I+1)$ [30].

Na Rys. 4 widnieje przykład zarejestrowanej linii spektralnej w atomie holmu, wraz z zapisem sygnału znacznika częstotliwości. Osiem głównych składowych widocznych na widmie odpowiada przejściom między podpoziomami struktury nadsubtelnej poziomów górnego i dolnego, o takich wartościach liczby F, że $\Delta F = \Delta J$, natomiast składowe o mniejszym natężeniu odpowiadają pozostałym przejściom dopuszczanym przez regułę wyboru dla liczby kwantowej F. Znając położenie składowych linii spektralnych na skali częstotliwościowej można obliczyć wartości stałych struktury

nadsubtelnej A i B. Zapisane podczas przeprowadzania eksperymentu widmo zostaje poddane analizie ilościowej za pomocą programu „Fitter" [31].
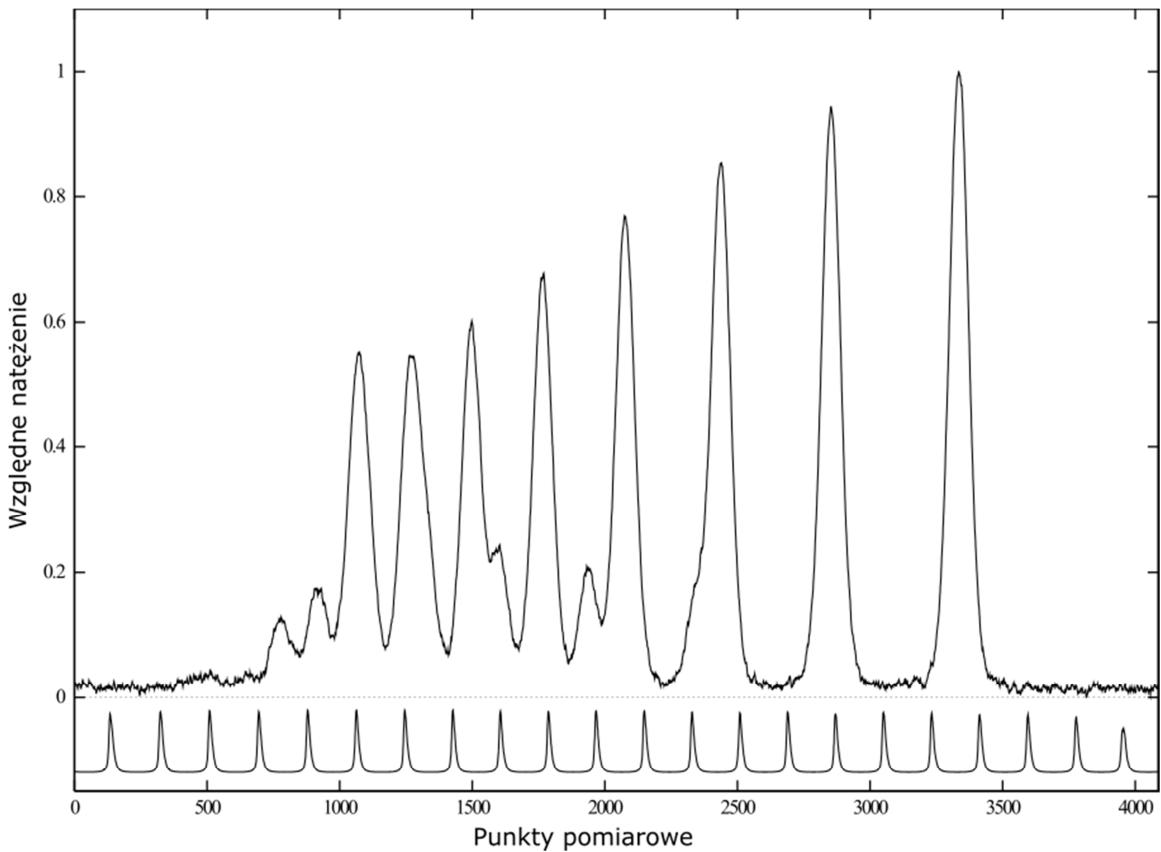
Rys. 4 Przykład zarejestrowanej linii spektralnej 19952,86 cm^{-1} (pomiędzy poziomami E = 20493,77 cm^{-1}, J = 13/2 i E = 40446,63 cm^{-1}, J = 15/2), wraz z sygnałem znacznika częstotliwości. Obraz pochodzi z programu "Fitter".

W pierwszym kroku zostaje utworzona skala częstotliwości, odpowiadająca mierzonemu skanowi, na podstawie wartości FSR interferometru oraz odległości między zarejestrowanymi maksimami interferencyjnymi. Następnie algorytm programu pozwala na dopasowanie krzywej teoretycznej do zapisanego sygnału poprzez iteracyjną optymalizację parametrów takich jak stałe struktury nadsubtelnej dolnego poziomu energetycznego oraz górnego poziomu elektronowego. Krzywa teoretyczna powstaje przez sumowanie składowych, z których każda może być odwzorowana przez profil Gaussa, Lorentza lub Voita. Położenia i natężenia składowych są obliczane na podstawie wzorów (2) i (3).

$$\nu = \nu_{cg} + \alpha_o A_o + \beta_o B_o - \alpha_u A_u - \beta_u B_u, \qquad (3)$$

gdzie ν_{cg} jest położeniem środka ciężkości struktury nadsubtelnej linii widmowej na skali częstotliwości, a α i β są stałymi z równania (1) dla poziomu górnego (o) i dolnego (u).

W przypadku mocno zaszumionych linii można powiązać wzajemnie wartości natężenia linii i dopasowywać je za pomocą jednego parametru. Jednak, ze względu na zjawisko nasycenia, zazwyczaj takie powiązanie można stosować tylko w przypadku grup

składowych o tej samej wartości ΔF. Najdokładniejsze wyniki można uzyskać w sytuacji, w której stałe A i B dla jednego z poziomów pomiędzy którymi zachodzi przejście są znane, a jedynymi dopasowywanymi parametrami są stałe drugiego z poziomów. Przykład krzywej teoretycznej dopasowanej do skanu eksperymentalnego, poprzez optymalizację stałych struktury nadsubtelnej poziomu górnego 40446,63 cm^{-1}, $J = 15/2$, przy parametrach znanych dla poziomu dolnego 20493,77 cm^{-1}, $J = 13/2$, przedstawiony został na Rys. 5. Pomimo zastosowania metody detekcji fazoczułej, dla dużej grupy badanych linii spektralnych stosunek sygnału do szumu w dalszym ciągu jest niewystarczający do przeprowadzenia optymalnego dopasowania wartość stałych A i B. Zwłaszcza składowe odpowiadające przejściom, dla których $\Delta F = \Delta J$ mogą pozostawać na poziomie szumu dla pojedynczego pomiaru. Z tego powodu, w trakcie przeprowadzania eksperymentu kilkunastokrotnie rejestrowane są te same linie spektralne, przy tych samych warunkach doświadczalnych. Zabieg ten pozwala na zwiększenie stosunku sygnału do szumu poprzez uśrednianie poszczególnych widm, a także pozwala na zebranie próby statystycznej zoptymalizowanych wartości stałych struktury nadsubtelnej, które dla poszczególnych skanów mogą różnić się między sobą.
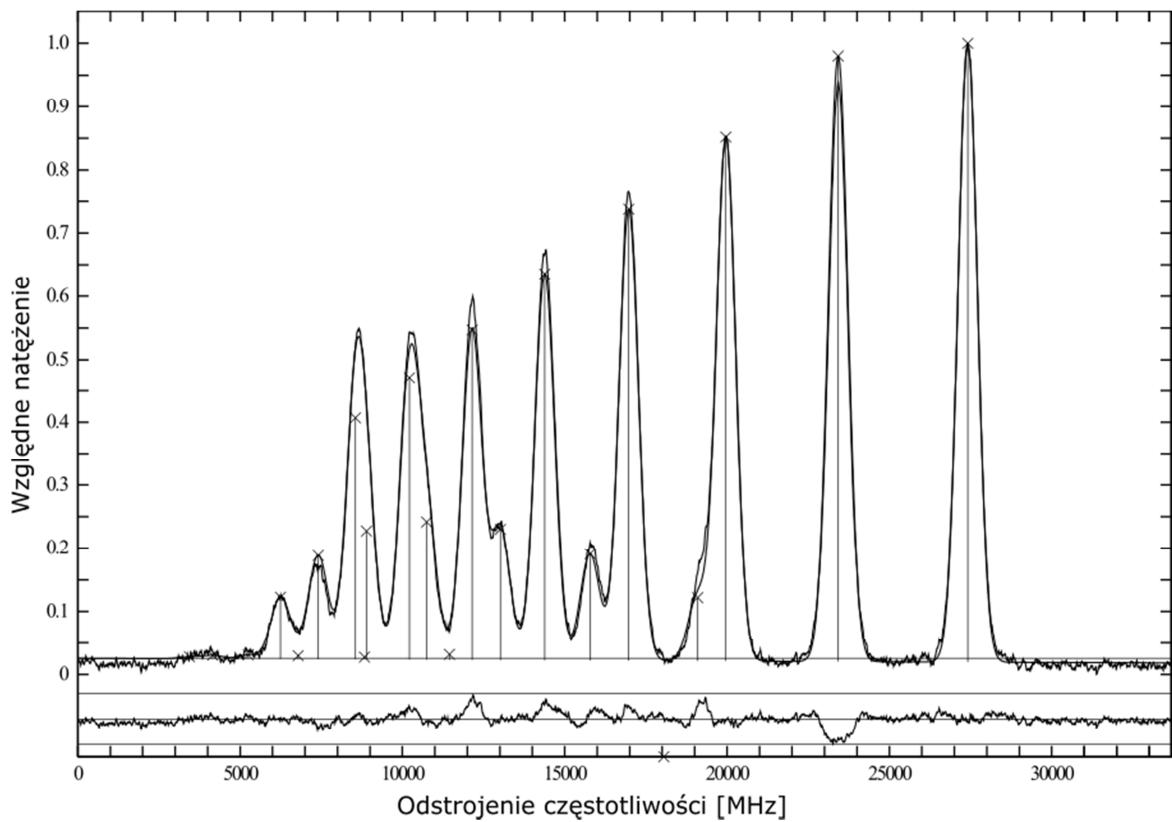
Rys. 5 Linia 19952,86 cm^{-1} zarejestrowana podczas eksperymentu, wraz z dopasowaną krzywą przy optymalnych wartościach stałych struktury nadsubtelnej. Obraz z programu "Fitter".

2.3. Pomiar czynników g_J Landégo

Zewnętrzne pole magnetyczne znosi degenerację poziomów energetycznych atomu ze względu na magnetyczną liczbę kwantową m_F. Zjawisko to, dla pól magnetycznych o natężeniu mniejszym niż wewnętrzne pole atomu, nosi nazwę efektu Zeemana. Stan atomu opisany całkowitym momentem pędu F ulega rozszczepieniu na $2F + 1$ podpoziomów zeemanowskich. W obserwowanym widmie linii spektralnej objawia się to rozdzieleniem poszczególnych składowych, które jest proporcjonalne do indukcji zewnętrznego pola magnetycznego oraz wartości czynników g_J Landégo obydwu poziomów, pomiędzy którymi zachodzi przejście promieniste. Przejścia promieniste pomiędzy poszczególnymi poziomami zeemanowskimi, oprócz reguł wyboru dla przejść dipolowych, muszą spełniać również reguły wyboru związane z polaryzacją. Światło laserowe spolaryzowane liniowo, w kierunku równoległym do linii pola magnetycznego może wywołać przejścia pomiędzy poziomami o tej samej magnetycznej liczbie kwantowej - $\Delta m_F = 0$ (polaryzacja π), natomiast przy polaryzacji prostopadłej do indukcji magnetycznej dopuszczalne są przejścia $\Delta m_F = \pm 1$ (polaryzacja σ). W zależności od przygotowanej polaryzacji światła wzbudzającego obserwowane są różne kształty widma. Przykład struktury nadsubtelnej linii widmowej, w obecności pola magnetycznego, zarejestrowanej przy obydwu polaryzacjach został przedstawiony na Rys. 6.

W celu przeprowadzenia badań struktury nadsubtelnej atomu holmu zmodyfikowanej poprzez efekt Zeemana w zewnętrznym polu magnetycznym konieczne było dokonanie modyfikacji w układzie pomiarowym opisanym w rozdziale 2.1. Pole magnetyczne było wytwarzane w eksperymencie za pomocą jednego z dwóch układów sztabkowych magnesów neodymowych. Pierwszy układ dwóch magnesów umieszczony jest bezpośrednio nad katodą wnękową i wytwarza w jej wnętrzu pole magnetyczne o indukcji około 500-600 G. W drugiej konfiguracji pojedyncze sztabki silniejszych magnesów neodymowych umieszczone są równolegle po dwóch stronach katody wnękowej, wytwarzając bardziej jednorodne pole o indukcji w przedziale 1900-2000 G. Pomimo, że układ magnesów w drugiej konfiguracji zapewnia kilkukrotnie silniejsze pole magnetyczne, a przez to bardziej wyraźne rozszczepienie struktury nadsubtelnej na składowe zeemanowskie, większość pomiarów spektroskopowych została przeprowadzona z wykorzystaniem magnesów ustawionych w pierwszej konfiguracji. Było to podyktowane efektem ubocznym umieszczenia źródła atomów w obecności silniejszego zewnętrznego pola magnetycznego, który wyraźnie ograniczał czas prowadzenia eksperymentu w sposób ciągły. Chmura atomów holmu w silniejszym polu magnetycznym ulegała odchyleniu, przez co warstwa metalu osadzała się na ceramikach izolujących katodę wnękową od anod, do których doprowadzane było wysokie napięcie, tworząc zwarcie elektryczne. Wskazane zjawisko w znacznym stopniu ograniczało czas prowadzenia badań, przez co zrezygnowano z korzystania z silniejszego

zestawu magnesów. Jak wykazano podczas prowadzenia badań w ramach niniejszej pracy doktorskiej rozszczepienie zeemanowskie wywołane polem magnetycznym o indukcji rzędu 500 G jest wystarczające do wyznaczenia wartości czynników g_J Landégo, na podstawie zarejestrowanych linii spektralnych.

Dodatkową niezbędną modyfikacją, względem układu doświadczalnego stosowanego w pomiarach stałych struktury nadsubtelnej w atomie holmu bez obecności pola magnetycznego, jest wprowadzenie polaryzatora liniowego oraz rotatora polaryzacji przed wejściem wiązki laserowej do lampy wyładowczej z katodą wnękową. Wykorzystanie rotatora polaryzacji pozwala na zmianę pomiędzy polaryzacjami π i σ bez dodatkowych strat mocy optycznej.

Widma zarejestrowane przy wiązce laserowej spolaryzowanej w kierunkach prostopadłym i równoległym do linii zewnętrznego pola magnetycznego były wyposażane w skalę częstotliwości za pomocą programu „Fitter", w analogiczny sposób jak skany linii spektralnych wykorzystywanych do pomiaru stałych struktury nadsubtelnej. Do przeprowadzenia obliczeń wartości czynników g_J wykorzystany został program przygotowany w tym celu przez członków grupy badawczej z Zakładu Inżynierii i Metrologii Kwantowej (dr hab. Bogusław Furmann, prof. PP) oraz Zakładu Robotyki (dr hab. Jarosław Ruczkowski, prof. PP) Politechniki Poznańskiej.

W pierwszym kroku program obliczeniowy dokonuje diagonalizacji hamiltonianu, wyrażonego równaniem 4, opisującego energię atomu holmu w zewnętrznym polu magnetycznym, wyznaczając energie podpoziomów zeemanowskich poziomu górnego oraz dolnego. Informacje, takie jak natężenie zewnętrznego pola magnetycznego, moment pędu jadra atomowego oraz chmury elektronowej, czy wartości stałych struktury nadsubtelnej dla poziomów F i F', jak również początkowe wartości czynników g_J Landégo zostają wprowadzone na początku obliczeń. Na podstawie danych wejściowych program wyznacza stany własne oraz wektory własne, co bezpośrednio przekłada się na określenie pozycji poszczególnych składowych zeemanowskich widma na skali częstotliwości. W kolejnym etapie obliczeń wyznaczona jest funkcja rozkładu natężenia, która następnie za pomocą algorytmu Marquardta jest dopasowywana w sposób iteracyjny do zarejestrowanej eksperymentalnie linii widmowej w celu obliczenia wartości czynnika g_J. Podobnie jak w procedurze obliczania stałych struktury nadsubtelnej optymalne warunki obliczeniowe uzyskuje się kiedy czynnik g_J dla jednej z poziomów energetycznych, dolnego lub górnego, jest znany z literatury.

$$H_{FM,F'M} = \delta_{FF'} \left(A\,\frac{C}{2} + B\,\frac{\frac{3}{4}C(C+1)-I(I+1)J(J+1)}{2I(2I+1)J(2J+1)} \right) + \mu_B g_J H_{mag}(-1)^D \sqrt{(2F+1)(2F'+1)J(J+1)(2J+1)} \times E, (4)$$

gdzie μ_B jest magnetonem Bohra, $C = F(F+1) - J(J+1) - I(I+1)$, $D = F - M_F + J + I + F' + 1$ natomiast $E = \begin{pmatrix} F & 1 & F' \\ -M_F & 0 & M_F \end{pmatrix} \begin{Bmatrix} F & 1 & F' \\ J & I & J \end{Bmatrix}$.
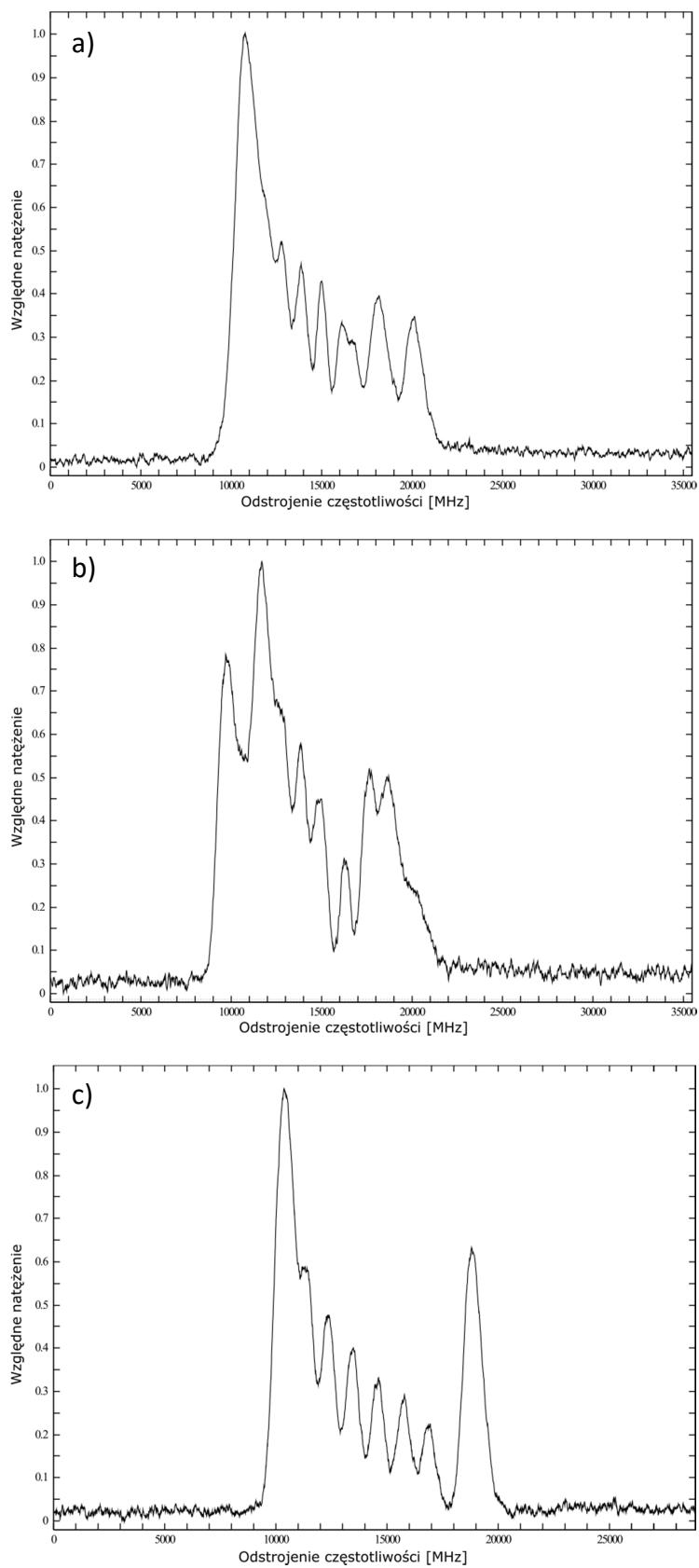
Rys. 6 Zarejestrowana linia 19281,49 cm^{-1} widoczna: a) w zewnętrznym polu magnetycznym, przy polaryzacji π, b) w zewnętrznym polu magnetycznym przy polaryzacji σ, c) bez zewnętrznego pola magnetycznego.

Istotnym warunkiem uzyskania prawidłowych wartości czynników g_J jest dobór wartości startowej. Algorytm zakłada, że wartość początkowa nie odbiega mocno od wartości docelowej. Jeżeli tak nie jest, to należy dokonać ponownej diagonalizacji z nową wartością startową. W obliczeniach stosowano zazwyczaj wartości startowe wynikające z dopasowania pół-empirycznego struktury subtelnej.

Ponadto, do wyznaczenia poprawnych wartości czynników g_J Landégo konieczna jest znajomość faktycznej wartości indukcji magnetycznej wewnątrz katody wnękowej. W celu kalibracji pola magnetycznego w przeprowadzonych badaniach wykorzystano linie spektralne gazu buforowego – argonu, dla których znane były literaturowe wartości czynników g_J obydwu poziomów energetycznych. Wykorzystując opisaną powyżej procedurę można obliczyć wartość indukcji magnetycznej, która następnie zostanie wykorzystana do obliczeń dla atomu holmu. Ze względu na istniejącą niejednorodność pola magnetycznego wewnątrz katody wnękowej pomiary kalibracyjne na liniach argonu wykonywane są dla różnych zakresów spektralnych, ponieważ dyspersja elementów optycznych wpływa na kierunek biegu wiązki laserowej podczas zmiany długości fali światła, a co za tym idzie również na miejsce w którym wzbudzane są atomy. Pomiar kalibracyjny przeprowadzany jest dla obydwu polaryzacji, ponieważ wiązki o polaryzacji π i σ ulegają nieznacznie innemu załamaniu podczas wprowadzaniu do lampy wyładowczej. Z tego powodu przy obydwu pomiarach można spodziewać się wzbudzenia atomów przy różnych polach magnetycznych. Podczas procedury obliczeniowej mającej na celu wyznaczenie wartości czynników g_J dla danej linii spektralnej przyjmowane są oddzielne wartości indukcji magnetycznej dla obydwu polaryzacji. Dodatkowym czynnikiem jaki należy uwzględnić jest fluktuacja pola magnetycznego powodowana niewielkimi ruchami układu magnesów zanurzonych w zbiorniku z ciekłym azotem, spowodowanych wrzeniem zawartości zbiornika. Na podstawie przeprowadzonych pomiarów oszacowano poziom zmian pola magnetycznego, spowodowanych wrzeniem ciekłego azotu, na około 2% wartości indukcji magnetycznej i przełożono je na dodatkowy składnik niepewności pomiarowej.

Podobnie jak w przypadku procedury obliczeniowej stałych struktury nadsubtelnej A i B prowadzone są wielokrotne zapisy badanych linii spektralnych, w celu poprawy stosunku sygnału do szumu. Wyznaczone wartości czynników g_J Landégo są uśredniane, a głównym przyczynkiem do niepewności pomiarowej jest odchylenie standardowe średniej arytmetycznej oraz niepewność znanej wartości czynnika g_J dla drugiego z poziomów biorących udział w przejściu promienistym.

3. Identyfikacja nowych poziomów energetycznych w atomie holmu

Trzecim aspektem, na który położony został nacisk podczas realizacji niniejszej pracy doktorskiej, jest poszerzenie wiedzy na temat struktury nadsubtelnej atomu holmu, poprzez identyfikację nieznanych dotąd poziomów energetycznych. Do przeprowadzenia badań w tym zakresie również wykorzystana została technika spektroskopii laserowej w katodzie wnękowej, z detekcją metodą *LIF*. Układ eksperymentalny jest tym samym, który wykorzystany został podczas badań ukierunkowanych na wyznaczenie stałych struktury nadsubtelnej znanych poziomów energetycznych.

Metodę poszukiwania nowych poziomów w strukturze nadsubtelnej atomu holmu, wykorzystaną w niniejszych badaniach, oparto o analizę dostępnych niesklasyfikowanych linii widmowych widocznych w widmie fourierowskim, udostępnionym dla bliskiego ultrafioletu oraz zakresu widzialnego [32] [33]. Przygotowany plik wejściowy zawiera zestawienie poziomów energetycznych należących do konfiguracji nieparzystych oraz parzystych, wraz z ich wartościami liczby kwantowej *J*, a także zestawienie linii widmowych w atomie holmu. Za pomocą dedykowanego programu, rozwiniętego w ramach działania grupy eksperymentalnej Zakładu Inżynierii i Metrologii Kwantowej, poszukiwane są koincydencje między sumą wartości liczb falowych linii widmowych oraz wartości energii znanych poziomów energetycznych, traktowanych jako poziomy dolne w zarejestrowanym przejściu spektralnym. Jeśli sumy wartości energetycznych dla przynajmniej dwóch kombinacji liczb falowych i poziomów dolnych są ze sobą zgodne (przy spełnieniu reguł wyboru dla przejść dipolowych) można założyć istnienie hipotetycznego, nieznanego dotąd, poziomu elektronowego. Następnie, program wykorzystywany przy badaniach stałych struktury nadsubtelnej generuje plik wyjściowy, w którym zawarte są wszystkie przejścia z założonego poziomu górnego, dozwolone przez reguły wyboru, które stanowią potencjalne kanały fluorescencji. W wygenerowanej liście przejść spektralnych są wzięte pod uwagę zarówno niesklasyfikowane linie widmowe jak i przejścia sklasyfikowane, dla których uwzględnione zostały wartości energii obydwu poziomów struktury nadsubtelnej oraz względne natężenie linii. Wykorzystany program przygotowuje listę kanałów fluorescencji z uwzględnieniem ustawienia monochromatora wykorzystywanego w eksperymencie.

Weryfikacja doświadczalna postawionej hipotezy polega na próbach rejestracji struktury nadsubtelnej niesklasyfikowanej linii widmowej w kilku przewidywanych kanałach fluorescencji. Podczas skanowania częstotliwości światła wzbudzającego wokół nominalnej wartości przejścia zapisywana jest jej wartość na początku skanu. Metodą *LIF* rejestrowany jest sygnał w kanałach fluorescencji, przewidywanych dla hipotetycznego poziomu górnego. Obserwacja niesklasyfikowanej linii spektralnej w przynajmniej kilku

różnych kanałach fluorescencji pozwala na wstępne potwierdzenie jego istnienia. Rejestracja badanej linii spektralnej przy odpowiednim stosunku sygnału do szumu pozwala na dodatkową analizę ilościową stałych struktury nadsubtelnej nowego poziomu energetycznego. Otrzymanie zbieżnych wyników obliczeń dla kilku niezależnych linii spektralnych stanowi dodatkowy argument potwierdzający założoną hipotezę. Rejestracja niesklasyfikowanych linii widmowych w dodatkowych kanałach fluorescencji, zbyt słabych aby pozwolić na obliczenie stałych A i B badanego poziomu, dostarcza dodatkowych informacji do analizy jakościowej, co pomaga w poprawnej weryfikacji postawionej hipotezy.

Dostępne widma fourierowskie w zakresie bliskiego ultrafioletu oraz zakresu widzialnego dla atomu holmu pozwalają na włączenie do przeprowadzonej analizy jakościowej dodatkowych niesklasyfikowanych linii spektralnych, których nie udało się zaobserwować w przeprowadzonym eksperymencie. Widmo Fouriera jest również bardzo istotne w procesie weryfikacji ostatecznej wartości energii nowych poziomów elektronowych w atomie holmu, poprzez porównanie przewidywanych wartości liczb falowych badanych linii spektralnych (definiowanych jako różnice pomiędzy hipotetyczną energią poziomu górnego oraz znanego poziomu dolnego), z ich wartościami zmierzonymi eksperymentalnie. Część linii spektralnych, rejestrowanych podczas badań doświadczalnych, posiada zbyt małą intensywność, aby włączyć je do procesu wyznaczania wartości energii nowych poziomów elektronowych. W takiej sytuacji wykorzystane zostają wybrane fragmenty widma fourierowskiego do określenia rzeczywistej wartości energii poziomu górnego w tego typu przejściach. Do wycięcia fragmentu widma wokół analizowanej linii spektralnej służy inny program, również rozwinięty w ramach działalności grupy badawczej Zakładu Inżynierii i Metrologii Kwantowej. Wyselekcjonowany fragment spektrum, o szerokości 1-2 cm^{-1}, zostaje zlinearyzowany przez ten sam program na podstawie informacji o rozdzielczości dostępnego widma fourierowskiego i wygenerowane zostają pliki wyjściowe w formacie wykorzystywanym przy analizie ilościowej struktury nadsubtelnej. Za pomocą programu „*Fitter*" wyznaczane jest przesunięcie środka ciężkości struktury nadsubtelnej nierejestrowanej linii spektralnej, względem hipotetycznej wartości energii poziomu górnego. Zabieg ten pozwala na uzupełnienie wyników uzyskanych na drodze eksperymentu w katodzie wnękowej i dokładniejsze wyznaczenie energii nowych poziomów.

Część hipotetycznych poziomów elektronowych w atomie holmu, których istnienie postulowane jest w ramach niniejszej pracy doktorskiej, nie spełnia wszystkich kryteriów wymaganych do ostatecznego potwierdzenia. Jest to spowodowane zbyt małą ilością kanałów fluorescencji zarejestrowanych podczas prowadzenia badań, lub widocznych w dostępnym widmie Fouriera, czy też zbyt dużą rozbieżnością wartości energii wśród zarejestrowanych linii wzbudzających dany poziom elektronowy. Przytoczone wątpliwości dotyczą dwóch poziomów konfiguracji nieparzystych, a także trzech

poziomów konfiguracji parzystych. Ich istnienie jest prawdopodobne, ale wymaga dodatkowej weryfikacji.

Na podstawie przeprowadzonych badań spektroskopowych potwierdzono istnienie oraz zidentyfikowano 62 poziomy energetyczne w strukturze nadsubtelnej atomu holmu: 54 konfiguracji nieparzystych oraz 8 konfiguracji parzystych, które nie były znane do tej pory. Dla wszystkich przytoczonych nowych poziomów elektronowych wyznaczono również stałe struktury nadsubtelnej oraz liczby kwantowe J.

4. Wykaz prac wchodzących w skład rozprawy doktorskiej

1. B. Furmann, D. Stefańska, M. Suski, S. Wilman, **M. Chomski**, ,,Hyperfine structure studies of the odd-parity electronic levels of the holmium atom. I: Levels with known energies", *Journal of Quantitative Spectroscopy & Radiative Transfer*, 2019, vol. 234, str. 115-123.

W niniejszej pracy badano stałe struktury nadsubtelnej A i B dla 43 poziomów elektronowych konfiguracji nieparzystych atomu holmu. Na podstawie analizy wyników uzyskanych dla 66 linii spektralnych metodą laserowo indukowanej fluorescencji, w lampie wyładowczej z katodą wnękową. Wartości stałych struktury nadsubtelnej, uzyskane dla 27 badanych poziomów energetycznych zostały wyznaczone po raz pierwszy w sposób doświadczalny. Dla 4 poziomów energetycznych skorygowane zostały liczby kwantowe J, względem dostępnych danych literaturowych. Jako dodatkowy element badań wyznaczono dokładniejsze wartości stałych struktury nadsubtelnej dla 3 poziomów konfiguracji parzystych, wykorzystywanych jako znane dolne poziomy w wybranych rejestrowanych liniach spektralnych. Dwa z tych poziomów cechują się liczbą kwantową $J = 17/2$ i mogłyby być wykorzystane jako poziomy górne przy drugim stopniu chłodzenia laserowego atomów holmu w pułapce magnetooptycznej. Opublikowane dane doświadczalne zostały wykorzystane w pół-empirycznej analizie struktury subtelnej i nadsubtelnej poziomów elektronowych atomu holmu, należących do konfiguracji nieparzystych, prowadzonych w naszej grupie badawczej.

2. B. Furmann, D. Stefańska, S. Wilman, **M. Chomski**, M. Suski, ,,Hyperfine structure studies of the odd-parity electronic levels in the holmium atom, II: New levels", *Journal of Quantitative Spectroscopy and Radiative Transfer*, 2019, vol. 235, str. 70–80.

Niniejsza praca skupia się na analizie niesklasyfikowanych linii spektralnych, w widmie atomu holmu, ukierunkowanej na identyfikację nieznanych do tej pory poziomów energetycznych i określeniu ich struktury nadsubtelnej. Na podstawie analizy ilościowej 113 niesklasyfikowanych linii spektralnych w atomie holmu, metodą laserowo indukowanej fluorescencji w lampie wyładowczej z katodą wnękową, zidentyfikowano 35 nieznanych dotąd poziomów elektronowych konfiguracji nieparzystych. Dla wszystkich zidentyfikowanych poziomów elektronowych wyznaczone zostały wartości stałych struktury nadsubtelnej. Nowo wyznaczone energie poziomów energetycznych pozwoliły na sklasyfikowanie 256 linii spektralnych w widmie atomu holmu, zarówno zarejestrowanych poprzez bezpośrednie wzbudzenie, jak i obserwowanych jako kanały fluorescencji. Opublikowane dane doświadczalne zostały wykorzystane w pół-empirycznej analizie struktury subtelnej i nadsubtelnej poziomów elektronowych atomu holmu, należących do konfiguracji nieparzystych, prowadzonych w naszej grupie badawczej.

3. D. Stefańska, B. Furmann, J. Ruczkowski, M. Elantkowska, P. Głowacki, **M. Chomski**, M. Suski, S. Wilman, ,,Investigations of the possible second-stage laser cooling transitions for the holmium atom magneto-optical trap", *Journal of Quantitative Spectroscopy and Radiative Transfer*, 2020, vol. 246 (106915).

Badania spektroskopowe, przeprowadzone w ramach niniejszej pracy, koncentrują się na opisie poziomów elektronowych w atomie holmu, które mogą zostać wykorzystane w chłodzeniu laserowym drugiego stopnia w pułapce magnetooptycznej. Przeanalizowano 5 przejść spektralnych z poziomu podstawowego na poziomy konfiguracji parzystych o liczbach kwantowych $J = 17/2$ oraz wyznaczono dla tych poziomów energetycznych wartości czynników g_J Landégo. Dodatkowo, zweryfikowane zostały wartości stałych struktury nadsubtelnej A i B badanych poziomów elektronowych, a także w ramach przeprowadzonych badań poprawiona została dokładność potwierdzonych wyników. Przeprowadzono również wstępną analizę pół-empiryczną czasów życia wybranych poziomów energetycznych w strukturze nadsubtelnej atomu holmu.

4. **M. Chomski**, B. Furmann, J. Ruczkowski, M. Suski, D. Stefańska, ,,Landé g$_J$ factors of the electronic levels of the holmium atom", *Journal of Quantitative Spectroscopy and Radiative Transfer*, 2021, vol. 274 (107865).

Niniejsza praca była ukierunkowana na pomiar czynników g_J Landégo dla poziomów energetycznych w atomie holmu. Badania prowadzone były metodą spektroskopii laserowej w lampie wyładowczej z katodą wnękową, umieszczoną w stałym zewnętrznym polu magnetycznym, oraz detekcją metodą laserowo indukowanej fluorescencji. Analiza rozszczepienia struktury nadsubtelnej badanych poziomów elektronowych, obserwowanego dla 69 linii spektralnych w wyniku działania efektu Zeemana, pozwoliła na wyznaczenie nieznanych dotąd doświadczalnych wartości czynników g_J dla 15 poziomów energetycznych konfiguracji nieparzystych i 18 poziomów należących do konfiguracji parzystych. Przeprowadzone badania pozwoliły również zweryfikować wartości literaturowe czynników g_J Landégo dla 6 poziomów energetycznych.

5. **M. Chomski**, M. Suski, S. Wilman, B. Furmann, J. Ruczkowski, D. Stefańska, ,,Landé g$_J$ factors of odd-parity electronic levels of the holmium atom", *Journal of Quantitative Spectroscopy and Radiative Transfer*, 2022, vol. 279 (108045).

Niniejsza praca zawiera wyniki doświadczalne czynników g_J Landégo dla 18 poziomów elektronowych w atomie holmu. Badania były oparte o rejestrację rozszczepienia Zeemana struktury nadsubtelnej metodą laserowo indukowanej fluorescencji w lampie wyładowczej z katodą wnękową, umieszczonej w stałym polu magnetycznym. Wyniki uzyskane na podstawie analizy rozszczepionej struktury nadsubtelnej 33 linii spektralnych pozwoliły na wyznaczenie nieznanych dotąd wartości czynników g_J

dla 12 poziomów energetycznych konfiguracji nieparzystych oraz jednego poziomu konfiguracji parzystej.

6. **M. Chomski**, B. Furmann, M. Suski, P. Głowacki, D. Stefańska, S. Mieloch, ,,Determination of the energies of new electronic levels of the holmium atom and investigation of their hyperfine structure'', *Journal of Quantitative Spectroscopy and Radiative Transfer*, 2023, vol. 297 (108480).

Niniejsza praca skoncentrowana była na analizę niesklasyfikowanych linii spektralnych w atomie holmu, w celu identyfikacji poziomów elektronowych o nieznanej dotąd wartości energii. Dane doświadczalne otrzymano metodą spektroskopii laserowej w lampie wyładowczej z katodą wnękową. Detekcja oparta była o metodę laserowo indukowanej fluorescencji. Analiza zarejestrowanych w sposób eksperymentalny 79 linii spektralnych, wraz z wybranymi niesklasyfikowanymi liniami widocznymi w widmie Fouriera oraz obserwowanymi kanałami fluorescencji pozwoliła na identyfikację 27 poziomów elektronowych w atomie holmu, dla których dotychczas nie były znane wartości energii. Dodatkowo, obliczone zostały nieznane dotąd wartości stałych struktury nadsubtelnej dla 31 poziomów elektronowych, w tym dla wszystkich nowo zidentyfikowanych poziomów.

Pozostałe publikacje współautorskie, niewchodzące w skład rozprawy doktorskiej

1. B. Furmann, D. Stefańska, **M. Chomski**, M. Suski, S. Wilman, ,,Hyperfine structure studies of the odd-parity electronic levels of the terbium atom'', *Journal of Quantitative Spectroscopy and Radiative Transfer*, 2019, vol. 237, 106613.

2. B. Furmann, **M. Chomski**, M. Suski, S. Wilman, D. Stefańska, ,,Investigations of the hyperfine structure and isotope shifts in the even-parity level system of atomic europium'', *Journal of Quantitative Spectroscopy and Radiative Transfer*, 2020, 251, 107070.

3. B. Furmann, J. Ruczkowski. **M. Chomski**, M. Suski, S. Wilman, D. Stefańska, ,,Landé gJ factors of the electronic levels of the europium atom'', *Journal of Quantitative Spectroscopy and Radiative Transfer*, 2020, 255, 107258.

4. P. Głowacki, D. Stefańska, J. Ruczkowski, M. Elantkowska, **M. Chomski**, B. Furmann, ,,Hyperfine structure investigations of Mn I'', *Journal of Quantitative Spectroscopy and Radiative Transfer*, 2022, 287, 108245.

5. M. Suski, **M. Chomski**, B. Furmann, J. Ruczkowski, D. Stefańska, ,,Landé gJ factors of even-parity electronic levels of the terbium atom", *Journal of Quantitative Spectroscopy and Radiative Transfer*, 2022, 288, 108270.

6. M. Suski, B. Furmann, **M. Chomski,** J. Ruczkowski, D. Stefańska, S. Mieloch, ,,Landé gJ factors of the odd-parity electronic levels of the terbium atom determined by laser spectroscopy", *Journal of Quantitative Spectroscopy and Radiative Transfer*, 2022, 291, 108342.

7. M. Suski, B. Furmann, **M. Chomski**, S. Mieloch, P. Głowacki, D. Stefańska, ,,Hyperfine structure investigations of the odd-parity electronic levels of the terbium atom", *Journal of Quantitative Spectroscopy and Radiative Transfer*, 2023, 298, 108492.

5. Wnioski

W ramach niniejszej pracy doktorskiej, na którą przedłożone zostało 6 spójnych tematycznie publikacji, przedstawione zostały wyniki badań doświadczalnych skoncentrowanych na identyfikacji nieznanych dotąd poziomów elektronowych w strukturze nadsubtelnej atomu holmu, a także wyznaczeniu doświadczalnym wartości ich parametrów charakterystycznych: energii, stałych struktury nadsubtelnej A i B oraz czynników Landégo g_J. Metodą badawczą wykorzystaną we wszystkich pracach składających się na niniejszą rozprawę doktorską jest spektroskopia laserowa z detekcją metodą laserowo indukowanej fluorescencji w lampie wyładowczej z katodą wnękową.

Na podstawie analizy niesklasyfikowanych linii spektralnych, zawartych w dostępnych widmach fourierowskich dla atomu holmu, dokonano identyfikacji 54 poziomów energetycznych konfiguracji nieparzystych oraz 8 poziomów konfiguracji parzystych. Dla wszystkich potwierdzonych doświadczalnie poziomów elektronowych wyznaczone zostały wartości energii, wartości stałych struktury nadsubtelnej A i B oraz określono liczby kwantowe J. Dodatkowo, na podstawie wyników uzyskanych dla nowych poziomów energetycznych wyznaczono wartości stałych A i B dla dwóch poziomów należących do konfiguracji nieparzystych, których energie były znane w literaturze, ale nie posiadały doświadczalnych danych na temat stałych struktury nadsubtelnej. W ramach badań ukierunkowanych na identyfikację energii nowych poziomów elektronowych udało się dodatkowo skorygować wartość dipolowej stałej magnetycznej A dla poziomu konfiguracji parzystej $E = 8427{,}11$ cm^{-1}, $J = 15/2$, która została błędnie zapisana w jednej z wcześniejszych publikacji na temat struktury nadsubtelnej atomu holmu [21].

W ramach analizy ilościowej znanych poziomów struktury nadsubtelnej wyznaczono nieznane dotąd eksperymentalne wartości magnetycznej stałej dipolowej A oraz elektrycznej stałej kwadrupolowej dla 27 poziomów konfiguracji nieparzystych w atomie holmu oraz zweryfikowano dane dla 16 poziomów, dla których dostępne były wartości literaturowe. Dla 3 poziomów elektronowych konfiguracji parzystych wyniki uzyskane w ramach niniejszej pracy doktorskiej są dokładniejsze niż w przypadku danych literaturowych. Dwa z wymienionych poziomów: $E = 8378{,}91$ cm^{-1}, $J = 17/2$ i $E = 20568{,}63$ cm^{-1}, $J = 17/2$ mogą potencjalnie stanowić poziom górny w chłodzeniu laserowym drugiego stopnia, realizowanym w pułapce magnetooptycznej. Przeprowadzone badania pozwalają na skorygowanie wartości liczby kantowej J dla 4 poziomów energetycznych konfiguracji nieparzystych. Poziom $E = 37426{,}02$ cm^{-1} był opisany w literaturze liczbą kwantową $J = 17/2$, jednak na podstawie analizy 5 linii spektralnych na ten poziom można określić jej prawidłową wartość jako $J = 15/2$. Na podstawie analizy jakościowej 2 linii spektralnych wzbudzających poziom $E = 37426{,}02$ cm^{-1} dokonano sugestii korekty liczby kwantowej J z wartości

literaturowej 13/2 na 11/2. Zaproponowana zmiana została podyktowana układem niediagonalnych składowych struktury nadsubtelnej widocznym w zarejestrowanych liniach jako pojedyncza grupa, co nie zgadza się z literaturową wartością liczby J. Na podstawie analogicznej analizy jakościowej pojedynczych linii spektralnych zasugerowano korektę liczby $J = 11/2$ na wartość 13/2 dla poziomu $E = 30589{,}44$ cm^{-1} oraz zmianę z $J = 19/2$ na $J = 17/2$ dla poziomu $E = 36677{,}81$ cm^{-1}.

Badania rozszczepienia Zeemana struktury nadsubtelnej atomu holmu zaowocowały dostarczeniem licznych danych doświadczalnych na temat czynników g_J Landégo. Dostępne dane literaturowe w tej tematyce są niezwykle ubogie, co w połączeniu z możliwym wykorzystaniem atomów holmu w roli materiału kwantowego przygotowywanego w pułapkach magnetooptycznych, stanowiło motywację do rozszerzenia badań struktury nadsubtelnej holmu o ten aspekt. W ramach niniejszej pracy doktorskiej wyznaczono 62 wartości czynników g_J Landégo, dla 34 poziomów konfiguracji nieparzystych i 28 poziomów konfiguracji parzystych. Dla 51 poziomów energetycznych będących obiektem badań spektroskopowych przedstawione wyniki są pierwszymi zmierzonymi w sposób doświadczalny. Pięć poziomów energetycznych konfiguracji parzystych, dla których po raz pierwszy wyznaczono wartości czynników g_J Landégo, zostało zasugerowanych pod kątem realizacji przejść chłodzących drugiego stopnia, o wąskim spektrum linii widmowej.

Pomimo ograniczeń związanych z wykorzystaniem silniejszego zestawu magnesów neodymowych, który powoduje osadzenie się materiału metalicznego na izolujących ceramikach i w efekcie zerwanie wyładowania poprzez zwarcie obwodu, uzyskane wyniki czynników Landégo mogą zostać uznane za wiarygodne. Rezultaty obliczeń uzyskane na podstawie tych samych linii spektralnych, rejestrowanych w obecności silniejszego i słabszego pola magnetycznego są zbieżne, co potwierdza, że zewnętrzne pole magnetyczne o wartości indukcji rzędu 500 G jest wystarczające do analizy ilościowej rozszczepienia Zeemana struktury nadsubtelnej atomu holmu.

W ramach cyklu sześciu publikacji, składającego się na niniejszą pracę doktorską, zidentyfikowano 62 poziomy elektronowe w atomie holmu. Na podstawie analizy niesklasyfikowanych linii spektralnych wyznaczono doświadczalne wartości parametrów charakteryzujących nowe poziomy w strukturze energetycznej, takie jak wartości ich energii, liczby kwantowe J oraz stałe struktury nadsubtelnej. Łącznie opublikowano nieznane dotąd wartości doświadczalne stałych struktury nadsubtelnej oraz wartości czynników g_J Landégo dla, kolejno 89 i 51 poziomów elektronowych atomu holmu. W ramach prowadzonych prac badawczych zweryfikowane zostały również wartości dla wybranych poziomów energetycznych, które posiadały zgłoszone wartości literaturowe.

Wyniki zawarte w przedłożonych publikacjach stanowią znaczne uzupełnienie danych doświadczalnych dla struktury nadsubtelnej atomu holmu. Pierwiastek ten

w ostatnich latach zyskuje na znaczeniu jako materiał kwantowy, o licznych zastosowaniach w dziedzinie przetwarzania informacji kwantowej, a także inżynierii i metrologii kwantowej. Z punktu widzenia tych zastosowań bardzo istotna jest rozwinięta wiedza na temat struktury nadsubtelnej wykorzystywanego pierwiastka oraz szeroka baza danych doświadczalnych wartości parametrów charakteryzujących poziomy elektronowe. Holm, ze względu na wyjątkowe właściwości magnetyczne, rozpatrywany jest również jako klasyczny nośnik ultra-gęstej pamięci magnetycznej. Dostarczone w ramach niniejszej pracy doktorskiej dane eksperymentalne mogą przyczynić się do dalszego wykorzystania holmu w roli materiału kwantowego do zastosowań technologicznych.

34

Bibliografia

[1]   D. R. Lide (ed.), CRC Handbook of Chemistry and Physics, Internet version 2005, CRC Press, Boca Raton, FL, 2005, https://www.academia.edu/download/63428029/CRC.Press.Handbook.of.Chemistry.and.Physics.85th.ed.eBook-LRN20200526-31167-1jwr0zm.pdf (dostęp z dnia 18.01.2023).

[2]   C. K. Gupta and N. Krishnamurthy, Extractive metallurgy of rare earths, CRC Press, 2004.

[3]   J. Emsley, *Nature's Building Blocks: An A-Z Guide to the Elements*, Oxford University Press, 2011, pp. 224-226.

[4]   R. P. MacDonald, "Uses for a Holmium Oxide Filter in Spectrophotometry", *Clinical Chemistry, vol. 10(12),* p. 1117–1120, 1964, DOI: https://doi.org/10.1093/clinchem/10.12.1117.

[5]   F. Natterer, K. Yang, W. Paul, *et. al.*, "Reading and writing single-atom magnets", *Nature 543,* pp. 226-228, 2017, DOI: https://doi.org/10.1038/nature21371.

[6]   F. Natterer, F. Donati, F. Patthey and H. Brune, "Thermal and Magnetic-Field Stability of Holmium Single-Atom Magnets", *Phys. Rev. Lett. 121, 027201,* 2018, DOI: https://doi.org/10.1103/PhysRevLett.121.027201.

[7]   P. R. Forrester, F. Patthey, E. Fernandes, D. P. Sblendorio, H. Brune and F. Natterer, "Quantum state manipulation of single atom magnets using the hyperfine interaction", *Phys. Rev. B 100, 180405(R),* 2019, DOI: https://doi.org/10.1103/PhysRevB.100.180405.

[8]   M. Saffman and K. Mølmer, "Scaling the neutral-atom Rydberg gate quantum computer by collective encoding in holmium atoms", *Phys. Rev. A 78, 012336,* 2008, DOI: https://doi.org/10.1103/PhysRevA.78.012336.

[9]   J. Miao, J. Hostetter, G. Stratis and M. Saffman, "Magneto-optical trapping of holmium atoms", *Phys. Rev. A 89, 041401(R),* 2014, DOI: https://doi.org/10.1103/PhysRevA.89.041401.

[10]   J. J. McClelland and J. L. Hanssen, "Laser Cooling without Repumping: A Magneto-Optical Trap for Erbium Atoms", *Phys. Rev. Lett. 96, 143005,* 2006, DOI: https://doi.org/10.1103/PhysRevLett.96.143005.

[11]   J. Hostetter, J. D. Pritchard, J. E. Lawler and M. Saffman, "Measurement of holmium Rydberg series through magneto-optical trap depletion spectroscopy", *Phys. Rev. A 91, 012507,* 2015, DOI: https://doi.org/10.1103/PhysRevA.91.012507.

[12] R. A. Haberstroh, T. I. Moran and S. Penselin, "Direct measurement of the nuclear magnetic dipole moment of Ho-165 with the atomic beam magnetic resonance method", *Zeitschrift für Physik, vol. 252,* p. 421–427, 1972, DOI: https://doi.org/10.1007/BF01379735.

[13] W. Dankwort and J. Ferch, "Reevaluation of the atomic gJ factor and the nuclear gJ factor of 165-Ho", *Z. Physik, vol. 267,* p. 239–241, 1974, DOI: 10.1007/BF01669226.

[14] A. E. Livingston and E. H. Pinnington, "Spectra of Neutral and Singly Ionized Holmium", *J. Opt. Soc. Am. vol. 61(10),* 1971, DOI: https://doi.org/10.1364/JOSA.61.1429_1.

[15] B. Burghardt, S. Buttgenbach, N. Glaeser, R. Harzer, G. Meisel, B. Roski and F. Traber, "Hyperfine structure measurements in metastable states of 165-Ho", *Zeitschrift fur Physik A Atoms and Nuclei 307 (3),* 1982, DOI: https://doi.org/10.1007/BF01438640.

[16] W. J. Childs, D. R. Cok and L. S. Goodman, "New line classifications in Ho I based on high-precision hyperfine-structure measurement of low levels", *J. Opt. Soc. Am. vol. 73 (2),* 1983, DOI: https://doi.org/10.1364/JOSA.73.000151.

[17] J. F. Wyart, P. Camus and J. Vergès, "Etude du spectre de l'holmium atomique: I. Spectre d'emission infrarouge niveaux d'émission infrarouge niveaux d'énergie de Ho I et structures hyperfines", *Physica B+C, vol. 92 (3),* 1977, DOI: https://doi.org/10.1016/0378-4363(77)90137-1.

[18] J. F. Wyart and P. Camus, "Etude du spectre de l'holmium atomique: II. Interprétation paramétrique des niveaux d'énergie et des structures hyperfines", *Physica B+C, vol. 93 (2),* 1978, DOI: https://doi.org/10.1016/0378-4363(78)90129-8.

[19] S. Kroger, J. F. Wyart and P. Luc, "Theoretical interpretation of hyperfine structures in doubly-excited configurations $4f^{10}5d6s6p$ and $4f^{10}5d^{2}6s$ and new energy levels in neutral holmium (Ho I)", *Physica Scripta 55 (579),* 1997, DOI: 10.1088/0031-8949/55/5/010.

[20] D. Stefańska and B. Furmann, "Hyperfine structure investigations for the odd-parity configuration system in atomic holmium", *Journal of Quantitative Spectroscopy and Radiative Transfer, vol. 206,* pp. 286-295, 2018, DOI: https://doi.org/10.1016/j.jqsrt.2017.11.019.

[21] D. Stefańska, J. Ruczkowski, M. Elantkowska and B. Furmann, "Fine- and hyperfine structure investigations of the even-parity configuration system of the atomic holmium", *Journal of Quantitative Spectroscopy and Radiative Transfer, vol. 209,* pp. 180-195, 2018, DOI: 10.1016/j.jqsrt.2018.01.010.

[22] D. Stefańska, B. Furmann and P. Głowacki, "Possibilities of investigations of the temporal variation of the α constant in the holmium atom", *Journal of Quantitative Spectroscopy and Radiative Transfer, vol. 213,* pp. 159-168, 2018,

DOI: https://doi.org/10.1016/j.jqsrt.2018.04.017.

[23] B. Furmann, D. Stefańska, M. Suski and S. Wilman, "Identification of new electronic levels in the holmium atom and investigation of their hyperfine structure", *Journal of Quantitative Spectroscopy & Radiative Transfer, vol. 219,* pp. 117-126, 2018,
DOI: https://doi.org/10.1016/j.jqsrt.2018.08.005.

[24] A. Kramida, Y. Ralchenko, J. Reader and NIST ASD Team, "NIST Atomic Spectra Database (ver. 5.10), [Online]", National Institute of Standards and Technology, Gaithersburg, 2023. [Online]. Available: https://physics.nist.gov/asd.

[25] H. Li, J. F. Wyart, O. Delieu and M. Lepers, "Anisotropic optical trapping as a manifestation of the complex electronic structure of ultracold lanthanide atoms: The example of holmium", *Phys. Rev. A 95, 062508,* 2017, DOI: https://doi.org/10.1103/PhysRevA.95.062508.

[26] M. Elantkowska, J. Ruczkowski, A. Sikorski and S. Wilman, "Fine- and hyperfine structure investigations of the odd-parity configuration system in atomic holmium", *Journal of Quantitative Spectroscopy and Radiative Transfer, vol. 237, 106642,* 2019,
DOI: https://doi.org/10.1016/j.jqsrt.2019.106642.

[27] C. Sneden and J. J. Cowan, "Genesis of the heaviest elements in the Milky Way Galaxy", *Science 299 (5603),* 2003, DOI: 10.1126/science.1077506.

[28] J. E. Lawler *et. al.*, "Improved Atomic Data for Ho II and New Holmium Abundances for the Sun and Three Metal-poor Stars", *ApJ 604 (850),* 2004, DOI: 10.1086/382068.

[29] D. Stefańska, M. Suski, A. Zygmunt, J. Stachera and B. Furmann, "Tunable single-mode cw energy-transfer dye laser directly optically pumped by a diode laser", *Optics & Laser Technology, vol. 120, 105673,* 2019, DOI: https://doi.org/10.1016/j.optlastec.2019.105673.

[30] I. I. Sobelman, Atomic Spectra and Radiative Transitions, New York: Springer-Verlag Berlin Heidelberg, 1979.

[31] G. Guthohrlein, *Fitter program,* Helmut Schmidt University Hamburg, 2004.

[32] N. Al-Labady *et. al.*, "Line Identification of Atomic and Ionic Spectra of Holmium in the Near-UV. Part I. Spectrum of Ho I", *The Astrophysical Journal Supplement Series, vol. 228 (16),* 2017, DOI: 10.3847/1538-4365/228/2/16.

[33] B. Özdalgiç *et. al.,* "Line Identification of Atomic and Ionic Spectra of Holmium in the Visible Spectral Range. I. Spectrum of Ho I", *The Astrophysical Journal Supplement Series, vol. 240 (27),* 2019, DOI: 10.3847/1538-4365/aaf9b2.

Załączniki

Poznań, 26.06.2023r.

mgr inż. Maciej Chomski
Instytut Badań Materiałowych i Inżynierii Kwantowej,
Wydział Inżynierii Materiałowej i Fizyki Technicznej,
Politechnika Poznańska
ul. Piotrowo 3
60-965 Poznań
e-mail: maciej.s.chomski@doctorate.put.poznan.pl, **tel.** +48 61 665 3229

Oświadczenie współautora artykułów naukowych

Oświadczam, że jestem współautorem następujących prac, składanych jako spójny tematycznie cykl publikacji naukowych w ramach mojej pracy doktorskiej:

1. B. Furmann, D. Stefańska, M. Suski, S. Wilman, M. Chomski, ,,*Hyperfine structure studies of the odd-parity electronic levels of the holmium atom. I: Levels with known energies*", Journal of Quantitative Spectroscopy & Radiative Transfer, 2019, vol. 234, str. 115-123.
2. B. Furmann, D. Stefańska, S. Wilman, M. Chomski, M. Suski, ,,*Hyperfine structure studies of the odd-parity electronic levels in the holmium atom, II: New levels*", Journal of Quantitative Spectroscopy and Radiative Transfer, 2019, vol. 235, str. 70–80.
3. D. Stefańska, B. Furmann, J. Ruczkowski, M. Elantkowska, P. Głowacki, M. Chomski, M. Suski, S. Wilman, ,,*Investigations of the possible second-stage laser cooling transitions for the holmium atom magneto-optical trap*", Journal of Quantitative Spectroscopy and Radiative Transfer, 2020, vol. 246 (106915).
4. M. Chomski, B. Furmann, J. Ruczkowski, M. Suski, D. Stefańska, ,,*Landé g_J factors of the electronic levels of the holmium atom*", Journal of Quantitative Spectroscopy and Radiative Transfer, 2021, vol. 274 (107865).
5. M. Chomski, M. Suski, S. Wilman, B. Furmann, J. Ruczkowski, D. Stefańska, ,,*Landé g_J factors of odd-parity electronic levels of the holmium atom*", Journal of Quantitative Spectroscopy and Radiative Transfer, 2022, vol. 279 (108045).
6. M. Chomski, B. Furmann, M. Suski, P. Głowacki, D. Stefańska, S. Mieloch, ,,*Determination of the energies of new electronic levels of the holmium atom and investigation of their hyperfine structure*", Journal of Quantitative Spectroscopy and Radiative Transfer, 2023, vol. 297 (108480).

Mój udział w niniejszych pracach polegał na:

Ad. 1 Pomocy w przygotowaniu układu pomiarowego, udziale w badaniach, pomocy w opracowaniu wyników prac badawczych.

Ad. 2 Pomocy w przygotowaniu układu pomiarowego, udziale w badaniach, pomocy w opracowaniu wyników prac badawczych.

Ad. 3 Pomocy w przygotowaniu układu pomiarowego, udziale w badaniach, pomocy w opracowaniu wyników prac badawczych.

Ad. 4 Opracowaniu wyników badań, przygotowaniu układu pomiarowego, udziale w pracach badawczych, redakcji manuskryptu oraz przygotowaniu odpowiedzi dla recenzentów.

Ad. 5 Opracowaniu oraz walidacji wyników badań, udziale w analizie formalnej, przygotowaniu układu pomiarowego, udziale w pracach badawczych, redakcji manuskryptu oraz przygotowaniu odpowiedzi dla recenzentów.

Ad. 6 Opracowaniu oraz walidacji wyników badań, udziale w analizie formalnej, przygotowaniu układu pomiarowego, udziale w pracach badawczych, redakcji manuskryptu oraz przygotowaniu odpowiedzi dla recenzentów.

Maciej Chomski

(podpis współautora)

Poznań, 26.06.2023r.

mgr inż. Sebastian Wilman
Instytut Badań Materiałowych i Inżynierii Kwantowej,
Wydział Inżynierii Materiałowej i Fizyki Technicznej,
Politechnika Poznańska
ul. Piotrowo 3
60-965 Poznań
e-mail: sebastian.b.wilman@doctorate.put.poznan.pl, tel. +48 61 665 3229

Oświadczenie współautora artykułów naukowych

Oświadczam, że opublikowałem z mgr. inż. Maciejem Chomskim następujące prace:

1. B. Furmann, D. Stefańska, M. Suski, S. Wilman, M. Chomski, „*Hyperfine structure studies of the odd-parity electronic levels of the holmium atom. I: Levels with known energies*", Journal of Quantitative Spectroscopy & Radiative Transfer, 2019, vol. 234, str. 115-123.
2. B. Furmann, D. Stefańska, S. Wilman, M. Chomski, M. Suski, „*Hyperfine structure studies of the odd-parity electronic levels in the holmium atom, II: New levels*", Journal of Quantitative Spectroscopy and Radiative Transfer, 2019, vol. 235, str. 70–80.
3. D. Stefańska, B. Furmann, J. Ruczkowski, M. Elantkowska, P. Głowacki, M. Chomski, M. Suski, S. Wilman, „*Investigations of the possible second-stage laser cooling transitions for the holmium atom magneto-optical trap*", Journal of Quantitative Spectroscopy and Radiative Transfer, 2020, vol. 246 (106915).
4. M. Chomski, M. Suski, S. Wilman, B. Furmann, J. Ruczkowski, D. Stefańska, „*Landé g_J factors of odd-parity electronic levels of the holmium atom*", Journal of Quantitative Spectroscopy and Radiative Transfer, 2022, vol. 279 (108045).

Mój udział w niniejszych pracach polegał na:

Ad. 1 Pomocy w przygotowaniu układu pomiarowego, udziale w badaniach, pomocy w opracowaniu wyników prac badawczych.

Ad. 2 Pomocy w przygotowaniu układu pomiarowego, udziale w badaniach, pomocy w opracowaniu wyników prac badawczych.

Ad. 3 Pomocy w przygotowaniu układu pomiarowego oraz udziale w badaniach.

Ad. 4 Udziale w pracach badawczych, pomocy w opracowaniu wyników prac badawczych oraz zebraniu funduszy.

Wyrażam zgodę na przedłożenie wyżej wymienionych prac przez mgr. inż. Macieja Chomskiego jako części rozprawy doktorskiej w formie spójnego tematycznie zbioru artykułów naukowych.

(podpis współautora)

Poznań, 26.06.2023r.

mgr inż. Marcin Suski
Instytut Badań Materiałowych i Inżynierii Kwantowej,
Wydział Inżynierii Materiałowej i Fizyki Technicznej,
Politechnika Poznańska
ul. Piotrowo 3
60-965 Poznań
e-mail: marcin.j.suski@doctorate.put.poznan.pl, **tel.** +48 61 665 3229

Oświadczenie współautora artykułów naukowych

Oświadczam, że opublikowałem z mgr. inż. Maciejem Chomskim następujące prace:

1. B. Furmann, D. Stefańska, M. Suski, S. Wilman, M. Chomski, *„Hyperfine structure studies of the odd-parity electronic levels of the holmium atom. I: Levels with known energies"*, Journal of Quantitative Spectroscopy & Radiative Transfer, 2019, vol. 234, str. 115-123.

2. B. Furmann, D. Stefańska, S. Wilman, M. Chomski, M. Suski, *„Hyperfine structure studies of the odd-parity electronic levels in the holmium atom, II: New levels"*, Journal of Quantitative Spectroscopy and Radiative Transfer, 2019, vol. 235, str. 70–80.

3. D. Stefańska, B. Furmann, J. Ruczkowski, M. Elantkowska, P. Głowacki, M. Chomski, M. Suski, S. Wilman, *„Investigations of the possible second-stage laser cooling transitions for the holmium atom magneto-optical trap"*, Journal of Quantitative Spectroscopy and Radiative Transfer, 2020, vol. 246 (106915).

4. M. Chomski, B. Furmann, J. Ruczkowski, M. Suski, D. Stefańska, *„Landé g_J factors of the electronic levels of the holmium atom"*, Journal of Quantitative Spectroscopy and Radiative Transfer, 2021, vol. 274 (107865).

5. M. Chomski, M. Suski, S. Wilman, B. Furmann, J. Ruczkowski, D. Stefańska, *„Landé g_J factors of odd-parity electronic levels of the holmium atom"*, Journal of Quantitative Spectroscopy and Radiative Transfer, 2022, vol. 279 (108045).

6. M. Chomski, B. Furmann, M. Suski, P. Głowacki, D. Stefańska, S. Mieloch, *„Determination of the energies of new electronic levels of the holmium atom and investigation of their hyperfine structure"*, Journal of Quantitative Spectroscopy and Radiative Transfer, 2023, vol. 297 (108480).

Mój udział w niniejszych pracach polegał na:

Ad. 1 Pomocy w przygotowaniu układu pomiarowego, udziale w badaniach, pomocy w opracowaniu wyników prac badawczych.

Ad. 2 Pomocy w przygotowaniu układu pomiarowego, udziale w badaniach, pomocy w opracowaniu wyników prac badawczych.

Ad. 3 Pomocy w przygotowaniu układu pomiarowego oraz udziale w badaniach.

Ad. 4 Udziale w pracach badawczych, pomocy w opracowaniu wyników prac badawczych.

Ad. 5 Udziale w pracach badawczych, pomocy w opracowaniu wyników prac badawczych.

Ad. 6 Udziale w pracach badawczych, pomocy w opracowaniu wyników prac badawczych.

Wyrażam zgodę na przedłożenie wyżej wymienionych prac przez mgr. inż. Macieja Chomskiego jako części rozprawy doktorskiej w formie spójnego tematycznie zbioru artykułów naukowych.

....
(podpis współautora)

Poznań, 26.06.2023r.

dr hab. Bogusław Furmann, prof. PP
Instytut Badań Materiałowych i Inżynierii Kwantowej,
Wydział Inżynierii Materiałowej i Fizyki Technicznej,
Politechnika Poznańska
ul. Piotrowo 3
60-965 Poznań
e-mail: boguslaw.furmann@put.poznan.pl, **tel.** +48 61 665 3226

Oświadczenie współautora artykułów naukowych

Oświadczam, że opublikowałem z mgr. inż. Maciejem Chomskim następujące prace:

1. B. Furmann, D. Stefańska, M. Suski, S. Wilman, M. Chomski, *„Hyperfine structure studies of the odd-parity electronic levels of the holmium atom. I: Levels with known energies"*, Journal of Quantitative Spectroscopy & Radiative Transfer, 2019, vol. 234, str. 115-123.
2. B. Furmann, D. Stefańska, S. Wilman, M. Chomski, M. Suski, *„Hyperfine structure studies of the odd-parity electronic levels in the holmium atom, II: New levels"*, Journal of Quantitative Spectroscopy and Radiative Transfer, 2019, vol. 235, str. 70–80.
3. D. Stefańska, B. Furmann, J. Ruczkowski, M. Elantkowska, P. Głowacki, M. Chomski, M. Suski, S. Wilman, *„Investigations of the possible second-stage laser cooling transitions for the holmium atom magneto-optical trap"*, Journal of Quantitative Spectroscopy and Radiative Transfer, 2020, vol. 246 (106915).
4. M. Chomski, B. Furmann, J. Ruczkowski, M. Suski, D. Stefańska, *„Landé g_J factors of the electronic levels of the holmium atom"*, Journal of Quantitative Spectroscopy and Radiative Transfer, 2021, vol. 274 (107865).
5. M. Chomski, M. Suski, S. Wilman, B. Furmann, J. Ruczkowski, D. Stefańska, *„Landé g_J factors of odd-parity electronic levels of the holmium atom"*, Journal of Quantitative Spectroscopy and Radiative Transfer, 2022, vol. 279 (108045).
6. M. Chomski, B. Furmann, M. Suski, P. Głowacki, D. Stefańska, S. Mieloch, *„Determination of the energies of new electronic levels of the holmium atom and investigation of their hyperfine structure"*, Journal of Quantitative Spectroscopy and Radiative Transfer, 2023, vol. 297 (108480).

Mój udział w niniejszych pracach polegał na:

Ad. 1 Określeniu metodologii, konceptualizacji prac badawczych, nadzorowaniu oraz udziale w badaniach, opracowaniu i walidacji wyników prac badawczych, analizie formalnej, zgromadzeniu funduszy, redakcji manuskryptu oraz przygotowaniu odpowiedzi dla recenzentów.

Ad. 2 Określeniu metodologii, konceptualizacji prac badawczych, nadzorowaniu oraz udziale w badaniach, opracowaniu i walidacji wyników prac badawczych, analizie formalnej, zgromadzeniu funduszy, redakcji manuskryptu oraz przygotowaniu odpowiedzi dla recenzentów.

Ad. 3 Pomocy w określeniu metodologii oraz konceptualizacji prac badawczych, nadzorowaniu oraz udziale w badaniach, udziale w opracowaniu i walidacji wyników prac badawczych, pomocy w analizie formalnej, przygotowaniu oprogramowania oraz zgromadzeniu funduszy.

Ad. 4 Pomocy w opracowaniu wyników badań oraz analizie formalnej, udziale w pracach badawczych, przygotowaniu oprogramowania, zgromadzeniu funduszy oraz pomocy w redakcji manuskryptu.

Ad. 5 Pomocy w opracowaniu wyników badań oraz analizie formalnej, udziale w pracach badawczych, przygotowaniu oprogramowania oraz pomocy w redakcji manuskryptu.

Ad. 6 Określeniu metodologii, konceptualizacji prac badawczych, pomocy w opracowaniu wyników badań oraz analizie formalnej, udziale w pracach badawczych, zgromadzeniu funduszy oraz pomocy w redakcji manuskryptu.

Wyrażam zgodę na przedłożenie wyżej wymienionych prac przez mgr. inż. Macieja Chomskiego jako części rozprawy doktorskiej w formie spójnego tematycznie zbioru artykułów naukowych.

(podpis współautora)

Poznań, 26.06.2023r.

dr hab. Danuta Stefańska
Instytut Badań Materiałowych i Inżynierii Kwantowej,
Wydział Inżynierii Materiałowej i Fizyki Technicznej,
Politechnika Poznańska
ul. Piotrowo 3
60-965 Poznań
e-mail: danuta.stefanska@put.poznan.pl, **tel.** +48 61 665 3232

Oświadczenie współautora artykułów naukowych

Oświadczam, że opublikowałam z mgr. inż. Maciejem Chomskim następujące prace:

1. B. Furmann, D. Stefańska, M. Suski, S. Wilman, M. Chomski, ,,*Hyperfine structure studies of the odd-parity electronic levels of the holmium atom. I: Levels with known energies*", Journal of Quantitative Spectroscopy & Radiative Transfer, 2019, vol. 234, str. 115-123.
2. B. Furmann, D. Stefańska, S. Wilman, M. Chomski, M. Suski, ,,*Hyperfine structure studies of the odd-parity electronic levels in the holmium atom, II: New levels*", Journal of Quantitative Spectroscopy and Radiative Transfer, 2019, vol. 235, str. 70–80.
3. D. Stefańska, B. Furmann, J. Ruczkowski, M. Elantkowska, P. Głowacki, M. Chomski, M. Suski, S. Wilman, ,,*Investigations of the possible second-stage laser cooling transitions for the holmium atom magneto-optical trap*", Journal of Quantitative Spectroscopy and Radiative Transfer, 2020, vol. 246 (106915).
4. M. Chomski, B. Furmann, J. Ruczkowski, M. Suski, D. Stefańska, ,,*Landé g_J factors of the electronic levels of the holmium atom*", Journal of Quantitative Spectroscopy and Radiative Transfer, 2021, vol. 274 (107865).
5. M. Chomski, M. Suski, S. Wilman, B. Furmann, J. Ruczkowski, D. Stefańska, ,,*Landé g_J factors of odd-parity electronic levels of the holmium atom*", Journal of Quantitative Spectroscopy and Radiative Transfer, 2022, vol. 279 (108045).
6. M. Chomski, B. Furmann, M. Suski, P. Głowacki, D. Stefańska, S. Mieloch, ,,*Determination of the energies of new electronic levels of the holmium atom and investigation of their hyperfine structure*", Journal of Quantitative Spectroscopy and Radiative Transfer, 2023, vol. 297 (108480).

Mój udział w niniejszych pracach polegał na:

Ad. 1 Pomocy w określeniu metodologii prac badawczych, udziale w badaniach, pomocy w opracowaniu i walidacji wyników prac badawczych, udziale w analizie formalnej, pomocy w redakcji i edycji manuskryptu.

Ad. 2 Pomocy w określeniu metodologii prac badawczych, udziale w badaniach, pomocy w opracowaniu i walidacji wyników prac badawczych, udziale w analizie formalnej, pomocy w redakcji i edycji manuskryptu.

Ad. 3 Określeniu metodologii oraz konceptualizacji prac badawczych, udziale w badaniach, opracowaniu i walidacji wyników prac badawczych, analizie formalnej, redakcji manuskryptu oraz przygotowaniu odpowiedzi dla recenzentów.

Ad. 4 Udziale w pracach badawczych, pomocy w redakcji i edycji manuskryptu.

Ad. 5 Udziale w pracach badawczych, pomocy w redakcji i edycji manuskryptu.

Ad. 6 Udziale w pracach badawczych, pomocy w edycji manuskryptu.

Wyrażam zgodę na przedłożenie wyżej wymienionych prac przez mgr. inż. Macieja Chomskiego jako części rozprawy doktorskiej w formie spójnego tematycznie zbioru artykułów naukowych.

(podpis współautora)

Poznań, 26.06.2023r.

mgr inż. Szymon Mieloch
Instytut Badań Materiałowych i Inżynierii Kwantowej,
Wydział Inżynierii Materiałowej i Fizyki Technicznej,
Politechnika Poznańska
ul. Piotrowo 3
60-965 Poznań
e-mail: szymon.mieloch@doctorate.put.poznan.pl, **tel.** +48 61 665 3229

Oświadczenie współautora artykułów naukowych

Oświadczam, że opublikowałem z mgr. inż. Maciejem Chomskim następującą pracę:

M. Chomski, B. Furmann, M. Suski, P. Głowacki, D. Stefańska, S. Mieloch, „Determination of the energies of new electronic levels of the holmium atom and investigation of their hyperfine structure", Journal of Quantitative Spectroscopy and Radiative Transfer, 2023, vol. 297 (108480).

Mój udział w niniejszej pracy polegał na: udziale w badaniach oraz pomocy w opracowaniu wyników badań.

Wyrażam zgodę na przedłożenie wyżej wymienionej pracy przez mgr. inż. Macieja Chomskiego jako części rozprawy doktorskiej w formie spójnego tematycznie zbioru artykułów naukowych.

....
(podpis współautora)

Poznań, 26.06.2023r.

dr hab. Jarosław Ruczkowski
Instytut Robotyki i Inteligencji Maszynowej,
Wydział Automatyki, Robotyki i Elektrotechniki,
Politechnika Poznańska
ul. Piotrowo 3
60-965 Poznań
e-mail: jaroslaw.ruczkowski@put.poznan.pl, **tel.** +48 61 665 3228

Oświadczenie współautora artykułów naukowych

Oświadczam, że opublikowałem z mgr. inż. Maciejem Chomskim następujące prace:

1. D. Stefańska, B. Furmann, J. Ruczkowski, M. Elantkowska, P. Głowacki, M. Chomski, M. Suski, S. Wilman, *„Investigations of the possible second-stage laser cooling transitions for the holmium atom magneto-optical trap"*, Journal of Quantitative Spectroscopy and Radiative Transfer, 2020, vol. 246 (106915).
2. M. Chomski, B. Furmann, J. Ruczkowski, M. Suski, D. Stefańska, *„Landé g_J factors of the electronic levels of the holmium atom"*, Journal of Quantitative Spectroscopy and Radiative Transfer, 2021, vol. 274 (107865).
3. M. Chomski, M. Suski, S. Wilman, B. Furmann, J. Ruczkowski, D. Stefańska, *„Landé g_J factors of odd-parity electronic levels of the holmium atom"*, Journal of Quantitative Spectroscopy and Radiative Transfer, 2022, vol. 279 (108045).

Mój udział w niniejszych pracach polegał na:

Ad. 1 Pomocy w opracowaniu metodologii badań, udziale w analizie formalnej, przygotowaniu oprogramowania.

Ad. 2 Udziale w analizie formalnej, przygotowaniu oprogramowania, pomocy w redakcji części manuskryptu.

Ad. 3 Udziale w analizie formalnej, przygotowaniu oprogramowania.

Wyrażam zgodę na przedłożenie wyżej wymienionych prac przez mgr. inż. Macieja Chomskiego jako części rozprawy doktorskiej w formie spójnego tematycznie zbioru artykułów naukowych.

....
(podpis współautora)
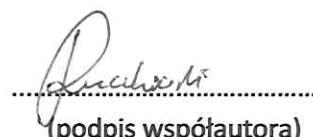
Poznań, 26.06.2023r.

dr inż. Przemysław Głowacki
Instytut Badań Materiałowych i Inżynierii Kwantowej,
Wydział Inżynierii Materiałowej i Fizyki Technicznej,
Politechnika Poznańska
ul. Piotrowo 3
60-965 Poznań
e-mail: przemyslaw.glowacki@put.poznan.pl, **tel.** +48 61 665 3222

Oświadczenie współautora artykułów naukowych

Oświadczam, że opublikowałem z mgr. inż. Maciejem Chomskim następujące prace:

1. D. Stefańska, B. Furmann, J. Ruczkowski, M. Elantkowska, P. Głowacki, M. Chomski, M. Suski, S. Wilman, „*Investigations of the possible second-stage laser cooling transitions for the holmium atom magneto-optical trap*", Journal of Quantitative Spectroscopy and Radiative Transfer, 2020, vol. 246 (106915).

2. M. Chomski, B. Furmann, M. Suski, P. Głowacki, D. Stefańska, S. Mieloch, „*Determination of the energies of new electronic levels of the holmium atom and investigation of their hyperfine structure*", Journal of Quantitative Spectroscopy and Radiative Transfer, 2023, vol. 297 (108480).

Mój udział w niniejszych pracach polegał na:

Ad. 1 Udziale w badaniach, pomocy w analizie formalnej.

Ad. 2 Udziale w badaniach, pomocy w opracowaniu wyników badań.

Wyrażam zgodę na przedłożenie wyżej wymienionych prac przez mgr. inż. Macieja Chomskiego jako części rozprawy doktorskiej w formie spójnego tematycznie zbioru artykułów naukowych.

....
(podpis współautora)

Poznań, 26.06.2023r.

dr hab. Magdalena Elantkowska
Instytut Badań Materiałowych i Inżynierii Kwantowej,
Wydział Inżynierii Materiałowej i Fizyki Technicznej,
Politechnika Poznańska
ul. Piotrowo 3
60-965 Poznań
e-mail: magdalena.elantkowska@put.poznan.pl, **tel.** +48 61 665 3222

Oświadczenie współautora artykułów naukowych

Oświadczam, że opublikowałam z mgr. inż. Maciejem Chomskim następującą pracę:

D. Stefańska, B. Furmann, J. Ruczkowski, M. Elantkowska, P. Głowacki, M. Chomski, M. Suski, S. Wilman, „*Investigations of the possible second-stage laser cooling transitions for the holmium atom magneto-optical trap*", Journal of Quantitative Spectroscopy and Radiative Transfer, 2020, vol. 246 (106915).

Mój udział w niniejszej pracy polegał na: pomocy w opracowaniu metodologii badań oraz udziale w analizie formalnej.

Wyrażam zgodę na przedłożenie wyżej wymienionej pracy przez mgr. inż. Macieja Chomskiego jako części rozprawy doktorskiej w formie spójnego tematycznie zbioru artykułów naukowych.

Magdalena Elantkowska

(podpis współautora)

Hyperfine structure studies of the odd-parity electronic levels of the holmium atom. I: Levels with known energies

B. Furmann*, D. Stefańska, M. Suski, S. Wilman, M. Chomski

Institute of Materials Research and Quantum Engineering, Faculty of Technical Physics, Poznan University of Technology, Piotrowo 3, Poznan 60–965, Poland

ARTICLE INFO

ABSTRACT

In this work investigations of the hyperfine structure of 66 spectral lines of the holmium atom were performed with the method of laser induced fluorescence in a hollow cathode discharge lamp. Altogether 43 odd-parity levels, involved as the upper levels in the transitions studied, were investigated. For about half of them the *hfs* constants *A* and *B* were evaluated for the first time. For some levels, already examined in earlier works, supplementary results were obtained; for a few levels it was possible to compare our results with earlier literature data. For 4 levels *J* quantum numbers were changed with respect to the available literature values. As a by-product, also improved *hfs* constants for the lower even-parity levels were determined. The data reported facilitated the semi-empirical fit of the fine and hyperfine structure of the odd-parity level system, performed in our group.

1. Introduction

Lanthanides constitute a group of elements with enormously rich atomic energy level structure, mostly due to the open f-electron shells in majority of low-lying configurations. Numerous elements of this series have a well-established position in astrophysical applications, mainly in analysis of stellar atmospheres [1,2]; particularly high lanthanides abundances are encountered for the so called peculiar stars.

Recently lanthanides gained considerable attention also because of their possible applications in quantum engineering and metrology; this applies in particular to the elements with more than half-filled f-electron shells, for which a surprisingly efficient method of laser cooling in magneto-optical traps (MOTs) was developed in the previous decade [3]. Holmium, which fulfills this criterion and possesses only one stable isotope $^{165}_{67}$Ho, is of particular interest. It belongs to the lanthanide elements which were already successfully laser-cooled; this was accomplished several years ago [4] and was strongly motivated by the concept to exploit the uniquely rich Zeeman-hyperfine splitting of the Ho I ground state for collective encoding of quantum registers [5]. Holmium was also proposed as one of the lanthanide elements suitable for the measurements of the temporal variation of the fine structure constant α [6].

Despite the extensive spectroscopic investigations performed, in particular within the last few years, the electronic levels structure

of the holmium atom is still far from being complete. Theory of atomic structure predicts tens of thousands of electronic levels for this atomic species, while only several hundreds were hitherto observed experimentally. For many levels the hyperfine structure is not known, and the general lack of experimental Lande g_J factors can be considered exceptional throughout the periodic table. In our earlier works concerning the atomic holmium [7–9] the state of knowledge concerning this kind of fundamental electronic levels' properties was already reviewed.

Fourier-spectroscopic investigations of holmium spectra (atomic, as well as ionized) were first performed in the IR region [10]; most lines could be classified as belonging to the holmium atom. In the last years extensive Fourier-spectroscopic studies in the UV [11,12] and very recently also in the visible spectral region [13,14] were reported. Such investigations provide an enormous progress in the issue of line classification; this method is, however, less suitable for analysis of the hyperfine structure of the levels involved.

In the present work the *hfs* constants *A* and *B* were determined for 43 odd-parity levels with known energies, half of them for the first time. For most of the remaining levels, investigated already in our earlier works, supplementary results allowed obtaining improved, in many cases more precise, *A* and *B* values. A few levels with available literature *A* and *B* constants were remeasured. The results obtained in this work were already included in the semi-empirical fine- and hyperfine structure fit for the odd-parity level system, performed in the theory team of our research group. Within the second part of the current project investigations aiming

* Corresponding author.
E-mail address: boguslaw.furmann@put.poznan.pl (B. Furmann).

at identification and *hfs* constants determination of new electronic levels, with hitherto unknown energies, were carried out (work under preparation for publication).

2. Experimental details

The experimental method and setup used in the investigations performed in this work were generally the same as in all our earlier works concerning the *hfs* studies in atomic holmium [7,8,15,16]. Most technical details were described in [7,8]; the methodology of the search of new electronic levels was briefly addressed in [15] and more extensively described in [16]. In the present work only a brief overview is provided.

All the investigations were performed by laser induced fluorescence (LIF) in a hollow cathode discharge lamp.

The laser light for excitation of the transitions studied was generated by single-mode tunable ring dye lasers (modified Coherent model CR 699–21). The total available spectral range extended over large part of the visible region - ca. 480–620 nm, and was obtained with three various dyes. The long-wavelength part of the spectral range (down to ca. 565 nm) was generated by DCM and Rhodamine 6 G, both optically pumped at $\lambda = 532$ nm by a frequency-doubled Nd^{3+}:YVO_4 laser. The short-wavelength region (up to ca. 540 nm) was obtained from Coumarin 498, pumped at $\lambda = 445$ nm by a diode laser. The amplitude-modulation of the exciting laser beam was applied, followed by phase-sensitive detection of the LIF signal. The applied variant of the LIF method takes advantage of spectral selection of the fluorescence signal (achieved by a monochromator SPM-2, Carl Zeiss Jena), which allows unique identification of individual decay channels from the upper levels.

The wavenumbers of the transitions investigated were measured by a wavemeter (Burleigh, model WA-1500). The values obtained proved consistent with the wavenumbers calculated as differences between the involved levels' energies published in NIST Atomic Spectra Database [17]. The relative frequency scale for the scans was provided by the frequency marker signal (calibrated Fabry-Perot interferometer with FSR ≈ 1500 MHz, wavelength-corrected), recorded along with the LIF spectra.

On the average 10–30 frequency scans were recorded for each transition, dependent on the signal-to-noise ratio.

3. Results

3.1. General remarks

In this work 66 spectral lines of the holmium atom were quantitatively investigated, all of them involving upper odd-parity levels with known energies, but the hyperfine structure either hitherto not investigated at all or investigated with Fourier spectroscopy, i.e. with relatively low spectral resolution. Altogether the *hfs* constants were determined for 43 levels with energies within the range of ca. 24000-41500 cm^{-1} and *J* quantum number values from 11/2 to 19/2.

Out of the total number of transitions, 50 were excited by the Coumarin 498 laser, 13 by the laser operated on Rhodamine 6G and the remaining 4 lines were investigated with the DCM laser. Laser spectroscopic investigations of many of the levels became feasible due to the recently published classification of numerous spectral lines based on Fourier-spectroscopic studies in the visible region [13]; the extended spectral range of laser radiation enabled us to examine many of the newly classified transitions. Most of the levels were investigated in at least 2 excitation transitions.

Details of the fitting procedure, including some particular issues deserving separate comment, are described in Section 3.2 below.

The spectral lines investigated are compiled in Table 1. In the columns 2 and 3 the information on the transitions is provided: air wavelengths and vacuum wavenumbers, respectively. In columns 4–7 the lower even-parity levels' parameters are given: energies, *J* values and *hfs* constants, the latter having been usually fixed in the fitting procedure (as explained below); in column 8 the respective references are cited. In columns 10–14 the energies, *J* values and *hfs* constants of the upper odd-parity levels are listed. The uncertainties of the *hfs* constants are mean standard deviations and reflect the scattering of the results between the individual scans or the groups of scans for each line.

In Table 2 a compilation of the final results concerning the odd-parity levels investigated is presented. The levels are ordered according to their *J* values, and for each *J* - according to their energies. In columns 1 and 2 the *J* and energy values of the levels are listed. Columns 3–5 are devoted to the constants *A* and columns 6–8 - the constants *B*: first the results obtained in the present work are given, and then the existing literature values (concerning 7 levels). The uncertainties of the *hfs* constants are single mean standard deviations, reflecting the scattering between the values obtained from individual transitions, except for the levels investigated in single transitions. In the latter cases a different estimate of the final uncertainties was adopted, including also systematic factors, as described in our earlier works [7,8].

Table 3 is devoted exclusively to the levels already investigated in our earlier work [7], for which supplementary results were now obtained. Columns 1 and 2 contain the levels' *J* values and energies, as in Table 2; in columns 3 and 4 the constants *A* and *B*, obtained on the individual lines, are listed. In columns 5 and 6 the wavelengths and the wavenumbers of the respective spectral lines are given; the last column 7 includes the adequate references (either the earlier work [7], or the line No in Table 1 in the present work). The uncertainties are single mean standard deviations.

Figs. 1 and 2 depict two selected examples of the recorded *hfs* spectra of the spectral lines.

3.2. Fitting procedure

The hyperfine structure of the spectral lines was evaluated in the same way as in our earlier works - with the use of the program "Fitter", developed in the group of Prof. Guthöhrlein in Hamburg. For each line either individual frequency scans, or the averaged groups containing several scans, were fitted separately, and the results were then averaged.

A few particular issues related to determination of the *hfs* constants of the levels by "Fitter" in some particular cases are discussed below.

Generally the *hfs* constants of the lower even-parity levels involved in the transitions investigated were determined in our earlier works from the analysis of multiple spectral lines and thus considered reliable. Thus it was decided to fix those constants in the fitting procedure and to determine only the constants for the upper odd-parity levels. There were, however, a few exceptions to this rule, concerning the lower even-parity levels 8378.91 cm^{-1} (*J* = 17/2), 8427.11 cm^{-1} (*J* = 15/2) and 20568.63 cm^{-1} (*J* = 17/2); a more detailed discussion od these particular cases is presented in Section 3.3.

Several spectral lines were encountered, for which the only fluorescence channel that could be efficiently used for observation of the LIF signal was positioned in close vicinity of the excitation wavelength. In such cases it proved impossible to eliminate totally the laser stray light, despite the use of appropriate filters in front of the monochromator entrance slit. Due to some interference effects the stray light intensity was not constant over the frequency scan range, often with a flat maximum positioned around the scan center. Since the program "Fitter" is equipped with very limited tools to fit the background (only linear dependence on the frequency detuning), the attempts of fitting the original spectra nec-

Table 1

Spectral lines of the holmium atom, investigated in order to determine the hyperfine structure constants for the upper odd-parity levels with known energies, along with the *A* and *B* values obtained. In most cases the *hfs* constants of the lower even-parity levels involved in the spectral lines were fixed at the available values in the least-squares fit procedure; the respective citations are given in a separate column. For some spectral lines the *hfs* constants of both the lower and the upper levels were determined independently (see Section 3). The energies of both the lower and the upper levels were taken from the NIST Atomic Spectra Database [17])

	Line		Lower Level					Upper Level					
No	λ_{air} (nm)	k_{vac} (cm^{-1})	E (cm^{-1})	J	A (MHz)		B (MHz)		ref.	E (cm^{-1})	J	A (MHz)		B (MHz)	
1	2	3	4	5	6		7		8	9	10	11		12	
1	482.579	20716.20	16709.82	17/2	1139.7	(0.8)	−2045	(41)	[16]	37426.02	15/2	1103.3	(0.9)	299	(42)
2	483.329	20684.08	9741.50	19/2	745.1	(1.4)	1747	(78)	[8]	30425.58	19/2	951.9	(1.5)	1808	(79)
3	486.630	20543.74	16882.28	15/2	479.3	(1.3)	−641	(26)	[15]	37426.02	15/2	1102.5	(1.4)	289	(27)
4	486.852	20534.39	20167.18	15/2	1335.9	(0.2)	1249	(5)	[15]	40701.57	17/2	655.5	(0.3)	42	(6)
5	488.540	20463.44	15136.06	15/2	862.4	(0.6)	234	(14)	[8]	35599.50	17/2	878.4	(0.7)	843	(24)
6	488.846	20450.63	16438.01	17/2	822.0	(0.4)	2000	(19)	[8]	36888.64	19/2	926.1	(0.5)	1742	(21)
7	490.208	20393.81	9741.50	19/2	745.1	(1.4)	1747	(78)	[8]	30135.31	17/2	1049.7	(1.5)	2400	(79)
8	490.861	20366.67	17059.35	13/2	556.1	(0.7)	−1217	(40)	[15]	37426.02	15/2	1101.4	(0.8)	356	(44)
9	491.688	20332.41	12339.04	15/2	806.7	(1.4)	−139	(19)	[8]	32671.45	15/2	846.0	(1.5)	1288	(31)
10	493.004	20278.17	20498.73	17/2	1124.9	(1.5)	381	(60)	[10]	40776.90	17/2	566.2	(1.6)	1236	(61)
11	494.842	20202.84	20498.73	17/2	1124.9	(1.5)	381	(60)	[10]	40701.57	17/2	656.2	(1.6)	53	(61)
12	495.431	20178.82	16709.82	17/2	1139.7	(0.8)	−2045	(41)	[16]	36888.64	19/2	927.3	(0.9)	1789	(42)
13	498.893	20038.78	21217.11	19/2	1081.5	(1.5)	864	(60)	[10]	41255.89	19/2	685.6	(1.6)	143	(61)
14	499.620	20009.63	11530.56	17/2	772.8	(1.2)	1011	(20)	[8]	31540.19	15/2	815.0	(1.3)	116	(21)
15	500.662	19967.99	16709.82	17/2	1139.7	(0.8)	−2045	(41)	[16]	36677.81	17/2	1238.8	(0.8)	251	(42)
16	502.052	19912.70	11530.56	17/2	772.8	(1.2)	1011	(20)	[8]	31443.26	15/2	1029.3	(1.3)	−1155	(21)
17	502.321	19902.04	20167.18	15/2	1335.9	(0.2)	1249	(5)	[15]	40069.22	13/2	768.3	(0.2)	848	(9)
18	502.649	19889.05	17883.57	19/2	1224.1	(1.6)	−152	(36)	[8]	37772.62	19/2	1218.4	(1.7)	−1629	(33)
19	504.723	19807.34	15081.12	13/2	891.0	(0.4)	119	(12)	[8]	34888.46	15/2	557.5	(0.5)	1378	(26)
20	505.125	19791.58	16438.01	17/2	822.0	(0.4)	2000	(19)	[8]	36229.59	19/2	881.0	(0.6)	702	(26)
21	505.906	19761.00	21494.89	21/2	1031.9	(1.2)	1258	(88)	[16]	41255.89	19/2	686.3	(1.3)	225	(89)
22	506.497	19737.95	15130.31	17/2	808.5	(1.8)	2120	(27)	[8]	34868.26	19/2	432.7	(1.9)	1302	(28)
23	506.645	19732.20	15136.06	15/2	862.4	(0.6)	234	(14)	[8]	34868.26	17/2	431.6	(0.7)	1249	(15)
24	511.110	19559.79	21217.11	19/2	1081.5	(1.5)	864	(60)	[10]	40776.90	17/2	565.6	(1.6)	1232	(61)
25	512.791	19495.71	9147.08	13/2	916.6	(0.5)	2668	(7)	[20]	28642.79	11/2	439.3	(0.6)	535	(10)
26	513.087	19484.46	21217.11	19/2	1081.5	(1.5)	864	(60)	[10]	40701.57	17/2	656.1	(1.6)	67	(61)
27	513.277	19477.22	12339.04	15/2	806.7	(1.4)	−139	(19)	[8]	31816.26	13/2	43.4	(1.7)	−1560	(55)
28	513.906	19453.41	15081.12	13/2	891.0	(0.4)	119	(12)	[8]	34534.53	13/2	808.9	(0.7)	615	(14)
29	514.397	19434.82	18337.80	17/2	1104.7	(1.2)	−1782	(20)	[16]	37772.62	19/2	1219.2	(1.3)	−1435	(21)
30	514.778	19420.42	18821.25	11/2	264.7	(0.6)	−446	(33)	[16]	38241.67	13/2	613.9	(0.9)	−698	(41)
31	516.066	19371.95	15130.31	17/2	808.5	(1.8)	2120	(27)	[8]	34502.26	19/2	921.8	(1.9)	3257	(30)
32	518.203	19292.07	8378.91	17/2	779.1	(0.4)	183	(12)	*	27670.98	19/2	1038.6	(0.3)	2233	(13)
33	518.488	19281.49	18337.80	17/2	1104.7	(1.2)	−1782	(20)	[16]	37619.29	19/2	1282.6	(1.3)	−1458	(21)
34	518.781	19270.60	8378.91	17/2	777.9	(0.5)	250	(30)	*	27649.51	15/2	991.6	(0.5)	1578	(28)
35	519.929	19228.03	15081.12	13/2	891.0	(0.4)	119	(12)	[8]	34309.15	13/2	1050.1	(0.6)	1495	(13)
36	520.406	19210.40	15136.06	15/2	862.4	(0.6)	234	(14)	[8]	34346.46	15/2	701.1	(0.7)	751	(16)
37	520.924	19191.32	18651.53	15/2	865.4	(1.4)	−2670	(19)	[16]	37842.85	15/2	1453.1	(1.5)	−974	(20)
38	521.677	19163.60	15130.31	17/2	808.5	(1.8)	2120	(27)	[8]	34293.91	17/2	906.6	(1.9)	295	(28)
39	523.325	19103.27	11322.31	21/2	694.6	(0.8)	3540	(11)	[8]	30425.58	19/2	950.8	(0.9)	1868	(12)
40	523.450	19098.71	12344.55	13/2	908.6	(0.6)	424	(23)	[8]	31443.26	15/2	1029.5	(0.7)	−1084	(24)
41	523.738	19088.22	18337.80	17/2	1104.7	(1.2)	−1782	(20)	[16]	37426.02	15/2	1100.5	(1.3)	248	(26)
42	524.803	19049.47	12344.55	13/2	908.6	(0.6)	424	(23)	[8]	31394.02	11/2	784.6	(0.7)	394	(24)
43	525.188	19035.49	12344.55	13/2	908.6	(0.6)	424	(23)	[8]	31380.04	13/2	750.0	(0.7)	861	(24)
44	526.594	18984.66	18858.19	13/2	467.8	(0.9)	−3185	(41)	[16]	37842.85	15/2	1455.4	(1.0)	−1078	(44)
45	529.093	18895.02	11530.56	17/2	772.8	(1.2)	1011	(20)	[8]	30425.58	19/2	951.2	(1.3)	1804	(21)
46	529.437	18882.72	15130.31	17/2	808.5	(1.8)	2120	(27)	[8]	34013.03	19/2	1077.5	(1.9)	1280	(28)
47	530.262	18853.37	15130.31	17/2	808.5	(1.8)	2120	(27)	[8]	33983.68	15/2	979.4	(1.9)	1283	(28)
48	532.489	18774.49	18651.53	15/2	865.4	(1.4)	−2670	(19)	[16]	37426.02	15/2	1101.3	(1.5)	415	(20)
49	533.589	18735.81	11689.77	19/2	735.5	(0.8)	3022	(36)	[8]	30425.58	19/2	953.0	(1.1)	1862	(75)
50	570.696	17517.59	9147.08	13/2	916.6	(0.5)	2668	(7)	[20]	26664.67	11/2	778.5	(0.6)	1443	(14)
51	571.058	17506.51	13082.93	11/2	1042.2	(1.8)	2359	(8)	[8]	30589.44	13/2	1444.3	(1.9)	−1245	(9)
52	577.767	17303.21	16709.82	17/2	1139.7	(0.8)	−2045	(41)	[16]	34013.03	19/2	1078.1	(0.9)	1195	(43)
53	577.997	17296.32	20568.63	17/2	793.5	(0.3)	3213	(16)	*	37864.95	17/2	1239.2	(0.3)	423	(13)
54	581.099	17203.99	20568.63	17/2	795.1	(1.5)	3286	(73)	*	37772.62	19/2	1220.5	(1.6)	−1528	(76)
55	595.672	16783.10	18651.53	15/2	865.4	(1.4)	−2670	(19)	[16]	35434.63	13/2	897.2	(1.5)	−1308	(21)
56	596.083	16771.55	12344.55	13/2	908.6	(0.6)	424	(23)	[8]	29116.10	11/2	496.0	(0.7)	−498	(24)
57	598.512	16703.47	11689.77	19/2	735.5	(0.8)	3022	(36)	[8]	28393.24	19/2	876.9	(1.1)	1250	(37)
58	599.347	16680.20	15136.06	15/2	862.4	(0.6)	234	(14)	[8]	31816.26	13/2	40.1	(0.7)	−1607	(16)
59	609.613	16399.31	18337.80	17/2	1104.7	(1.2)	−1782	(20)	[16]	34737.11	19/2	915.3	(1.3)	1939	(21)
60	610.998	16362.14	15081.12	13/2	891.0	(0.4)	119	(12)	[8]	31443.26	15/2	1028.0	(0.5)	−1133	(13)
61	613.352	16299.34	8378.91	17/2	778.5	(0.6)	217	(34)	*	24678.25	19/2	1212.1	(0.7)	−983	(43)
62	613.393	16298.24	12344.55	13/2	908.6	(0.6)	424	(23)	[8]	28642.79	11/2	437.3	(0.8)	619	(33)
63	637.251	15688.06	8427.11	15/2	844.6	(0.3)	597	(29)	*	24115.17	17/2	1192.4	(0.5)	−1682	(43)
64	637.379	15684.91	15855.28	15/2	1142.4	(1.1)	−410	(35)	[16]	31540.19	15/2	813.2	(1.2)	317	(36)
65	641.343	15587.98	15855.28	15/2	1142.4	(1.1)	−410	(35)	[16]	31443.26	15/2	1028.4	(1.2)	−1025	(36)
66	655.087	15260.94	15855.28	15/2	1142.4	(1.1)	−410	(35)	[16]	31116.22	17/2	1539.0	(1.2)	−1539	(36)

* *A* and *B* constants of the lower and the upper level determined indpendently

** *A* and *B* constants of the lower level fixed at the averages calculated from the values obtained for the remaining hitherto investigated lines
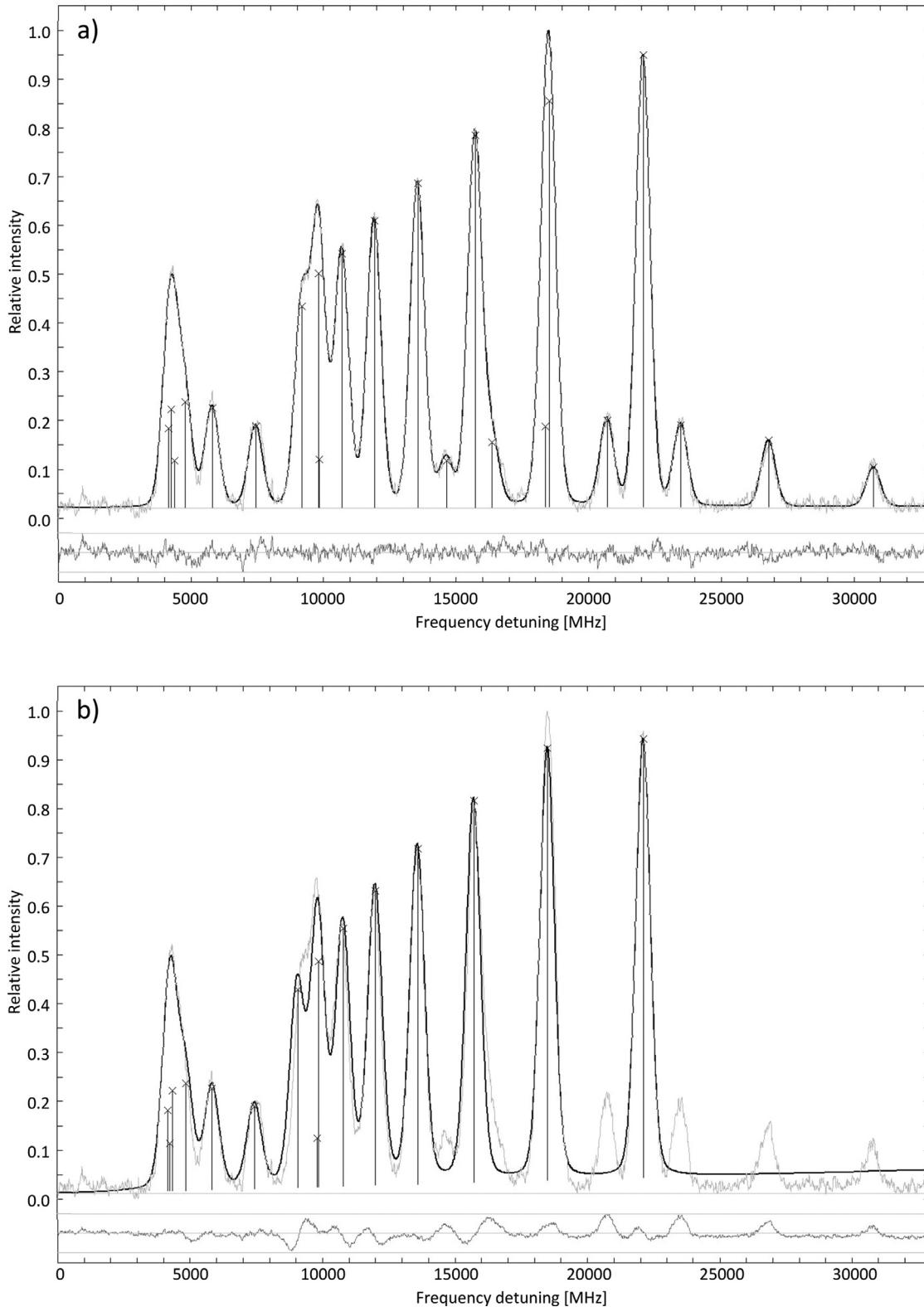
Fig. 1. Recorded spectral line λ = 532.489 nm, corresponding to the transition 18651.53 cm^{-1} ($J = 15/2$) → 37426.02 cm^{-1} in the holmium atom (line 49 in Table 1), along with the *hfs* components fitted by program "Fitter" (marked with vertical lines); two J quantum number values for the upper level were assumed: (a) 15/2, determined in the present work, (b) 17/2, hitherto proposed in the literature [19]. The lower traces represent the deviations of the experimental data from the theoretical curves and reflect the quality of the fit (the scaling factors amount to: 0.8897 and 0.2420, respectively). The horizontal lines at the value of relative intensity close to 0 represent the fitted background.
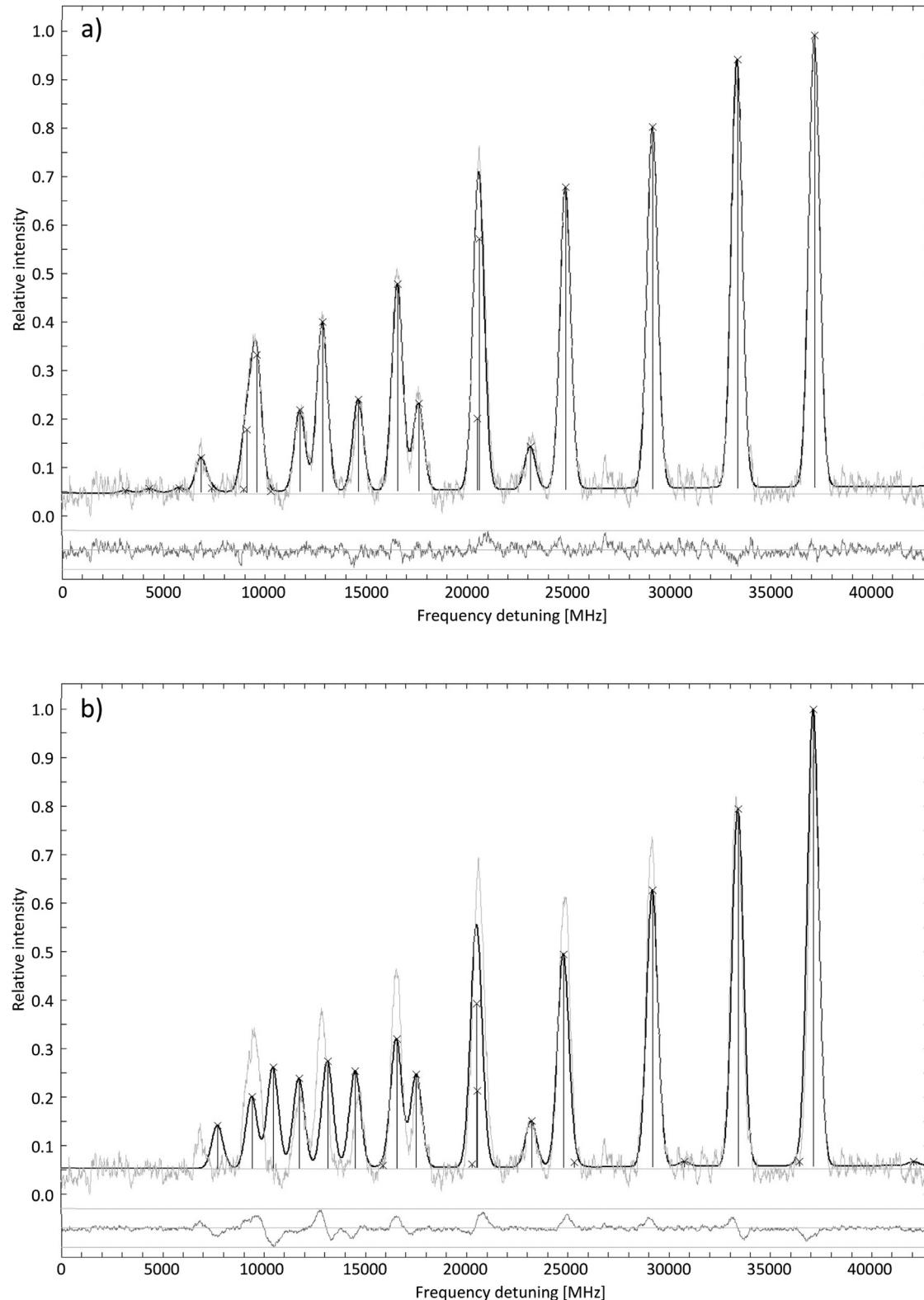
Fig. 2. Recorded spectral line λ = 571.058 nm, corresponding to the transition 13082.93 cm^{-1} ($J = 11/2$) → 30589.44 cm^{-1} in the holmium atom (line 52 in Table 1), along with the *hfs* components fitted by program "Fitter" (marked with vertical lines); two *J* quantum number values for the upper level were assumed: (a) 13/2, determined in the present work, (b) 11/2, hitherto proposed in the literature [10]. The lower traces represent the deviations of the experimental data from the theoretical curves and reflect the quality of the fit (the scaling factors amount to: 0.5123 and 0.1687, respectively). The horizontal lines at the value of relative intensity close to 0 represent the fitted background.

Table 2

Compilation of the hyperfine structure constants *A* and *B* for the odd-parity levels in the holmium atom investigated in this work; additionally, existing experimental literature data (concerning a few levels only) are presented for reference. In parentheses the full uncertainties (in MHz) are quoted.

Level		A (MHz)			B (MHz)		
J	E (cm⁻¹)	this work	[10]	[18]	this work	[10]	[18]
1	2	3	4	5	6	7	8
11/2							
	26664.67	778.0(2.0)[c]	783.6(3.0)		1443(83)[c]	1470(150)	
	28642.79	438.0(1.0)[b]			577(42)[b]		
	29116.10	496.0(2.3)[c]	498.3(4.5)		−498(107)[c]	−450(300)	
	31394.02	784.6(1.6)[c]			394(71)[c]		
13/2							
	30589.44	1444.3(3.6)[c]			−1245(92)[c]		
	31380.04	747.5(2.6)[a]			840(22)[a]		
	31816.26	41.8(1.7)[b]			−1584(24)[b]		
	34309.15	1051.2(0.5)[a]			1485(29)[a]		
	34534.53	807.0(1.0)[a]			658(27)[a]		
	35434.63	897.6(0.3)[a]			−1271(39)[a]		
	38241.67	613.9(2.4)[c]			−698(118)[c]		
	40069.22	768.3(1.9)[c]			848(110)[c]		
15/2							
	27649.51	991.6(1.4)[c]	996.0(3.0)		1578(88)[c]	1500(150)	
	31443.26	1028.8(0.4)[b]			−1099(30)[b]		
	31540.19	814.1(0.9)[b]			217(101)[b]		
	32671.45	848.8(1.1)[a]			1232(35)[a]		
	33983.68	979.7(0.6)[a]			1163(54)[a]		
	34346.46	697.2(4.0)[a]			799(48)[a]		
	34888.46	557.0(0.7)[a]			1442(36)[a]		
	37426.02	1101.8(0.5)[b]			321(30)[b]		
	37842.85	1454.3(1.2)[b]			−1026(52)[b]		
17/2							
	24115.17	1192.4(1.7)[c]			−1682(121)[c]		
	30135.31	1049.7(3.1)[c]	1050.9(3.0)		2400(195)[c]	2280(150)	
	31116.22	1539.0(2.5)[c]			−1539(124)[c]		
	34293.91	905.1(1.6)[a]			261(34)[a]		
	34868.26	431.2(0.6)[b]			1276(27)[b]		
	35599.50	882.0(4.0)[a]			887(44)[a]		
	36677.81	1238.8(2.1)[c]			251(116)[c]		
	37864.95	1239.2(1.8)[c]			423(101)[c]		
	40701.57	655.9(0.3)[b]			54(8)[b]		
	40776.90	565.9(0.3)[b]			1234(2)[b]		
19/2							
	24678.25	1212.1(1.9)[c]	1212.3(3.0)	1215.6(7.0)	−983(136)[c]	−1035(150)	−1057(24)
	27670.98	1038.6(1.5)[c]	1041.3(3.0)		2233(101)[c]	2130(150)	
	28393.24	876.6(0.4)[a]	877.8(3.0)		1245(6)[a]	1029(150)	
	30425.58	951.7(0.5)[b]			1835(18)[b]		
	34013.03	1077.9(0.2)[a]			1228(21)[a]		
	34502.26	921.8(2.6)[c]			3257(82)[c]		
	34737.11	915.4(0.1)[a]			1910(30)[a]		
	36229.59	880.7(0.4)[a]			718(16)[a]		
	36888.64	926.3(0.4)[a]			1750(40)[a]		
	37619.29	1285.2(2.6)[a]			−1363(95)[a]		
	37772.62	1219.4(0.7)[b]			−1531(56)[b]		
	41255.89	686.0(0.4)[b]			184(41)[b]		

[a] *A* and *B* constants determined as the averages from all lines involving this level investigated in the present study and in [7]

[b] *A* and *B* constants determined as the averages from all lines involving this level investigated in the present study

[c] *A* and *B* constants determined from single lines

essarily resulted in systematic shifts of the determined *hfs* constants (particularly *B*). In the cases where nonlinear background was observed, the spectra were first corrected in Microcal Origin by subtracting a polynomial least-squares fitted to the background, before they were further evaluated by "Fitter".

3.3. Even-parity lower levels examined independently

In the above mentioned exceptional cases of three even-parity levels, 8378.91 cm⁻¹ (*J* = 17/2), 8427.11 cm⁻¹ (*J* = 15/2) and 20568.63 cm⁻¹ (*J* = 17/2), we refrained from adopting the earlier *hfs* constants literature values as constraints in the fitting procedure. For these levels Fourier spectroscopy values were already available [10], these were, however, reported as belonging to the least precisely evaluated group of levels, with estimated uncertainties of 4.5 MHz for *A* constants and 300 MHz for *B* constants.

For the first level, 8378.91 cm⁻¹, also *hfs* constants determined from optogalvanic spectroscopy were reported [18]; these were, however, based on the analysis of a single line only. Thus, taking into account the limitations of the optogalvanic detection (i.e. the risk of simultaneous recording of various lines overlapping at the same narrow spectral region of the order of 1 cm⁻¹), those results could not be considered being undisputed. The second level, 8427.11 cm⁻¹, was not investigated in [18].

Independent studies of the *hfs* of the third level, 20568.63 cm⁻¹, were reported in our earlier works [7,8]; we

Table 3

Compilation of the hyperfine structure constants *A* and *B* for the odd-parity levels of the holmium atom, remeasured in this work. In parentheses the full uncertainties (in MHz) are quoted.

	Level		*hfs* constants		Line		
J	E (cm^{-1})		*A* (MHz)	*B* (MHz)	λ_{air}	k$_{vac}$	ref
1	2		3	4	5	6	7
13/2							
	31380.04		744.9(0.9)	818(12)	525.036	19041.00	[7]
			750.0(0.7)	861(24)	525.188	19035.49	this work, line No 43
	Mean values		747.5(2.6)	840(22)			
	34309.15		1050.1(0.6)	1495(13)	519.929	19228.03	this work, line No 35
			1051.2(0.4)	1440(18)	521.419	19173.09	[7]
			1051.2(0.6)	1443(20)	573.667	17426.87	[7]
			1052.2(0.4)	1560(44)	575.489	17371.72	[7]
	Mean values		1051.2(0.5)	1485(29)			
	34534.53		808.9(0.7)	615(14)	513.906	19453.41	this work, line No 28
			805.5(0.7)	655(15)	515.361	19398.47	[7]
			807.2(0.7)	705(49)	568.118	17597.10	[7]
	Mean values		807.0(1.0)	658(27)			
	35434.63		897.5(1.6)	−1311(55)	508.958	19642.50	[7]
			898.2(0.3)	−1195(27)	518.517	19280.42	[7]
			897.2(1.5)	−1308(21)	595.672	16783.10	this work, line No 55
	Mean values		897.6(0.3)	−1271(39)			
15/2							
	32671.45		846.0(1.5)	1288(31)	491.688	20332.41	this work, line No 9
			849.3(1.0)	1313(45)	491.822	20326.90	[7]
			851.9(1.2)	1124(17)	569.930	17541.14	[7]
			846.8(0.2)	1250(11)	594.501	16816.17	[7]
			849.8(0.4)	1187(9)	605.260	16517.24	[7]
	Mean values		848.8(1.1)	1232(35)			
	33983.68		978.3(0.6)	1139(23)	528.882	18902.56	[7]
			979.4(1.9)	1283(28)	530.262	18853.37	this work, line No 47
			980.9(0.4)	1030(34)	578.749	17273.86	[7]
			980.2(0.7)	1200(20)	579.626	17247.73	[7]
	Mean values		979.7(0.6)	1163(54)			
	34346.46		693.2(2.0)	846(25)	520.251	19216.15	[7]
			701.1(0.7)	751(16)	520.406	19210.40	this work, line No 36
	mean values		697.2(4.0)	799(48)			
	34888.46		557.5(0.5)	1378(26)	504.723	19807.34	this work, line No 19
			555.8(1.0)	1502(30)	505.979	19758.15	[7]
			557.8(0.5)	1445(17)	506.126	19752.40	[7]
	mean values		557.0(0.7)	1442(36)			
17/2							
	34293.91		906.6(1.9)	295(28)	521.677	19163.60	this work, line No 38
			903.5(0.2)	228(9)	521.834	19157.85	[7]
	mean values		905.1(1.6)	261(34)			
	35599.50		885.7(1.3)	930(28)	488.403	20469.19	[7]
			878.4(0.7)	843(24)	488.540	20463.44	this work, line No 5
	mean values		882.1(3.7)	887(44)			
19/2							
	28393.24		876.2(0.6)	1239(46)	585.629	17070.93	[7]
			876.9(1.1)	1250(37)	598.512	16703.47	this work, line No 57
	mean values		876.6(0.4)	1245(42)*			
	34013.03		1077.5(1.9)	1280(28)	529.437	18882.72	this work, line No 46
			1078.2(0.4)	1243(25)	568.831	17575.02	[7]
			1077.9(0.2)	1195(8)	576.890	17329.51	[7]
			1078.1(0.9)	1195(43)	577.767	17303.21	this work, line No 52
	mean values		1077.9(0.2)	1228(21)			
	34737.11		915.4(0.4)	1884(11)	509.885	19606.80	[7]
			915.3(1.3)	1939(21)	609.613	16399.31	this work, line No 59
	mean values		915.4(0.1)	1910(30)			
	36229.59		881.0(0.6)	702(26)	505.125	19791.58	this work, line No 20
			880.3(0.4)	733(21)	512.158	19519.77	[7]
	mean values		880.7(0.4)	718(16)			
	36888.64		926.1(0.5)	1742(21)	488.846	20450.63	this work, line No 6
			925.5(0.4)	1821(22)	494.786	20205.12	[7]
			927.3(0.9)	1789(42)	495.431	20178.82	this work, line No 12
			926.2(0.2)	1652(11)	526.029	19005.07	[7]
	mean values		926.3(0.4)	1750(40)			
	37619.29		1287.8(0.4)	−1268(34)	506.554	19735.72	[7]
			1282.6(1.3)	−1458(21)	518.488	19281.49	this work, line No 33
	mean values		1285.2(2.6)	−1363(95)			

* Uncertainty for the *hfs* constant *B* calculated on the basis of the uncertainties for individual spectral lines because of negligible statistical error value

Table 4

Hyperfine structure constants *A* and *B* for the even-parity levels in the holmium atom, investigated in this work as the lower levels in transitions and fitted independently; additionally, existing experimental literature data are presented for reference. In parentheses the full uncertainties (in MHz) are quoted.

Level		*A* (MHz)			*B* (MHz)		
J	E (cm^{-1})	this work	[10]	[18]	this work	[10]	[18]
1	2	3	4	5	6	7	8
15/2							
	8427.11	844.6(1.5)[c]	843.0(4.5)		597(108)[c]	801(300)	
17/2							
	8378.91	778.5(0.6)[b]	776.4(4.5)	784.7(6.0)	217(34)[b]	608(300)	601(23)
	20568.63	795.1(1.5)[a]	793.5(4.5)		3286(73)[a]	3180(300)	

[a] *A* and *B* constants determined as the averages from all lines involving this level investigated in the present study and in [7].

[b] *A* and *B* constants determined as the averages from all lines involving this level investigated in the present study

[c] *A* and *B* constants determined from single lines.

obtained the constants *A* and *B* from the analysis of a single line, with relatively large final uncertainties. Thus we considered this level as a case deserving further studies.

In six of the investigated transitions these three even-parity levels were involved, and four of the lines were found to be sufficient for an independent determination of the *hfs* constants of both upper and lower energy levels. The obtained *hfs* constants for the lower even-parity levels are presented in Table 2. For the two remaining lines these constants were used in the analysis of their *hfs*.

4. Discussion

4.1. Estimated accuracy of the results obtained

Among 43 electronic odd-parity levels investigated in this work, 16 (i.e. somewhat more than one third of the total number) were studied before in our earlier work [7]. The constants' values given there were sometimes based on the analysis of single spectral lines only, and thus additional possibilities of verification, in particular of the constants *B*, were sought.

The large scattering of *B* constants for the electronic levels of the holmium atom, as well as observed inconsistencies between various studies reported in the literature, was already discussed in [7,8]. A particularly high nuclear spin value of 7/2 results in very low and rather poorly differentiated Casimir coefficients related to the constants *B*. As a consequence, these constants are very sensitive to any changes in the *hfs* interval values and exhibit much worse consistency between results obtained from measurements on various spectral lines than is observed for elements with lower *I* values (e.g. terbium - $I = 3/2$ for the single stable isotope $^{159}_{65}$Tb). Another issue is concerned with typically very broad *hfs* structures of the spectral lines in holmium, extended over several tens of GHz; this requires broad frequency scans in laser-spectroscopic measurements. With the limited scan frequency resolution (in our experimental setup currently 4096 measurement points per scan, resulting in frequency increments usually exceeding 10 MHz per point) a somewhat decreased precision of determination of the frequency intervals between the *hfs* components may result.

The *hfs* results for most of the levels investigated in this work for the first time by us, were obtained from the analysis of various spectral lines (whenever investigation of more than one line for a particular level was possible), and found to be mutually consistent (with the typical relatively high uncertainties for the constants *B* taken into account). An exception constitutes the level 31540.91 cm^{-1} ($J = 15/2$), for which two spectral lines could be studied. Here the difference between the obtained *B* values was higher than the average. Unfortunately, so far no other lines involving this level could be observed in the accessible spectral region.

Altogether 15 levels (ca. 35%) could so far be investigated on single spectral lines only. Since some systematic factors were included in the total uncertainties quoted in such cases, the resulting precision of the *hfs* constants is lower than for the levels studied in multiple transitions. Certainly further investigations can improve the precision, if an extension of the available laser radiation spectral range, in particular towards shorter wavelengths, becomes possible.

Literature *hfs* constants' values are available for altogether 7 odd-parity levels - in most cases these are early Fourier-spectroscopic results [10] of limited precision, in one case (level 24678.25 cm^{-1} ($J = 19/2$)) also values from optogalvanic spectroscopy were published [18] (based on the analysis of a single spectral line). The general tendency of our *B* constants values to differ somewhat from those reported in [10] is still maintained. However, the differences are not substantial, ranging from several tens to ca. 200 MHz, and usually fall within the total uncertainty limits.

4.2. Changes of *J* quantum numbers

An important point is a change of the *J* quantum numbers for some odd-parity levels with respect to the earlier literature values. This concerns 4 levels; the individual cases are discussed below.

The most evident is the case of the level 37426.02 cm^{-1}; the earlier suggested *J* value was 17/2 [19], but our investigations clearly indicate the value 15/2. This level was involved in five excited transitions, one of them involving the lower even-parity level 17059.35 cm^{-1} with $J = 13/2$, which definitely excludes the possibility of $J = 17/2$ for the upper level in question. Additionally, in Fig. 1 as an example the spectral line $\lambda = 532.489$ nm, corresponding to the transition 18651.53 cm^{-1} ($J = 15/2$) → 37426.02 cm^{-1}, is presented with fitted *hfs* patterns corresponding to $J = 15/2$ and 17/2 for the upper level. The fit with $J = 17/2$ does not explain the observed spectrum.

The level 28642.79 cm^{-1} was examined in two spectral lines ($\lambda = 512.791$ nm and $\lambda = 613.393$ nm), both involving lower even-parity levels with $J = 13/2$. This value allows both the $J = 13/2$ suggested in [19] and the value $J = 11/2$ proposed in the present work. However, in each spectral line only one group of the off-diagonal *hfs* components is visible, indicating nonequal *J* values of both the levels involved, and this group corresponds to the excitations $F \rightarrow F - 1$, which means that the upper level's *J* value is lower than that of the lower level. Attempts of assuming $J = 13/2$ for the upper level in the fit procedure of the spectral lines mentioned resulted in theoretical curves inconsistent with the observed *hfs* patterns.

The levels 30589.44 cm^{-1} and 36677.81 cm^{-1} are involved in single lines only, $\lambda = 571.058$ nm and $\lambda = 500.662$ nm, respectively.

The first level was given with $J = 11/2$ in [10] and the transition investigated in the present work, $\lambda = 571.058$ nm, involves a $J = 11/2$ lower level. The observed *hfs* spectrum clearly corresponds to J value of the upper level higher than that of the lower level (the *hfs* pattern for this line is presented in Fig. 2 with theoretical curves fitted for two assumed J values of the upper level).

For the second level $J = 19/2$ was proposed in [19]. The *hfs* pattern of the studied spectral line involving this level evidently includes two groups of the off-diagonal *hfs* components, positioned on both sides of the group of main (diagonal) components; this is characteristic of equal J quantum numbers of both levels involved. Since the lower level of the transition $\lambda = 500.662$ nm is assigned with $J = 17/2$, the upper level has also certainly $J = 17/2$.

4.3. Auxiliary results for the even-parity levels

As already mentioned in Section 3, three lower even-parity levels: 8378.91 cm^{-1}, 8427.11 cm^{-1} and 20568.63 cm^{-1}, were analyzed independently in the present work. For these levels earlier literature Fourier spectroscopy *hfs* constants [10] fall into the lowest precision category reported, and the optogalvanic spectroscopy results for the level 8378.91 cm^{-1} [18] are not considered to be reliable. Our values of the constants A, presented in Table 4, are in good agreement with the literature data mentioned, and they are more precise. Our constants B differ somewhat from the literature values; nevertheless, the differences are not very large, and we believe our results to be reliable.

5. Conclusions

In this work the hyperfine structure constants of 43 odd-parity levels in the holmium atom were determined on the basis of laser spectroscopic investigations in a hollow cathode discharge lamp, involved in 66 excited transitions covering various parts of the visible spectral range. The levels examined are in broad energy range of ca. 23500–41500 cm^{-1} and most of them were studied for the first time.

In the case of 4 odd-parity levels, investigations performed in this work indicated the necessity of assigning J quantum number values different from those hitherto proposed in the literature.

The new results greatly facilitated the semi-empirical analysis of the fine and hyperfine structure of the odd-parity level system in the holmium atom, which is in progress in our research group.

As a by-product, more precise hyperfine structure constants were determined for 3 even-parity levels, two of them with $J = 17/2$, possibly suitable as the upper levels of second-stage laser cooling transitions in magneto-optical traps.

Acknowledgments

References

[1] Sneden C, Cowan JJ. Genesis of the heaviest elements in the milky way galaxy. Science 2003;299(5603):70–5.

[2] Winckler N, Dababneh S, Heil M, Käppeler F, Gallino R, Pignatari M. Lanthanum: an s- and r-process indicator. Astrophys J 2006;647(1):685–91.

[3] McClelland JJ, Hanssen JL. Laser cooling without repumping: a magneto-optical trap for erbium atoms. Phys Rev Lett 2006;96:143005.

[4] Miao J, Hostetter J, Stratis G, Saffman M. Magneto-optical trapping of holmium atoms. Phys Rev A 2014;89:041401.

[5] Saffman M, Mølmer K. Scaling the neutral-atom rydberg gate quantum computer by collective encoding in holmium atoms. Phys Rev A 2008;78:012336.

[6] Dzuba VA, Flambaum VV. Relativistic corrections to transition frequencies of Ag I, Dy I, Ho I, Yb II, Yb III, Au I and Hg II and search for variation of the fine-structure constant. Phys Rev A 2008;77:012515.

[7] Stefanska D, Furmann B. Hyperfine structure investigations for the odd-parity configuration system in atomic holmium. J Quant Spectros Rad Trans 2018;206:286–95.

[8] Stefanska D, Ruczkowski J, Elantkowska M, Furmann B. Fine- and hyperfine structure investigations of the even-parity configuration system in atomic holmium. J Quant Spectros Rad Trans 2018a;209:180–95.

[9] Stefanska D, Werbowy S, Krzykowski A, Furmann B. Lande g_J factors for even–parity electronic levels in the holmium atom. J Quant Spectros Rad Trans 2018b;210:136–40.

[10] Wyart J-F, Camus P, Vergès J. Etude du spectre de L'holmium atomique: i. spectre d'émission infrarouge niveaux d'énergie de ho i et structures hyperfines. Phys C 1977;92(3):377–96.

[11] Al-Labady N, Özdalgiç B, Er A, Güzelçimen F, Öztürk IK, Kröger S, et al. Line identification of atomic and ionic spectra of holmium in the near-UV. part i. spectrum of ho i. Astrophys J Suppl Ser 2017;228(2):16.

[12] Başar G, Al-Labady N, Özdalgiç B, GüzelÇÍmen F, Er A, Öztürk IK, et al. Line identification of atomic and ionic spectra of holmium in the near-UV. II. spectra of ho II and ho III. Astrophys J Suppl Ser 2017;228(2):17.

[13] Özdalgiç B, GüzelçÍmen F, Öztürk IK, Kröger S, Kruzins A, Tamanis M, et al. Line identification of atomic and ionic spectra of holmium in the visible spectral range. i. spectrum of ho i. Astrophys J Suppl Ser 2019a;240(2):27.

[14] Özdalgiç B, Başar G, GüzelçÍmen F, Öztürk IK, Ak T, Bilir S, et al. Line identification of atomic and ionic spectra of holmium in the visible spectral range. II. spectrum of ho II and ho III. Astrophys J Suppl Ser 2019b;240(2):28.

[15] Stefanska D, Furmann B, Głowacki P. Possibilities of investigations of the temporal variation of the α constant in the holmium atom. J Quant Spectros Rad Trans 2018c;213:159–68.

[16] Furmann B, Stefanska D, Suski M, Wilman S. Identification of new electronic levels in the holmium atom and investigation of their hyperfine structure. J Quant Spectros Rad Trans 2018;219:117–26.

[17] Kramida A, Yu Ralchenko, Reader J, NIST ASD Team. NIST atomic spectra database (Ver. 5.5.1). National Institute of Standards and Technology, Gaithersburg, MD.; 2017. http://physics.nist.gov/asd.

[18] Reddy MN, Ahmad SA, Rao GN. Laser optogalvanic spectroscopy of holmium. J Opt Soc Am B 1992;9:22–6.

[19] Kröger S, Wyart J-F, Luc P. Theoretical interpretation of hyperfine structures in doubly-excited configurations 4F^{10}5D6S6P and 4F^{10}5D^{2}6S and new energy levels in neutral holmium (ho i). Physica Scripta 1997;55:579.

[20] Childs WJ, Cok DR, Goodman LS. New line classifications in ho i based on high-precision hyperfine-structure measurement of low levels. J Opt Soc Am 1983;73(2):151–5.

Hyperfine structure studies of the odd-parity electronic levels in the holmium atom. II: New levels

B. Furmann*, D. Stefańska, S. Wilman, M. Chomski, M. Suski

Institute of Materials Research and Quantum Engineering, Faculty of Technical Physics, Poznan University of Technology, Piotrowo 3, Poznan 60-965, Poland

ARTICLE INFO

ABSTRACT

This work is devoted to investigations of unclassified spectral lines in atomic holmium, aiming at identification of new electronic levels and determination of their hyperfine structure. Altogether 113 unclassified lines were investigated with the method of laser induced fluorescence in a hollow cathode discharge lamp. As a result, 35 odd-parity electronic levels with previously unknown energies were identified; for all of them the hyperfine structure constants *A* and *B* were also determined. The data reported greatly facilitated the semi-empirical fit of the fine and hyperfine structure of the odd-parity level system, performed in our group.

© 2019 Elsevier Ltd. All rights reserved.

1. Introduction

Holmium belongs to the lanthanides series - a group of elements with open 4f electronic shell, resulting in a particularly complex energy level structure. Due to the "collapse" of the wavefunction of the 4f-electrons the average energy values of various configurations are very close to one another, which results in particularly strong configuration mixing. Thus it is extremely difficult to achieve satisfactory description of the fine and the hyperfine structure, as well as other characteristic features of the electronic levels (e.g. Landé g_J factors), with *ab initio* theoretical methods. Much better results can be obtained with the use of semi-empirical methods; however, a prerequisite of their application is the availability of possibly extensive experimental databases.

On one side the complexity of the electronic levels structure may constitute a considerable challenge for the theory of complex atoms, as noted above, and on the other side it opens numerous application possibilities. It is well known, for example, that correct interpretation of the spectra of lanthanide elements is crucial for various issues in astrophysics. In this context, the knowledge of electronic levels and correct classification of the spectral lines improves the precision of estimation for the abundances of the nuclei of a particular element in the object (e.g. star) investigated. Since creation of various isotopes, often of very similar mass values, requires different conditions (slow or fast neutron capture), evaluation of the abundances of various elements allows gaining insight

in the history of the universe. Numerous research studies were devoted to this topic, and further possibilities still emerge.

Within the last dozen years this group of elements was extensively investigated also for other reasons - important applications in quantum engineering and metrology were found, in particular for the heavier lanthanides with more than half-filled 4f shell; some of these applications directly exploit the extreme complexity of the electronic levels structure.

Holmium is one of the elements with particularly interesting applications proposed and gradually developed. An exceptionally rich Zeeman-hyperfine structure of the ground state of the holmium atom (the total number of sublevels amounts to 128, which is the highest value for any stable isotope) was proposed as a basis for collective encoding of quantum registers [1]. This concept, which requires cold atoms for successful realization, naturally constituted the motivation for laser cooling of holmium atoms; this was achieved in a magneto-optical trap (MOT) a few years ago by the same research group [2], with the use of the laser cooling method developed for the lanthanide elements [3].

The uniquely high density of the electronic levels structure in the lanthanide elements makes them also suitable for performing precise investigations of the possible temporal drift of the fine structure constant α. A successful experiment is in progress on dysprosium [4,5], but suitable electronic transitions in other lanthanide elements were also proposed; holmium is one of the most promising alternative cases considered [6].

Spectroscopic studies performed over many years by various research groups, particularly intensified recently, resulted in identification and often also determination of the characteristic properties of numerous electronic levels of both parities in the holmium

---

atom. However, the description of the electronic level structure of this element is still very limited. Only several hundreds of levels, out of tens of thousands predicted by theory, were identified experimentally, and only for part of them hyperfine splittings were determined. Landé g_J factors for atomic holmium are generally missing - the values are known for merely a few tens of the electronic levels. A more comprehensive review on the basic properties of the electronic levels in the holmium atom was already presented in our earlier works on this element [7–9]. In our most recent work [10] the hyperfine structure of 45 further odd-parity levels was investigated.

Comprehensive Fourier-spectroscopic investigations of holmium spectra reported within the last two years, first in UV [11,12] and recently extended into the visible spectral region [13,14], proved that still numerous spectral lines of this element remain unclassified. In conclusions of both the works concerning the holmium atom [11,13] the authors emphasized that achievement of further progress in classification of the spectral lines of this element demands determination of the energies and essential properties of new electronic levels. This motivated us to undertake the search for unknown levels, which might possibly be involved in unclassified transitions.

So far most of the new levels that could be identified from our studies were of the odd parity; some of them were already reported in our recent works: 5 levels with $J = 11/2$ or $13/2$ (and possible applications in experimental schemes proposed for the measurement of the temporal drift of α constant) in [15] and 21 levels with various J values, ranging from 11/2 to 21/2, in [16]. Most of those levels (21) allowed successful interpretation of altogether 65 previously unclassified spectral lines observed by Fourier spectroscopy, reported in [13].

In the present work further 35 new odd-parity levels in the holmium atom were identified, and their properties (energy values and the *hfs A* and *B* constants) were determined; these allow classification of further over 200 spectral lines. The results obtained enabled achievement of important progress in the semi-empirical fine- and hyperfine structure fit for the odd-parity level system, performed in the theory team of our research group.

2. Procedure of the search for new electronic levels

In this work the same procedure of the search of new electronic levels was applied as in most cases examined in our previous work [16]; this approach was described there in detail and is only briefly reviewed below.

The search procedure was restricted to the transitions involving only upper odd-parity levels with unknown energies. Thus various relatively low-lying even-parity levels were considered as the lower levels of the unclassified spectral lines, mainly extracted from the available Fourier spectra compilations [11,13,17]. Addition of the transitions' wavenumbers result in hypothetic energies of the upper levels, while the selection rules for the electric dipole transitions determine the allowed range of their J values.

Then these hypothetic levels were selected, whose existence would allow classification of the highest number of the lines observed in the Fourier spectrum. With the use of the dedicated program, compilations of all the transitions involving the particular levels, allowed by the selection rules concerning the quantum number J, were generated. These transitions, whose wavelengths lied within the generation ranges of our lasers, were tested through the measurements of their hyperfine structure with the LIF method. It was also checked, in which possible fluorescence channels the same *hfs* pattern of the line was observed. If, upon the assumption of the literature values of the constants A and B of the lower levels, the evaluated constants A and B for the upper level under study were found mutually consistent for the

transitions investigated, the existence of the levels was considered proven.

As in the previous work [16], not all the postulated upper odd-parity levels could be successfully verified. It is possible that many unclassified spectral lines correspond to transitions between both levels with hitherto unknown energies; some lines might also have erroneously been assigned to the spectrum of neutral atom. Certainly some of the unclassified lines involve lower odd-parity and the upper even-parity levels - the case which is not considered in the present work.

3. Experimental details

The experimental method and setup used in the investigations performed in this work were generally the same as in all our earlier works concerning the *hfs* studies in atomic holmium [7,8,15,16]. Most technical details were described in [7,8]; the methodology of the search of new electronic levels was briefly addressed in [15] and more extensively described in [16]. In the present work only a brief overview is provided.

All the investigations were performed by laser induced fluorescence (LIF) in a hollow cathode discharge lamp.

The laser light for excitation of the transitions studied was generated by single-mode tunable ring dye lasers (modified Coherent model CR 699-21). The total spectral range used covered the central part of the visible region - ca. 480–620 nm, and was obtained with three various dye solutions. The long-wavelength part of the spectral range (down to ca. 565 nm) was generated by Rhodamine 6G, optically pumped at $\lambda = 532$ nm by a frequency-doubled Nd^{3+}:YVO_4 laser. The short-wavelength region (up to ca. 540 nm) was obtained from Coumarin 498, pumped at $\lambda = 445$ nm by a diode laser, and the gap between the two regions was filled by an energy transfer binary dye mixture: Coumarin 498 (donor) + Pyrromethene 556 (acceptor), directly pumped by the same diode laser.

In the method applied the frequency of the laser radiation is scanned over the range of 5–50 GHz around the center of gravity of the spectral line investigated. The amplitude-modulation of the exciting laser beam was applied, followed by phase-sensitive (lock-in) detection of the LIF signal.

The readings of the frequency scan start wavenumbers of the transitions investigated were provided by a wavemeter (Burleigh, model WA-1500). The relative frequency scale for the scans was based on the frequency marker signal (FSR ≈ 1500 MHz, wavelength-corrected), recorded along with the LIF spectra. The relative centers of gravity of the spectral lines could be determined from the least-squares fits of the *hfs* spectra, yielding the absolute wavenumbers upon addition of the recorded start values.

The applied variant of the LIF method takes advantage of spectral selection of the fluorescence signal, which allows unique identification of individual decay channels from the upper levels. The wavelengths of the induced fluorescence were selected by tuning of the grating monochromator (SPM-2, Carl Zeiss Jena). Since all the transitions studied involved upper odd-parity levels, in most cases with hitherto unknown energies, the possibly extensive knowledge of the fluorescence transitions was desired to facilitate their identification. In interpretation of the fluorescence channels relative intensities, the limitations encountered in UV region, resulting from the parameters of the monochromator applied for spectral selection (discussed in more detail in [16]), were taken into account.

The issue of the possible collisional coupling of the excited levels (partial transfer of the laser induced population to other levels, due to collisions), which can occur under typical buffer gas pressure of 3–$4{\cdot}10^{-1}$ mbar [7], was extensively discussed in [16]. In this work, due to the relatively broad spectral range covered by

our lasers, many of the fluorescence channels could also be verified as direct excitation transitions. In some cases the quality of the spectra was not sufficient for independent determination of the *hfs* constants, although usually it was possible to check the consistency of the *hfs* patterns observed with the *A* and *B* constants of both levels involved, determined from other transitions. Such spectral lines are not reported in this work as the excitation transitions. In some rare cases the LIF signal proved very weak and unsuitable for any kind of quantitative evaluation, but the patterns observed in various fluorescence channels were evidently reproduced (e.g. identical positions of the distinguishable components).

On the average 10–30 frequency scans were recorded for each transition, dependent on the signal-to-noise ratio.

4. Results

In this work 113 spectral lines of the holmium atom were quantitatively investigated as excitation transitions, all of them involving upper new odd-parity levels, with previously unknown energies ranging from ca. 29500 cm^{-1} to ca. 40000 cm^{-1} and the *J* quantum numbers from 9/2 to 19/2; obviously, the hyperfine structure of those levels was also not known before.

Almost all newly identified electronic levels were involved in at least 2 excitation transitions suitable for precise determination of the hyperfine structure constants *A* and *B* (some of them in 5–6 transitions, and one level even in 7 transitions). In many cases more excitation lines were observed, but not reported here because of the low signal quality. For all the levels several fluorescence channels could be observed, the strongest ones generally located in near UV. There were, however, two exceptions of the levels investigated in single excitation transitions; these cases are described in more detail in Section 5.

In order to determine the unknown levels' energies, the absolute wavenumbers of the transitions involving those levels were first evaluated. The values obtained were found consistent with the tabularized wavenumbers of the respective unclassified spectral lines [11,13]. The levels' energies were calculated by addition of the experimentally determined transitions' wavenumbers to the known energies of the lower even-parity levels involved [18].

The hyperfine structure of the spectral lines was evaluated in the same way as in our earlier works - with the use of the program "Fitter", developed in the group of Prof. Guthöhrlein in Hamburg. For each line either individual frequency scans, or the averaged groups containing several scans, were fitted separately, and the results were then averaged.

The *hfs* constants of the lower even-parity levels involved in the transitions investigated were reported in our earlier works as resulting from investigations of several spectral lines. Accordingly, those constants were used as constraints in the fitting procedure and only the constants for the upper odd-parity levels were evaluated. There was one exception, concerning the lower even-parity level 18757.87 cm^{-1} ($J = 9/2$), discussed in more detail below.

The spectral lines investigated are compiled in Table 1. In the columns 2 and 3 the information on the transitions is provided: air wavelengths and vacuum wavenumbers, respectively. In columns 4–7 refer the lower even-parity levels' parameters are given: energies, *J* values and *hfs* constants, the latter having been generally fixed in the fitting procedure (as explained above); in column 8 the respective references are cited. In columns 10–14 the energies, *J* values and *hfs* constants of the upper odd-parity levels are listed. The uncertainties of the *hfs* constants are mean standard deviations and reflect the scattering of the results between the individual scans or the groups of scans for each line.

In the above mentioned exceptional case of one even-parity level, 18757.87 cm^{-1} ($J = 9/2$), we did not adopt our earlier *hfs* constants values as constraints in the fitting procedure. This level

was investigated by us in only one spectral line, reported in our earlier work [16], and in our opinion deserved further verification. Currently another transition involving this level was investigated: $\lambda = 613.584$ nm (Table 1, No 111). It appeared strong and could be recorded with high signal-to-noise ratio, making independent determination of the *hfs* constants of both levels involved possible. The final *hfs* constants of the even-parity level 18757.87 cm^{-1} ($J = 9/2$), calculated as the averages from the values obtained previously and for the spectral line just discussed, thus amount to: $A = 1147.6(0.3)$ MHz, $B = 316(12)$ MHz.

In Table 2 the final results concerning the odd-parity levels with previously unknown energies are compiled. The levels are grouped according to their *J* values; within each group the levels are order with increasing energies. Columns 1 and 2 contain the levels' *J* values and energies, columns 3 and 4 are devoted to the *hfs* constants *A* and *B*, respectively. The remaining columns of Table 2 contain the information on the expected fluorescence channels from the upper odd-parity levels identified in this work, resulting from the coincidence analysis (Section 2). In most cases at least a few fluorescence channels could be observed; some lines could also be investigated as direct excitation transitions. In columns 5–7 the fluorescence lines' wavelengths, wavenumbers and available relative intensities (from several sources [11,13,17,18]) are included, columns 8 and 9 contain the energies and the *J* values of the terminating lower even-parity levels. In column 10 additional remarks were entered; the particularly strong fluorescence channels were indicated, and the lines observed also as excitation transitions were referred to the respective lines' numbers in Table 1.

The uncertainties of the levels' energies are single mean standard deviations, calculated from the values obtained in the analysis of individual transitions studied. Almost all the uncertainties for the *hfs* constants *A* and *B* are also single mean standard deviations, reflecting the scattering between the values obtained for individual transitions, except for two categories:

1. the levels investigated in single transitions,
2. the levels investigated in two transitions, where the *hfs* constants *B* were accidentally very similar (while the general tendency is rather high scattering of the values).

In the first case an estimate of the final uncertainties including also systematic factors was adopted, as described in our earlier works [7,8]. In the second case the final uncertainties were calculated from the uncertainties observed for individual spectral lines.

Table 3, entirely included in Supplemental Material, contains a compilation of all the hitherto unclassified spectral lines, that could be classified as transitions involving the newly identified odd-parity levels in the holmium atom. Classification was based on direct observation of the spectral lines as transitions involving the particular levels - either as direct excitation transitions or as fluorescence channels. Obviously, the wavenumbers of the transitions observed in the present work were checked against the literature values from Fourier spectroscopic investigations, reported in [11,13,17]. Moreover, the consistency between the literature *hfs* patterns' widths presented in the works cited, and the widths calculated from the *hfs* constants of the lower and upper levels of the spectral lines examined in the present work was checked.

Table 3 constitutes an extension of the respective tables listing the observed spectral lines in [11,13], in the spectral region covered in the present work. In columns 1 and 2 the transitions' wavelengths and wavenumbers are listed, column 3 contains the relative intensities, quoted directly from [11,13], observed under argon as the buffer gas (the intensities observed in neon atmosphere and the ratios of intensities for both buffer gases, important for interpretation of Fourier spectra, were omitted as irrelevant for our experiment). In column 4 additional comments are provided [11,13] (e.g. blending of the line pattern, possible assignment
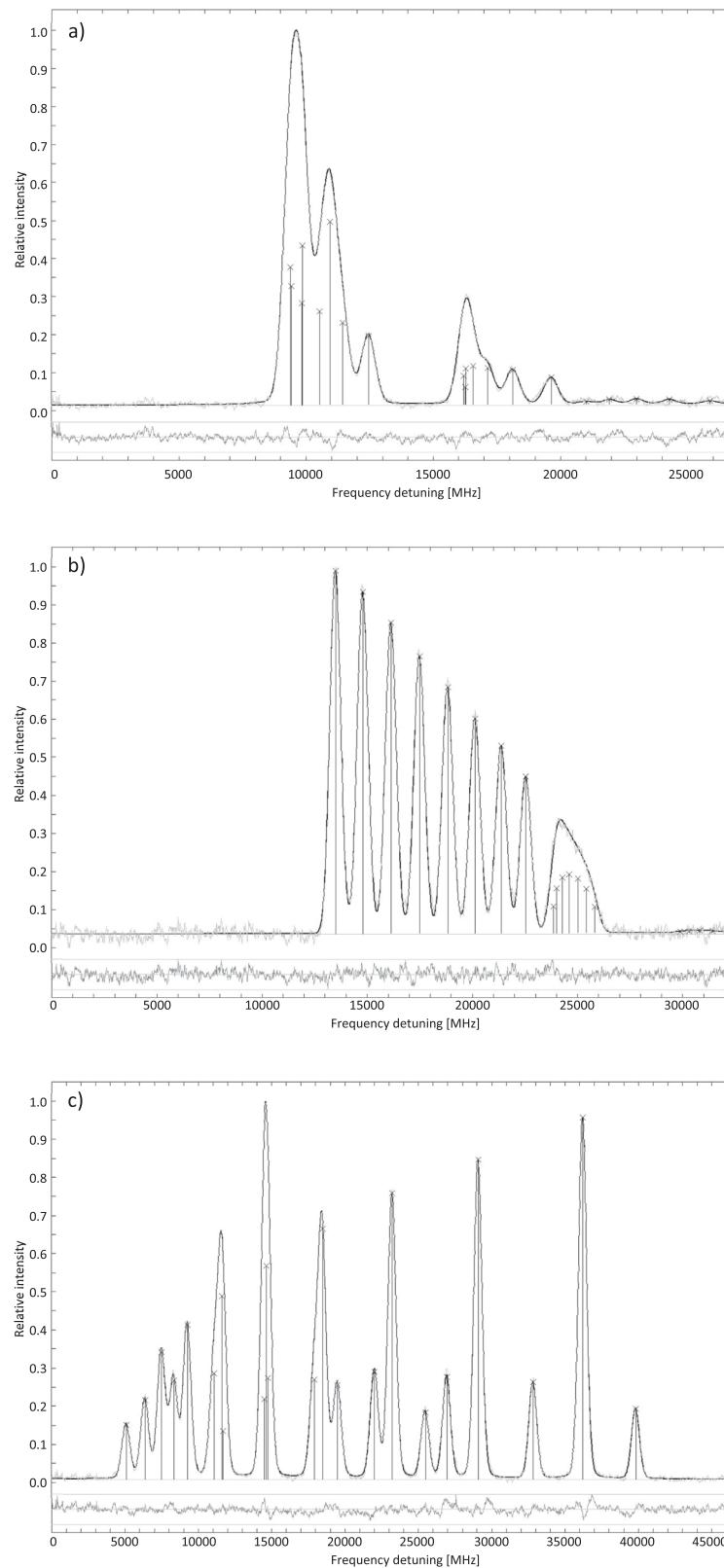
Fig. 1. Examples of the recorded *hfs* patterns of spectral lines involving new odd-parity levels in the holmium atom, along with the components fitted by program "Fitter" (marked with vertical lines): a) λ = 515.324 nm (line 54 in Table 1: 18651.53 cm^{-1}, J = 15/2 → 38051.38 cm^{-1}, J = 13/2), b) λ = 539.769 nm (line 68 in Table 1: 15130.31 cm^{-1}, J = 17/2 → 33651.60 cm^{-1}, J = 15/2), c) λ = 568.433 nm (line 80 in Table 1: 18858.19 cm^{-1}, J = 13/2 → 36445.54 cm^{-1}, J = 13/2). The lower traces, representing the deviations of the experimental data from the respective theoretical curves (scaling factors: 1.4593, 0.8755 and 1.4833, respectively), show the quality of the fit. The horizontal lines at the value of relative intensity close to 0 represent the fitted background.

Table 1

Spectral lines of the holmium atom, investigated in order to determine the hyperfine structure constants for the upper odd-parity levels with previously unknown energies, along with the values obtained. The *hfs* constants of the lower even-parity levels involved in the spectral lines were generally fixed at the available values in the least-squares fit procedure (one exception - the line λ = 613.584 nm, marked by a single asterisk, is described in Section 4). The respective citations are given in a separate column (in most cases the data origin from our earlier works on holmium [8,15,16], for the constants *B* rounded to 1 MHz, if neccecary). The energies of the lower levels were taken from the NIST Atomic Spectra Database [18], while those of the upper levels were experimentally determined in this work (for details see Section 4).

No	λ_air (nm)	k_vac (cm⁻¹)	Lower Level E (cm⁻¹)	J	A (MHz)		B (MHz)		ref.	Upper Level E (cm⁻¹)	J	A (MHz)		B (MHz)	
1	2	3	4	5	6		7		8	9	10	11		12	
1	481.761	20751.40	16154.21	15/2	903.5	(0.9)	439	(31)	[16]	36905.61	15/2	1299.0	(1.0)	−430	(35)
2	482.903	20702.32	16709.82	17/2	1139.7	(0.8)	−2045	(41)	[16]	37412.14	17/2	1126.3	(0.9)	1367	(42)
3	482.927	20701.30	13082.93	11/2	1042.2	(1.8)	2359	(8)	[8]	33784.23	13/2	796.5	(1.9)	784	(12)
4	485.155	20606.22	13082.93	11/2	1042.2	(1.8)	2359	(8)	[8]	33689.15	13/2	1257.8	(1.9)	523	(9)
5	486.415	20552.83	15081.12	13/2	891.0	(0.4)	119	(12)	[8]	35633.95	15/2	1238.2	(0.5)	1966	(13)
6	486.959	20529.86	16882.28	15/2	479.3	(1.3)	−641	(26)	[15]	37412.14	17/2	1126.2	(1.4)	1385	(58)
7	487.392	20511.64	16154.21	15/2	903.3	(0.9)	439	(31)	[16]	36665.85	15/2	1008.5	(1.0)	1374	(35)
8	487.582	20503.64	15130.31	17/2	808.5	(1.8)	2120	(27)	[8]	35633.95	15/2	1239.2	(1.9)	2006	(22)
9	488.441	20467.60	16438.01	17/2	822.0	(0.4)	2000	(19)	[8]	36905.61	15/2	1299.5	(0.5)	−784	(20)
10	489.266	20433.08	17059.35	13/2	556.1	(0.7)	−1217	(40)	[15]	37492.43	13/2	1066.6	(1.1)	220	(52)
11	490.230	20392.91	16735.95	13/2	882.7	(1.7)	−26	(30)	[16]	37128.86	13/2	845.5	(1.8)	148	(104)
12	490.823	20368.27	15130.31	17/2	808.5	(1.8)	2120	(27)	[8]	35498.58	19/2	1090.0	(1.9)	728	(28)
13	491.671	20333.14	18491.21	11/2	842.0	(2.0)	−380	(29)	[15]	38824.35	13/2	872.7	(2.1)	451	(30)
14	491.717	20331.22	18564.90	13/2	869.3	(0.3)	389	(19)	[15]	38896.12	11/2	1005.1	(0.7)	432	(37)
15	492.684	20291.33	16154.21	15/2	903.3	(0.9)	439	(31)	[16]	36445.54	13/2	1062.8	(1.0)	472	(32)
16	492.986	20278.87	12344.55	13/2	908.6	(0.6)	424	(23)	[8]	32623.42	13/2	771.8	(0.7)	1774	(24)
17	492.988	20278.82	15081.12	13/2	891.0	(0.4)	119	(12)	[8]	35359.94	13/2	620.3	(0.5)	560	(13)
18	493.459	20259.45	18564.90	13/2	869.3	(0.3)	389	(19)	[15]	38824.35	13/2	870.8	(0.5)	453	(34)
19	494.327	20223.88	15136.06	15/2	862.4	(0.6)	234	(14)	[8]	35359.94	13/2	620.0	(0.7)	573	(15)
20	495.015	20195.79	16709.82	17/2	1139.7	(0.8)	−2045	(41)	[16]	36905.61	15/2	1300.0	(0.9)	−556	(52)
21	495.121	20191.43	16937.43	11/2	1024.0	(0.6)	1883	(19)	[15]	37128.86	13/2	842.2	(0.8)	158	(25)
22	495.829	20162.61	18491.21	11/2	842.0	(2.0)	−380	(29)	[15]	38653.82	13/2	657.9	(2.1)	−591	(30)
23	497.987	20075.24	11530.56	17/2	772.8	(1.2)	1011	(20)	[8]	31605.80	19/2	1166.9	(1.3)	750	(22)
24	498.914	20037.93	18858.19	13/2	467.8	(0.9)	−3185	(41)	[16]	38896.12	11/2	1011.0	(1.0)	466	(42)
25	499.015	20033.89	18564.90	13/2	869.3	(0.3)	389	(19)	[15]	38598.79	13/2	825.6	(0.4)	−813	(22)
26	499.715	20005.82	18337.80	17/2	1104.7	(1.2)	−1782	(20)	[16]	38343.62	15/2	959.4	(1.3)	−541	(34)
27	499.803	20002.29	18651.53	15/2	865.4	(1.4)	−2670	(19)	[16]	38653.82	13/2	655.9	(1.5)	−565	(20)
28	500.613	19969.94	15081.12	13/2	891.0	(0.4)	119	(12)	[8]	35051.06	11/2	972.4	(0.5)	1218	(25)
29	500.962	19956.03	16709.82	17/2	1139.7	(0.8)	−2045	(41)	[16]	36665.85	15/2	1011.2	(0.9)	1119	(42)
30	501.182	19947.26	18651.53	15/2	865.4	(1.4)	−2670	(19)	[16]	38598.79	13/2	826.7	(1.5)	−717	(20)
31	501.260	19944.17	18564.90	13/2	869.3	(0.3)	389	(19)	[15]	38509.07	15/2	221.1	(0.4)	−1178	(20)
32	501.471	19935.77	12344.55	13/2	908.6	(0.6)	424	(23)	[8]	32280.32	11/2	587.3	(1.5)	−404	(112)
33	501.968	19916.03	11689.77	19/2	735.5	(0.8)	3022	(36)	[8]	31605.80	19/2	1167.9	(0.9)	682	(37)
34	502.570	19892.17	18337.80	17/2	1104.7	(1.2)	−1782	(20)	[16]	38229.97	17/2	243.3	(1.3)	−1275	(21)
35	503.447	19857.54	18651.53	15/2	865.4	(1.4)	−2670	(19)	[16]	38509.07	15/2	221.7	(1.5)	−1118	(20)
36	504.081	19832.57	18821.25	11/2	264.7	(0.6)	−446	(33)	[16]	38653.82	13/2	656.0	(0.7)	−695	(34)
37	505.021	19795.63	18858.19	13/2	467.8	(0.9)	−3185	(41)	[16]	38653.82	13/2	657.4	(1.0)	−630	(42)
38	505.036	19795.05	12339.04	15/2	806.7	(1.4)	−139	(19)	[8]	32134.09	15/2	545.1	(1.5)	1512	(20)
39	505.171	19789.75	9741.50	19/2	745.1	(1.4)	1747	(78)	[8]	29531.25	17/2	1218.2	(1.5)	122	(79)
40	505.453	19778.72	18564.90	13/2	869.3	(0.3)	389	(19)	[15]	38343.62	15/2	959.8	(0.4)	−750	(20)
41	505.483	19777.54	18821.25	11/2	264.7	(0.6)	−446	(33)	[16]	38598.79	13/2	826.4	(0.7)	−789	(34)
42	506.429	19740.60	18858.19	13/2	467.8	(0.9)	−3185	(41)	[16]	38598.79	13/2	828.2	(1.0)	−828	(42)
43	507.677	19692.09	18651.53	15/2	865.4	(1.4)	−2670	(19)	[16]	38343.62	15/2	959.2	(1.5)	−759	(21)
44	508.741	19650.88	18858.19	13/2	467.8	(0.9)	−3185	(41)	[16]	38509.07	15/2	224.3	(1.0)	−1225	(42)
45	509.402	19625.38	15081.12	13/2	891.0	(0.4)	119	(12)	[8]	34706.50	15/2	755.7	(1.0)	−728	(86)
46	510.390	19587.40	18756.22	15/2	852.7	(0.8)	2679	(33)	[16]	38343.62	15/2	961.4	(0.9)	−542	(36)
47	510.624	19578.44	18651.53	15/2	865.4	(1.4)	−2670	(19)	[16]	38229.97	17/2	242.6	(1.5)	−1148	(20)
48	510.682	19576.19	15130.31	17/2	808.5	(1.8)	2120	(27)	[8]	34706.50	15/2	747.9	(2.0)	−436	(45)
49	510.901	19567.81	15792.13	11/2	1026.5	(3.6)	887	(57)	[16]	35359.94	13/2	619.8	(3.7)	643	(58)
50	511.615	19540.49	13082.93	11/2	1042.2	(1.8)	2359	(8)	[8]	32623.42	13/2	771.9	(1.9)	1719	(9)
51	512.555	19504.66	15855.28	15/2	1142.4	(1.1)	−410	(35)	[16]	35359.94	13/2	622.5	(1.2)	619	(36)
52	513.033	19486.48	18564.90	13/2	869.3	(0.3)	389	(19)	[15]	38051.38	13/2	963.7	(0.4)	330	(20)
53	513.529	19467.68	16735.95	13/2	882.7	(1.7)	−26	(30)	[16]	36203.63	15/2	1045.3	(1.8)	813	(31)
54	515.324	19399.85	18651.53	15/2	865.4	(1.4)	−2670	(19)	[16]	38051.38	13/2	965.6	(1.5)	378	(20)
55	519.095	19258.93	15792.13	11/2	1026.5	(3.6)	887	(57)	[16]	35051.06	11/2	970.3	(3.7)	1200	(59)
56	519.882	19229.78	15855.28	15/2	1142.4	(1.1)	−410	(35)	[16]	35085.06	13/2	736.9	(1.2)	1197	(36)
57	520.759	19197.39	13082.93	11/2	1042.2	(1.8)	2359	(8)	[8]	32280.32	11/2	585.5	(1.9)	−418	(10)
58	520.873	19193.19	18858.19	13/2	467.8	(0.9)	−3185	(41)	[16]	38051.38	13/2	967.8	(1.0)	256	(42)
59	524.119	19074.34	18337.80	17/2	1104.7	(1.2)	−1782	(20)	[16]	37412.14	17/2	1125.1	(1.3)	1445	(24)
60	525.404	19027.68	15081.12	13/2	891.0	(0.4)	119	(12)	[8]	34108.80	11/2	885.5	(0.5)	521	(14)
61	528.091	18930.85	16154.21	15/2	903.3	(0.9)	439	(31)	[16]	35085.06	13/2	735.0	(1.0)	1240	(32)
62	531.341	18815.06	16683.52	19/2	739.7	(0.5)	3389	(12)	[8]	35498.58	19/2	1090.5	(0.6)	675	(13)
63	532.541	18772.68	15792.13	11/2	1026.5	(3.6)	887	(57)	[16]	34564.81	9/2	1216.1	(3.7)	1450	(60)
64	534.522	18703.11	15081.12	13/2	891.0	(0.4)	119	(12)	[8]	33784.23	13/2	790.3	(0.5)	787	(13)
65	537.253	18608.03	15081.12	13/2	891.0	(0.4)	119	(12)	[8]	33689.15	13/2	1254.8	(0.5)	554	(13)

Table 1 (*continued*)

	Line		Lower Level					Upper Level			
No	λ_{air} (nm)	k_{vac} (cm^{-1})	E (cm^{-1})	J	A (MHz)	B (MHz)	ref.	E (cm^{-1})	J	A (MHz)	B (MHz)
1	2	3	4	5	6	7	8	9	10	11	12
66	538.417	18567.81	18337.80	17/2	1104.7 (1.2)	−1782 (20)	[16]	36905.61	15/2	1300.0 (1.3)	−697 (25)
67	538.844	18553.09	15136.06	15/2	862.4 (0.6)	234 (14)	[8]	33689.15	13/2	1253.8 (0.7)	567 (20)
68	539.769	18521.29	15130.31	17/2	808.5 (1.8)	2120 (27)	[8]	33651.60	15/2	749.2 (1.9)	2557 (28)
69	539.937	18515.54	15136.06	15/2	862.4 (0.6)	234 (14)	[8]	33651.60	15/2	748.1 (0.7)	2476 (15)
70	545.152	18338.42	17059.35	13/2	556.1 (0.7)	−1217 (40)	[15]	35397.77	15/2	687.9 (0.8)	1712 (41)
71	545.799	18316.67	15792.13	11/2	1026.5 (3.6)	887 (57)	[16]	34108.80	11/2	884.7 (3.7)	600 (58)
72	545.846	18315.11	16735.95	13/2	882.7 (1.7)	−26 (30)	[16]	35051.06	11/2	972.1 (1.8)	1212 (32)
73	547.239	18268.49	16438.01	17/2	822.0 (0.4)	2000 (19)	[8]	34706.50	15/2	751.6 (0.5)	−320 (20)
74	554.960	18014.32	18651.53	15/2	865.4 (1.4)	−2670 (19)	[16]	36665.85	15/2	1009.8 (1.5)	1226 (20)
75	560.220	17845.19	16719.62	9/2	1209.3 (3.0)	2139 (150)	[17]	34564.81	9/2	1229.2 (3.1)	1435 (151)
76	560.575	17833.87	15855.28	15/2	1142.4 (1.1)	−410 (35)	[16]	33689.15	13/2	1256.3 (1.2)	682 (36)
77	565.656	17673.67	15136.06	15/2	862.4 (0.6)	234 (14)	[8]	32809.73	17/2	862.9 (0.9)	2712 (17)
78	566.777	17638.73	18564.90	13/2	869.3 (0.3)	389 (19)	[15]	36203.63	15/2	1044.4 (0.4)	816 (20)
79	567.241	17624.29	18821.25	11/2	264.7 (0.6)	−446 (33)	[16]	36445.54	13/2	1063.4 (0.7)	413 (34)
80	568.433	17587.35	18858.19	13/2	467.8 (0.9)	−3185 (41)	[16]	36445.54	13/2	1065.0 (1.0)	373 (42)
81	569.384	17557.98	20493.40	11/2	1012.5 (0.7)	641 (28)	[15]	38051.38	13/2	964.6 (0.8)	537 (31)
82	569.574	17552.10	18651.53	15/2	865.4 (1.4)	−2670 (19)	[16]	36203.63	15/2	1045.5 (1.5)	920 (20)
83	569.741	17546.89	22476.89	17/2	743.7 (3.0)	609 (150)	[17]	40023.78	17/2	1068.4 (3.1)	611 (151)
84	570.132	17534.94	16154.21	15/2	903.3 (0.9)	439 (31)	[16]	33689.15	13/2	1254.1 (1.0)	739 (35)
85	570.515	17523.16	22500.62	15/2	747.4 (0.8)	431 (37)	[8]	40023.78	17/2	1062.8 (0.9)	718 (45)
86	572.992	17447.41	18756.22	15/2	852.7 (0.8)	2679 (33)	[16]	36203.63	15/2	1046.3 (0.9)	740 (34)
87	573.975	17417.54	20074.89	15/2	827.6 (3.2)	1561 (40)	[16]	37492.43	13/2	1069.2 (3.3)	124 (42)
88	576.361	17345.44	18858.19	13/2	467.8 (0.9)	−3185 (41)	[16]	36203.63	15/2	1047.6 (1.1)	776 (42)
89	577.032	17325.25	20167.18	15/2	1335.9 (0.2)	1249 (5)	[15]	37492.43	13/2	1065.7 (0.3)	149 (15)
90	580.082	17234.16	20258.27	13/2	1426.8 (1.6)	1755 (70)	[8]	37492.43	13/2	1068.5 (1.7)	119 (71)
91	581.158	17202.25	20849.13	11/2	988.6 (1.7)	80 (71)	[8]	38051.38	13/2	968.5 (1.8)	358 (72)
92	582.683	17157.23	22866.55	19/2	764.7 (3.0)	954 (150)	[17]	40023.78	17/2	1068.7 (3.1)	581 (151)
93	588.681	16982.42	18651.53	15/2	865.4 (1.4)	−2670 (19)	[16]	35633.95	15/2	1241.1 (1.5)	1968 (21)
94	589.652	16954.45	15855.28	15/2	1142.4 (1.1)	−410 (35)	[16]	32809.73	17/2	864.3 (1.2)	2782 (37)
95	590.093	16941.78	16709.82	17/2	1139.7 (0.8)	−2045 (41)	[16]	33651.60	15/2	749.1 (0.9)	2477 (42)
96	591.005	16915.65	16735.95	13/2	882.7 (1.7)	−26 (30)	[16]	33651.60	15/2	749.3 (1.8)	2502 (31)
97	593.911	16832.87	18564.90	13/2	869.3 (0.3)	389 (19)	[15]	35397.77	15/2	684.7 (0.5)	1735 (37)
98	596.788	16751.72	16937.43	11/2	1024.0 (0.6)	1883 (19)	[15]	33689.15	13/2	1256.2 (0.7)	591 (24)
99	600.086	16659.67	22414.04	13/2	818.9 (0.8)	587 (35)	[8]	39073.71	15/2	887.3 (0.9)	−248 (36)
100	600.235	16655.52	16154.21	15/2	903.3 (0.9)	439 (31)	[16]	32809.73	17/2	863.1 (1.0)	2819 (32)
101	600.739	16641.55	18756.22	15/2	852.7 (0.8)	2679 (33)	[16]	35397.77	15/2	688.4 (0.9)	1640 (34)
102	602.571	16590.96	20074.89	15/2	827.6 (3.2)	1561 (40)	[16]	36665.85	15/2	1011.0 (3.3)	1131 (41)
103	603.221	16573.09	22500.62	15/2	747.4 (0.8)	431 (37)	[8]	39073.71	15/2	886.7 (0.9)	−230 (38)
104	603.703	16559.85	18491.21	11/2	842.0 (2.0)	−380 (29)	[15]	35051.06	11/2	974.6 (2.1)	1264 (30)
105	604.443	16539.58	18858.19	13/2	467.8 (0.9)	−3185 (41)	[16]	35397.77	15/2	691.0 (1.0)	1694 (45)
106	606.402	16486.16	18564.90	13/2	869.3 (0.3)	389 (19)	[15]	35051.06	11/2	970.8 (0.4)	1262 (20)
107	606.794	16475.49	15130.31	17/2	808.5 (1.8)	2120 (27)	[8]	31605.80	19/2	1167.1 (1.9)	858 (31)
108	607.126	16466.49	21584.89	13/2	1220.4 (1.5)	−681 (60)	[17]	38051.38	13/2	966.0 (1.6)	592 (62)
109	610.640	16371.72	16438.01	17/2	822.0 (0.4)	2000 (19)	[8]	32809.73	17/2	864.0 (0.5)	2710 (20)
110	610.680	16370.65	20074.89	15/2	827.6 (3.2)	1561 (40)	[16]	36445.54	13/2	1061.9 (3.3)	494 (43)
111	613.584	16293.19	18757.87	9/2	1147.6 (0.3)	316 (12)	*	35051.06	11/2	974.6 (0.2)	1299 (15)
112	614.143	16278.36	20167.18	15/2	1335.9 (0.2)	1249 (5)	[15]	36445.54	13/2	1060.5 (0.3)	372 (10)
113	616.952	16204.23	20241.31	13/2	998.0 (1.8)	270 (17)	[15]	36445.54	13/2	1065.6 (1.9)	181 (21)

* *A* and *B* constants of the lower and the upper level determined indpendently

to Ho II or Ho III spectrum). The following columns 5 and 6 include the respective *hfs* widths from [11,13] (with sign designation) and obtained in this work; since for many spectral lines the *hfs* pattern sign could not be determined from Fourier spectroscopy, differences between the literature *hfs* widths and those determined in our study were not calculated. In column 7 the observed transitions' wavenumber differences (determined in this work and those from Fourier spectroscopy) are listed. Finally, columns 8–11 contain the energies and *J* quantum number values of the assigned upper and lower levels.

Fig. 1 depicts three selected examples of the recorded *hfs* spectra of the spectral lines.

5. Discussion

Within this work altogether 35 new odd-parity levels of the holmium atom were identified, and their basic characteristics (energies and *hfs* constants) were quantitatively evaluated.

5.1. Levels' identification criteria

The minimum criteria for identification of a new upper (odd-parity) level, assumed in this work, were the following:

Table 2

Compilation of the energy values and the hyperfine structure constants A and B for the new odd-parity levels in the holmium atom investigated in this work, along with the expected fluorescence channels (the respective spectral lines and the terminating even-parity levels). In parentheses the uncertainties for the levels' energies (uncertainty of the last digit) and the *hfs* constants (uncertainty value in MHz) are quoted. The literature intensities of the fluorescence channels were taken from several sources [11,13,17,18]; these corresponded to the transitions with the literature wavelengths closest to the wavelengths observed. Some of the fluorescence channels were also observed as excitation transitions; for them the respective line numbers in Table 1 are quoted in the last column.

Upper level		*hfs* constants		Fluorescence channel			Lower level		Remarks
J	E (cm^{-1})	A (MHz)	B (MHz)	λ_{air} (nm)	k_{vac} (cm^{-1})	relative intensity	E (cm^{-1})	J	
1	2	3	4	5	6	7	8	9	10
9/2									
	34564.81(9)[a]	1222.7(6.6)[a]	1443(115)[a]*	465.378	21481.88	29	13082.93	11/2	strong
				532.541	18772.68	22	15792.13	11/2	line No 63
				560.220	17845.19	7	16719.62	9/2	line No 75
11/2									
	32280.32(3)[a]	586.4(0.9)[a]	−411(80)[a]*	432.157	23133.24	4	9147.08	13/2	
				501.471	19935.77		12344.55	13/2	line No 32
				520.759	19197.39	17	13082.93	11/2	line No 57
				581.261	17199.20	15	15081.12	13/2	
				606.327	16488.19	6	15792.13	11/2	
				656.807	15220.97	18	17059.35	13/2	
	34108.80(3)[a]	885.1(0.4)[a]	561(40)[a]	400.500	24961.72	39	9147.08	13/2	
				459.340	21764.25	10	12344.55	13/2	
				475.472	21025.87		13082.93	11/2	
				525.404	19027.68	4	15081.12	13/2	line No 60
				545.799	18316.67	7	15081.12	13/2	line No 71
	35051.06(4)[a]	972.1(0.9)[a]	1243(16)[a]	385.932	25903.98	53	9147.08	13/2	strong
				440.279	22706.51	11	12344.55	13/2	not observed
				455.077	21968.13	36	13082.93	11/2	
				500.613	19969.94	6	15081.12	13/2	line No 28
				519.095	19258.93	11	15792.13	11/2	line No 55
				545.846	18315.11	16	16735.95	13/2	line No 72
				603.703	16559.85		18491.21	11/2	line No 104
				606.402	16486.16	11	18564.90	13/2	line No 106
				613.584	16293.19	4	18757.87	9/2	line No 111
	38896.12(4)[a]	1008.0(3.0)[a]	449(17)[a]	457.815	21836.77	43	17059.35	13/2	
				491.717	20331.22	19	18564.90	13/2	line No 14
				496.429	20138.25		18757.87	9/2	not evaluated
				498.914	20037.93	7	18858.19	13/2	line No 24
13/2									
	32623.42(3)[a]	771.9(0.1)[a]	1747(28)[a]	425.841	23476.34	9	9147.08	13/2	
				492.853	20284.38		12339.04	15/2	
				492.986	20278.87	19	12344.55	13/2	line No 16
				511.615	19540.49	18	13082.93	11/2	line No 50
				569.893	17542.30	3	15081.12	13/2	not observed
				571.683	17487.36	3	15136.06	15/2	not observed
				596.204	16768.14	10	15855.28	15/2	
				607.026	16469.21	4	16154.21	15/2	not observed
	33689.15(7)[a]	1255.5(0.7)[a]	609(34)[a]	407.349	24542.07	198	9174.08	13/2	strong
				468.251	21350.11	5	12339.04	15/2	not observed
				468.372	21344.60	7	12344.55	13/2	
				485.155	20606.22		13082.93	11/2	line No 4
				537.253	18608.03	12	15081.12	13/2	line No 65
				538.844	18553.09	9	15136.06	15/2	line No 67
				560.575	17833.87	9	15855.28	15/2	line No 76
				570.132	17534.94	6	16154.21	15/2	line No 84
				596.788	16751.72	5	16937.43	11/2	line No 98
	33784.23(3)[a]	793.4(3.1)[a]	785(13)[a]*	394.255	25357.12	180	8427.11	15/2	
				405.777	24637.15	33	9147.08	13/2	
				466.175	21445.19	4	12339.04	15/2	not observed
				482.927	20701.28	21	13082.93	11/2	line No 3
				534.522	18703.11	10	15081.12	13/2	line No 64
	35085.06(3)[a]	736.0(1.0)[a]	1219(22)[a]	375.016	26657.95	38	8427.11	15/2	
				519.882	19229.78	9	15855.28	15/2	line No 56
				528.091	18930.85	9	16154.21	15/2	line No 61
	35359.94(4)[a]	620.7(0.7)[a]	599(20)[a]	371.188	26932.83	15	8427.11	15/2	not observed
				434.266	23020.90	31	12339.04	15/2	
				434.370	23015.39		12344.55	13/2	
				448.767	22277.01	8	13082.93	11/2	
				492.988	20278.82	19	15081.12	13/2	line No 17
				494.327	20223.88	7	15136.06	15/2	line No 19
				510.901	19567.81	10	15792.13	11/2	line No 49
				512.555	19504.66	6	15885.28	15/2	line No 51
	36445.54(6)[a]	1063.2(0.8)[a]	384(46)[a]	366.217	27298.46	150	9147.08	13/2	strong
				414.709	24106.50		12339.04	15/2	
				414.804	24100.99		12344.55	13/2	

Table 2 (continued)

J	E (cm⁻¹)	A (MHz)	B (MHz)	λ_air (nm)	k_vac (cm⁻¹)	relative intensity	E (cm⁻¹)	J	Remarks
	Upper level			Fluorescence channel			Lower level		
		hfs constants							
1	2	3	4	5	6	7	8	9	10
				467.937	21364.42	4	15081.12	13/2	
				469.143	21309.48	7	15136.06	15/2	
				484.046	20653.41		15792.13	11/2	not observed
				492.684	20291.33	8	16154.21	15/2	line No 15
				567.241	17624.29		18821.25	11/2	line No 79
				568.433	17587.35	3	18858.19	13/2	line No 80
				610.680	16370.65		20074.89	15/2	line No 110
				614.143	16278.36		20167.18	15/2	line No 112
				616.952	16204.23	11	20241.31	13/2	line No 113
	37128.86(3)ᵃ	843.9(1.7)ᵃ	153(76)ᵃ*	403.367	24784.31	15	12344.55	13/2	
				453.434	22047.74		15081.12	13/2	
				454.567	21992.80		15136.06	15/2	
				468.544	22047.74	4	15792.13	11/2	not observed
				469.935	21273.58	5	15855.28	15/2	not observed
				490.230	20392.91	6	16735.95	13/2	line No 11
				495.121	20191.43	13	16937.43	11/2	line No 21
	37492.43(6)ᵃ	1067.5(0.9)ᵃ	153(24)ᵃ	409.561	24409.50	7	13082.93	11/2	not observed
				447.174	22356.37	5	15136.06	15/2	
				462.039	21637.15	21	15855.28	15/2	strong
				468.512	21338.22	39	16154.21	15/2	strong
				489.266	20433.08	8	17059.35	13/2	line No 10
				573.975	17417.54	6	20074.89	15/2	line No 87
				577.032	17325.25		20167.18	15/2	line No 89
				580.082	17234.16	8	20258.27	13/2	line No 90
	38051.38(2)ᵃ	966.0(0.8)ᵃ	409(53)ᵃ	388.808	25712.34	3	12339.04	15/2	strong
				449.125	22259.25		15792.13	11/2	
				476.238	20992.03	6	17059.35	13/2	strong
				511.101	19560.17		18491.21	11/2	
				513.033	19486.48	14	18564.90	13/2	line No 52
				515.324	19399.85	31	18651.53	15/2	line No 54
				519.873	19230.13	11	18821.25	11/2	
				520.873	19193.19	8	18858.19	13/2	
				556.128	17976.49	8	20074.89	15/2	
				558.998	17884.19	17	20167.18	15/2	
				569.384	17557.98		20493.40	11/2	line No 81
				581.158	17202.24	3	20849.13	11/2	line No 91
				587.845	17006.56		21044.81	13/2	
				607.126	16466.49		21584.89	13/2	line No 108
	38598.79(3)ᵃ	826.7(0.6)ᵃ	−787(25)ᵃ	380.703	26259.75		12339.04	15/2	
				391.802	25515.86	7	13082.93	11/2	
				425.093	23517.67		15081.12	13/2	
				438.345	22806.66	11	15792.13	11/2	
				460.350	21716.51	6	16882.28	15/2	
				497.186	20107.58	5	18491.21	11/2	
				499.015	20033.89	8	18564.90	13/2	line No 25
				501.182	19947.26	6	18651.53	15/2	line No 30
				505.483	19777.54	6	18821.25	11/2	line No 41
				506.429	19740.60	16	18858.19	13/2	line No 42
	38653.82(4)ᵃ	656.8(0.6)ᵃ	−620(29)ᵃ	495.829	20162.61	6	18491.21	11/2	line No 22
				499.803	20002.29	7	18651.53	15/2	line No 27
				504.081	19832.57	12	18821.25	11/2	line No 36
				505.021	19795.63	46	18858.19	13/2	line No 37
	38824.35(4)ᵃ	872.0(1.0)ᵃ	452(33)ᵃ*	377.461	26485.31	48	12339.04	15/2	
				491.671	20333.14	5	18491.21	11/2	line No 13
				493.459	20259.45	9	18564.90	13/2	line No 18
15/2									
	32134.09(4)ᵇ	545.1(3.5)ᵇ	1512(131)ᵇ	421.698	23706.98	53	8427.11	15/2	
				434.906	22987.01	23	9147.08	13/2	not observed
				505.036	19795.05	22	12339.04	15/2	line No 38
				505.177	19789.54		12344.55	13/2	
	33651.60(7)ᵃ	748.9(0.3)ᵃ	2503(19)ᵃ	469.197	21307.05	146	12344.55	13/2	
				590.093	16941.78	6	18858.19	13/2	line No 95
				591.005	16915.65	55	18858.19	13/2	line No 96
	34706.50(5)ᵃ	751.7(2.3)ᵃ	−495(122)ᵃ	379.722	26327.59		8378.91	17/2	
				509.402	19625.38		15081.12	13/2	line No 45
				510.682	19576.19	26	15130.31	17/2	line No 48
				530.322	18851.22		15855.28	15/2	not evaluated
				547.239	18268.49	49	16438.01	17/2	line No 73
	35397.77(4)ᵃ	688.0(1.3)ᵃ	1695(21)ᵃ	370.007	27018.86	76	8378.91	17/2	
				545.152	18338.42	17	17059.35	13/2	line No 70
				593.911	16832.87		18564.90	13/2	line No 97
				600.739	16641.55	15	18756.22	15/2	line No 101

Table 2 (*continued*)

Upper level		hfs constants		Fluorescence channel			Lower level		Remarks
J	E (cm^{-1})	A (MHz)	B (MHz)	λ_{air} (nm)	k$_{vac}$ (cm^{-1})	relative intensity	E (cm^{-1})	J	
1	2	3	4	5	6	7	8	9	10
				604.442	16539.58		18858.19	13/2	line No 105
	35633.95(6)[a]	1239.5(0.9)[a]	1980(14)[a]	366.800	27255.04		8378.91	17/2	
				367.450	27206.84	21	8427.11	15/2	strong
				377.438	26486.87		9147.08	13/2	strong
				429.158	23289.40	7	12339.04	15/2	
				486.415	20552.83		15081.12	13/2	line No 5
				487.582	20503.64	10	15130.31	17/2	line No 8
				538.220	18574.60	9	17059.35	13/2	
				588.681	16982.42	8	18651.53	15/2	line No 93
				595.933	16775.76	8	18858.19	13/2	not evaluated
	36203.63(3)[a]	1045.8(0.6)[a]	813(31)[a]	418.913	23864.59	72	12339.04	15/2	strong
				419.010	23859.08	13	12344.55	13/2	strong
				513.530	19467.68	7	16735.95	13/2	line No 53
				566.777	17638.73		18564.90	13/2	line No 78
				569.574	17552.10	4	18651.53	15/2	line No 82
				572.992	17447.41		18756.22	15/2	line No 86
				576.361	17345.44		18858.19	13/2	line No 88
	36665.85(7)[a]	1009.9(0.7)[a]	1212(59)[a]	363.285	27518.77		9147.08	13/2	
				397.734	25135.29		11530.56	17/2	
				411.046	24321.30	18	12344.55	13/2	
				463.161	21584.73		15081.12	13/2	strong
				480.391	20810.57	22	15855.28	15/2	strong
				487.392	20511.64	7	16154.21	15/2	line No 7
				500.962	19956.03	18	16709.82	17/2	line No 29
				554.960	18014.32	9	18651.53	15/2	line No 74
				602.571	16590.96	11	20074.89	15/2	line No 102
	36905.61(5)[a]	1299.6(0.3)[a]	−617(78)[a]	393.976	25375.05	6	11530.56	17/2	strong
				406.942	24566.57	24	12339.04	15/2	strong
				459.229	21769.55	8	15136.06	15/2	
				474.919	21050.33	43	15855.28	15/2	strong
				481.761	20751.40	29	16154.21	15/2	line No 1
				488.441	20467.60	9	16438.01	17/2	line No 9
				495.015	20195.79	85	16709.82	17/2	line No 20
				538.417	18567.81	106	18337.80	17/2	line No 66
	38343.62(4)[a]	960.0(0.5)[a]	−648(62)[a]	384.439	26004.58		12339.04	15/2	
				384.520	25999.07		12344.55	13/2	
				429.756	23262.50	8	15081.12	13/2	strong
				430.666	23213.31		15130.31	17/2	
				430.773	23207.56	4	15136.06	15/2	
				462.110	21633.80	6	16709.82	17/2	strong
				462.669	21607.67	6	16735.95	13/2	
				465.824	21461.34	23	16882.28	15/2	not observed
				469.699	21284.27		17059.35	13/2	strong
				499.715	20005.82	11	18337.80	17/2	line No 26
				505.453	19778.72		18564.90	13/2	line No 40
				507.677	19692.09		18651.53	15/2	line No 43
				510.390	19587.40		18756.22	15/2	line No 46
	38509.07(4)[a]	222.0(1.0)[a]	−1174(31)[a]	370.560	26978.51	3	11530.56	17/2	strong
				382.008	26170.03		12339.04	15/2	
				382.089	26164.52		12344.55	13/2	
				462.260	21626.79		16882.28	15/2	
				466.076	21449.72		17059.35	13/2	
				495.616	20171.27		18337.80	17/2	
				501.260	19944.17		18564.90	13/2	line No 31
				503.447	19857.58	62	18651.53	15/2	line No 35, strong
				508.741	19650.88		18756.22	15/2	line No 44, strong
	39073.71(3)[a]	887.0(0.3)[a]	−239(37)[a]*	417.634	23937.65	38	15136.06	15/2	strong
				600.086	16659.67		22414.04	13/2	line No 99
				602.358	16596.90		22476.89	17/2	
				603.221	16573.09		22500.62	15/2	line No 103
17/2									
	29531.25(3)[b]	1218.2(3.0)[b]	122(182)[b]	473.708	21104.14	58	8427.11	15/2	strong
				505.171	19789.75	23	9741.50	19/2	line No 39
	32809.73(2)[a]	863.6(0.4)[a]	2756(27)[a]	409.204	24430.82	78	8378.91	17/2	strong
				410.012	24382.62	174	8427.11	15/2	strong

Table 2 (*continued*)

Upper level		hfs constants		Fluorescence channel			Lower level		Remarks
J	E (cm^{-1})	A (MHz)	B (MHz)	λ_{air} (nm)	k_{vac} (cm^{-1})	relative intensity	E (cm^{-1})	J	
1	2	3	4	5	6	7	8	9	10
				433.375	23068.23	8	9741.50	19/2	
				469.812	21279.17		11530.56	17/2	
				565.656	17673.67	23	15136.06	15/2	line No 77
				589.652	16954.45	4	15855.28	15/2	line No 94
				600.235	16655.52	25	16154.21	15/2	line No 100
				610.640	16371.72	172	16438.01	17/2	line No 109, strong
				619.937	16126.21	15	16683.52	19/2	
	37412.14(7)[a]	1125.9(0.4)[a]	1399(24)[a]	361.291	27670.64		9741.50	19/2	
				386.266	25881.58		11530.56	17/2	strong
				388.657	25722.37		11689.77	19/2	strong
				398.721	25073.10		12339.04	15/2	strong
				448.786	22276.08		15136.06	15/2	
				463.760	21556.86	15	15855.28	15/2	strong
				470.281	21257.93		16154.21	15/2	
				482.903	20702.32		16709.82	17/2	line No 2
				486.959	20529.86		16882.28	15/2	line No 6
				511.928	19528.57		17883.57	19/2	
				524.119	19074.34	40	18337.80	17/2	line No 59, strong
				532.883	18760.61	4	18651.53	15/2	not observed
	38229.97(1)[a]	243.0(0.4)[a]	−1212(64)[a]	374.434	26699.41	17	11530.56	17/2	
				432.785	23099.66	4	15130.31	17/2	not observed
				446.808	22374.69	11	15855.28	15/2	
				452.859	22075.76	6	16154.21	15/2	
				458.756	21791.96	4	16438.01	17/2	not observed
				464.551	21520.15	12	16709.82	17/2	
				468.304	21347.69	115	16882.28	15/2	
				502.570	19892.17	23	18337.80	17/2	line No 34
				510.624	19578.44		18651.53	15/2	line No 47
	40023.78(5)[a]	1067.0(2.0)[a]	637(42)[a]	401.598	24893.47	193	15130.31	17/2	strong
				569.744	17546.89	3	22476.89	17/2	line No 83
				570.515	17523.14		22500.62	15/2	line No 85
				582.683	17157.23	22	22866.55	19/2	line No 92
19/2									
	31605.80(2)[a]	1167.3(0.4)[a]	763(52)[a]	497.987	20075.24		11530.56	17/2	line No 23
				501.968	19916.03	28	11689.77	19/2	line No 33
				606.794	16475.49	100	15130.31	17/2	line No 107, strong
	35498.58(2)[a]	1090.2(0.3)[a]	702(27)[a]	417.105	23968.02	26	11530.56	17/2	strong
				490.823	20368.27	7	15130.31	17/2	line No 12
				531.341	18815.06	6	16683.52	19/2	line No 62

[a] Energies and hfs constants determined as the averages from all the hitherto investigated lines
[b] Energies and hfs constants determined from single lines * Uncertainties for the hfs constants B calculated on the basis of the uncertainties for individual spectral lines; for details see text (Section 4)

- at least one excitation transition from a lower level with known energy and previously determined hfs constants A and B to the upper level in question could be quantitatively investigated,
- the total hfs pattern width of the respective spectral line (calculated from the constants A and B of both levels involved) proved consistent with the hfs reported for the corresponding unclassified spectral line on the basis of Fourier spectroscopic investigations,
- at least one additional fluorescence channel could be unambiguously established in the spectral region currently accessible for our detection system (monochromator for fluorescence wavelength selection and photomultiplier), i.e. from near UV to IR.

Of course multiple excitation possibilities and multiple fluorescence channels were always sought, and the mutual consistency of the hfs constants determined from the analysis of various transitions was checked.

33 levels were investigated in multiple spectral lines and the data obtained can be considered fully reliable within the estimated uncertainty limits.

Two levels: 32134.04 cm^{-1} ($J = 15/2$) and 29531.25 cm^{-1} ($J = 17/2$) were quantitatively investigated in single lines only. In these cases other excitation lines within the spectral range accessible at the time of realization of the experiment proved very weak, but observed fluorescence channels were strong and unequivocal; thus the existence of these levels is certainly undoubtful and their energies are correct to the accuracy quoted. The total hfs patterns widths of the investigated spectral lines proved fairly consistent with Fourier spectroscopic values [13], and we believe that also the hfs constants of the levels mentioned are correct. Nevertheless, if other laser excitation options become possible (after any extension of the accessible laser light spectral region), measurements aimed at confirmation of the results hitherto obtained are planned.

5.2. Fluorescence channels

For the majority of levels numerous fluorescence channels (some of them observed also as excitation transitions) could be tested. For many levels 8–10 fluorescence transitions could be confirmed, and for the level 38051.38 cm^{-1} ($J = 13/2$) altogether 14 channels were observed, out of which 5 were additionally verified in direct excitation.

In some cases the number of the spectral lines, that could be assigned to particular levels beyond doubt, was lower. This occurred in particular in the cases where one of the decay channels from the level examined proved particularly strong, which re-

sulted in necessarily much lower decay probabilities for other possible channels. In such cases the sensitivity of our fluorescence detection system often did not allow observation of those weak fluorescence lines. This was for instance the case for the level 29531.25 cm^{-1} ($J = 17/2$). Also the fluorescence channels in UV, with wavelengths below ca. 360 nm, were beyond the detection capabilities of our experimental setup, because of the spectral limits of the monochromator applied.

5.3. Hyperfine structure constants

In most cases the *hfs* constants for obtained from the analysis of various transitions proved mutually consistent, at least within the maximum statistical uncertainty limits. Several exceptions were noted, where the differences between the extreme values slightly exceeded the sum of their statistical errors, indicating the possible influence of some systematic factors. This concerned mainly the constants *B*; as is customary in the holmium atom, these exhibit rather large scattering (the probable reasons were discussed in our earlier works concerning this element).

6. Conclusions

Within this work 35 odd-parity electronic levels in the holmium atom with hitherto unknown energies, ranging from ca. 30000 cm^{-1} to ca. 40000 cm^{-1}, were identified, on the basis of investigations on 113 direct excitation transitions with the method of laser induced fluorescence in a hollow cathode discharge. For most of the levels examined numerous fluorescence channels, spectrally selected in the experiment, could be observed.

The method of searching for the new levels applied in the present work, based on finding coincidences between the wavenumbers of the unclassified spectral lines and the possible energy differences between the hypothetic upper and the known lower levels, and their subsequent experimental verification, proved so far reasonably efficient. However, the selected most probable options were hitherto tested, where the expected estimated energies of the new levels were obtained from the largest numbers of coincidences. Since the numbers of coincidences indicating the energies of still further new levels are smaller and will gradually decrease in the course of experiments, the increasing probability of accidental coincidences will have to be taken into account. On the other hand, the increasing number of the electronic levels with known parameters will make the cases where both the levels involved in an unclassified line are known levels, which can possibly be recognized on the basis of their hyperfine structures.

For the newly identified levels the *hfs* constants *A* and *B* were evaluated. For the majority of the levels, which were investigated in more than one spectral line each, the values evaluated from the analysis of individual lines proved generally mutually consistent, which constitutes an additional confirmation of the correctness of the determined levels' properties. Two levels could so far be directly excited in single transitions only (although of course fluorescence channels other than excitation transitions were observed); for these levels further investigation possibilities will be searched for.

The results concerning the newly identified odd-parity levels in the holmium atom were exploited in classification of 256 spectral lines of atomic holmium; this number includes both the lines observed as direct excitation transitions and those observed as fluorescence channels from the new levels. Moreover, the data were already included in the semi-empirical analysis of the fine- and the hyperfine structure of the odd-parity level system, carried out in

our research group; it seems that their inclusion helped to solve some of the previously encountered problems, and the final results are expected in the near future.

Supplementary material

Supplementary material associated with this article can be found, in the online version, at doi:10.1016/j.jqsrt.2019.06.005

References

[1] Saffman M, Mølmer K. Scaling the neutral-atom Rydberg gate quantum computer by collective encoding in holmium atoms. Phys Rev A 2008;78:012336.

[2] Miao J, Hostetter J, Stratis G, Saffman M. Magneto-optical trapping of holmium atoms. Phys Rev A 2014;89:041401.

[3] McClelland JJ, Hanssen JL. Laser cooling without repumping: a magneto-optical trap for erbium atoms. Phys Rev Lett 2006;96:143005.

[4] Cingöz A, Lapierre A, Nguyen A-T, Leefer N, Budker D, Lamoreaux SK, et al. Limit on the temporal variation of the fine-structure constant using atomic dysprosium. Phys Rev Lett 2007;98:040801.

[5] Leefer N, Weber CTM, Cingöz A, Torgerson JR, Budker D. New limits on variation of the fine-structure constant using atomic dysprosium. Phys Rev Lett 2013;111:060801.

[6] Dzuba VA, Flambaum VV. Relativistic corrections to transition frequencies of Ag I, Dy I, Ho I, Yb II, Yb III, Au I, and Hg II and search for variation of the fine-structure constant. Phys Rev A 2008;77:012515.

[7] Stefanska D, Furmann B. Hyperfine structure investigations for the odd-parity configuration system in atomic holmium. J Quant Spectrosc Radiat Transf 2018;206:286–95.

[8] Stefanska D, Ruczkowski J, Elantkowska M, Furmann B. Fine- and hyperfine structure investigations of the even-parity configuration system in atomic holmium. J Quant Spectrosc Radiat Transf 2018;209:180–95.

[9] Stefanska D, Werbowy S, Krzykowski A, Furmann B. Lande g_j factors for even–parity electronic levels in the holmium atom. J Quant Spectrosc Radiat Transf 2018;210:136–40.

[10] Furmann B, Stefańska D, Suski M, Wilman S, Chomski M. Hyperfine structure studies of the odd-parity electronic levels in the holmium atom. I: levels with known energies. J Quant Spectrosc Radiat Transf 2019;234:115–23.

[11] Al-Labady N, Özdalgiç B, Er A, Güzelçimen F, Öztürk IK, Kröger S, et al. Line identification of atomic and ionic spectra of holmium in the near-UV. Part I. spectrum of Ho I. Astrophys J Suppl Ser 2017;228(2):16.

[12] Başar G, Al-Labady N, Özdalgiç B, Güzelçimen F, Er A, Öztürk IK, et al. Line identification of atomic and ionic spectra of holmium in the near-UV. II. spectra of Ho II and Ho III. Astrophys J Suppl Ser 2017;228(2):17.

[13] Özdalgiç B, Güzelçimen F, Öztürk IK, Kröger S, Kruzins A, Tamanis M, et al. Line identification of atomic and ionic spectra of holmium in the visible spectral range. i. spectrum of ho i. Astrophys J Suppl Ser 2019;240(2):27.

[14] Özdalgiç B, Başar G, Güzelçimen F, Öztürk IK, Ak T, Bilir S, et al. Line identification of atomic and ionic spectra of holmium in the visible spectral range. II. spectrum of Ho II and Ho III. Astrophys J Suppl Ser 2019;240(2):28.

[15] Stefanska D, Furmann B, Głowacki P. Possibilities of investigations of the temporal variation of the α constant in the holmium atom. J Quant Spectrosc Radiat Transf 2018;213:159–68.

[16] Furmann B, Stefanska D, Suski M, Wilman S. Identification of new electronic levels in the holmium atom and investigation of their hyperfine structure. J Quant Spectrosc Radiat Transf 2018;219:117–26.

[17] Wyart J-F, Camus P, Vergès J. Etude du spectre de l'holmium atomique: I. Spectre d'émission infrarouge niveaux d'énergie de Ho I et structures hyperfines. Physica C 1977;92(3):377–96.

[18] Kramida A, Yu Ralchenko, Reader J, NIST ASD Team. NIST Atomic Spectra Database (ver. 5.5.1). Gaithersburg, MD: National Institute of Standards and Technology; 2017. [2017] [Online]. Available: http://physics.nist.gov/asd.

Investigations of the possible second-stage laser cooling transitions for the holmium atom magneto-optical trap

D. Stefańska [a],[*], B. Furmann [a], J. Ruczkowski [b], M. Elantkowska [a], P. Głowacki [a], M. Chomski [a], M. Suski [a], S. Wilman [a]

[a] *Institute of Materials Research and Quantum Engineering, Faculty of Technical Physics, Poznan University of Technology, Piotrowo 3, Poznan 60-965, Poland*
[b] *Institute of Control, Robotics and Information Engineering, Faculty of Electrical Engineering, Poznan University of Technology, Piotrowo 3A, Poznan 60-965, Poland*

ARTICLE INFO

ABSTRACT

In this work laser-spectroscopic investigations of selected electronic levels in the holmium atom are performed in the context of possible second-stage laser cooling transitions which can be considered in a magneto-optical trap. Five transitions were directly recorded by the method of laser induced fluorescence in a hollow cathode discharge. The hyperfine structure constants A and B for the upper even-parity $J = 17/2$ levels, evaluated in earlier works, were generally confirmed, and their accuracy was improved; thus the frequency differences between the hyperfine structure components, relevant for the possibility of application of the hyperfine repumping, could be determined. Investigations of the Zeeman-hyperfine structure of these spectral lines were performed in order to evaluate the Landé g_J factors of the upper levels; these were reported for the first time. Semi-empirical preliminary calculations of the lifetimes of the even-parity levels in question were also carried out, allowing estimation of the expected Doppler limits for the possible narrow-band laser cooling at the respective transitions. The degree of similarity between the g_J factors of the upper levels of the cooling transitions and the ground state is important for the efficiency of the sub-Doppler laser cooling in a magneto-optical trap. The results presented might facilitate the choice of the most favorable option of obtaining narrow-band laser cooling of the holmium atoms.

© 2020 Elsevier Ltd. All rights reserved.

1. Introduction

Holmium is an element belonging to the heavier ones in the lanthanide series, with more than half-filled 4f electronic shell. Its single stable isotope $^{165}_{67}$HO possesses a relatively high nuclear spin $I = 7/2$ and is characterized with a particularly rich structure of its electronic levels; for instance the holmium atom has an exceptionally high number of the hyperfine Zeeman sublevels in its ground state with $J = 15/2$: $(2J + 1) \times (2I + 1) = 128$, which is the highest number for any stable isotope. Moreover, large nuclear moments' values (the magnetic dipole moment amounts to $\mu = 4.17(3)\mu_N$, and the electric quadrupole moment range between 2.716-3.6 barn are reported [1]) yield very large hyperfine splittings of the electronic levels, the ground state included. Due to these particular features the atomic holmium has recently attracted much attention as a possible candidate for important applications in quantum engineering and metrology.

Already a decade ago a proposal of application of the Ho I ground state Zeeman sublevels for collective encoding of qubits in quantum registers [2] was put forward. Another possible application, proposed in [3], concerned the possible use of nearly degenerate pairs of electronic levels for the measurement of the temporal variation of the fine structure constant α (in our earlier work [4] a proposal of experimental realization of this concept, similar to the experiment successfully run on dysprosium for over a decade [5,6], was presented). Also the idea of searching for the possibility of achieving electromagnetically induced negative refraction as a result of coherent excitation of nearly degenerate electric dipole and magnetic dipole transitions (as originally proposed in [7,8]) was considered for the holmium atom.

The idea of Saffman and Mølmer [2] strongly inspired the efforts towards laser cooling of this element in a magneto-optical trap (MOT) with the use of the method developed for the lanthanide elements [9] (a brief review is given below); cooling of holmium at the first-stage transition was achieved a few years ago [10] by the same research group. Because of the apparent similarity of Landé g_J factors of the upper and the lower level, an efficient

polarization gradient cooling in MOT could also be applied and the temperatures down to below 100 μK, considerably lower than the Doppler limit of the cooling transition (780 μK), were achieved (sub-Doppler cooling). Nevertheless, still further cooling with application of a selected second-stage narrow-line cooling transition might greatly facilitate practical realization of the proposed encoding of *hfs*-Zeeman qubits [2], as well as other possible applications.

Application of the second-stage cooling transitions, with Doppler limits lower than for the first-stage transition, would be strongly desirable. The transitions proposed in [10] are dispersed over very broad spectral region, from violet (close to the first-stage transition) to the near IR. So far this research group reported some progress on further narrow-line cooling [11,12]. However, transitions with lower expected Doppler limits might prove more favorable.

The knowledge of the explicit structure of a particular spectral line is a prerequisite of its possible application for laser cooling; this requires prior spectroscopic studies with relatively high resolution. In the present work the hyperfine structure patterns of 5 possible second-stage cooling transitions (4 of them proposed in [10] - No 3-6) were analyzed on the basis of the experimental studies performed by the method of laser induced fluorescence (LIF) in a hollow cathode discharge. Also investigations of the g_J factors of the upper levels involved in the transitions studied were performed. Moreover, a semi-empirical analysis of the oscillator strengths of the spectral lines yielded some preliminary predictions concerning the lifetimes of the levels in question; the analysis is still in progress and will be reported separately [13].

2. Fundamentals of laser cooling of atomic holmium

In the holmium atom the main first-stage cooling transition already utilized is the hyperfine structure component $F = 11 \rightarrow F' = 12$ of the line $4f^{11}6s^2$ $^4I^o_{15/2} \rightarrow 4f^{11}6s6p$ (15/2, 1), $J = 17/2$ - 24360.81 cm^{-1}. The wavelength amounts to $\lambda = 410.384$ nm, and the Doppler limit of 780 μK results from the natural transition linewidth. The experimental value of g_J factor of the upper level is not known, but some theoretical predictions are available [14–16], very similar to the Landé g_J factor of the ground state; this allowed for efficient sub-Doppler polarization gradient cooling also in relatively strong magnetic fields, and achieving the MOT temperature well below the Doppler limit.

Altogether 8 possible second-stage cooling transitions were proposed [10], 6 of them being closed cycling transitions. According to some conference contributions of the same research group [11,12], laser cooling at the $\lambda = 412.020$ nm transition, with a Doppler limit of 55 μK, is currently being developed. However, neither of the longer-wavelength transitions, with lower expected Doppler limits, has been realized until now.

Generally all the transitions from the ground state to the even-parity $J = 17/2$ levels with energies lower than the value already mentioned can be considered as possible candidates for the second-stage cooling transitions. There are, however, some practical reasons for exclusion of some options. In particular, the lowest-lying odd-parity level with $15/2 \leq J \leq 19/2$ has the energy of 18572.28 cm^{-1}, and for all the considered possible cooling transitions to the even-parity levels positioned higher than that the relative probabilities of the optical leaks have to be taken into account. If a particular candidate cooling transition is not strong itself, this issue might be critical.

There are 5 known (i.e. experimentally observed) even-parity $J = 17/2$ levels with energies between 18572.28 cm^{-1} and 24360.81 cm^{-1}: 20498.73 cm^{-1}, 20568.63 cm^{-1}, 22476.89 cm^{-1}, 23498.57 cm^{-1} and 24263.96 cm^{-1}; the last two were already considered in [10] in the context of the second-stage cooling of atomic holmium, and tests of the very last option were reported [11,12].

At a first glance this seems to be a rather demanding scheme, since the transition involves a two-electron change (f $\rightarrow$ d, s $\rightarrow$ d) in the SL-coupling scheme approximation; however, the experimentally observed spectral line is quite strong, as reported in the NIST database [17]. Among the levels not considered in [10], 20498.73 cm^{-1} and 22476.89 cm^{-1} are also involved in two-electron change transitions, which are not present in the NIST compilation and thus are probably very weak. On the other hand, the transition to the level 20568.63 cm^{-1} (a one-electron change transition) is reported in [17], with moderate intensity.

3. Experimental details

Within this work experimental investigations of the *hfs* of 5 selected spectral lines of the holmium atom, possibly applicable as second-stage narrow-line laser cooling transitions in MOT, were performed. Moreover, Landé g_J factors of the upper even-parity $J = 17/2$ levels involved in these transitions were evaluated on the basis of investigations of magnetic splittings in the hyperfine structure.

The investigations of the *hfs* applied the same experimental method and setup as in the authors' recent works concerning the odd-parity levels [16] and the even-parity levels [18] in the holmium atom, where the general description was provided and the conditions specific for holmium hollow cathode discharge were presented; the reader is referred there for details. In the following text only a brief overview is given.

The method applied was laser induced fluorescence (LIF) in a hollow cathode discharge with spectral selection of the fluorescence channels (decay transitions from the upper level), performed with the use of a monochromator. Since the transitions investigated were cycling (in one case almost cycling), no other direct fluorescence channels than the transitions back to the ground state were available; these could not be used for observation of LIF signal due to the relatively high level of the scattered laser light. Instead, collisional fluorescence channels, resulting from an exchange of the laser excited population of the upper levels involved in the transitions with other electronic levels of comparable energies (the issue of collisional fluorescence channels was discussed in more detail in one of our recent works [19]).

As the source of exciting radiation cw tunable single mode lasers were used, covering the spectral region ca. 480-680 nm (modified Coherent, model CR 699-21, or its self-assembled variant with shortened resonator).

The most long-wavelength line No 1, positioned in the red spectral region ($\lambda = 660.747$ nm, upper level 15130.31 cm^{-1}), was examined with the laser operated on the dye DCM. Two subsequent lines: No 2 ($\lambda = 608.179$ nm, upper level 16438.01 cm^{-1}) and 3 ($\lambda = 598.285$ nm, upper level 16709.82 cm^{-1}) in the yellow-orange region were excited by a Rhodamine 6G laser. Both the long wavelength dyes were optically pumped by a frequency doubled Nd:YVO$_4$ laser, Coherent model Verdi V-10. For excitation of line No 4 in the green-yellow region ($\lambda = 545.190$ nm, upper level 18337.80 cm^{-1}) an energy transfer dye laser (ETDL) on the mixture of Coumarin 498 (donor) and Pyrromethene 556 (acceptor), optically pumped by a diode laser [20], was applied. For the last line No 5 in the blue-green region ($\lambda = 486.039$ nm, upper level 20568.63 cm^{-1}) a Coumarin 498 dye laser, also optically pumped by a diode laser [21], was used. As expected, no signal at the transition to the upper level 20498.73 cm^{-1} at $\lambda = 487.699$ nm could be detected. The transition to the upper level 22476.89 cm^{-1} at $\lambda = 444.777$ nm is outside the spectral region currently accessible with our lasers; the same applies to the IR transitions proposed in [10].

Intensity modulation of the laser beam and phase-sensitive detection of the resulting fluorescence were applied.

A frequency marker signal (FSR ≈ 1500 MHz, wavelength-corrected) was recorded, which facilitated construction of the relative frequency scale for the spectra. The wavenumbers of the spectral lines excited were determined with the use of a wavemeter (Burleigh, model WA-1500). The procedure involves a direct measurement at the beginning of each scan and a further determination of the center of gravity of the line in the least-squares fitting program.

Modification of the experimental setup adequate for investigations of the Zeeman-*hfs* splittings were essentially described in our earlier work on g_J factors for holmium atom even-parity levels [22].

A pair of permanent magnets was placed in the proximity of the hollow cathode discharge lamp, providing a moderately uniform magnetic field of the flux of ca. 600 Gs along the interaction path with the exciting laser beam. The magnitude of the magnetic field was calibrated by recording several spectral lines in argon (which is a buffer gas used in the discharge), each involving both electronic levels with precisely known g_J factors; the calibration lines were distributed over the total spectral range covered in the investigations performed.

Distinction between the Zeeman σ and π components was achieved by the control of the exciting laser light polarization. The degree of linear polarization of the laser beams exiting the dye lasers used was found quite high (in all cases exceeding 99.8 %), but nevertheless polarization was further improved with the use of a polarizing prism. Linear polarization perpendicular or parallel to the magnetic field direction is required in order to select σ and π components, respectively. Both polarization orientations could be obtained with the use of a broad-band polarization rotator. Unfortunately, minor parasitic admixtures of the orthogonal polarization were still found in the spectra, probably due to the reflections of the exciting laser beam on the hollow cathode discharge lamp windows; these admixtures were accounted for in the fitting procedure of the spectra.

The magnetic flux observed for the π components was by ca. 5 % lower than for the σ components, most likely due to the minor shift of the exciting laser beam path through the discharge.

Typically 10-20 frequency scans were recorded for each transition, dependent on the observed signal-to-noise ratio; in the case of Zeeman-*hfs* measurements, this number applied separately to each of the polarizations.

4. Results

4.1. Hyperfine structure patterns of the possible second-stage cooling transitions

The hyperfine structure of the ground state $^4I^o_{15/2}$ was investigated by high-precision method of magnetic resonance on an atomic beam (ABMR) [23], yielding the values of the *hfs* constants up to the order of electric hexadecapole. The constants A and B, responsible for the structure at the precision level relevant for our present studies, are as follows: $A = 800.583173(36)$ MHz, $B = -1668.07870(330)$ MHz.

The *hfs* constants of the upper levels of all the transitions examined in the present work were also known before: the early literature Fourier spectroscopy results were already available in 1977 [24], and recently these levels were remeasured with higher precision by LIF in a hollow cathode discharge lamp in our earlier works concerning the holmium atom [16,18,19,25] - each level could be observed in more than one spectral line and our final results were the statistical means of the values obtained.

For reevaluation of the hyperfine structure in the spectra recorded for the transitions investigated, suitable for second-stage laser cooling, the program "Fitter" (developed in the research group of Prof. Guthöhrlein in Hamburg) was applied, as in all our earlier works. Obviously the highly precise values of the *hfs* constants A and B of the ground state were always fixed in the fitting procedure. The constants A and B for the upper levels were evaluated independently and compared to the earlier results available; the obtained results are presented in Table 1. The layout of the table is as follows: in column 2 the cooling transitions wavelengths are listed, in column 3 - the energies of the upper levels; columns 4-5 and 6-7 include the *hfs* constants A and B, respectively - the values obtained directly from the analysis of the possible cooling transitions, compared to those obtained in our earlier works, from the analysis of other spectral lines; finally, in column 8 the respective references are cited. The uncertainties quoted, including both the statistical and the systematic factors, were calculated as in our earlier works [16,18] (recently the procedure adopted was described in more detail in [26]). As in [10], the transitions are ordered according to the increasing upper level energies, i.e. with decreasing wavelengths.

Table 2 constitutes a compilation of the basic spectral features of the transitions investigated, important from the point of view of practical realization of laser cooling procedure. As in the previous table, in columns 2 and 3 the transitions wavelengths and the upper levels' energies are quoted. Then the frequency detuning of the relevant *hfs* components from the lines' center of gravity are provided, as observed in the recorded spectra: for $F = 11 \rightarrow F' = 12$ (cooling) in column 4 and $F = 10 \rightarrow F' = 11$ (hyperfine repumping) in column 5; column 6 contains the differences of the above detunings, important for the possibility of obtaining both frequencies from a common laser beam.

The spectra recorded are presented in Figs. 1 and 2.

4.2. Landé g_J factors of the upper levels

The Landé g_J factors of the upper levels of the possible second-stage cooling transitions were evaluated directly from the observed Zeeman splitting of the transitions considered. Evaluation of the Zeeman-*hfs* of the spectra was performed with the use of the software developed in our research group. The program itself was tested on other spectral lines of holmium (already published in our earlier work [22]), and additional tests are planned with the use of the spectral lines of another element, involving the levels with known g_J values; description of the software and its tests will be published separately.

The g_J factor of the ground state was already known with an extremely high precision from ABMR measurements [27]; the value amounts to 1.1951429(25), and it was obviously fixed in the fitting procedure. Also the minor admixtures of the orthogonal polarization, observed in the spectra, were directly taken into account in the fitting procedure. However, due to the limited resolution and signal-to-noise ratios of the recorded spectra, as well as some saturation effects, which could not be fully eliminated, the accuracy of the obtained g_J factors for the upper levels is moderate. It should be emphasized, however, that the values are consistent with the earlier predictions of the semi-empirical analysis of the fine structure for the even-parity level system in the holmium atom performed in our research group [18] and in another work [15].

Attempts to improve the precision of the experimental g_J values are also planned for the near future. For verification (and possibly also increase of the precision) some other spectral lines can be examined, involving the even-parity levels in question as the lower levels and selected odd-parity levels (whose g_J factors are already known or can be determined from the separate studies) as the upper levels. However, due to the exceptional scarcity of experimental data on the Landé factors in the holmium atom (as compared to other elements) this procedure is expected to be very tedious, and perhaps no significant progress should be expected soon.

Table 1

Spectral lines of the holmium atom investigated in the context of possible second-stage laser cooling in a magneto-optical trap. The *hfs* constants of the ground state: $A_g = 800.583173(36)$ MHz and $B_g = -1668.07870(330)$ MHz [23] were fixed in the fitting procedure for calculation of the A and B constants of the upper levels; the uncertainties include both the statistical and the systematic factors (see text, Section 4.1). Since all the upper levels were already investigated in other transitions in our earlier works on the holmium atom, the previously obtained *hfs* constants values are also presented for comparison; still earlier (and usually less precise) results by other authors are not included - these were quoted and discussed in our works [18,25]

Line		Upper Level					
No	λ_{air}	E	A (MHz)		B (MHz)		ref.
	(nm)	(cm^{-1})	this work	earlier works	this work	earlier works	
1	2	3	4	5	6	7	8
1	660.747	15130.31	806.2(0.8)	808.5(1.8)	2074(50)	2120(27)	[18]
2	608.179	16438.01	818.9(0.9)	822.0(0.4)	2050(54)	2000(19)	[18]
3	598.285	16709.82	1136.4(1.3)	1139.7(0.8)	−2060(87)	−2045(41)	[19]
4	545.190	18337.80	1105.2(1.3)	1104.7(1.2)	−1865(86)	−1782(20)	[19]
5	486.039	20568.63	791.8(1.0)	795.1(1.5)	3324(65)	3286(73)	[25]

Table 2

Spectral features of the transitions of the holmium atom investigated in the context of possible second-stage laser cooling in a magneto-optical trap. The observed frequency detuning of the relevant *hfs* components vs. the centers of gravity of the lines are given (see also Figs. 1 and 2): for $F = 11 \rightarrow F' = 12$ (cooling) and $F = 10 \rightarrow F' = 11$ (hyperfine repumping), as well as their differences

Line		Upper level	Frequency detuning (MHz)		
No	λ_{air}	E	$\nu_{11 \rightarrow 12}$	$\nu_{10 \rightarrow 11}$	$\Delta\nu =$
	(nm)	(cm^{-1})	(cooling)	(hyperfine repumping)	$= \nu_{11\rightarrow 12} - \nu_{10\rightarrow 11}$
1	2	3	4	5	6
1	660.747	15130.31	3930	1890	2040
2	608.179	16438.01	4320	2140	2180
3	598.285	16709.82	12750	8000	4750
4	545.190	18337.80	11840	7410	4430
5	486.039	20568.63	3790	1560	2230

Table 3

Lande g_J factors of the even-parity levels with $J = 17/2$ - upper levels of the possible second-stage cooling transitions. The errors quoted for the experimental values are statistical and were calculated as described in Section 4.2. For comparison the theoretically predicted g_J factors were quoted after [15] ($g^{(1)}_{J,calc}$) and [18] ($g^{(1)}_{J,calc}$), in slightly different approaches to the semi-empirical analysis of the fine structure, along with the respective differences $\Delta g^{(1,2)}_J = g_{J,exp} - g^{(1,2)}_{J,calc}$. Additionally, g^{LS}_J values calculated for the dominating *LS* components are quoted [18] to indicate the deviations from the pure *LS*-coupling

No	E (cm^{-1})	main *LS* component		[%]	g^{LS}_J	$g^{(1)}_{J,calc}$ [15]	$g^{(2)}_{J,calc}$ [18]	$g_{J,exp}$ [this work]	$\Delta g^{(1)}_J$	$\Delta g^{(2)}_J$
1	2	3		4	5	6	7	8	9	10
1	15130.31	$4f^{10}(^5I)5d6s^2$	^6L	31.5	1.109	1.148	1.150	1.144(0.013)	−0.004	−0.006
2	16438.01	$4f^{10}(^5I)5d6s^2$	^6K	32.1	1.208	1.147	1.148	1.137(0.002)	−0.010	−0.011
3	16709.82	$4f^{11}(^4I)6s6p$	^6I	34.3	1.295	1.229	1.223	1.189(0.010)	−0.040	−0.034
4	18337.80	$4f^{11}(^4I)6s6p$	^6I	52.3	1.295	1.239	1.242	1.230(0.021)	−0.009	−0.012
5	20568.63	$4f^{10}(^5I)5d6s^2$	^4L	45.6	1.078	1.099	1.100	1.084(0.033)	−0.015	−0.016

In Table 3 the g_J factors of the interesting even-parity $J = 17/2$ levels, evaluated from the hitherto available experimental results, are listed and compared to the theoretically predicted ones, based on the semi-empirical analysis [15,18]. Columns 2-4 contain the levels' energies, the main eigenvector components and their per cent content; in column 5 the g_J factors calculated in the *LS* coupling scheme are given for reference, columns 6 and 7 include the literature theoretically predicted g_J factors from the semi-empirical analysis, in column 8 the experimental g_J factors obtained in this work are listed, and finally columns 9 and 10 include the differences between the experimental and the theoretical values.

The uncertainties of the experimental g_J factors quoted in the table are purely statistical. These were calculated from the uncertainty propagation formula: $\sigma = \sqrt{\sigma^2_{\sigma s} + \sigma^2_{\pi s} + \sigma^2_{pol}}$, where $\sigma_{\sigma s}$ and $\sigma_{\pi s}$ denote the mean standard deviations reflecting the differences between the values obtained for individual scans (or small averaged groups of scans) within each polarization separately, while σ_{pol} is related to the scattering between the values obtained for both polarizations. Of course because of the limited numbers of values averaged the respective mean standard deviations include the appropriate Student-Fisher coefficients. Unfortunately, the in-
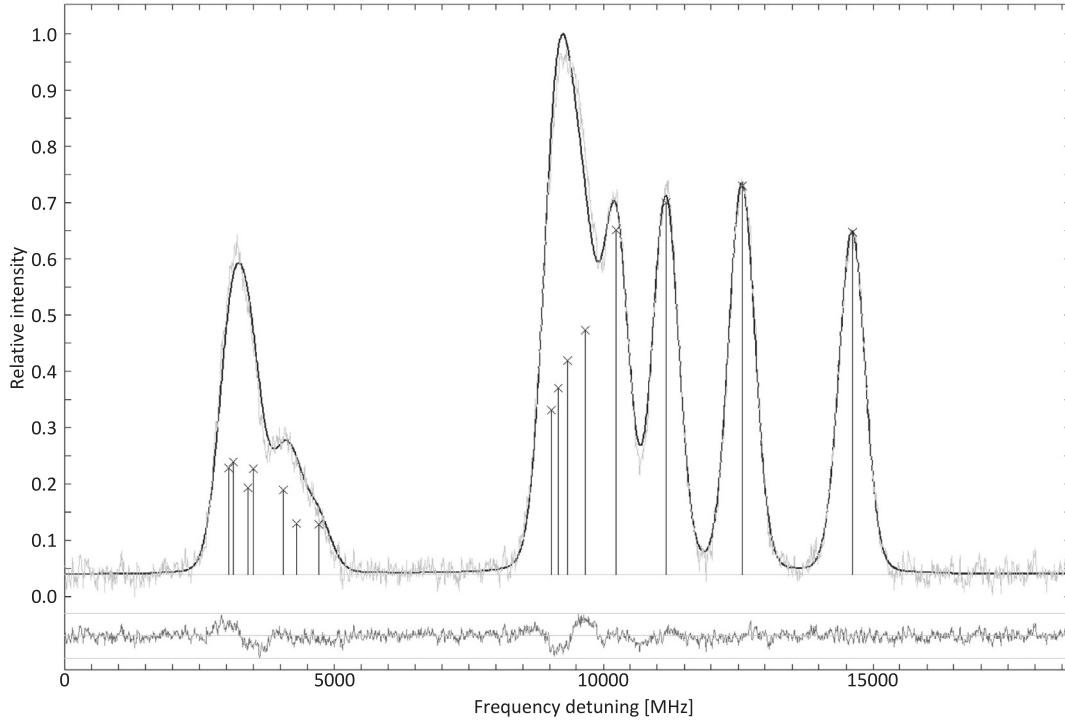
Fig. 1. Recorded *hfs* patterns of the spectral line $\lambda = 660.747$ nm in the holmium atom, considered for the second-stage laser cooling in MOT (Table 1 No 1), along with the components fitted by program "Fitter" (marked with vertical lines); additionally a diagram of the hyperfine splittings of the levels involved (the ground state and the level 15130.31 cm^{-1}) are presented and the *hfs* components relevant for laser cooling ($F = 11 \rightarrow F' = 12$ (cooling) and $F = 10 \rightarrow F' = 11$ (hyperfine repumping)) are indicated with a black and a dark gray arrow, respectively; the center of gravity of the line is marked with a light gray arrow. The lower trace in the spectrum represent the deviation of the experimental data from the respective fitted curve. The horizontal line at the value of relative intensity close to 0 represents the fitted background

formation on g_J factors is "encoded" not only in the positions of the individual components, but also in their intensities; under our experimental conditions the uncertainties of the latter are hard to estimate, thus no attempt of evaluation of the systematic uncertainties for the g_J values could be undertaken.

It should be emphasized, that the experimental values, although certainly of limited precision, are reported for the first time.

The example of the recorded spectra for both σ and π polarizations - the line No 1 ($\lambda = 660.747$ nm) - is depicted in Fig. 3.

4.3. Estimated lifetimes of the upper levels

Since for three out of five second-stage cooling transitions considered neither the oscillator strengths or the lifetimes of the upper levels are known, it is not possible to evaluate the respective Doppler limits (or the expected optimum detunings from the resonance). A direct experimental lifetime value was reported only for the level 16709.82 cm^{-1} - it amounts to 1090 ns [28]; for the cycling transition from the ground state to the level 16438.01 cm^{-1}
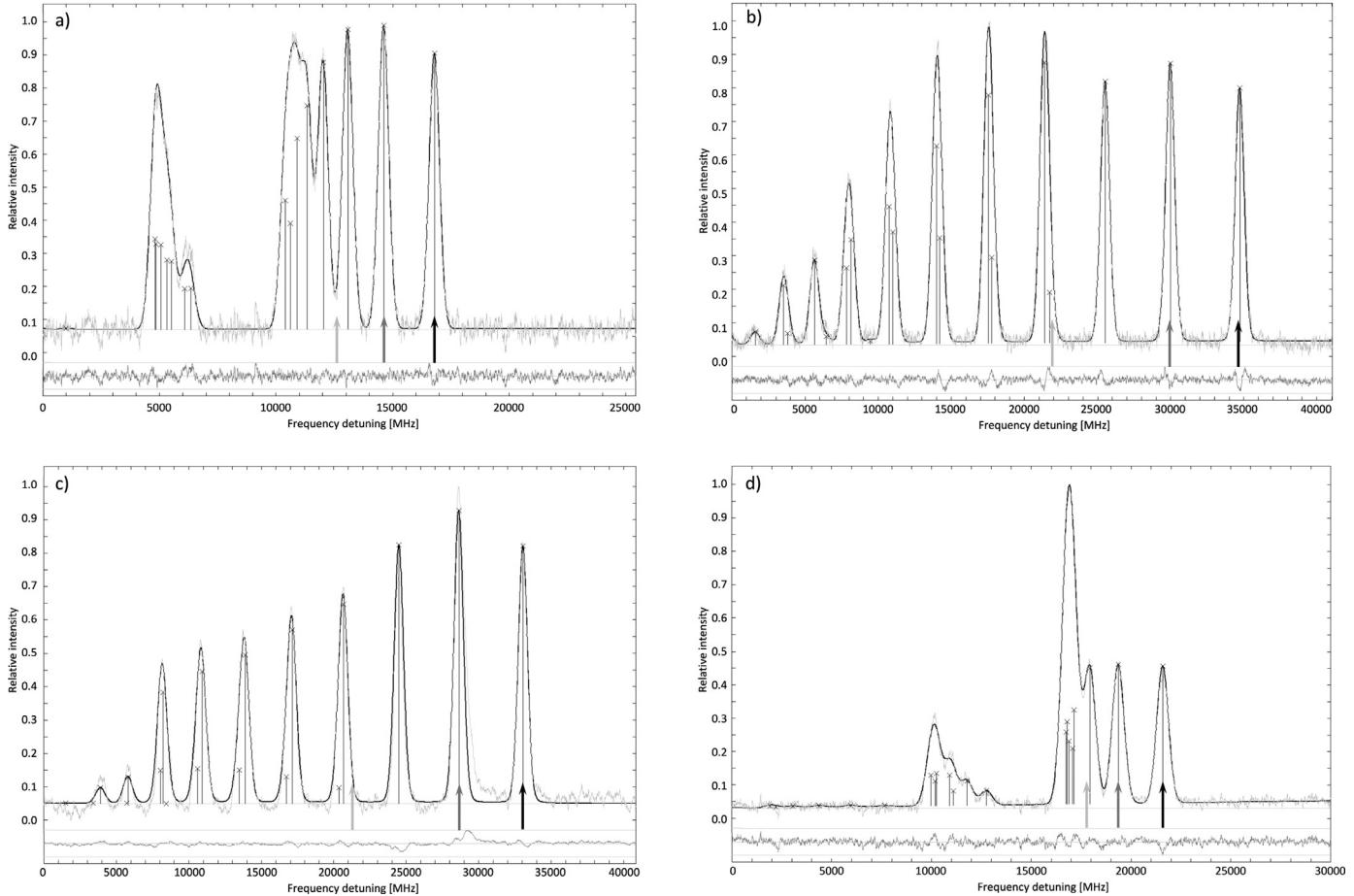
Fig. 2. Recorded *hfs* patterns of other investigated possible second-stage cooling transitions in the holmium atom (Table 1); : a) λ = 608.179 nm, No 2, b) λ = 598.285 nm, No 3, c) λ = 545.190 nm, No 4, d) λ = 486.039 nm, No 5. The components fitted by program "Fitter" are marked with vertical lines, the lower traces represent the deviations of the experimental data from the respective fitted curve, and the horizontal lines at the value of relative intensity close to 0 represent the fitted background. The relevant *hfs* components $F = 11 \rightarrow F' = 12$ (cooling) and $F = 10 \rightarrow F' = 11$ (hyperfine repumping) are indicated with black and dark gray arrows, respectively; the centers of gravity of the lines are marked with light gray arrows

an oscillator strength *f* was determined [29], which allows evaluation of the upper level's lifetime, yielding the value of 4069 ns. No facilities for the electronic levels' lifetimes are currently available in our laboratory, thus no supplementary experimental results can be supplemented.

However, for a number of other electronic levels of both parities in the holmium atom the lifetimes were measured [28,29], and for many transitions the oscillator strengths were determined [29,30]. Based on these data, a semi-empirical analysis of the oscillator strengths is in progress in our research group, exploiting the approach described in more detail for the case of the scandium and titanium atoms [31,32]. Thus, the respective lifetimes for the levels relevant for laser cooling can be predicted from a semi-empirical analysis of the oscillator strengths, based on the experimental values concerning other levels.

For the purpose of determination of the radiative lifetimes, our semi-empirical method was applied [31,32]. The angular coefficients of the transition matrix in pure *LS* coupling were calculated from straightforward Racah algebra. The transition matrix was transformed into the actual intermediate coupling by the fine structure eigenvectors obtained using semi-empirical method. The transition radial integrals are treated as free parameters in the least squares fit to the experimental oscillator strengths. The radiative lifetime of an excited state can be written as a reciprocal of the sum of transition probabilities for all possible de-excitaion channels.

It should be stressed that the recently *hfs* constants for a number of levels, based on the Fourier spectroscopic investigations [33], allowed to verify or, in some cases, correct the calculated eigenvector compositions for numerous even-parity levels, which greatly facilitated the calculation of the oscillator strengths of the transitions involving those as the upper levels.

In Table 4 selected results of the semi-empirical fit are presented. The even-parity levels reported are arranged according to their *J* quantum numbers, with increasing energies. The calculated lifetimes are compared to the experimental data available for the particular levels [28,29].

5. Discussion

5.1. Hyperfine structure patterns of the possible second-stage cooling transitions

As already mentioned, the *hfs* constants for the upper even-parity $J = 17/2$ levels considered were already known from our earlier works concerning atomic holmium. It has to be emphasised, however, that the *hfs* electric quadrupole constants B in the holmium atom are hard to determine precisely and the values obtained by various authors with various experimental techniques, or even under slightly different experimental conditions (e.g. various spectral lines involving the same electronic level) often differ by up to a few hundreds of MHz. Such differences can be attributed
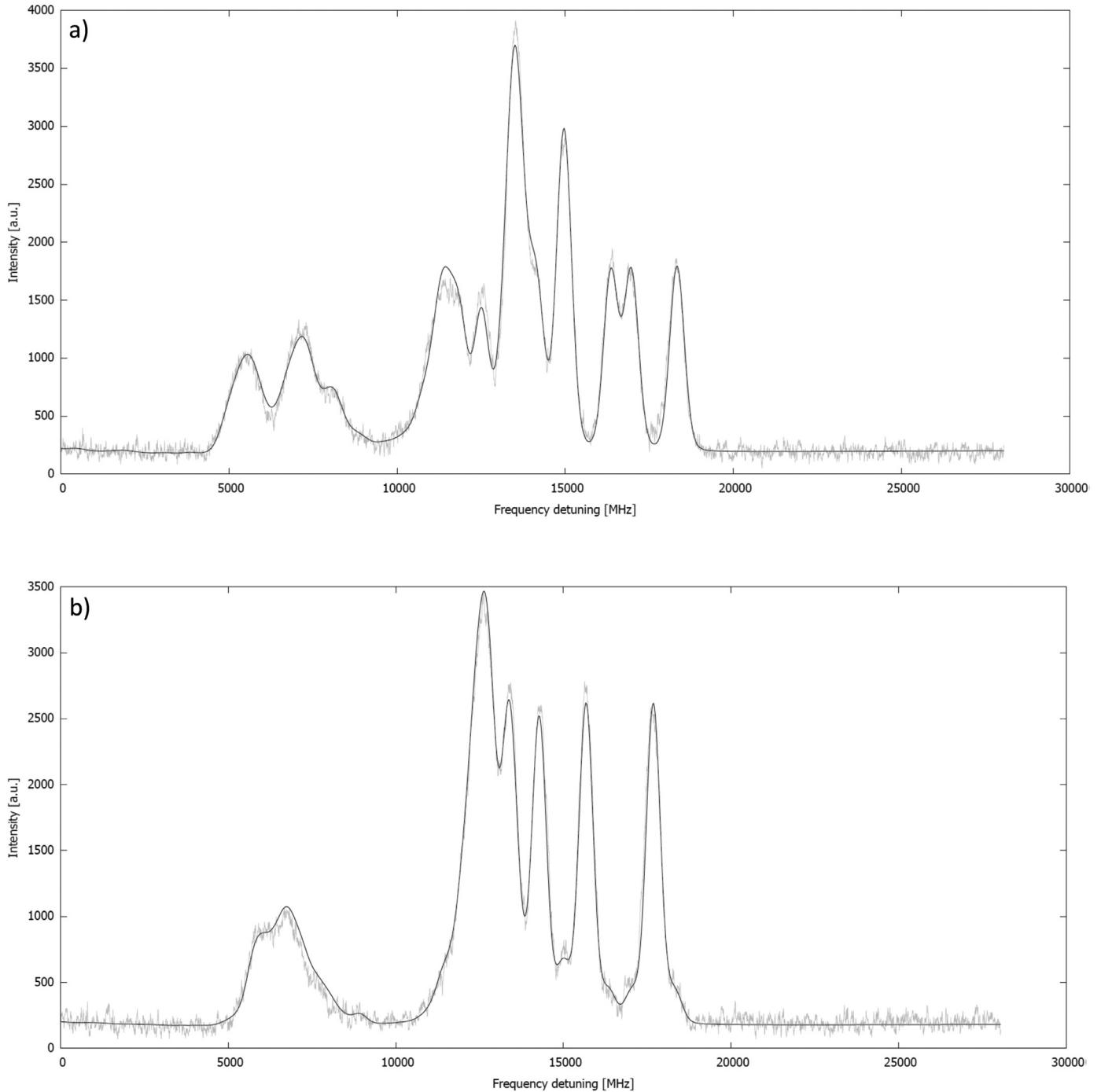
Fig. 3. Recorded Zeeman-*hfs* patterns of the spectral line $\lambda = 660.747$ nm in the holmium atom, considered for second-stage laser cooling in MOT (Table 1, No 1), for two polarizations: a) σ, b) π, along with the curves least-squares fitted by the software developed

to very low Casimir coefficients describing the contributions of the constant B to the hyperfine sublevels of a particular level. At a limited precision of determination of particular *hf* intervals this inevitably yields large uncertainties of the constants B, and can further result in somewhat inaccurate predictions of the *hfs* patterns for the spectral lines, which are not directly investigated. Thus we considered it necessary to record directly the transitions possibly suitable for second-stage laser cooling in order to discuss the relevant features more reliably.

As reported in [10], for the first-stage cooling transition at $\lambda = 410.384$ nm a *hfs* pattern with intensities of the main components *decreasing* with increasing frequency is observed, i.e. the cooling

component $F = 11 \rightarrow F' = 12$ lies *below* the hyperfine repumping component $F = 10 \rightarrow F' = 11$, by ca. 610 MHz. For all the possible second-stage cooling transitions considered in this work the opposite tendency occurs - the cooling component is positioned *above* the one suitable for the hyperfine repumping; an example of the line 15130.31 cm^{-1}, presented along with the hyperfine splittings of the levels involved and the relevant components indicated (Fig. 1), should facilitate the analysis. The frequency differences between the components mentioned always exceed 2 GHz, and for two lines ($\lambda = 598.285$ nm and $\lambda = 545.190$ nm) the values of almost 5 GHz are observed. In the case of the second-stage cooling transition currently tested by the group from the University of

Table 4

Preliminary results of the radiative lifetimes calculations (for brief description see text, Section 4.3) for the even-parity levels of the holmium atom; in the cases where experimental lifetimes are available, a good agreement between those values and the predicted ones can be noted; all lifetimes are expressed in ns.

Energy (cm^{-1})	J	this work	[28]	[29]
32039.760	9/2	26.9	29.1[a]	
32785.210	9/2	26.2	28.2[a]	
22413.140	11/2	943	1150[a]	
29069.780	11/2	11.4	9.4[a]	
30423.600	11/2	11.8	12.5[a]	
31903.280	11/2	83.7	82.2[a]	
32837.210	11/2	6.4	7.3[a]	
17059.350	13/2	1330	1530[a]	
18858.190	13/2	5240	3580[c]	
20241.310	13/2	318	414[a]	400(40)
22157.860	13/2	1305		
22978.190	13/2	101	104[a]	109(7)
24014.220	13/2	8.3	9.4[a]	11.1(8)
24740.520	13/2	18.0	22.1[a]	25(2)
29751.910	13/2	5.4	5.0[a]	
16882.280	15/2	2144	2720[b]	
18756.220	15/2	4110	4200[c]	
20074.890	15/2	793	862[a]	
23445.280	15/2	264	268[a]	250(15)
24660.800	15/2	4.9	5.0[a]	6.0(4)
25272.630	15/2	122	158[a]	155(6)
29642.600	15/2	4.7	4.7[a]	
15130.310	17/2	10700		
16438.010	17/2	4830		4069[d]
16709.820	17/2	1086	1090[a]	
18337.800	17/2	34100		
20568.630	17/2	6180		
24263.960	17/2	71.5	70.2[a]	72(8)
24360.810	17/2	4.7	4.9[a]	6.3(5)

[a] uncertainty ± 5%
[b] uncertainty ± 10%
[c] uncertainty ± 15%
[d] recalculated from experimental f_{ik} value

Wisconsin, at λ = 412.020 nm, so far no experimental *hfs* constants of the upper level were published; a rough estimate of the respective detuning, obtained with the predicted values from the semi-empirical fit of the hyperfine structure [18], is ca. 400 MHz.

The cooling laser beam frequency should be red-detuned from the respective $F = 11 \rightarrow F' = 12$ component by the value of the order of γ (the natural transition linewidth). For all the second-stage cooling transitions considered the optimum detuning is expected not to exceed 1 MHz, which is irrelevant at the estimation accuracy level. If both frequency components (cooling and hyperfine repumping) are to be extracted from the same laser beam, as desired, frequency detuning values of 2-5 GHz could be challenging; nevertheless, in each case, if considered necessary, this should be possible to realize by an appropriate modulator (e.g. Newport electro-optic phase modulators with operating frequencies up. to 7.5 GHz are available for the whole spectral range of 360-1600 nm). The Zeeman slower beam need not be considered in this context - for this purpose the beam red-detuned from the first-stage cooling transition would be preferred (as in the cases of Er [34,35] and Dy [36]).

5.2. Landé g$_J$ factors of the upper levels

As discussed before, similarity of Landé g_J factors of the ground state and the upper level of a laser cooling transition allows for efficient sub-Doppler cooling in a MOT. The g_J factor of the ground state is known very precisely, but no experimental values for the upper levels of any cooling transitions were obtained so far. For some cases, however, theoretical estimates were available. For the upper level of the already successfully realized first-stage cooling

transition, 24360.81 cm^{-1} there are three very similar estimates: 1.18 [14] (calculated in $J - J$-coupling approximation), 1.176 [15] and 1.182 [18] (both latter obtained form the semi-empirical fits of the fine structure, in various configuration bases). These predicted values differ from the g_J factor of the ground state by only ca. 0.01-0.02 - a value larger than in the case of erbium, but comparable to the case of dysprosium.

Experimental values of the g_J factors of the upper level of the second-stage cooling transitions considered, obtained in this work, are compared to the theoretically predicted values from the already addressed approaches to the semi-empirical fine structure fit [15,18] (Table 3). In all the cases the experimental values prove lower than the predicted ones. The respective differences amount to no more than −0.02, with one exception of the level 16709.82 cm^{-1} (the experimental value up to 0.04 lower then predicted, with the predicted values differing by 0.006 between various approaches). Taking into account the limited precision of the experimental data (the statistical uncertainties ranging from 0.002 to 0.033), this level of consistency should be considered very good.

Since the g_J factors reported were evaluated from single spectral lines (i.e. the possible cooling transitions), investigations on other transitions would be desired, whenever the experimental possibilities arise. The exceptional case of the level 16709.82 cm^{-1} certainly requires further studies in the future, in order to verify the value currently obtained. Also confirmation of the g_J value for the level 16438.01 cm^{-1}, burdened with a particularly small *statistical* uncertainty, should be sought.

5.3. Estimated laser cooling temperature limits

As mentioned in Section 4.3, the information on the lifetimes of the upper levels of the possible second-stage cooling transitions is rather scarce, and we have to rely mainly on the theoretically predicted values. So far only preliminary results are available, allowing rough estimates of the important parameters concerning laser cooling at the transitions considered in this work. The reliability of the results obtained can be verified by the consistency of the predicted oscillator strengths or lifetimes with the available experimental data. In particular, the lifetime of the upper level of the first-stage cooling transition, 24360.81 cm^{-1} is correctly reproduced ($\tau_{exp} = 4.9$ ns, $\tau_{theor} = 4.7$ ns), and for the cumulative branching ratio of the leaking transitions the order 10^{-5} is obtained, as in [10]. For the level 16709.82 cm^{-1} the experimental lifetime of 1090 ns [28] is perfectly reproduced. The final results of the analysis will be reported separately [13].

The lifetimes predicted for the upper levels of the considered possible second-stage cooling transitions range from ca. 1 μs (level 16709.82 cm^{-1}) to ca. 34 μs (level 18337.80 cm^{-1}), yielding the respective Doppler limit values between 3.2 μK and 0.1 μK. The lifetime value predicted in semi-empirical analysis for the level 16709.82 cm^{-1} is perfectly consistent with the experimental result (the only one directly available).

The lower limit temperatures for the sub-Doppler cooling, i.e. photon recoil limits, can easily be calculated - these range from ca. 0.26 μK for the longest-wavelength transition to ca. 0.48 μK for the shortest-wavelength one.

5.4. Cooling transitions - overview

In the following paragraphs specific features of the individual transitions are discussed in more detail.

Transition λ = 660.747 nm (upper level 15130.31 cm^{-1})...

The appropriate wavelength can be generated either with a dye laser operated on DCM dye, with a diode laser or a Ti:sapphire laser (short-wavelength option). The hyperfine repumping *hfs* com-

ponent lies ca. 2040 MHz lower than the cooling component (Fig. 1).

The predicted lifetime of the upper level was roughly estimated as 10.7 μs - since the respective transition is cycling, this value results in the Doppler limit of ca. 0.36 μK, comparable with the respective photon recoil limit. The difference between the Landé g_J factor of the upper level and that of the ground level amounts to $\Delta g_J \approx -0.045$; thus a moderate efficiency of sub-Doppler laser cooling can be expected.

Transition $\lambda = 608.179$ nm (upper level 16438.01 cm^{-1})
The wavelength for excitation of this transition can be obtained either with a dye laser operated on Rhodamine 6G, or with a frequency-doubled diode laser. The hyperfine repumping *hfs* component lies ca. 2180 MHz lower than the cooling component.

The Doppler limit of 0.91 μK (only ca. 3 times higher than the photon recoil limit), estimated from the experimental oscillator strength of the transition [29], was already quoted in [10]; the lifetime predicted by the semi-empirical fit exceeds the evaluated experimental value by ca. 20 %. The difference of the relevant g_J factors is somewhat larger than for the previous transition: $\Delta g_J \approx -0.055$; the expected sub-Doppler cooling efficiency is not expected to be high.

Transition $\lambda = 598.285$ nm (upper level 16709.82 cm^{-1})
The transition wavelength can be accessed in the same way as for the previous transition discussed. The hyperfine repumping *hfs* component is positioned ca. 4750 MHz below the cooling component.

The Doppler limit is expected at 3.2 μK [10]; as already mentioned, the agreement between the experimental and the theoretically predicted lifetime values is perfect.

The experimentally determined g_J factors do not differ much: $\Delta g_J \approx -0.006$ - this difference is smaller than e.g. for the case of the main cooling transition in atomic dysprosium ($\Delta g_J = -0.022$ [37]) or thullium ($\Delta g_J = -0.021$ [38]), and probably very similar to the main cooling transition for atomic holmium. Thus a significant efficiency of sub-Doppler cooling may probably be expected. However, since the experimental g_J value is not consistent with the earlier semi-empirical predictions within the statistical error limits, its further verification in the future is planned.

Transition $\lambda = 545.190$ nm (upper level 18337.80 cm^{-1})
The wavelength of this transition is not easily achieved. It can certainly be obtained with the use of a frequency-doubled diode laser; it is also possible to generate it with a dye laser, but the choice of the dye in not that obvious as in previous two cases. The laser can be operated e.g. on Coumarin 498, Coumarin 510, Coumarin 540, Rhodamine 110 or Pyrromethene 556, provided an appropriate pump laser (preferably an argon ion laser operated on selected lines in the visible range) is available. With some effort one may also consider frequency doubling of a Ti:Sapphire laser; however, the required fundamental wavelength of ca. 1091 nm lies at the very edge of the gain curve of this laser type.

The hyperfine repumping *hfs* component is positioned ca. 4430 MHz below the cooling component.

The semi-empirical preliminary prediction of the lifetime of the upper level is ca. 34.1 μs, resulting in the expected Doppler limit of ca. 0.10 μK (below the photon recoil limit). The difference of the g_J factors amounts to $\Delta g_J \approx 0.035$ - the sub-Doopler cooling should thus be moderately efficient.

Transition $\lambda = 486.039$ nm (upper level 20568.63 cm^{-1})
The relevant wavelength can be generated directly by a diode laser, or by a frequency-doubled Ti:Sapphire laser; another choice may be a dye laser operated on Coumarin 480 or Coumarin 498, if a suitable pump source is available. The hyperfine repumping *hfs* component lies ca. 2230 MHz below the cooling component.

This is the only transition among the considered ones, which is not strictly cycling - there are five possible electric-dipole allowed

leaking transitions, although their absolute probabilities should be very low and the branching ratios should not exceed 10^{-6}. The predicted lifetime (attributed predominantly to the cooling transition from the ground state) amounts to ca. 6.2 μs, and thus the Doppler limit is expected at ca. 0.56 μK. The Landé g_J factors of the upper and the lower level differ considerably: $\Delta g_J \approx -0.085$, and only negligible sub-Doppler cooling might be expected.

6. Conclusions

In this work five optical transitions from the ground state of the type $J = 15/2 \rightarrow J' = 17/2$, which can be considered as the possible second-stage laser cooling transitions in a magneto-optical trap for atomic holmium, were directly recorded with the method of laser induced fluorescence (LIF) in a hollow cathode discharge lamp; four of the transitions were already proposed for this purpose in the work reporting successful laser cooling of the holmium atoms at the main cooling transition [10]. The *hfs* constants *A* and *B*, already known from our earlier investigations and, with generally lower precision, also from the studies by other authors, were currently remeasured. The same transitions were also recorded in the presence of the magnetic field, which yielded the possibility of evaluation of the Landé g_J factors of the upper levels involved for the first time; attempts to increase the accuracy of the latter through additional examination of other spectral lines are planned.

Direct observation of the transitions in question gives access to the features important from the point of view of the laser cooling procedure, e.g. the frequency detuning between the *hfs* components to be used for cooling ($F = 11 \rightarrow F' = 12$), and for the hyperfine repumping ($F = 10 \rightarrow F' = 11$). These values differ drastically from the detuning observed in the main cooling transition. Although obtaining such detuning values, if the hyperfine repumping should prove to be necessary, would not be trivial, it nevertheless seems technically feasible.

Taking into account all the features considered, i.e. the known or predicted probabilities of the possible cooling transitions and the semi-empirically predicted lifetimes of the upper levels (both features related to the natural linewidths and thus the cooling Doppler limits), as well as the differences between the Landé g_J factors of the upper levels and the ground state (determining the efficiency of sub-Doppler cooling), the availability of the sources of the excitation laser radiation, and finally the frequency detunings between the cooling and hyperfine repumping *hfs* components, the transitions No 1 ($\lambda = 660.747$ nm, upper level 15130.31 cm^{-1}) or 3 ($\lambda = 598.285$ nm, upper level 16709.82 cm^{-1}) seem the most promising. The transition No 5 ($\lambda = 486.039$ nm, upper level 20568.63 cm^{-1}) should perhaps not be further considered.

The results presented might facilitate the choice of the most favorable option of obtaining narrow-band laser cooling of the holmium atoms in MOT.

Declaration of Competing Interests

The authors declare that they have no known competing financial interests or personal relationships that could have appeared to influence the work reported in this paper.

CRediT authorship contribution statement

D. Stefańska: Conceptualization, Methodology, Validation, Formal analysis, Investigation, Writing - original draft, Writing - review & editing, Visualization. **B. Furmann:** Conceptualization, Methodology, Software, Validation, Formal analysis, Investigation, Supervision, Funding acquisition. **J. Ruczkowski:** Methodology, Software, Formal analysis. **M. Elantkowska:** Methodology, Formal

analysis. **P. Głowacki:** Formal analysis, Investigation. **M. Chomski:** Investigation. **M. Suski:** Investigation. **S. Wilman:** Investigation.

Acknowledgments

References

[1] Stone N. Table of nuclear magnetic dipole and electric quadrupole moments. Atomic Data and Nuclear Data Tables 2005;90(1):75–176. doi:10.1016/j.adt. 2005.04.001.

[2] Saffman M, Mølmer K. Scaling the neutral-atom Rydberg gate quantum computer by collective encoding in holmium atoms. Phys Rev A 2008;78. doi:10. 1103/PhysRevA.78.012336. 012336 (10pp).

[3] Dzuba VA, Flambaum VV. Relativistic corrections to transition frequencies of Ag I, Dy I, Ho I, Yb II, Yb III, Au I, and Hg II and search for variation of the fine-structure constant. Phys Rev A 2008;77. doi:10.1103/PhysRevA.77.012515. 012515 (6pp).

[4] Stefanska D, Furmann B, Głowacki P. Possibilities of investigations of the temporal variation of the α constant in the holmium atom. J Q Spectrosc Radiat Transf 2018;213:159–68. doi:10.1016/j.jqsrt.2018.04.017.

[5] Cingöz A, Lapierre A, Nguyen A-T, Leefer N, Budker D, Lamoreaux SK, et al. Limit on the temporal variation of the fine-structure constant using atomic dysprosium. Phys Rev Lett 2007;98. doi:10.1103/PhysRevLett.98.040801. 040801 (4pp).

[6] Leefer N, Weber CTM, Cingöz A, Torgerson JR, Budker D. New limits on variation of the fine-structure constant using atomic dysprosium. Phys Rev Lett 2013;111. doi:10.1103/PhysRevLett.111.060801. 060801 (5pp).

[7] Oktel MO, Müstecaplıoğlu OE. Electromagnetically induced left-handedness in a dense gas of three-level atoms. Phys Rev A 2004;70. doi:10.1103/PhysRevA. 70.053806. 053806 (7pp).

[8] Thommen Q, Mandel P. Electromagnetically induced left handedness in optically excited four-level atomic media. Phys Rev Lett 2006;96. doi:10.1103/ PhysRevLett.96.053601. 053601 (4pp).

[9] McClelland JJ, Hanssen JL. Laser cooling without repumping: a magneto-optical trap for erbium atoms. Phys Rev Lett 2006;96. doi:10.1103/PhysRevLett.96. 143005. 143005 (4pp).

[10] Miao J, Hostetter J, Stratis G, Saffman M. Magneto-optical trapping of holmium atoms. Phys Rev A 2014;89. doi:10.1103/PhysRevA.89.041401. 041401 (5pp).

[11] Milner W, Yip C, Booth D, Saffman M. Narrow-line cooling of neutral Holmium. In: APS Division of Atomic, Molecular and Optical Physics Meeting Abstracts; 2017. p. Q1.065.

[12] Yip C, Booth D, Zhou H, Collett J, Hostetter J, Saffman M. Optical Dipole Trapping of Holmium. In: APS Meeting Abstracts; 2018. p. T01.089.

[13] Ruczkowski J., Elantkowska M., Wilman S. 2019. To be published.

[14] Newman BK, Brahms N, Au YS, Johnson C, Connolly CB, Doyle JM, et al. Magnetic relaxation in dysprosium-dysprosium collisions. Phys Rev A 2011;83. doi:10.1103/PhysRevA.83.012713. 012713 (5pp).

[15] Li H, Wyart J-F, Dulieu O, Lepers M. Anisotropic optical trapping as a manifestation of the complex electronic structure of ultracold lanthanide atoms: The example of holmium. Phys Rev A 2017;95. doi:10.1103/PhysRevA.95.062508. 062508 (18pp).

[16] Stefanska D, Furmann B. Hyperfine structure investigations for the odd-parity configuration system in atomic holmium. J Q Spectrosc Radiat Transf 2018;206:286–95. doi:10.1016/j.jqsrt.2017.11.019.

[17] Kramida A., Yu. Ralchenko, Reader J., and NIST ASD Team. NIST Atomic Spectra Database (ver. 5.7.1), [Online]. Available: http://physics.nist.gov/asd [2019]. National Institute of Standards and Technology, Gaithersburg, MD.; 2019. 10.18434/T4W30F

[18] Stefanska D, Ruczkowski J, Elantkowska M, Furmann B. Fine- and hyperfine structure investigations of the even-parity configuration system in atomic holmium. J Q Spectrosc Radiat Transf 2018;209:180–95. doi:10.1016/j.jqsrt. 2018.01.010.

[19] Furmann B, Stefanska D, Suski M, Wilman S. Identification of new electronic levels in the holmium atom and investigation of their hyperfine structure. J Q Spectrosc Radiat Transf 2018;219:117–26. doi:10.1016/j.jqsrt.2018.08.005.

[20] Stefańska D, Suski M, Zygmunt J, Stachera J, Furmann B. Tunable single-mode cw energy-transfer dye laser directly optically pumped by a diode laser. Opt Laser Technol 2019;120. doi:10.1016/j.optlastec.2019.105673. 105673 (7pp).

[21] Stefanska D, Suski M, Furmann B. Tunable continuous wave single-mode dye laser directly pumped by a diode laser. Laser Phys Lett 2017;14(4). doi:10.1088/ 1612-202X/aa5f00. 045701 (7pp).

[22] Stefanska D, Werbowy S, Krzykowski A, Furmann B. Lande g_J factors for even-parity electronic levels in the holmium atom. J Q Spectrosc Radiat Transf 2018;210:136–40. doi:10.1016/j.jqsrt.2018.02.015.

[23] Dankwort W, Ferch J, Gebauer H. Hexadecapole interaction in the atomic ground state of ^{165}Ho. Zeitschrift für Physik 1974;267(3):229–37. doi:10.1007/ BF01669225.

[24] Wyart J-F, Camus P, Vergès J. Etude du spectre de l'holmium atomique: I. Spectre d'émission infrarouge niveaux d'énergie de Ho I et structures hyperfines. Phys C 1977;92(3):377–96. doi:10.1016/0378-4363(77)90137-1.

[25] Furmann B, Stefanska D, Suski M, Wilman S, Chomski M. Hyperfine structure studies of the odd-parity electronic levels in the holmium atom. I: Levels with known energies. J Q Spectrosc Radiat Transf 2019;234:115–23. doi:10.1016/j. jqsrt.2019.05.028.

[26] Furmann B, Stefanska D, Chomski M, Suski M, Wilman S. Hyperfine structure studies of the odd-parity electronic levels of the terbium atom. J Q Spectrosc Radiat Transf 2019;237. doi:10.1016/j.jqsrt.2019.106613. 106613 (8pp).

[27] Dankwort W, Ferch J. Reevaluation of the atomic g_J-factor and the nuclear g_I-factor of ^{165}Ho. Zeitschrift für Physik 1974;267(3):239–41. doi:10.1007/ BF01669226.

[28] DenHartog EA, Wiese LM, Lawler JE. Radiative lifetimes of Ho I and Ho II. J Opt Soc Am B 1999;16(12):2278–84. doi:10.1364/JOSAB.16.002278.

[29] Gorshkov VN, Komarovskii VA. Lifetimes of excited levels and oscillator strengths of Ho I and Ho II spectral lines. Opt Spectrosc 1979;47:350.

[30] Nave G. Atomic transition rates for neutral holmium (Ho I). J Opt Soc Am B 2003;20(10):2193–202. doi:10.1364/JOSAB.20.002193.

[31] Ruczkowski J, Elantkowska M, Dembczyński J. An alternative method for determination of oscillator strengths: The example of Sc II. J Q Spectrosc Radiat Transf 2014;145(Supplement C):20–42. doi:10.1016/j.jqsrt.2014.04.018.

[32] Ruczkowski J, Elantkowska M, Dembczyński J. Semi-empirical determination of radiative lifetimes for Sc II and Ti II. J Q Spectrosc Radiat Transf 2016;176(Supplement C):6–11. doi:10.1016/j.jqsrt.2016.02.018.

[33] Özdalgiç B, Başar G, Kröger S. Hyperfine structure analysis of atomic holmium in an FT spectrum in the visible spectral range. Astrophys J Suppl Ser 2019;244(2):41. doi:10.3847/1538-4365/ab4262.

[34] Berglund AJ, Hanssen JL, McClelland JJ. Narrow-line magneto-optical cooling and trapping of strongly magnetic atoms. Phys Rev Lett 2008;100. doi:10.1103/ PhysRevLett.100.113002. 113002 (4pp).

[35] Frisch A, Aikawa K, Mark M, Rietzler A, Schindler J, Zupanič E, et al. Narrow-line magneto-optical trap for erbium. Phys Rev A 2012;85. doi:10.1103/ PhysRevA.85.051401. 051401 (5pp).

[36] Lu M, Burdick NQ, Lev BL. Quantum degenerate dipolar fermi gas. Phys Rev Lett 2012;108. doi:10.1103/PhysRevLett.108.215301. 215301 (5pp).

[37] Ho Youn S, Lu M, Lev BL. Anisotropic sub-doppler laser cooling in dysprosium magneto-optical traps. Phys Rev A 2010;82. doi:10.1103/PhysRevA.82.043403. 043403 (5pp).

[38] Sukachev D, Sokolov A, Chebakov K, Akimov A, Kolachevsky N, Sorokin V. Sub-doppler laser cooling of thulium atoms in a magneto-optical trap. JETP Lett 2010;92:703–6. doi:10.1134/S0021364010220133.

Contents lists available at ScienceDirect

Journal of Quantitative Spectroscopy & Radiative Transfer

Landé g_J factors of the electronic levels of the holmium atom

M. Chomski [a], B. Furmann [a,*], J. Ruczkowski [b], M. Suski [a], D. Stefańska [a]

[a] Institute of Materials Research and Quantum Engineering, Faculty of Materials Engineering and Technical Physics, Poznan University of Technology, Piotrowo 3A, 60-965 Poznan, Poland
[b] Institute of Robotics and Machine Intelligence, Faculty of Control, Robotics and Electrical Engineering, Poznan University of Technology, Piotrowo 3A, 60-965 Poznan, Poland

ARTICLE INFO

ABSTRACT

In the present work measurements of Landé g_J factors for some electronic levels of the holmium atom are presented. The measurements were performed with the use of the Zeeman effect of the hyperfine structure, observed with the method of laser spectroscopy in a hollow cathode discharge lamp placed in constant magnetic field, with laser induced fluorescence detection. Investigation of 69 spectral lines of holmium in the spectral range 490–670 nm enabled for the first time the determination of g_J factors for 15 levels belonging to the odd-parity configurations of Ho and 18 levels belonging to the even-parity configurations.

1. Introduction

Holmium is an element belonging to lanthanides series and possesses only one stable isotope $^{165}_{67}$Ho. This is an element characterized by relatively high nuclear spin I = 7/2 and, because of that, its electronic levels′ structure is very rich. In addition, the large value of nuclear magnetic dipole moment and quite high nuclear electric quadrupole moment lead to rather large hyperfine splitting of the electronic levels. Due to the features mentioned above, holmium atom has been attracting attention for applications in quantum engineering and metrology. Holmium is believed to be good candidate for performing quantum processors based on large number of qubits [1]. The large hyperfine splitting and ground state multiplet splitting, which is characteristic for this element, turns out to be very useful for qubit preparation and readout. Moreover, the huge magnetic moment is an important property for long-range interacting dipolar systems. Laser cooling in magneto-optical traps is an efficient method for preparing the holmium qubits for quantum processing [2]. Investigation of the energy levels structure of this element aroused interest also due to the study of lanthanide elements wealth in stellar atmosphere [3,4].

Landé g_J factors are one of the key features, characteristic for the electronic levels, and help with their assignment to particular configurations. Determination of their values has significant impact on semi-empirical calculations performed for hyperfine structure (*hfs*). Moreover, accurate predictions of these factors' values can be helpful for the search of possible energy levels, suitable as upper levels of laser cooling transitions. For example, a new possible second-stage laser cooling transition for atomic holmium in a magneto-optical trap was proposed [5]. Efficient cooling of elements below the Doppler limit is necessary for applications in quantum engineering.

Despite the great importance of the Landé g_J factors in atomic and quantum physics there is still significant lack of experimental data on this issue. Properties of the ground state of holmium was precisely determined by Dankwort et al. [6]. Hyperfine structure parameters of other low-lying electronic energy levels were experimentally investigated also by Livingston and Pinnington [7], Burghardt et al. [8] and Kröger et al. [9]. Our research group delivered lots of data about the hyperfine structure magnetic dipole *A* and electric quadrupole *B* constants of atomic holmium in the previous years [10–16]. In the works [12,14,16] we also presented the values of energies and hyperfine structure constants of many new, previously not observed electronic levels in the holmium atom. The work of other groups [9,17–19] has also contributed to extending the knowledge about the energies of holmium electronic levels and their hyperfine structure.

---

* Corresponding author.
E-mail address: boguslaw.furmann@put.poznan.pl (B. Furmann).

Semi-empirically predicted Landé g_J factors for numerous even-parity [9,11,20] as well as odd-parity [9,20,21] electronic levels were calculated. An experiment to determine the empirical values of Landé g_J factors for even-parity energy levels in holmium was also carried out, by the method of laser induced fluorescence in a hollow cathode discharge lamp [22]. In total, 47 experimental values of Landé g_J factors of even- and 17 values of odd-parity electronic energy levels have been known. In this work new experimental values of g_J factors for 22- even and 17 odd-parity electronic energy levels in the holmium atom are included. Some of the presented results were obtained for the first time, and some others can be compared with previously published g_J factors. The presented corrections may help to explain significant discrepancies between the measured values of the *hfs* A and B constants, and those resulting from semi-empirical calculations, which appeared for some of the levels measured in the previous works, including ones with very low energies (several cm^{-1}). The differences between semi-empirically predicted and experimental values can reach several MHz for magnetic dipole constants A and even over 100 MHz for electric quadrupole constants B. Some of re-measured Landé factors are related to energy levels considered for laser cooling of the holmium atom [5]. Reported g_J factors can help with verification of previously obtained results.

2. Experimental details

In order to measure the Landé factors, the hyperfine structure of spectral lines split in a magnetic field was recorded. The method was disseminated by a group from the University of Gdańsk, that, in cooperation with a group of prof. Laurentius Windholz from Graz, published a number of papers, including those concerning the measurements of g_J factors in lanthanide atoms [23–28]. Investigations were carried out with the use of a similar method and experimental setup as in our previous research of holmium hyperfine structure constants A and B [10–16] or g_J factors of holmium and europium atom [22,29]. A detailed description of both the procedure and the setup was provided in [30]. This section provides a brief review of the experimental details.

The source of the atoms was a discharge in a hollow cathode lamp. After setting the initial laser frequency at the center of the tested line, the frequency was scanned over the range of 10–50 GHz. The g_J factors measurement requires alternating the polarization of laser beam between the vertical and horizontal direction (the π and σ polarization components respectively). Selection of the polarization components was realized by the polarization rotator.

To precisely calculate the g_J factors one should know the value and distribution of magnetic field inside the hollow cathode. The appropriate magnetic flux was ensured by the presence of one of the two sets of different bar neodymium magnets, which can be placed both above the hollow cathode or symmetrically on two sides of the discharge lamp. In the former configuration the magnetic flux is approximately 500–600 G. The latter configuration gave much higher (ca. 1900–2000 G) and more homogeneous magnetic field, but because of significant deviation of the path of the charge carriers the discharge wasn't stable enough to allow full-scale research. Due to this effect the insulator in discharge lamp setup was covered in conductive evaporated material and the short circuit appeared. This disadvantage forced us to perform most of research in lower magnetic field, with both magnets placed above the hollow cathode discharge lamp.

Optical excitation of holmium atoms was achieved by different dye lasers, depending on the spectral range. Four dye lasers have been used during the investigations: for blue-green region of the spectrum (ca. 490–525 nm) excitation was provided by a single-mode ring dye laser (modified Coherent CR 699-21) oper-

ated on Coumarin 498 dye. The semiconductor pump laser emitting a wavelength 445 nm (Lasever Inc., China, model LSR445SD-4W) was applied. The yellow-orange part of the spectrum (ca. 570–610 nm) was covered by another single-mode ring dye laser (also a modified Coherent CR 699-21) operated on Rhodamine 6G dye and optically pumped by a frequency doubled Nd:YVO$_4$ laser (Coherent, Verdi V-10). Spectral lines in the red region (ca. 625–670 nm) were excited by a ring laser operated on the DCM dye solution and optically pumped by the same light source as Rhodamine 6G dye. The remaining lines between 535nm and 560nm were investigated with a ring dye laser operated on a mixture of two dyes: Coumarin 498 and Pyrromethane 556, which constituted an energy transfer system, with the former dye as the donor and the latter as the acceptor. The pump laser was exactly the same as with single Coumarin 498 dye. The laser beam's wavelength was controlled with the wavemeter readings (Burleigh, WA-1500) and the single mode operation was checked with a mode analyzer.

The fluorescence light from decay transitions was directed, by the system of mirrors and filters, to the grating monochromator SPM-2, where spectral selection was performed. The light, after passing through the monochromator, was impingent on the photomultiplier (Hamamatsu R-375) with preamplifier, where the current signal was generated. The amplitude modulation of laser beam by the mechanical chopper for the phase-sensitive detection of the fluorescence signal was applied. The signal to noise ratio was enhanced with a phase-sensitive amplifier; the signal was further directed to the computer for scan recording. In order to create a frequency scale for the scans, along with the laser induced fluorescence signal also the transmission signal of a temperature stabilized FP interferometer with FSR=1500 MHz was recorded.

The experimental conditions were similar to those presented in earlier works concerning holmium and terbium laser spectroscopy. The discharge ignition was performed in the presence of argon as a buffer gas, after the lamp had been cooled with liquid nitrogen. The pressure in the hollow cathode lamp during the ignition was approximately equal to 0.55 mbar. During the experiment the pressure was decreasing, but has been kept not lower than 0.3 mbar. The discharge current in the hollow cathode was adjusted according to the fluorescence signal strength. It varied between 20 and 65 mA, but was typically kept at 40 mA.

To determine the magnetic field the Zeeman splitting of argon lines in various spectral regions was analysed. For the part of the spectrum covered by the DCM dye laser there were two argon lines: 15658.0735 cm^{-1} and 15580.9831 cm^{-1}. For the Rhodamine 6G dye laser's region a single line 17059.2145 cm^{-1} was recorded. Three more argon lines were investigated to determine the magnetic field in Coumarin 498 dye laser part of the spectrum: 19270.8263 cm^{-1}, 19365.8743 cm^{-1} and 19801.121 cm^{-1}. The recorded 15658.0735 cm^{-1} and 17059.2145 cm^{-1} argon lines, for both polarizations in lower and higher magnetic field, are presented in Figs. 1 and 2 respectively. The well known values of g_J factors of the corresponding energy levels [31,32] were assumed to calculate the mean magnetic field value during the experiment. These lines were recorded during every measurement session to determine magnetic field for each day. A particular obtained value, relevant for the particular measurement run, was then applied in the fitting procedure as a constant parameter to calculate the g_J factors of the holmium energy levels.

An important step in the preparation of the recorded scans for the g_J factors calculations was the application of the frequency scale based on the marker signal. The "Fitter" program, which has been successfully applied in our laboratory for *hfs* calculation for many years, was used for this purpose.
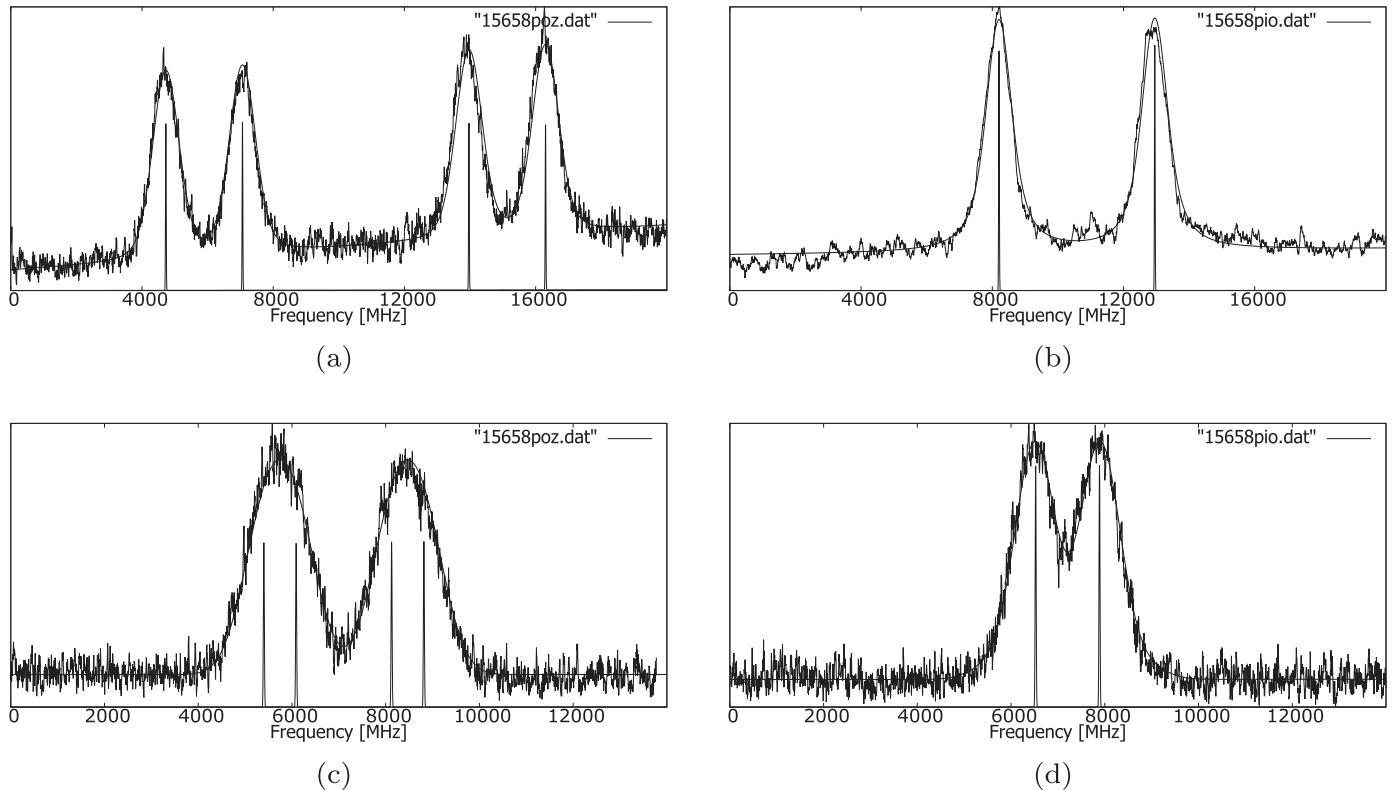
Fig. 1. Recorded Zeeman patterns of the spectral line $\lambda = 638.4717$nm (k=15658.0735 cm^{-1}) in the argon atom, along with the least-squares fitted curves for a) polarization σ at the magnetic field strength 1928 G b) polarization π at the magnetic field strength 1932 G, c) polarization σ at the magnetic field strength 602 G and d) polarization π at the magnetic field strength 607 G. The Zeeman splitting of this line was used to measure the magnetic field in DCM laser spectral range.
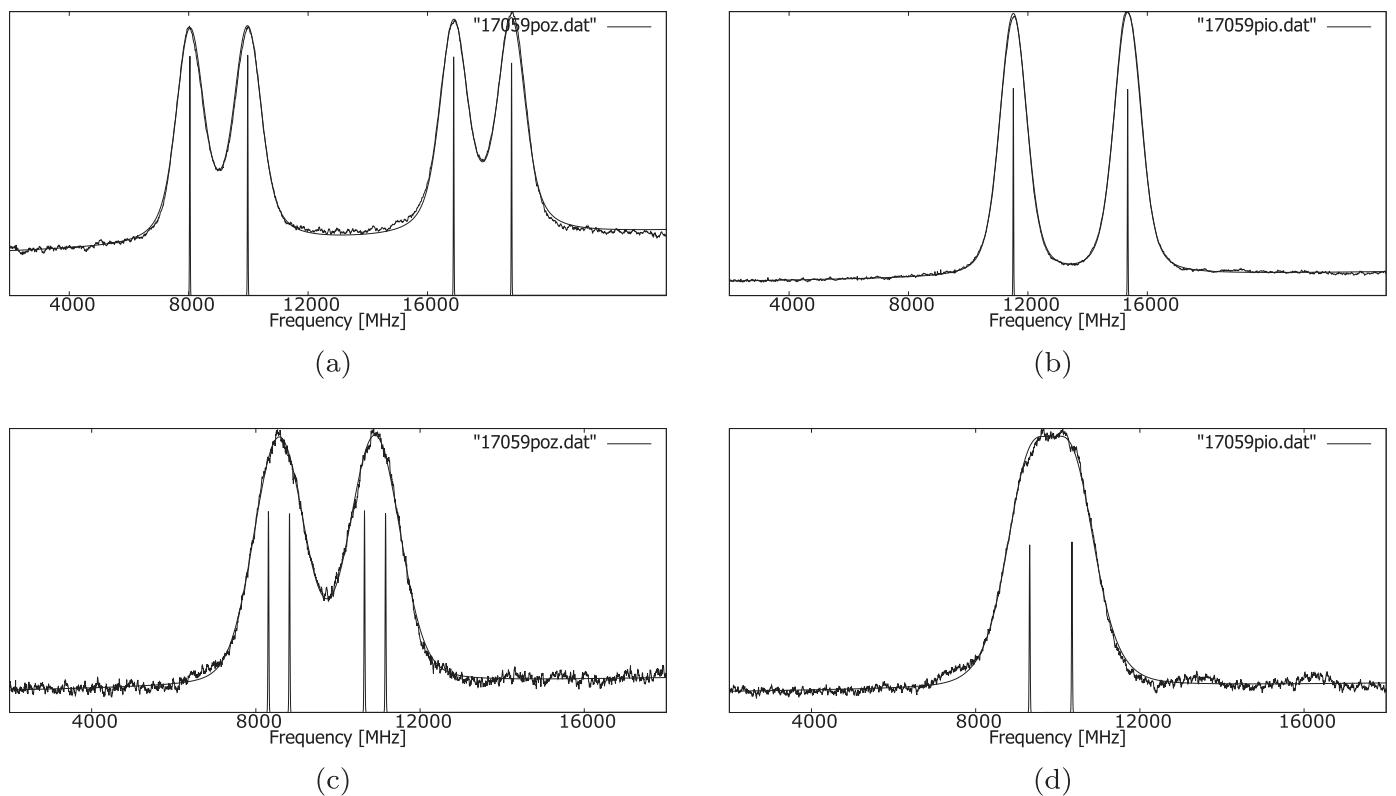
Fig. 2. Recorded Zeeman patterns of the spectral line $\lambda = 586.0310$ nm (k=17059.2145 cm^{-1}) in the argon atom, along with the least-squares fitted curves for a) polarization σ at the magnetic field strength 1915 G b) polarization π at the magnetic field strength 1922 G, c) polarization σ at the magnetic field strength 495 G and d) polarization π at the magnetic field strength 502 G. The Zeeman splitting of this line was used to measure the magnetic field in Rhodamine 6G laser spectral range.

3. Determination of g_J values

3.1. Hyperfine structure and Zeeman splitting

In an external magnetic field H_{mag}, the atomic eigenstates are linear combinations of the form:

$$|\psi M_F\rangle = \sum_F C_{M_F F} |\gamma JIF M_F\rangle. \tag{1}$$

The eigenvector amplitudes $C_{M_F F}$ can be obtained by diagonalization of the Hamiltonian matrix:

$$H_{FM_F, F'M_F} = \delta_{FF'}\left(A\frac{C}{2} + B\frac{\frac{3}{4}C(C+1) - I(I+1)J(J+1)}{2I(2I-1)J(2J-1)} \right)$$

$$+ \mu_B g_J H_{mag}(-1)^{F-M_F+J+I+F'+1}\sqrt{(2F+1)(2F'+1)J(J+1)(2J+1)}$$

$$\times \begin{pmatrix} F & 1 & F' \\ -M_F & 0 & M_F \end{pmatrix} \begin{Bmatrix} F & 1 & F' \\ J & I & J \end{Bmatrix}, \tag{2}$$

where $C = F(F+1) - J(J+1) - I(I+1)$, μ_B is the Bohr magneton and g_J is the Landé factor.

The intensity of an individual radiative transition between two Zeeman sublevels M_F and M_F' is proportional to the relevant transition probability. The experimentally observed line shape is a combination of individual Zeeman components, modified by the radiative broadening and instrumental effects.

3.2. Computational procedures

At the beginning of our computational procedures, the energies of Zeeman sublevels, relative to the fine structure energy $E(J)$, for both the upper and the lower level of the considered transition, are derived by means of diagonalization of Hamiltonian expressed by Eq. (2). The mandatory input data, concerning values of the magnetic field H_{mag}, nuclear spin I and electronic shell angular momentum J quantum numbers, the hyperfine structure A and B constants, as well as the initial values of Landé g_J factors for two energy levels involved, are loaded from an appropriate input file. The obtained eigenvalues and eigenvectors are adopted for determination of the relative positions in frequency scale and intensities of all the individual Zeeman components, separately for σ and π transitions.

In the next step, the intensity distribution function is determined as a sum of intensities for each abscissa value of the final pattern, with the use of evaluated splitting constants and line profile parameters. In an iterative procedure, this function is fitted to the experimentally observed line profile stored in the digital form, where values of Landé g_J factors for the upper and lower levels are adjustable parameters. In the calculations the Marquardt's algorithm [33] is applied. There is also a possibility to fine-tune the values of *hfs* constants, which is important especially when these constants are determined with significant measurement uncertainties.

In order to take into account the saturation effects, an additional parameter A_s (saturation rate) was introduced in the fitting procedure. Obtained values of saturation rate are in the range from 0.005 to 0.76. The large dispersion of the values of the saturation parameters results from a large number of measured lines of different intensities, a wide spectral range and a different value of the laser power used for each spectral range. The initial values of saturation parameters were selected on the basis of spectral lines' intensities and the probabilities of investigated transitions. The calculated decay rate of each Zeeman component (A_ν) of frequency ν was modified according to the following expression [34]:

$$A_\nu^{sat} = \frac{A_\nu}{1 + A_\nu/A_s} \tag{3}$$

A program using the Marquardt's algorithm to best fit the function parameters to the recorded spectra takes every individual Zeeman component as a Voigt's profile. Spectral lines, previously investigated by our research group with the same hollow cathode discharge current to calculate the *hfs A* and *B* constants, were fitted with the initial values of Gaussian and Lorentzian half-widths assumed as obtained from previous studies. For new lines the initial values of Lorentzian half-widths resulted from the literature lifetimes of the energy levels, while the values of Gaussian half-width parameters were adopted on the basis of the discharge current and the wavelength of the investigated transition.

4. Results

In this work altogether 74 spectral lines of atomic holmium were investigated for determination of Landé g_J factors, including 6 lines measured and analysed both under the stronger and the weaker magnetic field. It proved that applied magnetic field of ca. 500–600 G yielded sufficient Zeeman splitting of observed spectra. All of the investigated holmium lines are presented in Table 1.

To obtain the value of g_J factor of a particular upper energy level one should know the magnetic field strength and preferably g_J factor of the lower level (and vice versa, in the case of the need to determine the lower levels' factor the knowledge of the upper level's g_J factor is desired). Investigated transitions were excited from energy levels that don't belong to the ground multiplet. For this reason, both the g_J factors for the upper and lower levels were not precisely known. In this work, semi-empirically predicted g_J factors were taken as the initial values of g_J factors. The magnetic field was well-known from argon lines' investigation.

An iterative procedure of determination of g_J factors for both the levels involved in individual transitions is described below. First, the g_J factors of the lower energy levels were fixed at the semi-empirically predicted values, allowing calculation of g_J factors of the upper energy levels. Then, the obtained results were averaged. During the first step re-calculation of *hfs A* and *B* constants for the upper levels was also performed. Second, the procedure was reversed to make a correction in g_J values of the lower levels. In the following, the Landé g_J factors of the upper levels were calculated once again, with new g_J factors values of the lower levels. If the performed correction was valid, one should observe decreasing of mean standard deviations in comparison with those obtained in the first calculation for the upper levels. The adopted method resulted in significant reduction of mean standard deviation for the upper energy levels. The final Landé g_J factors obtained for the upper levels were used to re-correct the values of the Landé factors of the lower levels, again.

The final values for both the lower and the upper energy levels are summarized in Table 1. In the first group of columns the information on the transitions studied is provided: wavelengths and wavenumbers, respectively. The next two columns contain information about the lower levels of the investigated transitions: energies and J quantum numbers. The following column includes average experimental values of Landé g_J factors obtained from measurements performed for π and σ polarization. All of the Landé factors are listed with their uncertainties. Finally, the analogous sets of data for the upper energy levels are presented in columns 7–9.

The values obtained from final calculations were averaged for individual holmium energy levels. Among 17 odd-parity energy levels, one of them (28481.24 cm^{-1}) was involved in two spectral lines. From 3 to 7 results obtained from individual lines were used to average the remaining ones. In case of even-parity energy levels, the Landé g_J factor results were obtained from single lines in 3 cases: 16438.01 cm^{-1}, 18858.19 cm^{-1} and 20498.73 cm^{-1}. For 8 other levels results were averaged over g_J factors calculated from

2 lines excited from the level considered. From 3 to even 9 separate spectral lines were taken to the mean for the remaining half of investigated energy levels.

Table 2 contains experimental values for the *hfs* constants *A* and *B* of odd-parity energy levels obtained in this work, compared with literature data. Landé g_J factors averaged for individual energy levels investigated in this work are presented in Table 3. The results are reported separately for both parities. Information about studied energy levels is provided in second and third column: energies and *J* quantum numbers, respectively. The number of recorded spectral lines taken to the average is presented in fourth column. Following three columns include mean values of Landé g_J factors for particular energy levels, literature and semi-empirically predicted values, respectively.

Fig. 1 shows an example of recorded Zeeman spectra of an argon line, while in Fig. 2 all Zeeman components which form the investigated signal of another argon line are presented. The analysis of argon spectra in different spectral ranges led to determination of the magnetic field in the hollow cathode discharge lamp. In Figs. 3–8 examples of the spectra recorded in presence of the magnetic field and with the fitted Zeeman-*hfs* patterns are presented. Single Zeeman components are so close to each other that they can only be presented as a resultant envelope. The part of the spectrum in higher resolution, showing the individual Zeeman components, is presented in Fig. 4. The problem of simultaneous determination of the g_J factors of the upper and the lower electronic level of the studied transition required a special selection of the lines to be measured. The chance to increase the reliability of the results is, firstly, the use of more than one magnetic field strength value, and, secondly, the measurement of lines, the lower or upper levels of which are also involved in other transitions investigated. Both methods were used in the research, which is illustrated in the individual figures. Figs. 3 and 5 show the recorded Zeeman-*hfs* patterns of the spectral lines $\lambda = 585.629$ nm and $\lambda = 605.072$ nm, which were measured in both magnet systems. Figs. 6–8 show scans obtained in pairs for lines sharing a common upper or lower level.

The experimental uncertainty of calculated Landé g_J factors consists of two mean standard deviations for both fitted parameters of energy levels, uncertainty resulting from the selection of initial saturation parameters and the experimental error related to uncertainty of the magnetic field. Predicted fluctuations in the magnetic field, during the experiment, should not exceed 2%. To account for the contribution of the magnetic field variation to the total measurement uncertainty, the values of the g_J factors were calculated at 98% and 102% of the evaluated magnetic field values. The difference in obtained results was divided by 2 and assumed as Landé factors′ uncertainty resulting from the magnetic field. The total uncertainty for single electronic level, related to the single spectral line, was calculated according to the formula:

$$\Delta g_J = \sqrt{(SD_1)^2 + (SD_2)^2 + (\Delta g_{J,S})^2 + (\Delta g_{J,B})^2} \tag{4}$$

where $SD_{1,2}$ are the mean standard deviations for g_J of the upper and the lower electronic energy level, and the remaining two terms are the uncertainty related to saturation effect and the contribution of the magnetic field variation to the total measurement error, respectively.

5. Discussion

Most of the Landé g_J factors determined on the basis of the experimental investigations of the Zeeman structures of spectral lines in the atomic holmium, performed in this work, cannot be compared to any earlier experimental values. Only Landé factors for two odd-parity energy levels: 36229.59 cm^{-1} and 38345.80 cm^{-1}, as well as four even-parity energy levels:

(a)

(b)

(c)

(d)
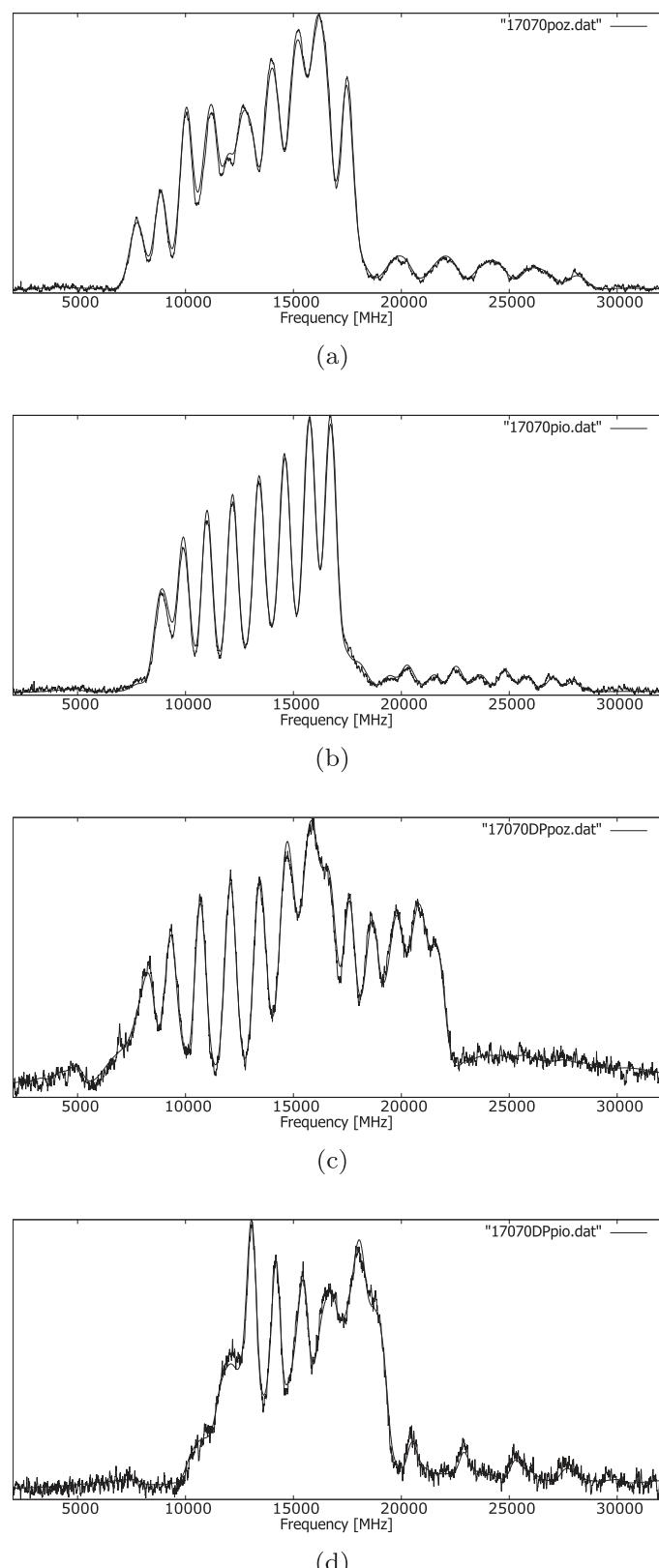
Fig. 3. Zeeman splitting of the hyperfine structure at two different values of magnetic field strength. Recorded Zeeman-*hfs* patterns of the spectral line $\lambda = 585.629$ nm (k=17070.93 cm^{-1}) in the holmium atom (Table 1, No 42 and 43), along with the least-squares fitted curves for a) polarization σ at the magnetic field strength 521.2 G, b) polarization π at the magnetic field strength 509.1 G, c) polarization σ at the magnetic field strength 1961 G, d) polarization π at the magnetic field strength 1955 G.

Table 1

Spectral lines of the holmium atom experimentally investigated in this work for the purpose of determination of the Landé g_J factors. For all lines the g_J factors for the upper odd-parity levels and lower even-parity levels were determined independently. Spectral lines recorded with stronger magnetic field (see text, Section 2.) are denoted by asterisks.

No	Line		Lower level			Upper level		
	λ_{air} (nm)	k_{vac} (cm^{-1})	E (cm^{-1})	J	$g_{J,av}$	E (cm^{-1})	J	$g_{J,av}$
1	2	3	4	5	6	7	8	9
1	489.237	20434.30	8427.11	15/2	1.2842(0.0087)	28861.41	17/2	1.1966(0.0074)
2	499.503	20014.33	8378.91	17/2	1.2668(0.0101)	28393.24	19/2	1.2405(0.0068)
3	499.661	20008.00	18337.80	17/2	1.2492(0.0089)	38345.80	15/2	1.1113(0.0075)
4	501.375	19939.59	9147.08	13/2	1.3518(0.0069)	29086.67	15/2	1.1689(0.0104)
5	501.443	19936.88	8378.91	17/2	1.2657(0.0073)	28315.79	15/2	1.2748(0.0078)
6	502.050	19912.70	11530.56	17/2	1.1962(0.0058)	31443.26	15/2	1.2119(0.0062)
7	502.658	19888.68	8427.11	15/2	1.2822(0.0109)	28315.79	15/2	1.2685(0.0095)
8	503.248	19865.38	8378.91	17/2	1.2690(0.0059)	28244.29	17/2	1.2313(0.0061)
9	504.472	19817.18	8427.11	15/2	1.2830(0.0063)	28244.29	17/2	1.2286(0.0077)
10	507.620	19694.27	18651.53	15/2	1.1901(0.0062)	38345.80	15/2	1.1088(0.0063)
11	512.160	19519.77	16709.82	17/2	1.2155(0.0100)	36229.59	19/2	1.2268(0.0063)
12	513.004	19487.61	18858.19	13/2	1.1116(0.0171)	38345.80	15/2	1.1083(0.0105)
13	518.650	19275.34	11530.56	17/2	1.1821(0.0146)	30805.90	17/2	1.2298(0.0080)
14	519.524	19243.03	11530.56	17/2	1.1945(0.0079)	30773.59	15/2	1.2711(0.0074)
15	521.538	19168.71	9147.08	13/2	1.3379(0.0136)	28315.79	15/2	1.2784(0.0108)
16	522.149	19146.28	9741.50	19/2	1.2233(0.0129)	28887.78	21/2	1.2449(0.0085)
17	522.869	19119.91	9741.50	19/2	1.2282(0.0094)	28861.41	17/2	1.1995(0.0086)
18	522.970	19116.13	11689.77	19/2	1.1852(0.0084)	30805.90	17/2	1.2098(0.0066)
19	523.450	19098.71	12344.55	13/2	1.2404(0.0067)	31443.26	15/2	1.2122(0.0061)
20	535.994	18651.74	9741.50	19/2	1.2274(0.0086)	28393.24	19/2	1.2159(0.0084)
21	540.309	18502.79	9741.50	19/2	1.2246(0.0088)	28244.29	17/2	1.2367(0.0086)
22	541.360	18466.86	12339.04	15/2	1.2540(0.0085)	30805.90	17/2	1.2061(0.0083)
23	542.471	18429.04	12344.55	13/2	1.2434(0.0086)	30773.59	15/2	1.2642(0.0076)
24	543.585	18391.26	8378.91	17/2	1.2755(0.0079)	26770.17	19/2	1.1876(0.0065)
25	551.476	18128.12	15855.28	15/2	1.2575(0.0106)	33983.40	17/2	1.2120(0.0085)
26	557.385	17935.94	12344.55	13/2	1.2339(0.0119)	30280.49	11/2	1.2531(0.0078)
27	558.760	17891.79	18337.80	17/2	1.2453(0.0089)	36229.59	19/2	1.2352(0.0058)
28	560.722	17829.19	16154.21	15/2	1.1949(0.0112)	33983.40	17/2	1.2094(0.0082)
29	569.141	17565.47	11322.31	21/2	1.2242(0.0077)	28887.78	21/2	1.2447(0.0063)
30	569.444	17556.11	11530.56	17/2	1.1921(0.0069)	29086.67	15/2	1.1783(0.0070)
31	571.165	17503.22	12339.04	15/2	1.2378(0.0080)	29842.26	13/2	1.2717(0.0094)
32	571.345	17497.71	12344.55	13/2	1.2466(0.0122)	29842.26	13/2	1.2535(0.0097)
33	576.846	17330.85	11530.56	17/2	1.1947(0.0080)	28861.41	17/2	1.1992(0.0064)
34	577.879	17299.88	16683.52	19/2	1.1699(0.0077)	33983.40	17/2	1.2179(0.0097)
35	577.879	17299.88*	16683.52	19/2	1.1728(0.0083)	33983.40	17/2	1.2141(0.0091)
36	578.758	17273.58	16709.82	17/2	1.2224(0.0076)	33983.40	17/2	1.2050(0.0080)
37	581.301	17198.01	11689.77	19/2	1.1892(0.0084)	28887.78	21/2	1.2329(0.0062)
38	581.317	17197.56	13082.93	11/2	1.2556(0.0151)	30280.49	11/2	1.2384(0.0067)
39	582.194	17171.64	11689.77	19/2	1.1807(0.0068)	28861.41	17/2	1.2007(0.0068)
40	582.194	17171.64*	11689.77	19/2	1.1834(0.0060)	28861.41	17/2	1.1979(0.0059)
41	582.625	17158.93	11322.31	21/2	1.2266(0.0052)	28481.24	21/2	1.2620(0.0060)
42	585.629	17070.93	11322.31	21/2	1.2329(0.0087)	28393.24	19/2	1.2362(0.0069)
43	585.629	17070.93*	11322.31	21/2	1.2328(0.0081)	28393.24	19/2	1.2362(0.0064)
44	587.082	17028.67	9741.50	19/2	1.2299(0.0140)	26770.17	19/2	1.2007(0.0242)
45	595.375	16791.47	11689.77	19/2	1.1818(0.0074)	28481.24	21/2	1.2603(0.0067)
46	595.597	16785.23	11530.56	17/2	1.1902(0.0069)	28315.79	15/2	1.2786(0.0069)
47	596.517	16759.33	13082.93	11/2	1.2461(0.0090)	29842.26	13/2	1.2671(0.0071)
48	597.130	16742.12	12344.55	13/2	1.2366(0.0087)	29086.67	15/2	1.1776(0.0064)
49	598.145	16713.73	11530.56	17/2	1.1885(0.0054)	28244.29	17/2	1.2400(0.0055)
50	598.145	16713.73*	11530.56	17/2	1.1957(0.0062)	28244.29	17/2	1.2329(0.0060)
51	598.512	16703.47	11689.77	19/2	1.1847(0.0082)	28393.24	19/2	1.2366(0.0053)
52	603.897	16554.52	11689.77	19/2	1.1809(0.0063)	28244.29	17/2	1.2317(0.0061)
53	603.897	16554.52*	11689.77	19/2	1.1826(0.0056)	28244.29	17/2	1.2309(0.0053)
54	605.072	16522.37	12339.04	15/2	1.2337(0.0067)	28861.41	17/2	1.2097(0.0086)
55	605.072	16522.37*	12339.04	15/2	1.2372(0.0066)	28861.41	17/2	1.2072(0.0082)
56	610.998	16362.14	15081.12	13/2	1.1816(0.0063)	31443.26	15/2	1.2095(0.0062)
57	625.380	15985.91	15130.31	17/2	1.1473(0.0086)	31116.22	17/2	1.2960(0.0063)
58	625.600	15980.16	15136.06	15/2	1.1716(0.0113)	31116.22	17/2	1.2900(0.0091)
59	625.737	15976.75	12339.04	15/2	1.2424(0.0059)	28315.79	15/2	1.2740(0.0079)
60	625.952	15971.24	12344.55	13/2	1.2447(0.0102)	28315.79	15/2	1.2687(0.0069)
61	635.520	15730.86	20498.73	17/2	1.3828(0.0141)	36229.59	19/2	1.2120(0.0096)
62	637.070	15692.47	15081.12	13/2	1.1846(0.0072)	30773.59	15/2	1.2634(0.0072)
63	637.760	15675.59	15130.31	17/2	1.1475(0.0119)	30805.90	17/2	1.2170(0.0061)
64	637.990	15669.84	15136.06	15/2	1.1744(0.0076)	30805.90	17/2	1.2078(0.0087)
65	639.310	15637.53	15136.06	15/2	1.1769(0.0070)	30773.59	15/2	1.2643(0.0078)
66	641.340	15587.98	15855.28	15/2	1.2576(0.0058)	31443.26	15/2	1.2149(0.0074)
67	652.056	15331.87	18651.53	15/2	1.1896(0.0128)	33983.40	17/2	1.2124(0.0070)
68	653.880	15289.05	16154.21	15/2	1.1929(0.0085)	31443.26	15/2	1.2190(0.0081)
69	655.090	15260.94	15855.28	15/2	1.2552(0.0095)	31116.22	17/2	1.2976(0.0083)
70	656.004	15239.61	11530.56	19/2	1.1926(0.0098)	26770.17	19/2	1.1977(0.0063)
71	657.740	15199.37	15081.12	13/2	1.1792(0.0087)	30280.49	11/2	1.2492(0.0076)
72	666.250	15005.25	16438.01	17/2	1.1549(0.0066)	31443.26	15/2	1.2126(0.0070)
73	668.680	14950.62	15855.28	15/2	1.2556(0.0108)	30805.90	17/2	1.2176(0.0079)
74	670.130	14918.31	15855.28	15/2	1.2635(0.0172)	30773.59	15/2	1.2717(0.0086)

Table 2
Values of the hyperfine structure constants *A* and *B* for the upper odd-parity levels of the holmium atom involved in the Zeeman-*hfs* investigations, known from literature [21] and obtained within this work.

No 1	E[cm^{-1}] 2	J 3	A[MHz] 4	B[MHz] 5	A$_{lit}$[MHz] 6	B$_{lit}$[MHz] 7
1	26770.17	19/2	729.0(1.0)	1283(41)	729.4(14)	1291(73)
2	28244.29	17/2	661.25(34)	711(27)	661.6(11)	731(27)
3	28315.79	15/2	876.0(9)	429(53)	875.7(12)	267(60)
4	28393.24	19/2	874.7(1.1)	1313(88)	876.6(4)	1245(6)
5	28481.24	21/2	1029.98(31)	2020(33)	1029.6(14)	2067(104)
6	28861.41	17/2	616.09(51)	−33(17)	615.9(5)	−78(21)
7	28887.78	21/2	955.0(1.0)	1760(23)	954.3(1)	1809(13)
8	29086.67	15/2	395.5(1.9)	−547(22)	396.1(28)	−550(34)
9	29842.26	13/2	1146.9(8)	380(28)	1149.1(5)	404(91)
10	30280.49	11/2	1188.2(1.7)	1632(9)	1193.7(16)	1623(50)
11	30773.59	15/2	836.7(7)	1199(28)	838.8(30)	1185(150)
12	30805.90	17/2	765.1(1.2)	−239(37)	764.5(24)	−293(51)
13	31116.22	17/2	1532.9(8)	−1586(39)	1539.0(25)	−1539(124)
14	31443.26	15/2	1028.8(5)	−1043(31)	1028.8(4)	−1099(30)
15	33983.40	15/2	1011.09(53)	1691(62)	1014.7(19)	1591(34)
16	36229.59	19/2	881.1(7)	704(16)	880.7(4)	718(16)
17	38345.80	15/2	520.93(16)	1163(144)	523.4(21)	471(102)

Table 3
Values of Landé *g$_J$* factors of the electronic levels of the holmium atom, determined in this work from the measurements of the Zeeman effect in the hyperfine structure, as well as theoretically predicted.

| No 1	E(cm^{-1}) 2	J 3	No of lines 4	$g_{J_{mean}}$ 5	$g_{J_{lit}}$ 6	$g_{J_{pred}}$ [11,21] 7
	even-parity	levels				
1	8378.91	17/2	4	1.269(0.010)		1.263
2	8427.11	15/2	3	1.283(0.008)		1.280
3	9147.08	13/2	2	1.347(0.039)		1.339
4	9741.50	19/2	5	1.227(0.007)		1.230
5	11322.31	21/2	4	1.229(0.010)		1.231
6	11530.56	17/2	9	1.192(0.008)		1.192
7	11689.77	19/2	8	1.183(0.007)		1.180
8	12339.04	15/2	5	1.241(0.014)		1.234
9	12344.55	13/2	6	1.241(0.010)		1.237
10	13082.93	11/2	2	1.250(0.027)		1.262
11	15081.12	13/2	3	1.182(0.009)		1.175
12	15130.31	17/2	2	1.147(0.006)	1.144(0.013)[5]	1.150
13	15136.06	15/2	4	1.175(0.009)		1.169
14	15855.28	15/2	5	1.257(0.009)		1.246
15	16154.21	15/2	2	1.194(0.009)		1.196
16	16438.01	17/2	1	1.155(0.019)	1.137(0.002)[5]	1.148
17	16683.52	19/2	2	1.171(0.010)		1.176
18	16709.82	17/2	2	1.219(0.020)	1.189(0.010)[5]	1.223
19	18337.80	17/2	2	1.247(0.013)	1.230(0.021)[5]	1.242
20	18651.53	15/2	2	1.190(0.006)		1.199
21	18858.19	13/2	1	1.112(0.086)		1.133
22	20498.73	17/2	1	1.383(0.062)		1.368
	odd-parity	levels				
1	26770.17	19/2	3	1.194(0.017)		1.204
2	28244.29	17/2	7	1.233(0.008)		1.229
3	28315.79	15/2	6	1.274(0.009)		1.263
4	28393.24	19/2	5	1.234(0.016)		1.239
5	28481.24	21/2	2	1.261(0.008)		1.266
6	28861.41	17/2	7	1.201(0.009)		1.092
7	28887.78	21/2	3	1.240(0.017)		1.251
8	29086.67	15/2	3	1.176(0.014)		1.143
9	29842.26	13/2	3	1.264(0.023)		1.133
10	30280.49	11/2	3	1.247(0.019)		1.202
11	30773.59	15/2	5	1.267(0.009)		1.265
12	30805.90	17/2	6	1.215(0.014)		1.208
13	31116.22	17/2	4	1.295(0.012)		1.289
14	31443.26	15/2	6	1.213(0.008)		1.210
15	33983.40	15/2	6	1.212(0.009)		1.229
16	36229.59	19/2	3	1.227(0.028)	1.230[9]	1.240
17	38345.80	15/2	3	1.110(0.008)	1.120[9]	1.057
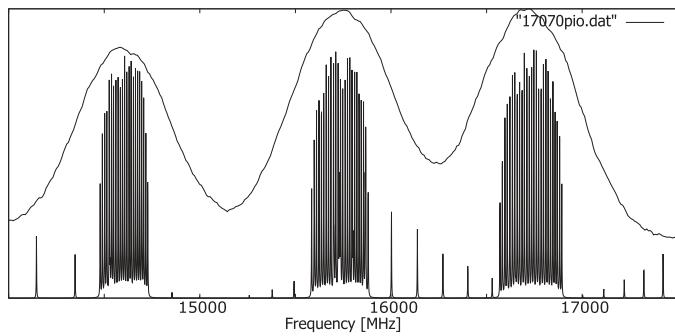
Fig. 4. The central part of the hyperfine line structure split in the magnetic field (polarization π, strength 509.1 G, k = 17070.93 cm^{-1} - the case presented in Fig. 3b) with symbolically marked positions of the Zeeman components.

15130.31 cm^{-1}, 16438.01 cm^{-1}, 16709.82 cm^{-1} and 18337.80 cm^{-1}, are available from the experimental reference data published by Kröger et al. [9] and our research grup [5], respectively. As far as the results for even-parity energy levels are concerned, the g_J factors' values for all compared levels are consistent, within the limits of the measurement uncertainties, with the values reported previously. This consistency is quite promising, but presented results will need further verification. For example, the level 16438.01 cm^{-1} was investigated in a single spectral line, so the average value was determined on the basis of two partial results (with π and σ polarization). Because of that, the obtained average value may be less reliable. Concerning the odd-parity energy levels, the experimental values of the g_J factor of 36229.59 cm^{-1} level determined in this study is consistent, within the limits of the measurement uncertainty, with the literature result, while for 38345.80 cm^{-1} level the respective results vary. However, the discrepancy is relatively small, taking into account that the measurement uncertainty was not determined for the compared literature data. Despite a clear shortage of available experimental data, a good agreement of the presented results with the values predicted by semi-experimental calculations can be observed.

Some small deviations between the values calculated for π and σ polarizations were observed. These differences may be caused by heterogeneity of the magnetic field across the path of the exciting laser beam. Another effect impairing the accuracy of the calculations is the presence of minor, but not negligible, σ components in the spectra which should contain only π components, and vice versa. This effect results from the imperfect parameters of the polarizer and the polarization rotator which transmit small amount of light that should be completely blocked in perfect situation. The presence of minor "*parasitic*" components is noticeable in case of strong spectral lines and strong exciting beam, but even in this situation the contribution of "*leaking*" components is at a level of ca. 0.1%. Despite the fact that the total measurement uncertainty is influenced by several different factors, the obtained uncertainties constitute only a few percent of the average values, which is a characteristic result for research performed with this method.

All experimental results summarized in Table 3 are very close to the values obtained by semi- empirical analysis of the hyperfine structure of the holmium atom. For 30 out of 39 investigated energy levels, the calculated Landé g_J factors agree with the predicted ones within the measurement uncertainties. The differences for the remaining results are quite small, not exceeding 11%. As can be concluded from the results presented in Table 2, the re-calculated values of the *hfs* constants A and B are also consistent with the literature data. Among 17 considered odd-parity electronic levels, results calculated for A constants of 10 levels don't differ from literature values by more than the determined measurement uncertainty. For remaining 7 levels, obtained results of A constants differ

(a)

(b)

(c)

(d)
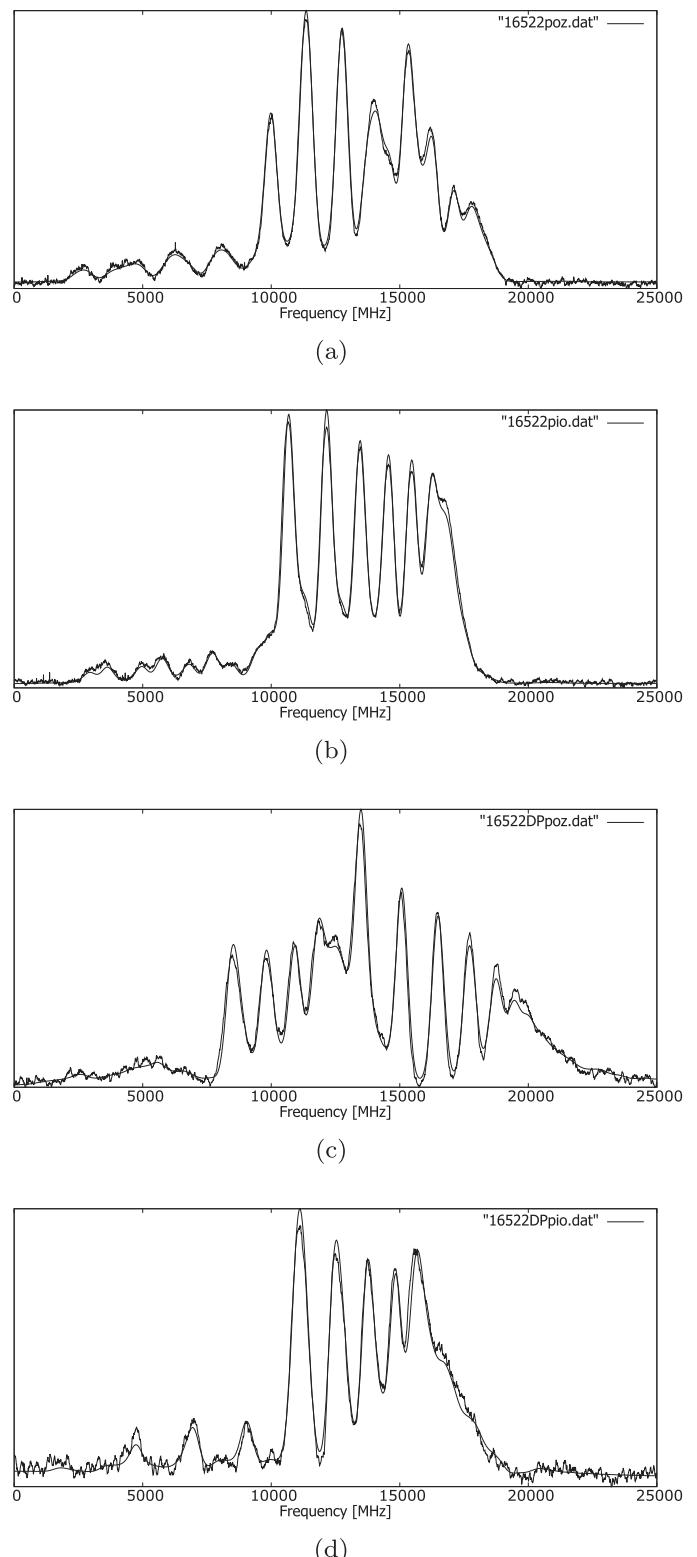
Fig. 5. Zeeman splitting of the hyperfine structure at two different values of magnetic field strength. Recorded Zeeman-*hfs* patterns of the spectral line $\lambda = 605.072$ nm (k=16522.37 cm^{-1}) in the holmium atom (Table 1, No 54 and 55), along with the least-squares fitted curves for a) polarization σ at the magnetic field strength 513.3 G, b) polarization π at the magnetic field strength 500.5 G, c) polarization σ at the magnetic field strength 1974 G, d) polarization π at the magnetic field strength 1929 G.
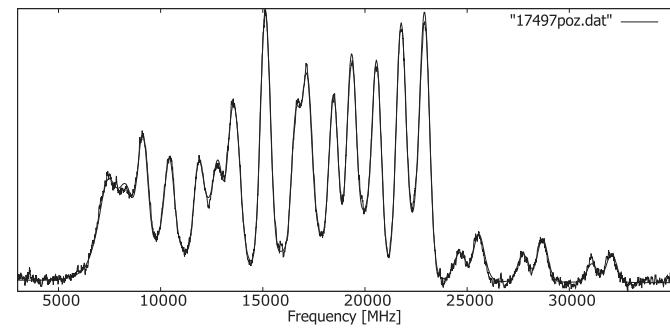
(a)
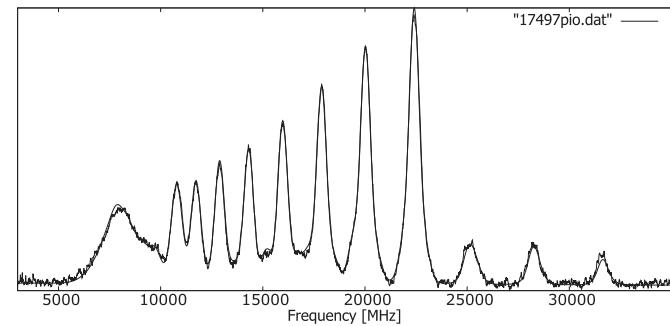
(b)
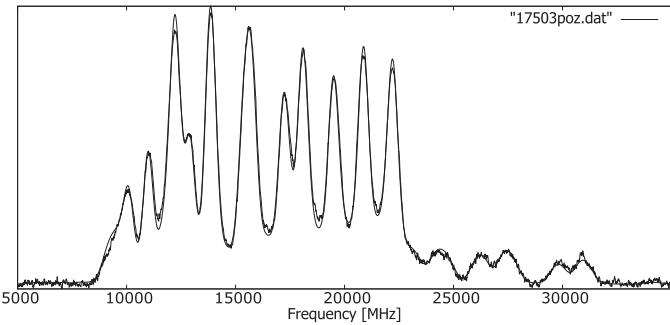
(c)
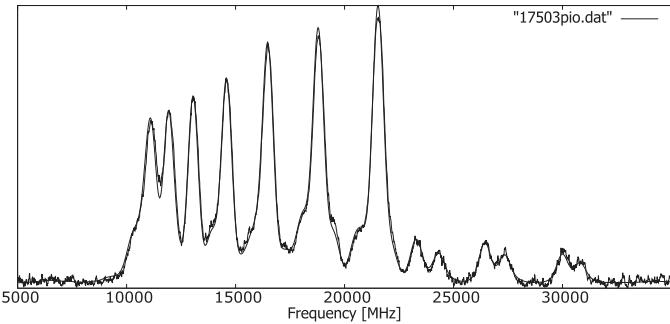
(d)

Fig. 6. Zeeman splitting of the hyperfine structure of two lines with the same upper level (E=29842.26 cm^{-1} J=13/2). Recorded Zeeman-*hfs* patterns of the spectral line λ = 571.345 nm (k=17497.71 cm^{-1}, Table 1, No 32), and λ = 571.165 nm (k=17503.22 cm^{-1}, Table 1, No 31) along with the least-squares fitted curves. a) line 17497.71 polarization σ at the magnetic field strength 510.3 G, b) line 17497.71 polarization π at the magnetic field strength 508.6 G, c)line 17503.22 polarization σ at the magnetic field strength 510.2 G, d) line 17503.22 polarization π at the magnetic field strength 505.9 G.
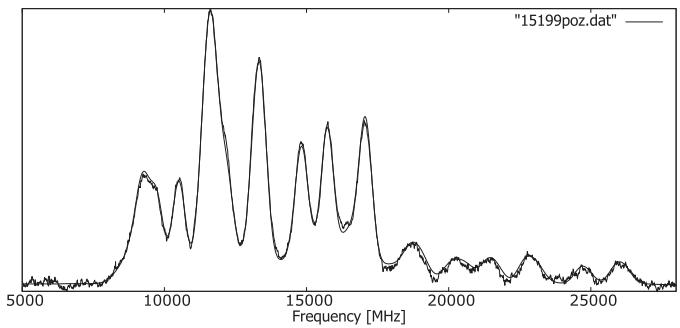
(a)
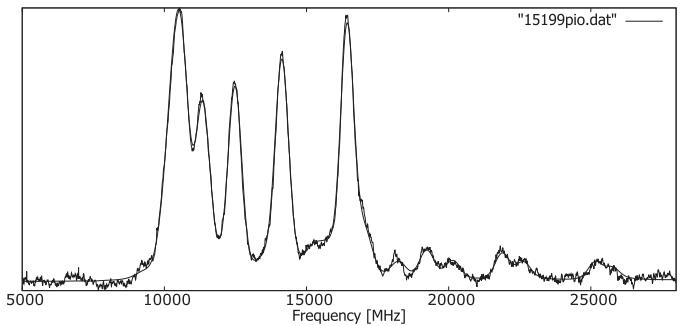
(b)
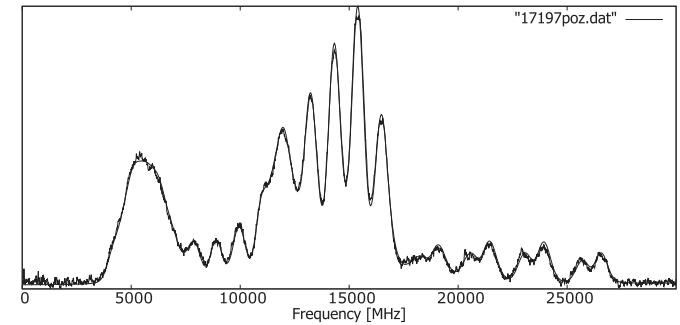
(c)
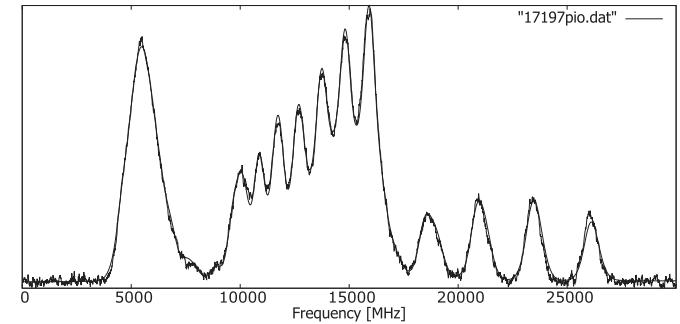
(d)

Fig. 7. Zeeman splitting of the hyperfine structure of two lines with the same upper level (E=30280.49 cm^{-1} J=11/2). Recorded Zeeman-*hfs* patterns of the spectral line λ = 657.740 nm (k=15199.37 cm^{-1}, Table 1, No 71), and λ = 581.317 nm (k=17197.56 cm^{-1}, Table 1, No 38) along with the least-squares fitted curves. a) line 15199.37 polarization σ at the magnetic field strength 600.8 G, b) line 15199.37 polarization π at the magnetic field strength 594.3 G, c)line 17197.56 polarization σ at the magnetic field strength 514. 3G, d) line 17197.56 polarization π at the magnetic field strength 508.6 G.
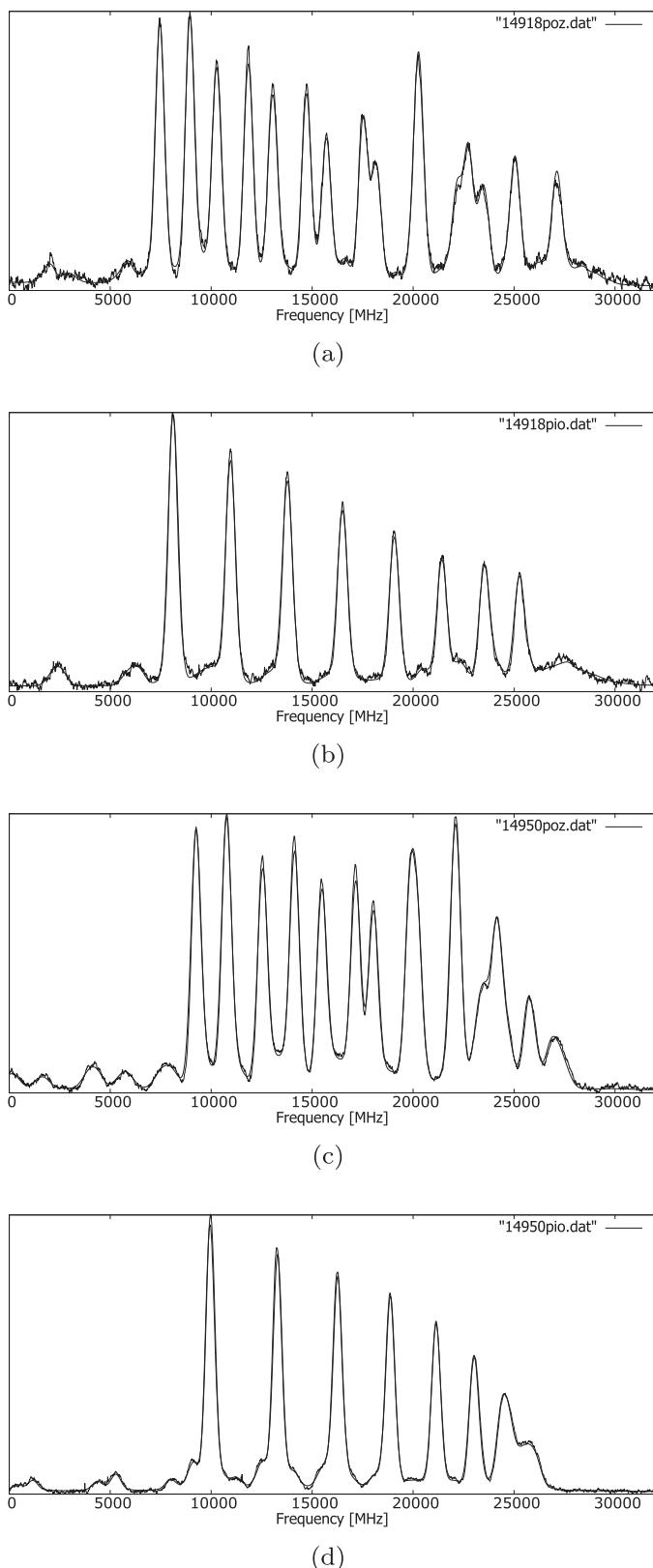
Fig. 8. Zeeman splitting of the hyperfine structure of two lines with the same lower level (E=15855.28 cm^{-1} J=15/2). Recorded Zeeman-*hfs* patterns of the spectral line λ = 670.130 nm (k=14918.31 cm^{-1}, Table 1, No 74), and λ = 668.680 nm (k=14950.62 cm^{-1}, Table 1, No 73) along with the least-squares fitted curves. a) line 14918.31 polarization σ at the magnetic field strength 618.6 G, b) line 14918.31 polarization π at the magnetic field strength 621.4 G, c) line 14950.62 polarization σ at the magnetic field strength 611.3 G, d) line 14950.62 polarization π at the magnetic field strength 621.6 G.

from literature values, but in most cases the inconsistencies don't exceed three times the mean standard deviation (the maximum statistical error). The most significant discrepancies were observed for 2 levels: 30280.49 cm^{-1} and 31116.22 cm^{-1}. Conerning calculated *B* constants, obtained results are consistent with previously published ones for 12 energy levels. Out of 5 cases, which differ from literature values by more than the estimated measurement errors, only the discrepancy for 38345.80 cm^{-1} level is significant. This case requires additional experimental verification, which will be carried out as soon as new experimental possibilities become available.

6. Conclusions

In this work experimental results of Landé g_J factors for 39 electronic levels of the holmium atom are presented, including 22 even-parity levels and 17 levels belonging to the odd-parity configurations. The measurements were performed with the LIF method in a hollow cathode discharge lamp with Zeeman splitting of spectra in a magnetic field. Among the investigated g_J factors, collected in Table 3, 33 were experimentally determined for the first time. One out of two results for odd-parity levels, and all of the even-parity levels, are in a good agreement with the earlier literature data. The result for the remaining odd-parity level is not consistent with the previously published one, within the measurement uncertainty, but one must notice that experimental uncertainty wasn't determined as far as the literature data for the odd-parity levels are concerned. The literature values obtained by our group earlier, and compared with current results in Table 3 were investigated in single spectral lines (considered as possible cooling transitions) and should be considered as preliminary results requiring further experimental verification. Presented values are mostly close to those predicted by the semi-empirical calculations, but in some cases the differences between the experimental and predicted values exceed the measurement uncertainties. Some lines were investigated both in stronger and weaker magnetic field, and obtained results are not significantly different.

Declaration of Competing Interest

The authors declare that they have no known competing financial interests or personal relationships that could have appeared to influence the work reported in this paper.

CRediT authorship contribution statement

M. Chomski: Data curation, Investigation, Formal analysis, Writing – original draft. **B. Furmann:** Data curation, Formal analysis, Funding acquisition, Investigation, Software. **J. Ruczkowski:** Formal analysis, Software. **M. Suski:** Data curation, Investigation. **D. Stefańska:** Investigation, Writing – original draft.

Acknowledgements

References

[1] Saffman M, Mølmer K. Scaling the neutral-atom Rydberg gate quantum computer by collective encoding in holmium atoms. Phys Rev A 2008;78:012336. doi:10.1103/physreva.78.012336.

[2] Miao J, Hostetter J, Stratis G, Saffman M. Magneto-optical trapping of holmium atoms. Phys Rev A 2014;89:041401. doi:10.1103/physreva.89.041401.

[3] Sneden C, Cowan JJ. Genesis of the heaviest elements in the milky way galaxy. Science 2003;299(5603):70–5. doi:10.1126/science.1077506.

[4] Lawler JE, Sneden C, Cowan JJ. Improved atomic data for Ho II and new holmium abundances for the sun and three metal-poor stars. Astrophys J 2004;604(2):850. doi:10.1086/382068.

[5] Stefańska D, Furmann B, Ruczkowski J, Elantkowska M, Glowacki P, Chomski M, et al. Investigations of the possible second-stage laser cooling transitions for the holmium atom magneto-optical trap. J Quant Spectrosc Radiat Transf 2020;246:106915. doi:10.1016/j.jqsrt.2020.106915.

[6] Dankwort W, Ferch J, Gebauer H. Hexadecapole interaction in the atomic ground state of ^{165}Ho. Z Phys 1974;267(3):229–37. doi:10.1007/bf01669225.

[7] Livingston AE, Pinnington EH. Spectra of neutral and singly ionized holmium. J Opt Soc Am 1971;61(10):1429–30. doi:10.1364/JOSA.61.1429_1.

[8] Burghardt B, Büttgenbach S, Glaeser N, Harzer R, Meisel G, Roski B, et al. Hyperfine structure measurements in metastable states of ^{165}Ho. Z Phys A 1982;307(3):193–200. doi:10.1007/bf01438640.

[9] Kröger S, Wyart J-F, Luc P. Theoretical interpretation of hyperfine structures in doubly-excited configurations 4f^{10}5d6s6p and 4f^{10}5d^{2}6s and new energy levels in neutral holmium (ho i). Phys Scr 1997;55:579. doi:10.1088/0031-8949/55/5/010.

[10] Stefanska D, Furmann B. Hyperfine structure investigations for the odd-parity configuration system in atomic holmium. J Quant Spectrosc Radiat Transf 2018;206:286–95. doi:10.1016/j.jqsrt.2017.11.019.

[11] Stefanska D, Ruczkowski J, Elantkowska M, Furmann B. Fine- and hyperfine structure investigations of the even-parity configuration system in atomic holmium. J Quant Spectrosc Radiat Transf 2018;209:180–95. doi:10.1016/j.jqsrt.2018.01.010.

[12] Stefanska D, Furmann B, Głowacki P. Possibilities of investigations of the temporal variation of the α constant in the holmium atom. J Quant Spectrosc Radiat Transf 2018;213:159–68. doi:10.1016/j.jqsrt.2018.04.017.

[13] Stefanska D, Furmann B. Hyperfine structure investigations for the odd-parity configuration system in atomic holmium. J Quant Spectrosc Radiat Transf 2018;206:286–95. doi:10.1016/j.jqsrt.2017.11.019.

[14] Furmann B, Stefanska D, Suski M, Wilman S. Identification of new electronic levels in the holmium atom and investigation of their hyperfine structure. J Quant Spectrosc Radiat Transf 2018;219:117–26. doi:10.1016/j.jqsrt.2018.08.005.

[15] Furmann B, Stefańska D, Suski M, Wilman S, Chomski M. Hyperfine structure studies of the odd-parity electronic levels of the holmium atom I: levels with known energies. J Quant Spectrosc Radiat Transf 2019;234:115–23. doi:10.1016/j.jqsrt.2019.05.028.

[16] Furmann B, Stefańska D, Wilman S, Chomski M, Suski M. Hyperfine structure studies of the odd-parity electronic levels in the holmium atom II: new levels. J Quant Spectrosc Radiat Transf 2019;235:70–80. doi:10.1016/j.jqsrt.2019.06.005.

[17] Wyart J-F, Camus P, Vergès J. Etude du spectre de l'holmium atomique: I. Spectre d'émission infrarouge niveaux d'énergie de Ho I et structures hyperfines. Physica C 1977;92(3):377–96. doi:10.1016/0378-4363(77)90137-1.

[18] Al-Labady N, Özdalgiç B, Er A, Güzelçimen F, Öztürk IK, Kröger S, et al. Line identification of atomic and ionic spectra of holmium in the near-UV. Part I. Spectrum of ho i. Astrophys J Suppl Ser 2017;228(2):16. doi:10.3847/1538-4365/228/2/16.

[19] Özdalgiç B, Güzelçimen F, Öztürk IK, Kröger S, Kruzins A, Tamanis M, et al. Line identification of atomic and ionic spectra of holmium in the visible spectral range. I. Spectrum of Ho I. Astrophys J Suppl Ser 2019;240(2):27. doi:10.3847/1538-4365/aaf9b2.

[20] Wyart J-F, Camus P. Etude du spectre de l'holmium atomique: II. Interprétation paramétrique des niveaux d'énergie et des structures hyperfines. Physica C 1978;93(2):227–36. doi:10.1016/0378-4363(78)90129-8.

[21] Elantkowska M, Ruczkowski J, Sikorski A, Wilman S. Fine- and hyperfine structure investigations of the odd-parity configuration system in atomic holmium. J Quant Spectrosc Radiat Transf 2019;237:106642. doi:10.1016/j.jqsrt.2019.106642.

[22] Stefanska D, Werbowy S, Krzykowski A, Furmann B. Lande g_J factors for even-parity electronic levels in the holmium atom. J Quant Spectrosc Radiat Transf 2018;210:136–40. doi:10.1016/j.jqsrt.2018.02.015.

[23] Grabowski D, Drozdowski R, Kwela J, Heldt J. Hyperfine structure and Zeeman effect studies in the 6p7p-6p7s transitions in Bi II. Z Phys D 1996;38:289–93. doi:10.1007/s004600050093.

[24] Werbowy S, Güney C, Windholz L. Experimental investigations of the Zeeman effect of new fine structure levels of lanthanum and praseodymium. Spectrochim Acta Part B 2016;116(Supplement C):16–20. doi:10.1016/j.sab.2015.11.003.

[25] Werbowy S, Güney C, Windholz L. Studies of Landé g_J-factors of singly ionized lanthanum by laser-induced fluorescence spectroscopy. J Quant Spectrosc Radiat Transf 2016;179(Supplement C):33–9. doi:10.1016/j.jqsrt.2016.03.009.

[26] Sobolewski Ł, Windholz L, Kwela J. Laser induced fluorescence spectroscopy used for the investigation of Landé g_J- factors of praseodymium energy levels. J Quant Spectrosc Radiat Transf 2017;194(Supplement C):24–30. doi:10.1016/j.jqsrt.2017.03.021.

[27] Sobolewski Ł, Windholz L, Kwela J. Determination of Lande g_J - factors of La I levels using laser spectroscopic methods: complementary investigations. J Quant Spectrosc Radiat Transf 2017;201(Supplement C):30–4. doi:10.1016/j.jqsrt.2017.06.030.

[28] Sobolewski Ł, Windholz L, Kwela J. Zeeman structure of red lines of lanthanum observed by laser spectroscopy methods. J Quant Spectrosc Radiat Transf 2017;201(Supplement C):180–3. doi:10.1016/j.jqsrt.2017.07.013.

[29] Furmann B, Ruczkowski J, Chomski M, Suski M, Wilman S, Stefańska D. Lande g_J factors of the electronic levels of the europium atom. J Quant Spectrosc Radiat Transf 2020;255:107258. doi:10.1016/j.jqsrt.2020.107258.

[30] Stefanska D, Furmann B. Hyperfine structure of the odd parity level system in the terbium atom. J Phys B 2017;50:175002. doi:10.1088/1361-6455/aa8370.

[31] Kramida A., Ralchenko Y., Reader J., and NIST ASD Team NIST Atomic Spectra Database (ver. 5.8), [Online]. Available: https://physics.nist.gov/asd [2021, May 6]. National Institute of Standards and Technology, Gaithersburg, MD.; 2020. 10.18434/T4W30F

[32] Salah W. Experimental measurements of the Landé g_J factor of some levels in argon atom situated near the first limit of ionization. Nucl Instrum Meth B 2002;196:25–30. doi:10.1016/S0168-583X(02)01251-X.

[33] Marquardt DW. An algorithm for least-squares estimation of nonlinear parameters. J Soc Ind App Math 1963;11(2):431–41. http://www.jstor.org/stable/2098941

[34] Sobolewski L, Windholz L, Kwela J. Landé g_J - factors of Nb I levels determined by laser spectroscopy. J Quant Spectrosc Radiat Transf 2020;249:107015. doi:10.1016/j.jqsrt.2020.107015.

Landé g_J factors of odd-parity electronic levels of the holmium atom

M. Chomski [a],*, M. Suski [a], S. Wilman [a], B. Furmann [a], J. Ruczkowski [b], D. Stefańska [a]

[a] *Institute of Materials Research and Quantum Engineering, Faculty of Materials Engineering and Technical Physics, Poznan University of Technology, Piotrowo 3A, Poznan 60-965, Poland*
[b] *Institute of Robotics and Machine Intelligence, Faculty of Control, Robotics and Electrical Engineering, Poznan University of Technology, Piotrowo 3A, Poznan 60-965, Poland*

ARTICLE INFO

ABSTRACT

In the present work results of Landé g_J factors measurements for 18 electronic levels of the holmium atom are presented. Recorded Zeeman spectra of the hyperfine structure, observed with the method of laser spectroscopy in a hollow cathode discharge lamp, placed in constant magnetic field, with laser induced fluorescence detection, were analyzed. Results obtained for 33 spectral lines of holmium in the spectral range of 488-677nm enabled the determination of the corresponding g_J factors. For 12 odd-parity levels of Ho I and one even-parity level these factors are determined for the first time.

© 2021 Elsevier Ltd. All rights reserved.

1. Introduction

Holmium is a lanthanide element, with one stable isotope $^{165}_{67}$Ho. It has relatively high nuclear spin I = 7/2 and is characterized by a large value of nuclear magnetic dipole moment and a quite high nuclear electric quadrupole moment. Holmium, as an element positioned close to the middle of the lanthanides series, possesses rich electronic levels' structure. Holmium is considered for applications in quantum engineering and metrology, as a good candidate for quantum processors implementation [1]. The Zeeman splitting of its ground state multiplet's hyperfine structure (*hfs*) is considered useful for qubit preparation and readout. For such use atoms have to be cooled below the Doppler limit and well-localized. Laser cooling in magneto-optical traps (MOT) is the first step towards preparing the holmium qubits for quantum processing applications [2].

This work is a continuation of the research aimed to the determination of Landé g_J factors of the energy levels of the holmium atom. Some results were recently published [3]. Values of g_J factors are significantly important for semi-empirical calculations performed for the fine structure of Ho and for laser cooling of Ho atoms in a MOT.

Although Landé g_J factors are one of the key features, characteristic for the electronic levels, there is still a significant lack of experimental data. In our previous work, focused on this topic, a brief review of the current state of knowledge on both the hyperfine structure and Landé g_J factors of the holmium atom, was included. Significant studies were carried out by, among others, Dankwort *et al.* [4], Livingston [5], Wyart *et al.* [6,7], Burghardt *et al.* [8] and many other research groups [9–11], including our experimental group [12–18]. In our recent work [3] new experimental values of Landé g_J factors for 15 levels belonging to the odd-parity configurations of atomic holmium and 18 levels belonging to the even-parity configurations are presented. In addition, for 6 energy levels earlier obtained experimental values have been redetermined. In total, 65 experimental values of Landé g_J factors for the even- and 32 values for the odd-parity electronic levels are hitherto known.

In the present work new experimental values of g_J factors for 17 odd-parity electronic levels in the holmium atom are included. Moreover, an experimental value for one even-parity level was obtained. Investigations were carried out using the same research method (laser induced fluorescence - LIF - in a hollow cathode discharge lamp) as before. Some of the previously obtained results were used as literature values for the lower energy levels to determine the g_J factors of the upper levels. Most of the presented experimental results for Landé g_J factors of atomic holmium energy levels were obtained for the first time.

2. Experimental details

The experimental method and setup used in the investigations performed in this work were generally the same as in our pre-

---

* Corresponding author.
E-mail address: maciej.s.chomski@doctorate.put.poznan.pl (M. Chomski).

vious work concerning Landé g_J factors determination for atomic holmium [3]. The hollow cathode discharge lamp placed in a constant magnetic field was the source of the studied atoms, and the tranistions in the atom were induced by various single-mode tunable ring dye lasers setups, operated on various dyes, dependent on the spectral range. The long-wavelength part of the spectral range was covered by DCM (using a modified Coherent CR599-21 dye laser) and Rhodamine 6G (use of a modified Coherent CR699-21 dye laser) dye solutions, both optically pumped by a frequency doubled Nd:YVO$_4$ laser (Coherent, Verdi V-10). The short-wavelength region was obtained from Coumarin 498 (using a modified Coherent CR699-21 laser), pumped by a blue diode laser. The investigated transitions were observed in a spectral range of ca. 488-677nm. The laser wavelength was controlled with a wavemeter (Burleigh, WA-1500) and the single mode operation was checked with a mode analyzer.

The magnetic field was generated by one of two available sets of different bar neodymium magnets. A stronger (ca. 1900–2000 G) or weaker (ca. 500–600 G) magnetic field could be applied, dependent on the chosen configuration. Most of the presented results were obtained in the weaker magnetic field, which is sufficient to record the Zeeman splitting of the hyperfine structure and allows a more stable discharge operation in the hollow cathode. The experimental conditions were similar to those presented in the earlier work. The discharge current in the hollow cathode was adjusted according to the fluorescence signal strength. It varied between 20 and 65 mA, but was typically kept at 40 mA. The pressure of the buffer argon gas was kept in the range of 0.3-0.6 mbar. Liquid nitrogen was used to cool the discharge lamp.

The fluorescence light, emitted by the excited holmium atoms, was directed by a system of mirrors and filters to a grating monochromator (SPM-2, Carl Zeiss Jena), where spectral selection was performed. The monochromator output was detected by a Hamamatsu R-375 photomultiplier with preamplifier, where the current signal was generated. Amplitude modulation of the laser beam by a mechanical chopper for phase-sensitive detection of the fluorescence signal was applied. The enhanced signal was further directed to a computer for recording of the hyperfine structure with Zeeman splitting. In order to create a frequency scale for the scans, along with the laser induced fluorescence signal also the transmission signal of a temperature stabilized FP interferometer with FSR=1500 MHz was recorded. Our experimental method, used for the measurements of g_J factors in lanthanide atoms, is similar to the one applied by a group from the University of Gdańsk, that, in cooperation with the group of prof. Laurentius Windholz from Graz University of Technology, published a number of papers on this topic [19–24]. The basic experimental setup for laser spectroscopic investigations with the LIF method has been used in our research group for many years.

Preparation of the recorded scans, by adding the proper frequency scale, was performed with the "Fitter" program, developed in the group of Prof. Guthöhrlein at Helmut Schmidt University in Hamburg, which has been successfully applied in our laboratory for *hfs* calculation for many years.

3. Determination of g_J values

3.1. Hyperfine structure and zeeman splitting

In the presence of an external magnetic field H_{mag}, the atomic eigenstates constitute linear combinations of the form:

$$|\psi M_F\rangle = \sum_F C_{M_F F}|\gamma JIFM_F\rangle. \tag{1}$$

The eigenvector amplitudes $C_{M_F F}$ are obtained through the diagonalization of the Hamiltonian matrix:

$$H_{FM_F, F'M_F'} = \delta_{FF'}\left(A\frac{C}{2} + B\frac{\frac{3}{4}C(C+1) - I(I+1)J(J+1)}{2I(2I-1)J(2J-1)}\right)$$
$$+ \mu_B g_J H_{mag}(-1)^{F-M_F+J+I+F'+1}\sqrt{(2F+1)(2F'+1)J(J+1)(2J+1)}$$
$$\times \begin{pmatrix} F & 1 & F' \\ -M_F & 0 & M_F \end{pmatrix}\begin{Bmatrix} F & 1 & F' \\ J & I & J \end{Bmatrix}, \tag{2}$$

where $C = F(F+1) - J(J+1) - I(I+1)$, μ_B is the Bohr magneton and g_J is the Landé factor.

The intensity of an individual transition between two Zeeman sublevels M_F and M_F' is proportional to the related transition probability. The experimentally observed line profile is a sum of individual Zeeman components, each having a line profile influenced by radiative broadening and instrumental effects.

3.2. Computational procedures

At the initial stage of our computational procedures, the energies of Zeeman sublevels, relative to the fine structure energy $E(J)$, for both the upper and the lower level of analysed transition, are obtained by means of diagonalization of Hamiltonian expressed by Eq. (2). The mandatory input data, regarding values of the magnetic field intensity H_{mag}, nuclear spin I and electronic shell total angular momentum J quantum numbers, the hyperfine structure A and B constants, as well as the initial values of Landé g_J factors for two energy levels involved, are loaded from an appropriate input file. The derived eigenvalues and eigenvectors are used for determination of the relative positions (on a frequency scale) and intensities of all the individual Zeeman components, both for σ and π transitions.

In the next stage, the intensity distribution function is constructed as a sum of intensities for each abscissa value of the final pattern, with the use of evaluated splitting constants and line profile parameters. In an iterative way, this function is fitted to the experimentally observed line profile recorded in digital form, where values of Landé g_J factors for the upper and lower levels serve as adjustable parameters. In the calculations the Marquardt's algorithm [25] is adopted. Our program allows also a fine tuning of the *hfs* constants values, which is important especially when these constants are determined with significant experimental uncertainties.

In order to include saturation effects, an additional parameter A_s (saturation rate) was added to the fitting procedure. Obtained values of the saturation rate are in the range from 0.005 to 0.76. The large range of the values of the saturation parameter is related to a large number of measured lines of various intensities, a wide spectral range and various values of the laser power available in various wavelengths. As a result of saturation, the proportions between the intensities of smaller and larger components are different than without saturation. If some part of the envelope results from high-intensity components lying too close to each other, the program can independently optimize only two of three parameters: the g_J factor, the Gaussian width and the saturation parameter. Thus, if individual high-intensity components are not sufficiently separated, the main criterion for selecting an appropriate g_J factor's value is the quality of the fit for low-intensity components. The initial values of saturation parameters were selected on the basis of spectral lines' intensities and the probabilities of investigated transitions. The calculated decay rate of each Zeeman component (A_ν) of frequency ν was modified according to the following expression [26]:

$$A_\nu^{sat} = \frac{A_\nu}{1 + A_\nu/A_s} \tag{3}$$

The program using the Marquardt's algorithm to best fit the function parameters to recorded spectra takes every individual Zeeman component as a Voigt's profile. Spectral lines, previously investigated by our research group with the same current to calculate *hfs A* and *B* constants, were fitted with the initial values of Gaussian and Lorentzian half widths as those obtained from previous studies. For new lines the initial value of the Lorentzian half width resulted from the literature lifetimes of energy levels, while the value of the Gaussian half width parameter was adopted on the basis of the intensity of the discharge current and the wavelength of the investigated transition.

4. Results

In this work altogether 33 spectral lines of atomic holmium were investigated for determination of Landé g_J factors. All of the investigated holmium lines are presented in Table 1. To obtain the value of a g_J factor of a particular upper energy level, one should know the magnetic flux and preferably the g_J factor of the lower level. The knowledge of the applied magnetic field is crucial to perform calculations of g_J factors. In order to determine the experimental parameter related to the magnetic field, selected argon spectral lines were investigated. For evaluation of the magnetic flux, the standard calculation procedure was reversed. The well-known Landé g_J factors values of the selected energy levels in argon were used for this purpose. Most of the recorded spectra of atomic holmium were investigated in the presence of a magnetic field of ca. 500–600 G, since our previous work proved that this

value is sufficient to obtain measurable Zeeman splitting. However, 4 lines were investigated with stronger magnetic field applied to the hollow cathode. Comparing results obtained from different spectral lines for the same upper energy level, investigated both in stronger and weaker magnetic field, confirmed that this parameter doesn't affect the calculations. Some of the even-parity holmium energy levels investigated previously were selected as the lower energy levels, so the values of g_J factors for most lower levels were adopted from the literature [3]. The only exception was the energy level 17883.57 cm^{-1}, which has not been experimentally investigated before. In this exceptional case, the semi-empirically predicted g_J factor was taken as the initial value during calculations.

Except for the case mentioned, the g_J factors of the lower energy levels were fixed at the known experimental values, facilitating calculation of g_J factors of the upper energy levels. Then, the obtained results were averaged for particular investigated energy levels. Among 17 odd-parity energy levels, 6 were involved in single spectral lines. In those cases the average g_J factor values were obtained from those determined for π and σ polarizations. The remaining 11 holmium odd-parity energy levels were involved in multiple spectral lines. For the even-parity energy level 17883.57 cm^{-1} the procedure was reversed. Final experimental results obtained for 3 upper odd-parity energy levels were fixed to perform the calculations of the lower level's new g_J factor.

The partial values for both the lower (even-parity) and the upper (odd-parity) energy levels are summarized in Table 1. In the first group of columns the information on the transitions studied

Table 1

Spectral lines of the holmium atom experimentally investigated in this work for the purpose of determination of the Landé g_J factors. For almost all of the lines the g_J factors for the lower even-parity levels were known from the previous work [3], except for the 17883.57 cm^{-1} level. Landé g_J factors for the upper odd-parity levels were determined from the experiment performed in this work.

	Line		Lower level			Upper level		
No	λ_{air} (nm)	k_{vac} (cm^{-1})	E (cm^{-1})	J	g_J [3]	E (cm^{-1})	J	$g_{J,av}$
1	2	3	4	5	6	7	8	9
1	483.329	20684.08	9741.50	19/2	1.227(0.007)	30425.58	19/2	1.2515(0.0078)
2	490.208	20393.81	9741.50	19/2	1.227(0.007)	30135.31	17/2	1.2934(0.0100)
3	502.649	19889.05	17883.57	19/2	1.261 [27]	37772.62	19/2	1.2132(0.0226)
4	502.911	19878.69	17883.57	19/2	1.261 [27]	37762.26	17/2	1.1719(0.0250)
5	506.554	19735.72	17883.57	19/2	1.261 [27]	37619.29	19/2	1.1798(0.0225)
6	509.885	19606.80	15130.31	17/2	1.147(0.006)	34737.11	19/2	1.2109(0.0068)
7	510.319	19590.14	18651.53	15/2	1.190(0.006)	38241.67	13/2	1.1757(0.0076)
8	512.781	19496.07	8427.11	15/2	1.283(0.008)	27923.18	17/2	1.2911(0.0104)
9	514.397	19434.82	18337.80	17/2	1.247(0.013)	37772.62	19/2	1.2510(0.0147)
10	514.671	19424.46	18337.80	17/2	1.247(0.013)	37762.26	17/2	1.1878(0.0138)
11	515.529	19392.13	18858.19	13/2	1.112(0.086)	38250.32	11/2	1.1651(0.0863)
12	516.309	19362.85	12344.55	13/2	1.241(0.010)	31707.40	11/2	1.2137(0.0114)
13	518.203	19292.07	8378.91	17/2	1.269(0.010)	27670.98	19/2	1.2530(0.0108)
14	518.488	19281.49	18337.80	17/2	1.247(0.013)	37619.29	19/2	1.1769(0.0137)
15	518.781	19270.60	8378.91	17/2	1.269(0.010)	27649.51	15/2	1.3194(0.0117)
16	520.082	19222.40	8427.11	15/2	1.283(0.008)	27649.51	15/2	1.3171(0.0087)
17	523.121	19110.73	18651.53	15/2	1.190(0.006)	37762.26	17/2	1.1913(0.0119)
18	523.325	19103.27	11322.31	21/2	1.229(0.010)	30425.58	19/2	1.2537(0.0107)
19	529.093	18895.02	11530.56	17/2	1.192(0.008)	30425.58	19/2	1.2472(0.0088)
20	536.397	18637.72	11689.77	19/2	1.183(0.007)	30327.49	17/2	1.1940(0.0080)
21	536.779	18624.47	13082.93	11/2	1.250(0.027)	31707.40	11/2	1.2215(0.0275)
22	540.319	18502.43	9147.08	13/2	1.347(0.039)	27649.51	15/2	1.3303(0.0391)
23	571.613	17489.50	12344.55	13/2	1.241(0.010)	29834.05	15/2	1.2293(0.0108)
24	579.345	17256.08	13082.93	11/2	1.250(0.027)	30339.01	13/2	1.2891(0.0275)
25	618.779	16156.38	15130.31	17/2	1.147(0.006)	31286.69	17/2	1.2426(0.0069)
26	625.562	15981.21	11689.77	19/2	1.183(0.007)	27670.98	19/2	1.2447(0.0079)
27	637.251	15688.06	8427.11	15/2	1.283(0.008)	24115.17	17/2	1.3176(0.0086)
28	641.501	15584.14	12339.04	15/2	1.241(0.014)	27923.18	17/2	1.2899(0.0142)
29	647.850	15431.41	15855.28	15/2	1.257(0.009)	31286.69	17/2	1.2561(0.0111)
30	652.967	15310.47	12339.04	15/2	1.241(0.014)	27649.51	15/2	1.3233(0.0143)
31	666.261	15005.00	15130.31	17/2	1.147(0.006)	30135.31	17/2	1.2872(0.0066)
32	666.516	14999.25	15136.06	15/2	1.175(0.009)	30135.31	17/2	1.2928(0.0111)
33	677.644	14752.93	15081.12	13/2	1.182(0.009)	29834.05	15/2	1.2354(0.0115)
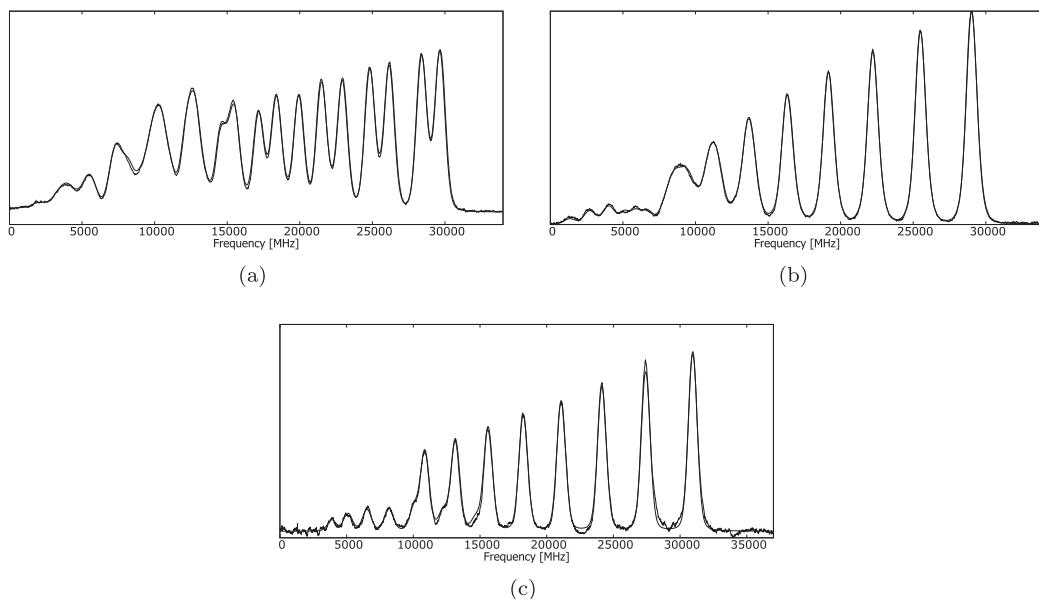
(a)

(b)

(c)

**Fig. 1.** Recorded *hfs* patterns of the spectral line λ = 518.488 nm (k=19281.49 cm⁻¹) in the holmium atom (Table 1, No 14), along with the least-squares fitted curves for: a) the Zeeman pattern with polarization σ, b) the Zeeman pattern with polarization π and c) the hyperfine structure pattern, unaffected by external magnetic field.

is provided: wavelengths and wavenumbers, respectively. The next two columns contain information about the lower levels of the investigated transitions: energies, *J* quantum numbers and the literature values of Landé g_J factors. The following columns include analogous sets of data for the upper energy levels and also experimental values of Landé g_J factors obtained from measurements performed for π and σ polarizations. All of the Landé factors are listed with their uncertainties.

Examples of the recorded spectra with the fitted Zeeman-*hfs* patterns are presented in Figs. 1–3. Single Zeeman components are so close to each other that they can only be presented as a resultant envelope. Some of investigated spectral lines share a common upper or lower level. This cases are represented by Figs. 2 and 3, respectively. Results obtained from 33 spec-

tral lines yielded new experimental values for 17 odd-parity and one even-parity electronic levels of atomic holmium. Averaged Landé g_J factors for all investigated energy levels are presented in Table 2.

Experimental uncertainties of the calculated Landé g_J factors consist of mean standard deviations for the fitted parameters of the upper energy levels, uncertainties of the literature Landé g_J factors and the experimental errors related to the uncertainty of the magnetic field determination. Estimated fluctuations of the magnetic field, during the experiment, should not exceed 2%. To account for the contribution of the magnetic field variation to the total measurement uncertainty, the values of the g_J factors were calculated at 98% and 102% of the evaluated magnetic field values. The differences in obtained results were divided by 2 and assumed

Table 2
Values of Landé g_J factors of electronic levels of the holmium atom, determined in this work from the measurements of the Zeeman effect in the hyperfine structure, available literature data and theoretically predicted values.

| No 1	E(cm⁻¹) 2	J 3	No of lines 4	gJ$_{mean}$ 5	gJ$_{lit}$ [9] 6	gJ$_{pred}$ [13,27] 7
	even-parity	level				
1	17883.57	19/2	3	1.270(0.023)		1.261
	odd-parity	levels				
1	24115.17	17/2	1	1.318(0.007)		1.320
2	27649.51	15/2	4	1.323(0.011)		1.318
3	27670.98	19/2	2	1.249(0.023)		1.230
4	27923.18	17/2	2	1.291(0.005)		1.284
5	29834.05	15/2	2	1.232(0.018)		1.209
6	30135.31	17/2	3	1.291(0.009)		1.281
7	30327.49	17/2	1	1.194(0.011)		1.196
8	30339.01	13/2	1	1.289(0.011)		1.314
9	30425.58	19/2	3	1.251(0.009)		1.247
10	31286.69	17/2	2	1.249(0.038)		1.264
11	31707.40	11/2	2	1.218(0.022)		1.181
12	34737.11	19/2	1	1.211(0.006)		1.197
13	37619.29	19/2	2	1.178(0.009)	1.350(0.04)	1.345
14	37762.26	17/2	3	1.184(0.024)	1.200(0.04)	1.171
15	37772.62	19/2	2	1.232(0.105)	1.240(0.04)	1.251
16	38241.67	13/2	1	1.176(0.011)	1.200(0.04)	1.214
17	38250.32	11/2	1	1.165(0.014)	1.200(0.04)	1.154
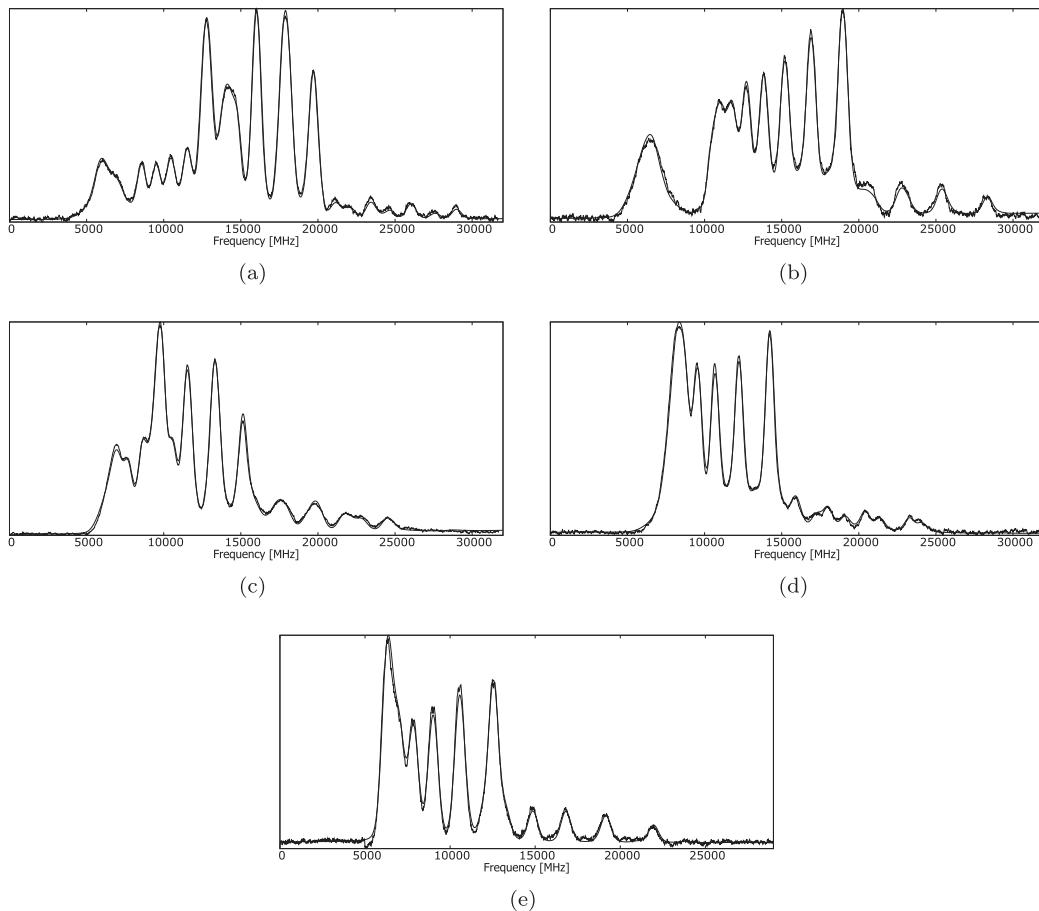
Fig. 2. Recorded *hfs* patterns of the spectral line $\lambda = 520.082$ nm (k=19222.40 cm^{-1}, Table 1, No 16), and $\lambda = 518.781$ nm (k=19270.60 cm^{-1}, Table 1, No 15), sharing a common upper level E=27649.51 cm^{-1} J=15/2, along with the least-squares fitted curves: a) Zeeman pattern of line at k=19222.40 cm^{-1} with polarization σ, b) Zeeman pattern of line at k=19222.40 cm^{-1} with polarization π, c) Zeeman pattern of line at k=19270.60 cm^{-1} with polarization σ, d) Zeeman pattern of line at k=19270.60 cm^{-1} with polarization π and e) hyperfine structure pattern of line at k=19270.60 cm^{-1}, unaffected by external magnetic field.

as Landé factors' uncertainties resulting from the magnetic field. The total uncertainty for a single electronic level, related to a single spectral line, was calculated according to the formula:

$$\Delta g_J = \sqrt{(\Delta g_{J,U})^2 + (\Delta g_{J,L})^2 + (\Delta g_{J,B})^2} \qquad (4)$$

where $\Delta g_{J,U}$ is the mean standard deviation for g_J of the upper energy level, $\Delta g_{J,L}$ is experimental uncertainty of the g_J factor value of the known lower energy level, and the remaining term is the uncertainty related to the contribution of the magnetic field variations to the total measurement error, respectively.

5. Discussion

Most of the Landé g_J factors investigated in this work cannot be compared to any earlier experimental values. Only results for 5 odd-parity energy levels are available from the experimental reference data published by Kröger [9]. Four g_J factors' values are consistent, within the limits of the measurement uncertainties, with the values reported previously. Only the result obtained for the 37619.29 cm^{-1} level disagrees with literature data.

Investigation of single spectral lines yielded the results for 6 energy levels. In these cases average g_J factors' values were calculated from scans for π and σ polarizations, and thus the obtained values may be less reliable.

Despite a clear shortage of the available experimental data, a good agreement of the presented results with the values predicted

by semi-experimental calculations can be observed. Exactly half of the experimental results summarized in Table 2 are consistent, within the limits of the measurement uncertainties, with the values obtained by a semi- empirical analysis of the hyperfine structure of the holmium atom. The Landé g_J factor calculated within this work for the single even-parity level (which has no earlier counterpart in the literature) is consistent with the predicted one. Obtained results can be generally considered in good agreement with predicted semi-empirical values. The relative difference between experimental and predicted g_J factor's value exceeds 5% only for the 37619.29 cm^{-1} level. As can be seen from Fig. 4, an attempt to fit a theoretical curve, assuming the available literature value, ended in failure. Moreover, this electronic level was investigated in the present work on two individual spectral lines and the obtained results are consistent with each other.

Some deviations between the values calculated for π and σ polarizations were observed during the experiment, however these discrepancies may be considered insignificant. Such differences were discussed in more detail in our previous work. Main sources of polarization dependent deviations are: heterogeneity of the magnetic field and the presence of minor σ components in the spectra which should contain only π components, and vice versa. Despite of the fact that the total measurement uncertainty is influenced by several different factors, the obtained uncertainties constitute only a few percent of the average values, which is a characteristic result for research performed with this method.
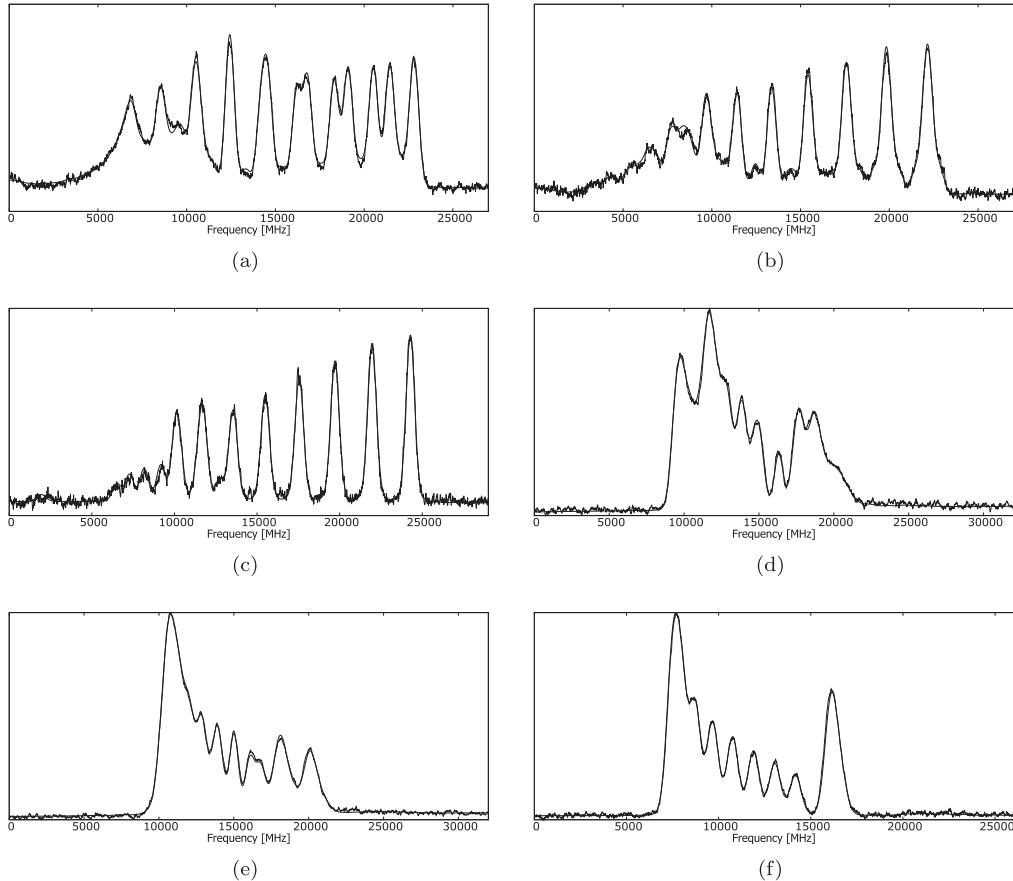
Fig. 3. Recorded Zeeman-*hfs* patterns of the spectral line $\lambda = 571.613$ nm (k=17489.50 cm^{-1}, Table 1, No 23), and $\lambda = 516.309$ nm (k=19362.85 cm^{-1}, Table 1, No 12), sharing a common lower level E=12344.55 cm^{-1} J=13/2, along with the least-squares fitted curves: a) Zeeman pattern of line at k=17489.50 cm^{-1} with polarization σ, b) Zeeman pattern of line at k=17489.50 cm^{-1} with polarization π,c) hyperfine structure pattern of line at k=17489.50 cm^{-1}, unaffected by external magnetic field, d) Zeeman pattern of line at k=19362.85 cm^{-1} with polarization σ, e) Zeeman pattern of line at k=19362.85 cm^{-1} with polarization π, f) hyperfine structure pattern of line at k=19362.85 cm^{-1}, unaffected by external magnetic field.
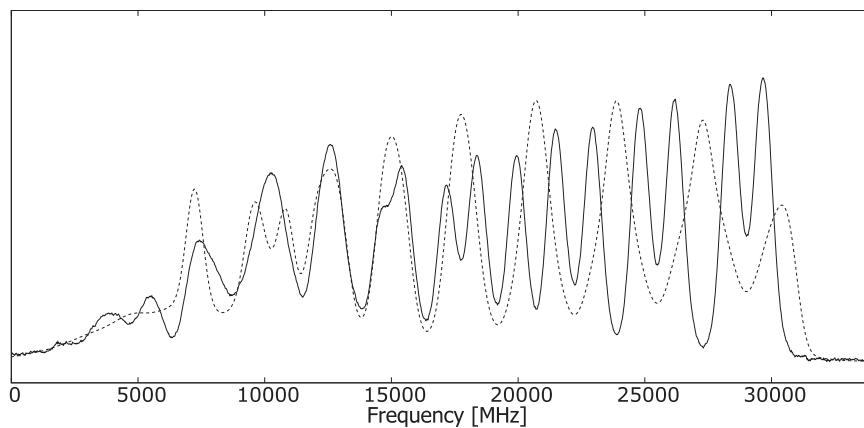
Fig. 4. Recorded Zeeman-*hfs* patterns of the spectral line $\lambda = 518.488$ nm (k=19281.49 cm^{-1}) in the holmium atom, along with the least-squares fitted curves. The solid line is a recorded pattern, while the dotted line represents an attempt to match a literature value [9]. The literatue value of the Landé g_J factor doesn't fit to the experimentally obtained spectrum.

6. Conclusions

In this work experimental results of Landé g_J factors for 18 electronic levels of the holmium atom are presented, including 17 odd-parity levels and one level belonging to the even-parity configurations. The measurements were performed with the LIF method in a hollow cathode discharge lamp with Zeeman splitting of spectra in a magnetic field. The parameters of the lower energy levels were known from our last work focused on this topic, which greatly facilitated calculation of new experimental values of g_J factors for the upper energy levels. Among the obtained results, presented in Table 2, 13 were experimentally determined for the first time. Half of the experimental values are consistent with semi-empirically predicted ones. Observed discrepancies for the remaining investigated levels were not unexpected, because of their relatively high energies. Four out of five odd-parity levels, which can be com-

pared with other experimental data, are in accordance with the previously published ones, within the measurement uncertainty. The largest difference between g_J factor obtained in this work, and both the predicted and the experimental literature data, concerns the 37619.29 cm^{-1} level, but the value reported previously doesn't fit to the recorded spectra.

Declaration of Competing Interest

The authors declare that they have no known competing financial interests or personal relationships that could have appeared to influence the work reported in this paper.

CRediT authorship contribution statement

M. Chomski: Data curation, Investigation, Formal analysis, Writing – original draft. **M. Suski:** Data curation, Investigation. **S. Wilman:** Data curation, Investigation, Funding acquisition. **B. Furmann:** Data curation, Formal analysis, Investigation, Software. **J. Ruczkowski:** Formal analysis, Software. **D. Stefańska:** Investigation, Writing – original draft.

Acknowledgments

References

[1] Saffman M, Mølmer K. Scaling the neutral-atom Rydberg gate quantum computer by collective encoding in holmium atoms. Phys Rev A 2008;78:012336. doi:10.1103/physreva.78.012336.

[2] Miao J, Hostetter J, Stratis G, Saffman M. Magneto-optical trapping of holmium atoms. Phys Rev A 2014;89:041401. doi:10.1103/physreva.89.041401.

[3] Chomski M, Furmann B, Ruczkowski J, Suski M, Stefańska D. Lande g_J factors of the electronic levels of the holmium atom. J Quant Spectrosc Radiat Transfer 2021;274:107865. doi:10.1016/j.jqsrt.2021.107865.

[4] Dankwort W, Ferch J, Gebauer H. Hexadecapole interaction in the atomic ground state of ^{165}Ho. Z Phys 1974;267(3):229–37. doi:10.1007/bf01669225.

[5] Livingston AE, Pinnington EH. Spectra of neutral and singly ionized holmium. J Opt Soc Am 1971;61(10):1429–30. doi:10.1364/JOSA.61.1429_1.

[6] Wyart J-F, Camus P, Vergès J. Etude du spectre de l'holmium atomique: I. Spectre d'émission infrarouge niveaux d'énergie de Ho I et structures hyperfines. Physica C 1977;92(3):377–96. doi:10.1016/0378-4363(77)90137-1.

[7] Wyart J-F, Camus P. Etude du spectre de l'holmium atomique: II. Interprétation paramétrique des niveaux d'énergie et des structures hyperfines. Physica C 1978;93(2):227–36. doi:10.1016/0378-4363(78)90129-8.

[8] Burghardt B, Büttgenbach S, Glaeser N, Harzer R, Meisel G, Roski B, Träber F. Hyperfine structure measurements in metastable states of ^{165}Ho. Z Phys A: At Nucl 1982;307(3):193–200. doi:10.1007/bf01438640.

[9] Kröger S, Wyart J-F, Luc P. Theoretical interpretation of hyperfine structures in doubly-excited configurations 4f^{10}5d6s6p and 4f^{10}5d^{2}6s and new energy levels in neutral holmium (Ho I). Phys Scr 1997;55:579. doi:10.1088/0031-8949/55/5/010.

[10] Al-Labady N, Özdalgiç B, Er A, Güzelçimen F, Öztürk IK, Kröger S, et al. Line identification of atomic and ionic spectra of holmium in the near-UV. Part I. Spectrum of Ho I. Astrophys J Suppl Ser 2017;228(2):16. doi:10.3847/1538-4365/228/2/16.

[11] Özdalgiç B, Güzelçímen F, Öztürk IK, Kröger S, Kruzins A, Tamanis M, et al. Line identification of atomic and ionic spectra of holmium in the visible spectral range. I. Spectrum of Ho I. Astrophys J Suppl Ser 2019;240(2):27. doi:10.3847/1538-4365/aaf9b2.

[12] Stefanska D, Furmann B. Hyperfine structure investigations for the odd-parity configuration system in atomic holmium. J Quant Spectrosc Radiat Transfer 2018;206:286–95. doi:10.1016/j.jqsrt.2017.11.019.

[13] Stefanska D, Ruczkowski J, Elantkowska M, Furmann B. Fine- and hyperfine structure investigations of the even-parity configuration system in atomic holmium. J Quant Spectrosc Radiat Transfer 2018;209:180–95. doi:10.1016/j.jqsrt.2018.01.010.

[14] Stefanska D, Furmann B, Głowacki P. Possibilities of investigations of the temporal variation of the α constant in the holmium atom. J Quant Spectrosc Radiat Transfer 2018;213:159–68. doi:10.1016/j.jqsrt.2018.04.017.

[15] Stefanska D, Furmann B. Hyperfine structure investigations for the odd-parity configuration system in atomic holmium. J Quant Spectrosc Radiat Transfer 2018;206:286–95. doi:10.1016/j.jqsrt.2017.11.019.

[16] Furmann B, Stefanska D, Suski M, Wilman S. Identification of new electronic levels in the holmium atom and investigation of their hyperfine structure. J Quant Spectrosc Radiat Transfer 2018;219:117–26. doi:10.1016/j.jqsrt.2018.08.005.

[17] Furmann B, Stefańska D, Suski M, Wilman S, Chomski M. Hyperfine structure studies of the odd-parity electronic levels of the holmium atom I: levels with known energies. J Quant Spectrosc Radiat Transfer 2019;234:115–23. doi:10.1016/j.jqsrt.2019.05.028.

[18] Furmann B, Stefańska D, Wilman S, Chomski M, Suski M. Hyperfine structure studies of the odd-parity electronic levels in the holmium atom II: new levels. J Quant Spectrosc Radiat Transfer 2019;235:70–80. doi:10.1016/j.jqsrt.2019.06.005.

[19] Grabowski D, Drozdowski R, Kwela J, Heldt J. Hyperfine structure and Zeeman effect studies in the 6p7p-6p7s transitions in Bi II. Z Phys D 1996;38:289–93. doi:10.1007/s004600050093.

[20] Werbowy S, Güney C, Windholz L. Experimental investigations of the Zeeman effect of new fine structure levels of lanthanum and praseodymium. Spectrochim Acta Part B 2016;116(Supplement C):16–20. doi:10.1016/j.sab.2015.11.003.

[21] Werbowy S, Güney C, Windholz L. Studies of Landé g_J-factors of singly ionized lanthanum by laser-induced fluorescence spectroscopy. J Quant Spectrosc Radiat Transfer 2016;179(Supplement C):33–9. doi:10.1016/j.jqsrt.2016.03.009.

[22] Sobolewski Ł, Windholz L, Kwela J. Laser induced fluorescence spectroscopy used for the investigation of Landé g_J- factors of praseodymium energy levels. J Quant Spectrosc Radiat Transfer 2017;194(Supplement C):24–30. doi:10.1016/j.jqsrt.2017.03.021.

[23] Sobolewski Ł, Windholz L, Kwela J. Determination of Lande g_J - factors of La I levels using laser spectroscopic methods: complementary investigations. J Quant Spectrosc Radiat Transfer 2017;201(Supplement C):30–4. doi:10.1016/j.jqsrt.2017.06.030.

[24] Sobolewski Ł, Windholz L, Kwela J. Zeeman structure of red lines of lanthanum observed by laser spectroscopy methods. J Quant Spectrosc Radiat Transfer 2017;201(Supplement C):180–3. doi:10.1016/j.jqsrt.2017.07.013.

[25] Marquardt DW. An algorithm for least-squares estimation of nonlinear parameters. J Soc Ind App Math 1963;11(2):431–41. http://www.jstor.org/stable/2098941

[26] Sobolewski L, Windholz L, Kwela J. Landé g_J - factors of Nb I levels determined by laser spectroscopy. J Quant Spectrosc Radiat Transfer 2020;249:107015. doi:10.1016/j.jqsrt.2020.107015.

[27] Elantkowska M, Ruczkowski J, Sikorski A, Wilman S. Fine- and hyperfine structure investigations of the odd-parity configuration system in atomic holmium. J Quant Spectrosc Radiat Transfer 2019;237:106642. doi:10.1016/j.jqsrt.2019.106642.

Determination of the energies of new electronic levels of the holmium atom and investigation of their hyperfine structure

M. Chomski*, B. Furmann, M. Suski, P. Głowacki, D. Stefańska, S. Mieloch

Institute of Materials Research and Quantum Engineering, Faculty of Materials Engineering and Technical Physics, Poznan University of Technology, Piotrowo 3A, 60-965 Poznan, Poland

ARTICLE INFO

ABSTRACT

In the present work 27 electronic energy levels of the holmium atom, with previously unknown energies, were identified for the first time. Experimental data were acquired with the method of laser spectroscopy in a hollow cathode discharge lamp, with laser induced fluorescence detection. Recorded patterns for 79 spectral lines of holmium in the spectral range 485–535 nm enabled determination of the hyperfine structure constants A and B for 23 odd-parity levels and 11 even-parity levels. For 31 levels the results are presented for the first time. The energy values for the previously unknown levels were determined, too.

© 2023 Elsevier Ltd. All rights reserved.

1. Introduction

Holmium is an element belonging to the lanthanides series - elements with an open 4f electronic shell. This element possesses one stable isotope $^{165}_{67}$Ho, and due to the relatively high nuclear spin I = 7/2 its electronic levels have rich hyperfine structure (*hfs*). Despite the fact that tens of thousands of energy levels are predicted according to the theory of its complex atomic structure, only a few hundred of them have been experimentally confirmed to date. For many of these levels fundamental parameters, such as the Landé g_J factors and *hfs* constants, have still not been determined. Description of this enormously rich atomic energy level structure with *ab initio* methods is extremely difficult, because of strong configuration mixing caused by collapse of the wavefunction of the 4f-electrons. Taking this into account, much better results can be obtained by semi-empirical methods. For the reasons given, a possibly large database of experimental values of the key parameters describing electronic energy levels is crucial for the further progress in the field of fine and hyperfine structure of lanthanides. A review of the basic properties of the electronic levels in the holmium atom was presented in our earlier works on this element [1–7].

Despite the difficulties in performing calculations, the rich energy level structure opens numerous application possibilities (in particular for holmium, but also for other elements in the lan-

thanides series). One of the most common uses is related to astrophysics. Correct interpretation of spectral lines plays a key role in determination of lanthanide elements' abundances in stellar atmospheres [8,9]. Small differences of the electronic levels' energies, common in the lanthanide elements, often allows to find allowed transitions at extremely low frequencies, which makes these elements also suitable for performing precise investigations of the possible time variations of the fine structure constant [10,11]. Holmium has attracted a lot of attention in recent years as a possibly good candidate for applications in quantum engineering. This element is considered for implementation of quantum processors on a large number of qubits [12]. Zeeman splitting of the ground state of holmium is beneficial for qubit preparation and readout.

For applications in quantum engineering and metrology atoms have to be cooled possibly below 100 μK. Laser cooling in magneto-optical traps (MOT) is the first step towards preparing qubits for quantum processing applications, and this was achieved for holmium a few years ago [13]. Further step is second-stage laser cooling using a narrow spectral transition. In one of our previous works we have investigated basic parameters for some of such transitions [14].

Reported Fourier-spectroscopic investigations of holmium provided confirmation of the existence of numerous unclassified spectral lines [15,16]. As an outcome of our previous works focused on this topic, altogether 194 spectral lines of atomic holmium were investigated, allowing to identify 61, previously not known, odd-parity electronic energy levels. For all investigated electronic levels the magnetic dipole A and the electric quadrupole B hyperfine structure constants were determined [5,11,17].

---

* Corresponding author.
 E-mail address: maciej.s.chomski@doctorate.put.poznan.pl (M. Chomski).

Table 1

Compilation of the investigated transitions of the holmium atom; each spectral line involves an upper energy level for which the hyperfine structure constants A and B are determined in the current study. Additionally, existing experimental literature data by other authors, concerning the lower energy levels, are included for reference. In parentheses the full uncertainties (in MHz) are quoted.

No	Line λ_{air} (nm)	k_{vac} (cm⁻¹)	Lower level E (cm⁻¹)	parity	J	A (MHz)		B (MHz)		ref.	Upper level E (cm⁻¹)	parity	J	A (MHz)		B (MHz)	
1	2	3	4	5	6	7		8		9	10	11	12	13		14	
1	485.624	20586.32	8427.11	e	15/2	839.3	(0.2)	385	(43)	a	29013.43	o	13/2	635.4	(0.3)	-576	(58)
2	503.223	19866.35	9147.08	e	13/2	916.5	(0.5)	2730	(30)	[18]	29013.43	o	13/2	635.3	(0.6)	-512	(33)
3	499.975	19995.43	12339.04	e	15/2	806.7	(1.4)	-139	(19)	[1]	32334.47	o	15/2	649.8	(1.5)	283	(37)
4	500.113	19989.92	12344.55	e	13/2	908.6	(0.6)	424	(23)	[1]	32334.47	o	15/2	650.2	(0.7)	544	(24)
5	512.187	19518.70	13094.42	o	9/2	884.5	(2.0)	1752	(22)	[1]	32613.12	e	9/2	898.9	(2.1)	1282	(39)
6	528.244	18925.38	15130.31	e	17/2	808.5	(1.8)	2120	(27)	[1]	34055.69	o	15/2	1064.1	(1.9)	1434	(29)
7	528.405	18919.63	15136.06	e	15/2	862.4	(0.6)	234	(14)	[1]	34055.69	o	15/2	1060.6	(0.7)	1408	(16)
8	501.019	19953.76	15081.12	e	13/2	891.0	(0.4)	119	(12)	[1]	35034.88	o	15/2	633.1	(0.5)	402	(38)
9	502.402	19898.82	15136.06	e	15/2	862.4	(0.6)	234	(14)	[1]	35034.88	o	15/2	629.8	(0.7)	327	(18)
10	521.242	19179.60	15855.28	e	15/2	1143.5	(2.4)	-367	(60)	[1]	35034.88	o	15/2	632.9	(2.5)	862	(63)
11	523.414	19100.02	16719.62	e	9/2	1209.3	(3.0)	2139	(150)	[20]	35819.64	o	11/2	706.8	(3.1)	812	(153)
12	523.862	19083.69	16735.95	e	13/2	883.6	(1.7)	-4	(64)	[1]	35819.64	o	11/2	702.0	(1.8)	661	(65)
13	532.893	18760.29	17059.35	e	13/2	556.4	(0.8)	-1332	(18)	[1]	35819.64	o	11/2	708.2	(1.5)	239	(33)
14	515.629	19388.40	16683.52	e	19/2	739.7	(0.5)	3389	(12)	[1]	36071.92	o	19/2	980.6	(0.6)	2043	(13)
15	502.110	19910.39	16735.95	e	13/2	883.6	(1.7)	-4	(64)	[1]	36646.34	o	11/2	942.5	(2.4)	-29	(76)
16	510.401	19586.99	17059.35	e	13/2	556.4	(0.8)	-1332	(18)	[1]	36646.34	o	11/2	953.1	(1.0)	-30	(30)
17	488.823	20451.60	16438.01	e	17/2	822.0	(0.4)	2000	(19)	[1]	36889.61	o	17/2	1151.5	(0.5)	-158	(25)
18	495.407	20179.79	16709.82	e	17/2	1135.6	(0.5)	-1984	(30)	[18]	36889.61	o	17/2	1148.0	(0.6)	-106	(50)
19	526.002	19006.04	17883.57	e	19/2	1220.50	(0.19)	-73	(12)	[18]	36889.61	o	17/2	1147.9	(0.2)	-114	(13)
20	486.662	20542.40	16709.82	e	17/2	1135.6	(0.5)	-1984	(30)	[18]	37252.22	o	17/2	1072.2	(0.6)	1209	(31)
21	528.550	18914.42	18337.80	e	17/2	1102.2	(0.4)	-1831	(13)	[18]	37252.22	o	17/2	1074.8	(0.5)	1295	(25)
22	524.763	19050.90	18572.28	o	15/2	805.8	(0.8)	1663	(318)	a	37623.18	e	15/2	644.8	(0.9)	95	(319)
23	533.025	18755.64	18867.40	o	13/2	1486.7	(0.2)	-848	(81)	[1]	37623.18	e	15/2	645.9	(0.5)	-257	(133)
24	523.121	19110.70	18651.53	e	15/2	863.40	(0.16)	-2740	(16)	[18]	37762.23	o	17/2	1297.5	(0.4)	-658	(31)
25	497.673	20087.91	17883.57	e	19/2	1220.50	(0.19)	-73	(12)	[18]	37971.48	o	17/2	1190.4	(0.2)	-336	(13)
26	517.456	19319.95	18651.53	e	15/2	863.40	(0.16)	-2740	(16)	[18]	37971.48	o	17/2	1190.9	(0.2)	-361	(19)
27	514.639	19425.69	18651.53	e	15/2	863.40	(0.16)	-2740	(16)	[18]	38077.21	o	13/2	1407.9	(0.2)	-217	(17)
28	520.173	19219.03	18858.19	e	13/2	465.45	(0.23)	-3158	(14)	[18]	38077.21	o	13/2	1411.4	(0.7)	-291	(57)
29	490.692	20373.68	17883.57	e	19/2	1220.50	(0.19)	-73	(12)	[18]	38257.25	o	19/2	117.6	(1.5)	-1485	(16)
30	501.882	19919.45	18337.80	e	17/2	1102.2	(0.4)	-1831	(13)	[18]	38257.25	o	19/2	118.5	(1.7)	-1293	(117)
31	507.249	19708.70	18564.90	e	13/2	868.8	(4.5)	594	(300)	[20]	38273.60	o	15/2	965.6	(4.6)	1215	(301)
32	512.221	19517.38	18756.22	e	15/2	849.3	(4.5)	3153	(300)	[20]	38273.60	o	15/2	965.3	(4.6)	1557	(301)
33	508.719	19651.74	18651.53	e	15/2	863.40	(0.16)	-2740	(16)	[18]	38303.27	o	17/2	943.7	(0.2)	1500	(17)
34	511.444	19547.05	18756.22	e	15/2	849.3	(4.5)	3153	(300)	[20]	38303.27	o	17/2	942.2	(4.6)	1943	(301)
35	506.798	19726.21	18756.22	e	15/2	849.3	(4.5)	3153	(300)	[20]	38482.43	o	13/2	671.2	(4.6)	797	(301)
36	508.475	19661.18	18821.25	e	11/2	265.5	(1.5)	-228	(60)	[20]	38482.43	o	13/2	673.9	(1.6)	584	(61)
37	509.432	19624.24	18858.19	e	13/2	465.45	(0.23)	-3158	(14)	[18]	38482.43	o	13/2	672.6	(0.3)	483	(15)
38	497.542	20093.18	18572.28	o	15/2	805.8	(0.8)	1663	(318)	a	38665.46	e	13/2	902.1	(0.9)	-959	(319)
39	504.963	19797.92	18867.40	o	13/2	1486.7	(0.2)	-848	(81)	[1]	38665.46	e	13/2	903.2	(0.3)	-721	(82)
40	515.625	19388.52	19276.94	o	15/2	1302.00	(0.15)	-1884	(60)	[20]	38665.46	e	13/2	898.3	(0.2)	-408	(61)
41	498.144	20068.90	18737.79	o	17/2	901.2	(0.3)	981	(150)	[20]	38806.69	e	17/2	725.5	(0.4)	5	(151)
42	511.897	19529.75	19276.94	o	15/2	1302.00	(0.15)	-1884	(60)	[20]	38806.69	e	17/2	725.3	(0.2)	-87	(61)
43	496.102	20151.52	18867.40	o	13/2	1486.7	(0.2)	-848	(81)	[1]	39019.06	e	11/2	1118.5	(0.4)	204	(91)
44	527.327	18958.30	20060.76	o	11/2	549.60	(0.15)	-549	(60)	[20]	39019.06	e	11/2	1105.6	(0.8)	255	(80)
45	492.132	20314.07	19276.94	o	15/2	1302.00	(0.15)	-1884	(60)	[20]	39591.01	e	13/2	1260.4	(0.2)	118	(61)
46	511.884	19530.25	20060.76	o	11/2	549.60	(0.15)	-549	(60)	[20]	39591.01	e	13/2	1263.3	(1.1)	-570	(97)
47	523.490	19097.24	20493.77	o	13/2	494.4	(0.3)	-1872	(150)	[20]	39591.01	e	13/2	1260.6	(0.4)	23	(151)
48	507.260	19708.28	20167.17	e	15/2	1336.8	(1.5)	1251	(60)	[20]	39875.45	o	13/2	1204.9	(1.6)	940	(61)
49	499.985	19995.03	20210.60	o	21/2	1022.2	(0.3)	-663	(5)	a	40205.63	e	21/2	599.8	(0.4)	-304	(6)
50	516.000	19374.45	20831.18	o	19/2	963.70	(0.11)	-1005	(77)	[1]	40205.63	e	21/2	600.4	(0.2)	-313	(78)
51	497.464	20096.34	20124.27	o	19/2	923.40	(0.15)	-789	(60)	[20]	40220.59	e	17/2	1047.0	(0.2)	1812	(65)
52	530.580	18842.05	21378.54	o	17/2	800.80	(0.13)	452	(65)	[1]	40220.59	e	17/2	1050.3	(0.2)	1525	(66)
53	533.596	18735.57	21485.02	o	19/2	804.3	(0.3)	3699	(150)	[20]	40220.59	e	17/2	1050.7	(0.4)	1679	(151)
54	493.365	20263.31	20167.18	e	15/2	1336.8	(1.5)	1251	(60)	[20]	40430.49	o	13/2	1066.4	(1.6)	81	(61)
55	515.701	19385.68	21044.81	e	13/2	964.9	(2.1)	2259	(99)	[1]	40430.49	o	13/2	1068.8	(3.3)	-309	(163)
56	501.243	19944.82	20493.77	o	13/2	494.4	(0.3)	-1872	(150)	[20]	40438.59	e	13/2	784.8	(0.4)	388	(151)
57	496.614	20130.74	20315.89	o	17/2	616.20	(0.15)	-1305	(60)	[20]	40446.63	e	15/2	773.3	(0.2)	-521	(61)
58	501.042	19952.86	20493.77	o	13/2	494.4	(0.3)	-1872	(150)	[20]	40446.63	e	15/2	772.9	(0.4)	-578	(151)
59	504.074	19832.82	20613.80	o	17/2	786.20	(0.15)	-1020	(60)	[20]	40446.63	e	15/2	772.5	(0.2)	-507	(61)
60	491.687	20332.48	20315.89	o	17/2	616.20	(0.15)	-1305	(60)	[20]	40648.38	e	17/2	662.6	(0.2)	-691	(61)
61	504.472	19817.20	20831.18	o	19/2	963.70	(0.11)	-1005	(77)	[1]	40648.38	e	17/2	664.0	(0.2)	-949	(78)
62	523.514	19096.36	21552.02	o	17/2	834.80	(0.19)	-804	(97)	[1]	40648.38	e	17/2	664.0	(0.2)	-985	(98)
63	536.497	18634.24	22014.13	o	15/2	650.40	(0.15)	-1332	(60)	[20]	40648.38	e	17/2	662.4	(0.2)	-631	(61)
64	492.028	20318.39	20498.73	e	17/2	1224.9	(1.5)	381	(60)	[20]	40817.12	o	19/2	796.2	(1.6)	1349	(61)
65	493.726	20248.49	20568.63	e	17/2	796.5	(2.4)	3358	(104)	[1]	40817.12	o	19/2	798.6	(2.5)	1489	(105)
66	510.062	19600.01	21217.11	e	19/2	1081.5	(1.5)	864	(60)	[20]	40817.12	o	19/2	796.0	(1.6)	1395	(61)
67	517.395	19322.23	21494.89	e	21/2	1033.2	(1.5)	1092	(60)	[20]	40817.12	o	19/2	798.3	(1.6)	1291	(61)

Table 1 (*continued*)

	Line		Lower level							Upper level					
No	λ_{air} (nm)	k_{vac} (cm^{-1})	E (cm^{-1})	parity	J	A (MHz)		B (MHz)		ref.	E (cm^{-1})	parity	J	A (MHz)		B (MHz)	
1	2	3	4	5	6	7		8		9	10	11	12	13		14	
68	485.407	20595.53	20493.40	e	11/2	1019.3	(0.3)	277	(170)	[a]	41088.93	o	13/2	706.4	(0.4)	352	(171)
69	498.760	20044.12	21044.81	e	13/2	964.9	(2.1)	2259	(99)	[1]	41088.93	o	13/2	706.2	(2.2)	5	(100)
70	488.742	20454.98	21044.81	e	13/2	964.9	(2.1)	2259	(99)	[1]	41499.79	o	13/2	958.1	(2.2)	78	(100)
71	518.731	19272.45	22227.34	e	15/2	1310.3	(1.4)	-2081	(71)	[2]	41499.79	o	13/2	957.7	(1.5)	-59	(74)
72	499.074	20031.52	22157.88	o	9/2	361.8	(0.3)	-522	(150)	[20]	42189.40	e	9/2	452.6	(0.4)	-921	(151)
73	508.226	19670.81	22518.59	o	11/2	681.30	(0.15)	-1188	(60)	[20]	42189.40	e	9/2	449.4	(0.2)	-537	(61)
74	510.169	19595.87	22593.53	o	11/2	772.5	(0.3)	246	(150)	[20]	42189.40	e	9/2	451.5	(0.4)	-530	(151)
75	496.631	20130.05	23375.28	e	25/2	971.7	(3.0)	2634	(150)	[20]	43505.33	o	25/2	536.2	(3.1)	2869	(151)
76	512.701	19499.10	24006.23	e	23/2	825.6	(3.0)	2130	(150)	[20]	43505.33	o	25/2	536.1	(3.1)	2595	(151)
77	493.013	20277.76	24006.23	e	23/2	825.6	(3.0)	2130	(150)	[20]	44283.99	o	23/2	618.4	(3.1)	2406	(151)
78	510.853	19569.65	24714.34	e	21/2	694.2	(3.0)	1761	(150)	[20]	44283.99	o	23/2	618.3	(3.1)	2579	(151)
79	533.500	18738.92	25545.07	e	21/2	1107.7	(1.7)	576	(96)	[1]	44283.99	o	23/2	623.0	(1.8)	2313	(97)

[a] - *A* and *B* constants fixed at the averages calculated from the values obtained for the remaining hitherto investigated lines

In the present work the results of further research, aimed to the identification of new energy levels in the holmium atom, are presented. Investigations were carried out using the method of laser spectroscopy in a hollow cathode discharge lamp, with laser induced fluorescence detection. Altogether 19 new odd-parity and 8 new even-parity electronic energy levels were identified. Their properties, such as energy values and *hfs A* and *B* constants, were also determined. Moreover, for two odd-parity levels and two even-parity level with known energies the *hfs A* and *B* constants were determined for the first time. The literature values of the hyperfine structure constants for the even-parity energy level $E = 8427.11$ cm^{-1} ($J = 15/2$), misspelled when reported in one of our previous works [2], were corrected. The *hfs* constants for two known odd-parity energy levels, $E = 29013.43$ cm^{-1} ($J = 13/2$) and $E = 39875.45$ cm^{-1} ($J = 13/2$), were verified.

2. Experimental details

Investigations carried out within this work were performed with the method that our group used in previous works on the hyperfine structure of atomic holmium [5,17], namely laser induced fluorescence (*LIF*) in a hollow cathode discharge lamp. Besides *LIF* detection, also the optogalvanic signal could be recorded. The investigated transitions in the holmium atom were excited by a single-mode tunable ring dye laser (modified Coherent CR699-21), operated on Coumarin 498 dye solution (485–535 nm), pumped by a blue diode laser. The fluorescence, emitted by the excited holmium atoms, was directed to a grating monochromator SPM-2 (Carl Zeiss Jena). To enhance the current signal from the photomultiplier, located at the output of monochromator, phase-sensitive detection of the fluorescence signal was applied.

The experimental conditions were similar to our previous research. The laser wavenumber was controlled with wavemeter readings (Burleigh, WA-1500), with nominal precision of 50 MHz, and the single mode operation was controlled with a mode analyzer. In order to create a frequency scale for the scans, along with the laser induced fluorescence signal also the transmission signal of a Fabry-Perot interferometer with free spectral range of 1500 MHz was recorded. The pressure of the buffer argon gas in the hollow cathode discharge lamp was kept in the range of 0.3–0.6 mbar. Liquid nitrogen was used to cool the discharge lamp. For evaluation of the *hfs* constants the program "Fitter", developed in the group of Prof. Guthöhrlein at Universität der Bundeswehr in Hamburg, was applied. The Fourier transform spectra (*FTS*) were available to us [15,16], and investigated unclassified lines were found there. As the experimental setup was essentially the same as in referred works, only a brief description of the method applied to search for and identify new energy levels is presented.

Regarding determination of unknown electronic energy levels, three experimental methods can be used:

1. Recording of the optogalvanic signal when scanning the laser frequency across a unclassified spectral line - the quantum *J* numbers and the *hfs* constants of both the upper and the lower levels are calculated from the registered spectra, then results for the lower levels assumed as the known ones are compared with the literature data and these levels are identified. The hypothetical energy value of an unknown upper electronic level is calculated by summing up the energy of the known lower electronic level and the wavenumber of the tested line. From the *J*-value of the assumed lower level we conclude *J* of the hypothetical level. Analysis of all atomic transitions allowed by the selection rules, from the hypothetical upper level to known lower levels, indicates predicted fluorescence channels, which are verified during the LIF experiment.
2. Analysis of unclassified FTS spectral lines - coincidences between the sums of known lower energy levels and wavenumbers of unclassified spectral lines, provided by the available FTS holmium spectra, are sought in this method. Such coincidences lead to introduction of one or several new hypothetical levels. The hypothetical upper energy levels are verified in the same way as in the optogalvanic method.
3. Manual searching of fluorescence channels - if there is no hypothesis regarding energy value and *J* quantum number of an unknown electronic level, the laser's wavenumber can be scanned continuously around the nominal value corresponding to an unclassified spectral line in order to provide its excitation. Simultaneously, the monochromator is slowly manually scanned over the entire accessible spectral range. Registered fluorescence signals are related to various possible upper energy levels. Comparing the results obtained from the recorded *hfs* analysis with the available database allows to identify an unknown upper energy level.

The optogalvanic signal recording is the preferred method, however because of the high noise level in the recorded signals this method was not applicable for the lines investigated in this paper. A second reason was that some of the known lower energy levels had values of *hfs* constants *A* and *B* similar to each other. The method mentioned in point no. 3 proved to be inefficient in conducting this research.

For the above reasons, it was necessary to apply the method based on the analysis of available unclassified spectral lines. In finding new hypothetical levels, predictions by semi-empirical simulations were very helpful. Possible fluorescence channels to lower

Table 2

Compilation of the energy values and the hyperfine structure constants *A* and *B* for the new odd-parity levels in the holmium atom investigated in this work, along with the observed fluorescence channels (spectral lines and lower even-parity levels). In parentheses the uncertainties for the levels' energies and the *hfs* constants are quoted. The literature values of the intensities of the fluorescence channels correspond to literature wavelengths closest to the wavelengths observed, and were reported by Al-Labady et al. [15] or Özdalgiç et al. [16], regarding spectral lines with the wavelengths shorter or longer than 400 nm, respectively. Fluorescence channels for which no intensities are given were evaluated from FTS provided by National Solar Observatory (https://nso.edu). Some of the fluorescence channels were also observed as excitation transitions; for them the respective line numbers in Table 1 are quoted in the last column.

J	Upper level E cm^{-1}	hfs constants A MHz	B MHz	Fluorescence channel λ_{air} nm	k$_{vac}$ cm^{-1}	relative intensity	Lower level E cm^{-1}	J	Remarks
1	2	3	4	5	6	7	8	9	10
11/2									
	35819.64(0.03)	705.2(2.8)	601(224)	439.694	22736.71	17	13082.93	11/2	strong
				482.060	20738.52		15081.12	13/2	weak
				523.414	19100.02	7	16719.62	9/2	line No 11
				523.862	19083.69	16	16735.95	13/2	line No 12
				529.452	18882.21	6	16937.43	11/2	FTS
				532.893	18760.29	13	17059.35	13/2	line No 13
	36646.34(0.03)	948.5(5.3)	-30(1)	363.543	27499.26	16	9147.08	13/2	strong
				411.376	24301.79	18	12344.55	13/2	strong
				424.267	23563.41	28	13082.93	11/2	strong
				502.110	19910.39	6	16735.95	13/2	line No 15
				507.243	19708.91	27	16937.43	11/2	FTS
				510.401	19586.99	36	17059.35	13/2	line No 16
				560.851	17825.09		18821.25	11/2	FTS
				562.016	17788.15	14	18858.19	13/2	FTS
				609.400	16405.03	7	20241.31	13/2	FTS
				610.031	16388.07	10	20258.27	13/2	FTS
	41088.94(0.04)	706.3(0.2)	139(170)	395.195	25296.80	31	15792.13	11/2	FTS
				413.936	24151.50	114	16937.43	11/2	FTS
				442.398	22597.72	21	18491.21	11/2	strong
				443.846	22524.03	4	18564.90	13/2	FTS
				448.955	22267.68	10	18821.25	11/2	strong
				485.407	20595.53	3	20493.40	11/2	line No 68
				498.760	20044.12	13	21044.81	13/2	line No 69
13/2									
	38077.21(0.02)	1408.9(1.7)	-239(35)	449.880	22221.93	10	15855.28	15/2	FTS
				468.445	21341.27	5	16735.95	13/2	observed
				471.679	21194.94	7	16882.28	15/2	observed
				475.653	21017.87	25	17059.35	13/2	strong
				514.639	19425.69	14	18651.53	15/2	line No 27
				520.173	19219.03		18858.19	13/2	linie No 28
	38482.43(0.02)	672.9(0.9)	559(99)	382.397	26143.39		12339.04	15/2	observed
				382.478	26137.88		12344.55	13/2	observed
				393.597	25399.50		13082.93	11/2	FTS
				440.593	22690.30	24	15792.13	11/2	strong
				464.015	21545.00	190	16937.43	11/2	FTS
				506.798	19726.21	3	18756.22	15/2	line No 35
				508.475	19661.18	18	18821.25	11/2	line No 36
				506.798	19726.21	40	18858.19	13/2	line No 37
				545.841	18315.25	16	20167.18	15/2	FTS
				548.060	18241.12	43	20241.31	13/2	FTS
	40430.49(0.03)	1067.8(2.3)	-233(210)	355.948	28085.94		12344.55	13/2	FTS
				365.559	27347.56	13	13082.93	11/2	strong
				394.376	25349.37	3	15081.12	13/2	weak
				424.541	23548.21		16882.28	15/2	FTS
				427.758	23371.14		17059.35	13/2	weak
				455.676	21939.28	25	18491.21	11/2	FTS
				457.211	21865.59		18564.90	13/2	FTS
				493.365	20263.31	29	20167.18	15/2	line No 54
				515.701	19385.68		21044.81	13/2	line No 55
	41499.79(0.02)	958(0.2)	45(58)	378.413	26418.67		15081.12	13/2	FTS
				379.201	26363.73		15136.06	15/2	FTS
				403.701	24763.84	15	16735.95	13/2	observed
				406.100	24617.51	28	16882.28	15/2	strong
				409.042	24440.44		17059.35	13/2	FTS
				440.822	22678.54	5	18821.25	11/2	FTS
				441.541	22641.60		18858.19	13/2	FTS
				470.269	21258.48		20241.31	13/2	FTS
				470.644	21241.52	9	20258.27	13/2	FTS
				488.742	20454.98	19	21044.81	13/2	line No 70
				501.997	19914.90		21584.89	13/2	FTS
				518.731	19272.45		22227.34	15/2	line No 71
				596.519	16759.27	60	24740.52	13/2	FTS

(continued on next page)

Table 2 (*continued*)

	Upper level	*hfs* constants		Fluorescence channel			Lower level		Remarks
J	E	*A*	*B*	λ_{air}	k_{vac}	relative	E	*J*	
	cm⁻¹	MHz	MHz	nm	cm⁻¹	intensity	cm⁻¹		
1	2	3	4	5	6	7	8	9	10
15/2									
	32334.47(0.04)	650.1(0.2)	492(105)	417.322	23955.56	8397	8378.91	17/2	strong
				418.163	23907.36		8427.11	15/2	weak[a]
				431.148	23187.39	48	9147.08	13/2	strong
				480.545	20803.91	27	11530.56	17/2	weak
				499.975	19995.43		12339.04	15/2	line No 3
				500.113	19989.92	40	12344.55	13/2	line No 4
				581.094	17204.16	8	15130.31	17/2	weak[a]
				581.288	17198.41		15136.06	15/2	weak[a]
				654.479	15275.12	13	17059.35	13/2	FTS
	34055.69(0.03)	1063.8(0.8)	1432(11)	389.347	25676.78		8378.91	17/2	weak
				390.079	25628.58		8427.11	15/2	weak
				401.354	24908.61	86	9147.08	13/2	strong
				460.464	21711.14	29	12344.55	13/2	weak
				528.244	18925.38	23	15130.31	17/2	line No 6
				528.405	18919.63	4	15136.06	15/2	line No 7
				576.346	17345.87	6	16709.82	17/2	FTS
	35034.88(0.02)	632.4(0.9)	445(168)	375.044	26655.97		8378.91	17/2	strong
				375.723	26607.77		8427.11	15/2	observed[a]
				386.173	25887.80		9147.08	17/2	observed[a]
				440.593	22690.33	24	12344.55	13/2	FTS
				501.019	19953.76	9	15081.12	13/2	line No 8
				502.402	19898.82		15136.06	15/2	line No 9
				521.242	19179.60	7	15855.28	15/2	line No 10
				614.131	16278.66	10	18756.22	15/2	FTS
				618.002	16176.69	12	18858.19	13/2	FTS
	38273.60(0.02)	965.4(0.2)	1449(160)	343.231	29126.52	6	9147.08	13/2	FTS
				385.477	25934.56		12339.04	15/2	FTS
				385.558	25929.05		12344.55	13/2	FTS
				431.053	23192.48	15	15081.12	13/2	FTS
				445.939	22418.32	5	15855.28	15/2	FTS
				451.965	22119.39	5	16154.21	15/2	observed
				457.840	21835.59	8	16438.01	17/2	observed
				507.249	19708.70	27	18564.90	13/2	line No 31
				512.221	19517.38	12	18756.22	15/2	line No 32
				514.911	19415.41		18858.19	13/2	observed[a]
				623.026	16046.26		22227.34	15/2	FTS
17/2									
	36889.60(0.02)	1148.5(1.3)	−117(18)	350.645	28510.70	8	8378.91	17/2	FTS
				488.823	20451.60		16438.01	17/2	line No 17
				494.762	20206.09		16683.52	19/2	observed[a]
				495.407	20179.79	22	16709.82	17/2	line No 18
				526.002	19006.04	11	17883.57	19/2	line No 19
				538.881	18551.80	32	18337.80	17/2	observed
				612.539	16320.97	4	20568.63	17/2	FTS
				681.834	14662.27	8	22227.34	15/2	FTS
	37252.22(0.02)	1073.1(1.3)	1237(41)	346.820	28825.11	6	8427.11	15/2	FTS
				363.391	27510.72	19	9741.50	19/2	FTS
				388.667	25721.66		11530.56	17/2	weak
				401.281	24913.18	13	12339.04	15/2	weak
				451.914	22121.91		15130.31	17/2	weak[a]
				452.031	22116.16	15	15136.06	15/2	weak
				486.662	20542.40	15	16709.82	17/2	line No 20
				528.550	18914.42	29	18337.80	17/2	line No 21
	37762.23(0.02)	1297.5(2.4)	−658(164)	340.232	29383.32	5	8378.91	17/2	FTS
				340.791	29335.12	2	8427.11	15/2	FTS
				356.777	28020.73	100	9741.50	19/2	FTS
				393.230	25423.19		12339.04	15/2	FTS
				456.348	21906.95	27	15855.28	15/2	strong
				468.819	21324.22	8	16438.01	17/2	FTS
				474.872	21052.41	46	16709.82	17/2	strong
				523.121	19110.70	23	18651.53	15/2	line No 24
	37971.48(0.03)	1190.6(0.3)	−346(13)	337.826	29592.57	6	8378.91	17/2	FTS
				354.132	28229.98	210	9741.50	19/2	FTS
				452.030	22116.20	15	15855.28	15/2	weak
				470.199	21261.66	63	16709.82	17/2	strong
				497.673	20087.91	14	17883.57	19/2	line No 25
				509.187	19633.68	72	18337.80	17/2	FTS
				517.456	19319.95	8	18651.53	15/2	line No 26

Table 2 (*continued*)

J	Upper level E cm^{-1}	*hfs* constants A MHz	B MHz	Fluorescence channel λ_{air} nm	k_{vac} cm^{-1}	relative intensity	Lower level E cm^{-1}	J	Remarks
1	2	3	4	5	6	7	8	9	10
	38303.27(0.02)	943.3(0.7)	1628(201)	350.018	28561.77	8	9741.50	19/2	FTS
				373.409	26772.71		11530.56	17/2	observed
				385.036	25964.23		12339.04	15/2	FTS
				431.416	23172.96	4	15130.31	17/2	observed[a]
				466.701	21420.99	30	16882.28	15/2	strong
				489.586	20419.70		17883.57	19/2	FTS
				508.719	19651.74	11	18651.53	15/2	line No 33
				511.444	19547.05		18756.22	15/2	line No 34
19/2									
	38257.25(0.03)	118.0(1.6)	-1400(121)	374.051	26726.69		11530.56	17/2	strong
				376.293	26567.48		11689.77	19/2	weak
				458.183	21819.24	14	16438.01	17/2	weak
				463.963	21547.43	62	16709.82	17/2	strong
				490.692	20373.68		17883.57	19/2	line No 29
				501.882	19919.45	93	18337.80	17/2	line No 30
	40817.12(0.01)	797.5(1.3)	1397(77)	410.072	24379.11		16438.01	17/2	FTS
				414.695	24107.30	6	16709.82	17/2	FTS
				444.728	22479.32	19	18337.80	17/2	observed
				492.028	20318.39		20498.73	17/2	line No 64
				493.726	20248.49		20568.63	17/2	line No 65
				510.062	19600.01	5	21217.11	19/2	line No 66
				517.395	19322.23		21494.89	21/2	line No 67
25/2									
	43505.33(0.06)	536.2(0.1)	2775(131)	464.453	21524.66		21980.67	23/2	strong
				496.631	20130.05	8	23375.28	25/2	line No 75
				512.701	19499.10	4	24006.23	23/2	line No 76

[a] - lines observed in the Fourier spectrum and confirmed in the current experiment, not included in determination of the upper levels' energy values, beacuse of too low *LIF* signal intensity

energy levels were found applying the selection rules and parity with regard to the hypothetical upper levels. The exciting laser was set to the nominal wavenumber of an unclassified spectral line, and then scanned around that value while searching a *LIF* signal. After observing a fluorescence signal in one fluorescence channel, the laser wavenumber was corrected to get optimal signal, and the monochromator was manually scanned in search for other predicted fluorescence channels. Observing a particular exciting spectral line in at least a few different channels allows one to assume that the excited state is identified correctly. If the signal to noise ratio was sufficiently good, the *hfs* pattern was recorded to determine the relevant parameters of the energy level, such as *hfs A* and *B* constants and quantum *J* number. Evaluated experimental data were compared for each unknown energy level. If the results from different spectral lines exciting the same upper level were found consistent, the existence of the investigated energy level could be confirmed.

Some observed fluorescence channels allowed to confirm the existence of an unknown upper level, but were too weak to allow the determination of the *hfs A* and *B* constants. Not every predicted energy level could be verified or identified, because of the lack of sufficiently strong fluorescence channels or registering of spectral lines involving two unknown energy levels.

3. Results

In this work altogether 79 spectral lines of the holmium atom were investigated. The conducted research allowed for identification of 19 odd-parity and 8 even-parity electronic levels with previously unknown energies within the range of ca. 32000–44000 cm^{-1}. Some additional spectral lines involving part of the investigated upper levels were also observed, but their quality did not allow for a quantitative analysis of the hyperfine structure, so they are not further discussed. Most of the evaluated upper energy levels were examined in at least two exciting transitions (only 4

investigated new energy levels were examined in single spectral lines). In each case at least a few fluorescence channels were identified, leading to a set of several transitions involving the investigated upper level, allowing its identification.

In order to determine the *hfs* constants of the investigated upper levels, the literature data for the known lower levels were fixed in the "Fitter" program. For two odd-parity lower levels and one even-parity lower level there were no experimental data on *hfs* constants available. In those situations the *hfs* constants of the lower levels were first fixed at the theoretical values obtained from our semi-empirical fit, and then the calculation procedure was reversed, i.e. performed with fixed newly evaluated *hfs* constants of the upper levels to determine the *hfs* constants of the lower levels. An additional exception was the even-parity level 8427.11 cm^{-1} ($J = 15/2$), for which the value of the magnetic dipole *A* constant was incorrectly published in one of the previous works [2]. For this lower level the *hfs* constants were recalculated with a spectral line recorded at two different fluorescence channels.

All the investigated spectral lines are listed in Table 1. Columns 2 and 3 include the information on the transitions (air wavelengths and vacuum wavenumbers, respectively), columns from 4 to 8 refer to the lower levels and contain such parameters as: energies, parities, *J* values, *hfs A* and *B* constants. Analogous information concerning the upper levels can be found in columns 10–14. The references to the literature values of the *hfs* constants of the lower levels, fixed during calculations, are listed in column 9.

Tables 2 and 3 include the final results obtained for new odd-parity and even-parity levels, respectively. The quantitative information concerning identified new energy levels is included in the first 4 columns: *J* values, energies and *hfs* constants, along with estimated uncertainties. Columns 5–7 include information about fluorescence channels used to identify new levels: air wavelengths, vacuum wavenumbers and the available relative intensities; the next two columns contain energies and *J* values of the lower levels involved in the fluorescence transitions. The last column includes

Table 3

Compilation of the energy values and the hyperfine structure constants *A* and *B* for the new even-parity levels in the holmium atom investigated in this work, along with the observed fluorescence channels (spectral lines and lower odd-parity levels). In parentheses the uncertainties for the levels' energies and the *hfs* constants are quoted. The literature values of intensities of the fluorescence channels correspond to literature wavelengths closest to the wavelengths observed, and were reported by Al-Labady et al. [15] or Özdalgiç et al. [16], regarding spectral lines with the wavelengths shorter or longer than 400 nm, respectively. Fluorescence channels for which no intensities are given were evaluated from FTS provided by National Solar Observatory (https://nso.edu). Some of the fluorescence channels were also observed as excitation transitions; for them the respective line numbers in Table 1 are quoted in the last column.

J	Upper level E cm⁻¹	hfs constants A MHz	B MHz	Fluorescence channel λ_air nm	k_vac cm⁻¹	relative intensity	Lower level E cm⁻¹	J	Remarks
1	2	3	4	5	6	7	8	9	10
9/2									
	32613.12(0.05)	898.9(2.1)	1282(58)	416.411	24007.96	162	8605.16	11/2	strong
				456.131	21917.37	5	10695.75	9/2	weak
				512.187	19518.70	16	13094.42	9/2	line No 5
13/2									
	38665.46(0.03)	901.6(1.8)	-781(218)	497.542	20093.18		18572.28	15/2	line No 38[a]
				504.963	19797.92	3	18867.54	13/2	line No 39
				515.625	19388.52	14	19276.94	15/2	line No 40
				537.349	18604.70	30	20060.76	11/2	FTS
				550.154	18171.69	22	20493.77	13/2	observed
				568.146	17596.24	1242	21069.22	15/2	observed
	39591.01(0.05)	1260.7(0.8)	26(184)	475.633	21018.73		18572.28	15/2	FTS
				482.410	20723.47	11	18867.54	13/2	observed
				492.132	20314.07	15	19276.94	15/2	line No 45
				511.884	19530.25	9	20060.76	11/2	line No 46
				523.490	19097.24	6	20493.77	13/2	line No 47[a]
				539.755	18521.79	4	21069.22	15/2	observed
15/2									
	37623.18(0.03)	645.1(0.6)	59(57)	524.763	19050.90	14	18572.28	15/2	line No 22
				529.363	18885.39	5	18737.79	17/2	FTS[a]
				533.025	18755.64	21	18867.54	13/2	line No 23
				544.919	18346.24	44	19276.94	15/2	observed[a]
				577.631	17307.29	17	20315.89	17/2	weak
				583.629	17129.41	16	20493.77	13/2	weak
	40446.63(0.02)	772.9(0.4)	-530(29)	463.282	21579.09	48	18867.54	13/2	strong
				496.614	20130.74	48	20315.89	17/2	line No 57
				501.042	19952.86	5	20493.77	13/2	line No 58
				504.074	19832.82	36	20613.81	17/2	line No 59
				542.369	18432.50	11	22014.13	15/2	FTS
				592.909	16861.32	234	23585.31	13/2	FTS
17/2									
	38806.69(0.02)	725.4(0.1)	-65(40)	498.144	20068.90	19	18737.79	17/2	line No 41
				511.897	19529.75	15	19276.94	15/2	line No 42
				549.513	18192.88	10	20613.81	17/2	weak
				556.158	17975.51	6	20831.18	19/2	FTS
				563.622	17737.47	16	21069.22	15/2	observed
	40220.59(0.04)	1048.3(1.7)	1733(116)	461.80	21648.31	8	18572.28	15/2	strong
				465.358	21482.80	7	18737.79	17/2	strong
				477.338	20943.65	16	19276.94	15/2	observed
				497.464	20096.34	16	20124.25	19/2	line No 51
				509.886	19606.78	7	20613.81	17/2	FTS
				530.580	18842.05	38	21378.54	17/2	line No 52
				533.596	18735.57	12	21485.02	19/2	line No 53
21/2									
	40205.63(0.02)	600.1(0.3)	-307(5)	499.985	19995.03	34	20210.60	21/2	line No 49
				516.000	19374.45	112	20831.18	19/2	line No 50
				534.022	18720.61		21485.02	19/2	observed[a]
				588.265	16994.42	158	23211.21	19/2	FTS

[a] - lines observed in the Fourier spectrum and confirmed in the current experiment, not included in determination of the upper levels' energy values, beacuse of too low *LIF* signal intensity

some remarks on evaluated exciting transitions and fluorescence channels. Spectral lines used to determine the values of new energy levels, existing in available Fourier spectra, but not observed in our experiment, are denoted as "FTS".

The proper identification of the investigated unknown upper energy levels was verified by comparing the predicted wavenumbers, resulting from the difference between expected upper levels and known lower levels, with actual wavenumbers observed in our present investigations. The exact value of the energy for a particular new upper level was determined for each transition as the sum of the energy of its lower level and the respective transition's wavenumber; the values corresponding to all relevant transitions

observed experimentally were then averaged. If the investigated spectral line was present in the Fourier spectrum analysis reported for near-UV [15] or visible range [16], the parameters of the *hfs* pattern recorded in our experiment (e.g. line pattern width and increasing or decreasing tendency of the *hfs* components' intensities with increasing frequency) were compared with the available data. Consistency of the results obtained within this work with the literature values allows to confirm the occurrence of the transition between the known lower level and a hypothetical upper level. When the investigated transition was observed in an available Fourier spectrum, but not evaluated by the authors, the center of gravity of its hyperfine structure was calculated on the basis of the

Table 4

Compilation of the energy values and the hyperfine structure constants A and B for the probably existing new odd-parity levels in the holmium atom. Presented energy levels are uncertain and require further verification.

	Upper level	hfs constants		Fluorescence channel			Lower level		Remarks
J	E cm^{-1}	A MHz	B MHz	λ_{air} nm	k_{vac} cm^{-1}	relative intensity	E cm^{-1}	J	
1	2	3	4	5	6	7	8	9	10
19/2									
	36071.92(0.05)	980.6(1.5)	2043(103)	360.999	27693.01		8378.91	17/2	weak[a]
				403.933	24749.61	23	11322.31	21/2	FTS
				410.020	24382.15	178	11689.77	19/2	strong
				515.629	19388.40	14	16683.52	19/2	line No 14
23/2									
	44283.99(0.09)	619.3(1.9)	2481(113)	438.683	22789.10		21494.89	21/2	observed[a]
				448.238	22303.32	4	21980.67	23/2	observed
				477.940	20917.28		23366.71	21/2	FTS
				478.136	20908.71	18	23375.28	25/2	observed
				493.013	20277.76	12	24006.23	23/2	line No 77
				510.853	19569.65	19	24714.34	21/2	line No 78
				533.500	18738.92		25545.07	21/2	line No 79[a]

[a] - lines observed in the Fourier spectrum and confirmed in the current experiment, not included in determination of the upper levels' energy values, beacuse of too low *LIF* signal intensity

Table 5

Compilation of the energy values and the hyperfine structure constants A and B for the probably existing new even-parity levels in the holmium atom. Presented energy levels are uncertain and require further verification.

	Upper level	hfs constants		Fluorescence channel			Lower level		Remarks
J	E cm^{-1}	A MHz	B MHz	λ_{air} nm	k_{vac} cm^{-1}	relative intensity	E cm^{-1}	J	
1	2	3	4	5	6	7	8	9	10
9/2									
	42189.40(0.05)	451.4(1.4)	-698(192)	451.776	22128.64		20060.76	11/2	weak[a]
				499.074	20031.52	23	22157.88	9/2	line No 72
				508.226	19670.81	12	22518.59	11/2	line No 73
				510.169	19595.87		22593.53	11/2	line No 74[a]
				538.165	18576.48		23612.92	11/2	weak[a]
11/2									
	39019.06(0.03)	1111.8(6.5)	231(26)	496.102	20151.52	23	18867.54	13/2	line No 43[a]
				527.327	18958.30	10	20060.76	11/2	line No 44
				539.653	18525.29	11	20493.77	13/2	observed
13/2									
	40438.59(0.04)	784.8(2.0)	388(91)	457.196	21866.31		18572.28	15/2	FTS
				472.421	21161.65	6	19276.94	15/2	FTS
				501.243	19944.82		20493.77	13/2	line No 56
				533.023	18755.69	21	21682.90	15/2	observed[a]

[a] - lines observed in the Fourier spectrum and confirmed in the current experiment, not included in determination of the upper levels' energy values, beacuse of too low intensity

Table 6

Compilation of the hyperfine structure constants A and B for the known energy levels of the holmium atom investigated in this work, along with the available literature values of the hfs constants.

Upper level			A (MHz)		B (MHz)		
J	E cm^{-1}	parity	this work	literature	this work	literature	Ref.
1	2	3	4	5	6	7	8
9/2							
	20493.40	e	1019.3(1.4)		277(70)		
13/2							
	29013.43	o	635.4(0.2)	636.3(2.0)	-561(47)	-392(65)	[18]
	39875.45	o	1204.9(1.2)	1203.8(0.4)	940(71)	957(15)	[20]
15/2							
	8427.11	e	839.3(0.2)	783.0(4.5)	385(43)	801(300)	[2]
	18572.28	o	805.8(0.8)		1663(318)		
17/2							
	40648.25	e	663.0(0.8)		-761(151)		
21/2							
	20210.60	o	1022.2(1.3)		-663(95)		

(a)

(b)
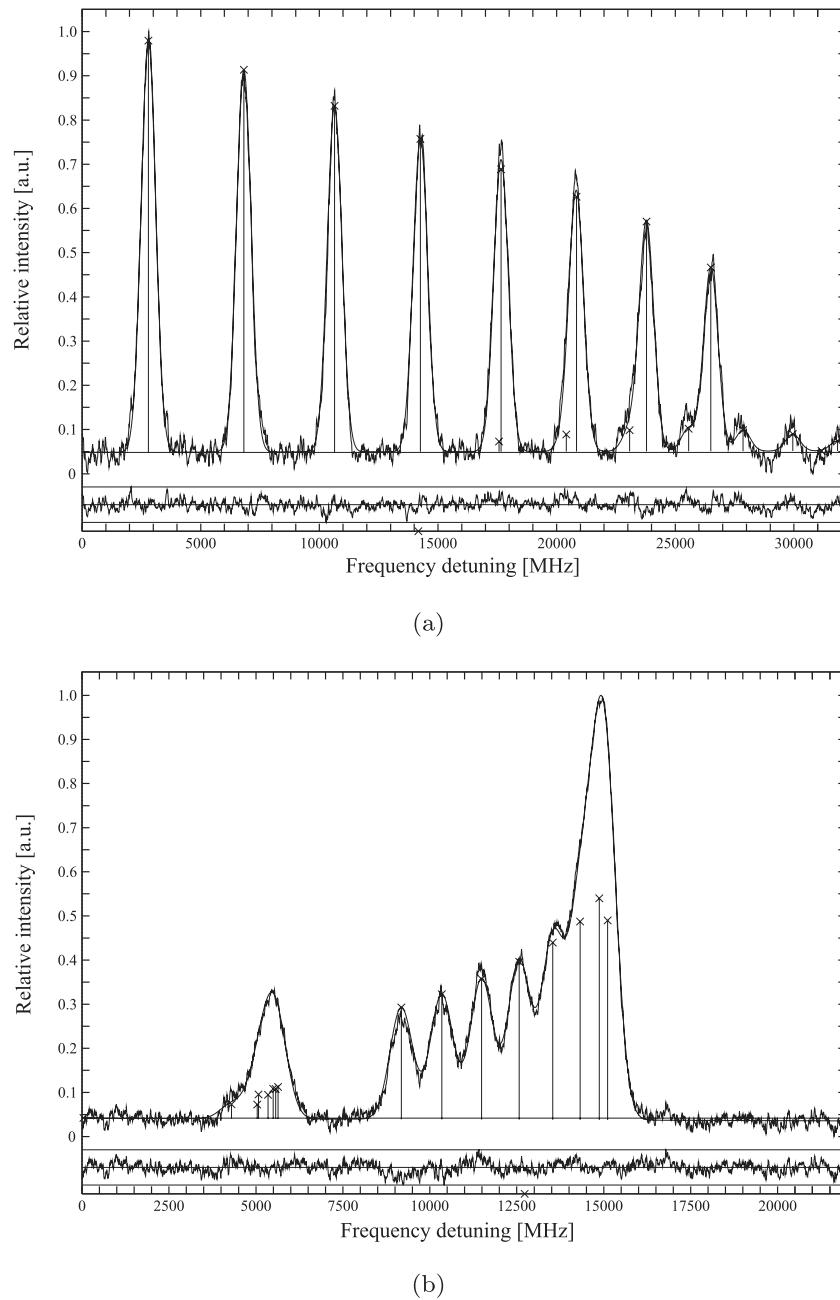
Fig. 1. Recorded *hfs* patterns of spectral lines of the holmium atom, involving the new odd-parity upper energy level E=40817.12 cm^{-1} J=19/2, along with the components fitted with the program "Fitter" (vertical lines): a) λ =517.395 nm (k=19322.23 cm^{-1}) (line no 67 in Table 1: 21494.89 cm^{-1} J=21/2 → 40817.12 cm^{-1} J=19/2), b) λ =493.726 nm (k=20248.49 cm^{-1}) (line no 65 in Table 1: 20568.63 cm^{-1} J=17/2 → 40817.12 cm^{-1} J=19/2). The lower traces represent the deviations of the experimental data from the fitted theoretical curves.

fit of the respective part of the Fourier spectrum using the *hfs* constants' values determined in the current work.

Some of the investigated upper levels could not be identified with certainty, due to the small number of fluorescence channels recorded experimentally with the *LIF* method, or visible in the Fourier spectrum, in relation to the number of possible transitions available. Other issue in identification of a particular new electronic level was too large variation in the energies obtained from various transitions. Those cases are included in Table 4 for odd-parity energy levels and Table 5 for even-parity energy levels. The existence of these levels is possible, but requires further investigation.

The hyperfine structure was investigated quantitatively also for 4 odd-parity and 3 even-parity levels with known energies. Per-

formed calculations allowed to determine the *hfs* constants, for the first time, for two odd-parity and two even-parity energy levels. Moreover, as already mentioned, the experimental value of *hfs* magnetic dipole constant *A* for 8427.11 cm^{-1} (*J* = 15/2) even-parity energy level [2] was corrected, and values of *hfs* constants for two odd-parity levels were confirmed. Results obtained for the energy level 29013.43 cm^{-1} (*J* = 13/2) have lower measurement uncertainty than for the reported literature value [18]. The results for levels with known energies are contained in Table 6. Columns 1–3 include basic information about the levels: *J* values, energies and parities. Columns 4 and 5 include experimental values of magnetic dipole *hfs* constants *A*, obtained within this work and reported in the literature, respectively. The following two columns include the same set of data for electric quadrupole *hfs* constants *B*. The last

(a)

(b)
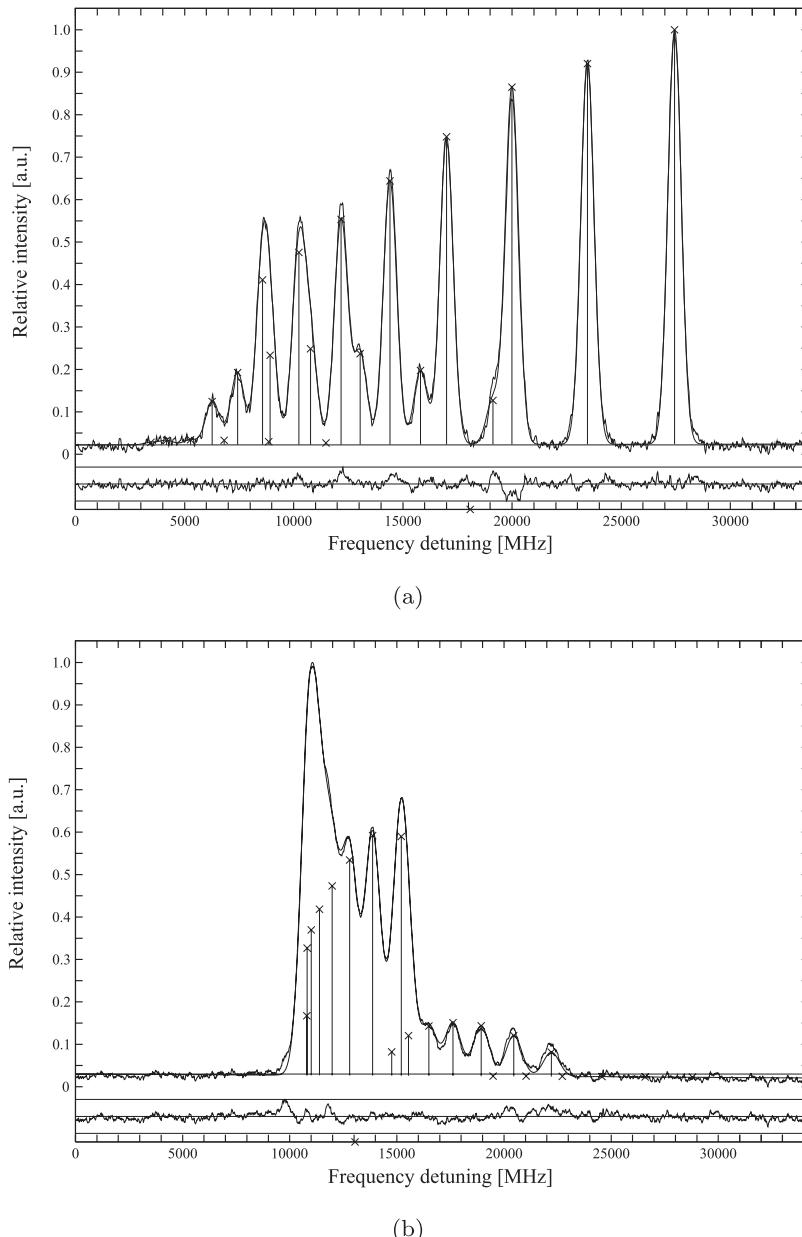
Fig. 2. Recorded *hfs* patterns of spectral lines of the holmium atom, involving the new even-parity upper energy level E=40446.63 cm^{-1} J=15/2, along with the components fitted with the program "Fitter" (vertical lines): a) λ =501.042 nm (k=19952.86 cm^{-1}) (line no 58 in Table 1: 20493.77 cm^{-1} J=13/2 → 40446.63 cm^{-1} J=15/2), b) λ =496.614 nm (k=20130.74 cm^{-1}) (line no 57 in Table 1: 20315.89 cm^{-1} J=17/2 → 40446.63 cm^{-1} J=15/2). The lower traces represent the deviations of the experimental data from the fitted theoretical curves.

column includes references to experimental values reported in the literature.

Examples of recorded hyperfine structures of the investigated lines are presented in Figs. 1 and 2, for an odd-parity and an even-parity upper energy level, respectively.

4. Discussion

The values of *hfs A* and *B* constants obtained for the upper levels in investigated spectral lines, presented in Table 1, are listed along with their total uncertainties. For each transition such uncertainty was determined as a combination of the uncertainty for the *hfs* constants of the lower level and the standard mean deviation for the *hfs* constants of the upper level, calculated for multiple recorded spectra of a particular line. The highest uncertainties can obviously be observed for spectral lines excited from those

lower levels, for which the literature values of the *hfs* constants' uncertainties are relatively high. For some investigated lines lower values of signal to noise ratio caused higher standard deviations of electric quadrupole *B* constants, but nevertheless results for their magnetic dipole *A* constants are consistent between different recorded scans. In order to determine the final *hfs* constants' values for the upper energy levels examined in more than one transition, a weighted average method was applied. Individual weights were determined on the basis of the fit quality parameter. The experimental uncertainties of the *hfs* constants for investigated electronic levels are standard deviations of the weighted average, or - for levels investigated in single spectral line - combinations of statistical and systematic errors.

For the majority of the studied cases the results obtained for the new levels are consistent among different transitions, concerning both energies and *hfs* constants. Only for one confirmed odd-

parity energy level 36646.34 cm^{-1} ($J = 11/2$) the uncertainty of A constant exceeds 3 MHz. This level was investigated in two transitions (lines No 15 and 16 in Table 1), which yielded quite divergent results for the magnetic dipole constant. However, the evaluated energy of this level exhibits good consistency within 10 different transitions, so despite the high uncertainty of the A constant the mentioned level may be regarded as confirmed. Further research may be required to determine the final value of its *hfs A* constant.

As already mentioned in Section 3, some investigated energy levels cannot yet be confirmed. The odd-parity energy level 44283.99 cm^{-1} ($J = 23/2$) was evaluated from 3 spectral lines and directly observed in 3 fluorescence channels, but two of the mentioned transitions were not visible in the available Fourier spectrum. Results obtained from 4 remaining transitions and one additional fluorescence channel present in FTS are not sufficiently consistent and still leave some question marks. Other four energy levels included in Tables 4 and 5 show better consistency, but there were too little confirmed fluorescence channels in order to assume their existence with certainty.

The final issue to consider is the analysis of the *hfs* results obtained for electronic levels with known energies. For four out of seven evaluated known energy levels *hfs A* and *B* constants were experimentally determined for the first time. For two of these levels final values were calculated from single spectral lines: 20493.40 cm^{-1} ($J = 9/2$) and 20210.60 cm^{-1} ($J = 21/2$). Experimental results obtained for the former level are in good agreement with semi-empirically predicted *hfs* constants reported in [2], but for the latter one there is a significant discrepancy between the experimental and the predicted values reported in [19]. However, further comparison of the available experimental values for the odd-parity levels with the semi-empirical predictions shows that this difference is comparable to other cases. Among the energy levels with available literature values of *hfs* constants, obtained results are consistent within the uncertainty limits with earlier reported values in 2 out of 3 cases. For 8427.11 cm^{-1} ($J = 15/2$) even-parity energy level magnetic dipole *hfs A* constant was corrected, as its previously reported value was misspelled [2].

5. Conclusions

Within this work the results of laser-spectroscopic investigations of the hyperfine structure of the holmium atom are presented. Numerous unclassified spectral lines were analyzed, allowing the identification of 19 new odd-parity and 8 new even-parity electronic levels in the energy range of ca. 32000–44000 cm^{-1}. Identification of new energy levels was based on the analysis of the selected fluorescence channels observed by the method of laser induced fluorescence in the hollow cathode discharge lamp. Additionally, as a result of performed research, two odd-parity and three even-parity levels were reported as probable new electronic levels, demanding further verification.

For all of the reported new energy levels, of course also the values of *hfs A* and *B* constants were experimentally determined for the first time. For the majority of the reported energy levels obtained values are consistent within the limits of the measurement uncertainties among the spectral lines associated with a given level. Performed investigations also allowed to determine experimental values of the *hfs* constants, for the first time, for two known odd-parity and two known even-parity levels, and to correct the *hfs A* constant for one even-parity level.

The new experimental results, included in this work, will be incorporated in further semi-empirical analysis of the fine and hyperfine structure of the holmium atom.

Declaration of Competing Interest

The author delcare that they have no known competing financial interests or personal relationship that could have appeared to influence the work reported in this paper.

CRediT authorship contribution statement

M. Chomski: Data curation, Investigation, Formal analysis, Writing – original draft. **B. Furmann:** Methodology, Formal analysis, Data curation, Investigation. **M. Suski:** Data curation, Investigation. **P. Głowacki:** Data curation, Investigation. **D. Stefańska:** Investigation, Writing – review & editing. **S. Mieloch:** Data curation, Investigation.

Data availability

No data was used for the research described in the article.

References

[1] Stefanska D, Furmann B. Hyperfine structure investigations for the odd-parity configuration system in atomic holmium. J Quant Spectrosc Radiat Transf 2018;206:286–95. doi:10.1016/j.jqsrt.2017.11.019.

[2] Stefanska D, Ruczkowski J, Elantkowska M, Furmann B. Fine- and hyperfine structure investigations of the even-parity configuration system in atomic holmium. J Quant Spectrosc Radiat Transf 2018;209:180–95. doi:10.1016/j.jqsrt.2018.01.010.

[3] Stefanska D, Werbowy S, Krzykowski A, Furmann B. Lande g_J factors for even-parity electronic levels in the holmium atom. J Quant Spectrosc Radiat Transf 2018;210:136–40. doi:10.1016/j.jqsrt.2018.02.015.

[4] Furmann B, Stefańska D, Suski M, Wilman S, Chomski M. Hyperfine structure studies of the odd-parity electronic levels of the holmium atom I: levels with known energies. J Quant Spectrosc Radiat Transf 2019;234:115–23. doi:10.1016/j.jqsrt.2019.05.028.

[5] Furmann B, Stefańska D, Wilman S, Chomski M, Suski M. Hyperfine structure studies of the odd-parity electronic levels in the holmium atom II: New levels. J Quant Spectrosc Radiat Transf 2019;235:70–80. doi:10.1016/j.jqsrt.2019.06.005.

[6] Chomski M, Furmann B, Ruczkowski J, Suski M, Stefańska D. Lande g_J factors of the electronic levels of the holmium atom. J Quant Spectrosc Radiat Transf 2021;274:107865. doi:10.1016/j.jqsrt.2021.107865.

[7] Chomski M, Suski M, Wilman S, Furmann B, Ruczkowski J, Stefańska D. Lande g_J factors of odd-parity electronic levels of the holmium atom. J Quant Spectrosc Radiat Transf 2022;279:108045. doi:10.1016/j.jqsrt.2021.108045.

[8] Sneden C, Cowan JJ. Genesis of the heaviest elements in the Milky Way Galaxy. Science 2003;299(5603):70–5. doi:10.1126/science.1077506.

[9] Lawler JE, Sneden C, Cowan JJ. Improved atomic data for Ho II and new holmium abundances for the sun and three metal-poor stars. Astrophys J 2004;604(2):850. doi:10.1086/382068.

[10] Dzuba VA, Flambaum VV. Relativistic corrections to transition frequencies of Ag I, Dy I, Ho I, Yb II, Yb III, Au I, and Hg II and search for variation of the fine-structure constant. Phys Rev A 2008;77:012515. doi:10.1103/PhysRevA.77.012515.

[11] Stefanska D, Furmann B, Głowacki P. Possibilities of investigations of the temporal variation of the α constant in the holmium atom. J Quant Spectrosc Radiat Transf 2018;213:159–68. doi:10.1016/j.jqsrt.2018.04.017.

[12] Saffman M, Mølmer K. Scaling the neutral-atom Rydberg gate quantum computer by collective encoding in holmium atoms. Phys Rev A 2008;78:012336. doi:10.1103/physreva.78.012336.

[13] Miao J, Hostetter J, Stratis G, Saffman M. Magneto-optical trapping of holmium atoms. Phys Rev A 2014;89:041401. doi:10.1103/physreva.89.041401.

[14] Stefańska D, Furmann B, Ruczkowski J, Elantkowska M, Glowacki P, Chomski M, Suski M, Wilman S. Investigations of the possible second-stage laser cooling transitions for the holmium atom magneto-optical trap. J Quant Spectrosc Radiat Transf 2020;246:106915. doi:10.1016/j.jqsrt.2020.106915.

[15] Al-Labady N, Özdalgiç B, Er A, Güzelçimen F, Öztürk IK, Kröger S, Kruzins A, Tamanis M, Ferber R, Başar G. Line identification of atomic and ionic spectra of holmium in the near-UV. Part I. Spectrum of Ho I. Astrophys J Suppl Ser 2017;228(2):16. doi:10.3847/1538-4365/228/2/16.

[16] Özdalgiç B, Güzelçimen F, Öztürk IK, Kröger S, Kruzins A, Tamanis M, et al. Line identification of atomic and ionic spectra of holmium in the visible spectral range. I. Spectrum of Ho I. Astrophys J Suppl Ser 2019;240(2):27. doi:10.3847/1538-4365/aaf9b2.

[17] Furmann B, Stefanska D, Suski M, Wilman S. Identification of new electronic levels in the holmium atom and investigation of their hyperfine structure. J Quant Spectrosc Radiat Transf 2018;219:117–26. doi:10.1016/j.jqsrt.2018.08.005.

[18] Başar G, Başar G, Özdalgiç B, Öztürk I, Güzelçimen F, Bingöl D, et al. Laser spectroscopic investigation of atomic holmium in the wavelength range from 780 nm to 830 nm: Hyperfine structure measurements and a new energy level. J Quant Spectrosc Radiat Transf 2020;243:106809. doi:10.1016/j.jqsrt.2019.106809.

[19] Elantkowska M, Ruczkowski J, Sikorski A, Wilman S. Fine- and hyperfine structure investigations of the odd-parity configuration system in atomic holmium. J Quant Spectrosc Radiat Transf 2019;237:106642. doi:10.1016/j.jqsrt.2019.106642.

[20] Wyart J-F, Camus P, Vergès J. Etude du spectre de l'holmium atomique: I. Spectre d'émission infrarouge niveaux d'énergie de Ho I et structures hyperfines. Physica C 1977;92(3):377–96. doi:10.1016/0378-4363(77)90137-1.